Post-translational modifications in mitochondrial dynamics

Laura Jade Lee

School of Biochemistry

August 2018

A dissertation submitted to the University of Bristol
in accordance with the requirements for award of the degree of
Doctor of Philosophy in the Faculty of Life Sciences

56189 words

Abstract

Ischaemic heart disease (IHD) is a leading cause of morbidity and mortality worldwide. IHD occurs when blood-flow to the heart is occluded, depriving the tissue of oxygen and glucose. Paradoxically, restoration of blood supply can cause further damage, termed reperfusion injury. The resultant oxidative stress (OS) causes multiple pathologies including profound mitochondrial damage.

Mitochondrial function is closely linked to their dynamics; continual fission and fusion facilitate mitochondrial-trafficking and ATP-distribution. Mitochondrial fission is mediated by the dynamin-like GTPase Drp1, which is recruited to mitochondria by its receptor Mff. Over-expression of Drp1 or Mff results in highly fragmented, dysfunctional mitochondria. The regulation of Drp1 by post-translational modifications (PTMs) is well-established, whereas regulation of Mff PTMs is less defined.

The aim of this PhD was to determine if, and how, manipulation of Mff PTMs can protect against mitochondrial damage incurred by IHD.

I show that OS causes phosphorylation of Mff, which promotes its SUMOylation. Mff SUMOylation subsequently leads to its ubiquitination and degradation. We propose that this is a protective response to limit mitochondrial fragmentation. Non-SUMOylatable Mff mutants have significantly reduced ubiquitination and slower turnover, indicating the activity of a SUMO-targeted ubiquitin ligase (STUbL).

I demonstrate that Mff is ubiquitinated by at least three ligases, and test the hypothesis that Parkin, a known ligase of Mff, could be recruited via a SUMO-dependent mechanism. While Parkin interacts non-covalently with SUMO, its recruitment to Mff is SUMO-independent. I then show that Parkin ubiquitinates Mff at its SUMOylatable lysine, whereas Fbxo7, a component of the Skp1-Cul1-Fbx ligase complex, mediates ubiquitination of Mff at a site independent of both SUMO and Parkin.

Given its dependence on OS, we propose that specific manipulation of the novel STUbL pathway could be a viable clinical intervention in recovery from IHD. This project therefore provides a solid foundation for further study.

Acknowledgements

First and foremost, I am hugely grateful to Jeremy. From the first time he interviewed me (and turned me down), his unwavering support has been crucial in getting me to this point. He has always had confidence in me, even when I'm being "too negative." Thank you for allowing me to be so independent and for calmly letting me make my own (frequent) mistakes, for teaching me to always ask questions, no matter how stupid they may seem, and for never being short of a few inspirational (and several four-letter) words of wisdom when the going gets tough.

A massive thanks to Kev, for his cunning plans and exceptional guidance, for not laughing (too much) at my mistakes, and for reminding me of the importance of stop codons. To Suko, thank you for holding the lab together in the face of our collective stupidity – we are all extremely grateful for everything you do, and for turning the occasional blind eye to some of the more foolish things we do. Dan, thank you for your Fbxo7-expertise and unrivalled knowledge of faculty-wide gossip dating back over a decade.

Many thanks to Nadiia for torturing all those hearts with me, and to Andrew and Tatyana, for donating and assisting with the torture contraption. Chun, thank you for the pickled hearts and introduction to Kung Fu, though I've yet to find a use for either. Thank you to Ruth and Caroline for taking me under your collective wing when I arrived here, bewildered, and for never turning down a swift (few) pint(s) since. To Phil, thank you for being a terrible lightweight but worthy arm-wrestling opponent. Paul, thanks for introducing me to Cheesy Fridays, and thank you to the rest of the Henley/Hanley lab for enduring them.

Luis, I couldn't have asked for a better bench-mate – our fungus is still going strong. Richard, thank you for suffering with me through the many Mff meetings. Alex, Sonam, Vanilla and Jodie, thank you for the numerous morning coffees, plentiful afternoon teas, and occasional scientific discussion.

To my mum and dad, thank you for all of your support, and for always taking an interest in my work despite not really understanding it. Matt, thanks for letting me be the more intelligent and more attractive sibling – at least you eventually grew taller than me.

And lastly, to Roz. Thank you for walking into my life nine years ago and sticking around ever since. You've been a constant through six homes, two degrees and eight series of Great British Bake Off. Thank you for always believing in me, keeping me fed over the last few months, and making sure we never run out of teabags.

*"Everything is sh*t. You just have to keep on working until you die."*
- Professor Jeremy Henley, 2017

Author’s Declaration

I declare that the work in this dissertation was carried out in accordance with the requirements of the University's Regulations and Code of Practice for Research Degree Programmes and that it has not been submitted for any other academic award. Except where indicated by specific reference in the text, the work is the candidate's own work. Work done in collaboration with, or with the assistance of, others, is indicated as such. Any views expressed in the dissertation are those of the author.

SIGNED: ..... DATE: .....

Table of Contents

List of Figures

Chapter 1 Introduction

Chapter 3 Ex vivo modelling of Ischaemia/Reperfusion injury

Chapter 4 Regulation of Mff by Parkin and Fbxo7

Chapter 5 SUMO regulates mitochondrial dynamics

Chapter 6 General Discussion

Chapter 8 Appendix

List of Tables

Chapter 1 Introduction

Chapter 2 Materials & Methods

Chapter 6 General Discussion

List of Abbreviations

Abbreviation	Full description
AD	Alzheimer's disease
ANOVA	Analysis of variance
AMP/ADP/ATP	Adenosine mono-/di-/tri-phosphate
APC/C	Anaphase-promoting complex
BCA	Bicinchoninic acid
BSA	Bovine serum albumin
CCCP	Carbonyl cyanide m-chlorophenyl hydrazone
CFP	Cyan fluorescent protein
CHX	Cycloheximide
CRL	Cullin RING ligase
CVD	Cardiovascular disease
DA	Dopaminergic neurons
DeSI	deSUMOylating isopeptidase
dH_2O	Distilled water
DMEM	Dulbecco's modified Eagle medium
DMSO	Dimethyl sulphoxide
DNA	Deoxyribonucleic acid
Drp1	Dynamin-related protein I
dsRNA	Double-stranded RNA
DTT	Dithiothreitol
DUB	De-ubiquitinating peptidase
Dyn2	Dynamin II
E (n)	Embryonic day
E1	Ubiquitin-activating enzyme
E2	Ubiquitin-conjugating enzyme
E3	Ubiquitin ligase
EC	Excitation-contraction
ECL	Enhanced chemiluminescence
EDTA	Ethylenediaminetetraacetic acid
EGTA	Ethylene glycol-bis-(β-aminoethyl ether)-N,N,N',N'-tetraacetic acid

ER	Endoplasmic reticulum
ESCRT	Endosomal sorting complexes required for transport
FAT10	Human Leukocyte Antigen-F adjacent Transcript 10
FBS	Foetal bovine serum
FBXO	F-box domain containing proteins
Fbxo7	F-box only protein 7
FCCP	Carbonyl cyanide-4-(trifluoromethoxy)phenylhydrazone
GFP	Green fluorescent protein
GluK/R	Kainate receptor subunit
GST	Glutathione S-transferase
GTP/GDP	Guanosine tri-/di-phosphate
HA	Hemagglutinin
HECT	Homologous to the E6AP carboxyl terminus
HEK	Human embryonic kidney
HIF	Hypoxia-inducible factor
HRP	Horse radish peroxidase
I/R	Ischaemia/reperfusion
IBR	In-between RINGs domain
IHD	Ischaemic heart disease
IMS	Intermembrane space (of mitochondria)
INF2	Inverted formin 2
IPC	Ischaemic pre-conditioning
IPTG	Isopropyl β-D-thiogalactopyranoside
ISG15	interferon stimulated gene 15
KCl	Potassium chloride
kDa	Kilo Dalton
LB	Luria-Bertani
MAM	Mitochondria-associated ER membrane
MAPL	Mitochondria-associated protein ligase
MEF	Murine embryonic fibroblast
Mff	Mitochondrial Fission Factor
Mfn	Mitofusin
MiD	Mitochondrial Dynamics Protein
MIM	Mitochondrial inner membrane (also IMM)

MOM	Mitochondrial outer membrane (also OMM)
mPTP	Mitochondrial permeability transition pore
mRNA	Messenger RNA
NADH	Nicotinamide adenine dinucleotide (NAD) + hydrogen (H)
Nedd8	neural precursor cell-expressed, developmentally downregulated gene 8
NEM	N-ethylmaleimide
NO	Nitric oxide
NPC	nuclear pore complex
OGD	Oxygen- and glucose-deprivation
PBS	Phosphate-buffered saline
PCR	Polymerase chain reaction
PD	Parkinson's disease
Pen/Strep	Penicillin and Streptomycin
PFA	Paraformaldehyde
PH	Pleckstrin homology
PIAS	Protein inhibitor of activated STAT
PINK1	PTEN-induced putative kinase I
PLL	Poly-L-lysine
PM	Plasma membrane
PML	Promyelocytic leukaemia protein
PRD/PRR	Proline-rich domain/region
PTM	Post-translational modification
RanBP	Ran binding protein
RanGAP	Ran-GTPase-activating protein
RBR	RING-between-RING E3 ligase
REP	Repressor element
RING	Really interesting new gene
RNA	Ribonucleic acid
ROS	Reactive oxygen species
RT-PCR	Reverse transcription PCR
SAE	SUMO activating enzyme
SCF	Skp1-Cul1-F-box-type CRL

SDS-PAGE	Sodium dodecyl sulphate polyacrylamide gel electrophoresis
SENP	Sentrin-specific protease
shParkin	Short hairpin RNA targeted to Parkin
shRNA	Short hairpin ribonucleic acid
shSCR	Short hairpin RNA with scrambled targeting sequence
siFbxo7	Small interfering RNA targeted to Fbxo7
siLuc	Small interfering RNA targeted firefly luciferase
SIM	SUMO-interacting motif
siRNA	Small interfering RNA
STUbL	SUMO-targeted ubiquitin ligase
SUMO	Small ubiquitin-like modifier
SUMO-Ub	SUMO-ubiquitin hybrid chain
TAE	Tris-acetate ethylenediaminetetraacetic acid
TBS-T	Tris-buffered saline containing tween
TEMED	Tetramethylethylenediamine
tRNA	Transfer RNA
tSIM-UIMs	Tandem SUMO-interacting motifs and ubiquitin-interacting motifs
UBC9	Ubiquitin conjugating protein 9
UBL	Ubiquitin-like protein/modifier
Ubl	Ubiquitin-like domain
UFD	Ubiquitin fusion degradation
UIM	Ubiquitin-interacting motif
UPD	Unique Parkin domain (RING0)
UPR	Unfolded protein response
UPS	Ubiquitin proteasome system
USPL1	Ubiquitin-specific protease-like I
WB	Western blot
WT	Wildtype
YFP	Yellow fluorescent protein

Chapter 1 Introduction

1.1 Mitochondrial dynamics regulate their function

The mitochondrion is an organelle found in most eukaryotic cells, but varies considerably between cell types in size, structure and number. For example, red blood cells have no mitochondria, but hepatocytes may have more than 2000 (Voet and Voet, 2011). Mitochondria are bound by a double membrane and are generally 0.75-3µm in diameter (Wiemerslage and Lee, 2016). These organelles are highly compartmentalised with structures for specific processes in the generation of adenosine triphosphate (ATP); 90% of cellular ATP is generated by mitochondria, resulting in mitochondria colloquially being referred to as "the powerhouse of the cell" (Pessayre et al., 2002).

1.1.1 Mitochondria: discovery and evolution

As reviewed previously (Ernster and Schatz, 1981), intracellular structures retrospectively believed to be mitochondria were first observed in the 1840s, although it was not until the late 1800s that they were recognised to be ubiquitously distributed throughout cell types, and of functional importance. The respiratory chain was not described until the discovery of cytochromes in 1925, and cellular respiration was not attributed specifically to mitochondria until the late 1940s.

Despite the dependence of most eukaryotic cells on mitochondria for energy conversion, it is now widely accepted that they were originally prokaryotic cells, engulfed by eukaryotic cells to ultimately form an endosymbiotic relationship (Keeling and Archibald, 2008). It is thought that an anaerobic cell endocytosed an aerobic bacterium but was unable to digest it. The cytoplasm of the anaerobic cell, abundant in partially-digested carbohydrates, allowed the aerobic bacterium to flourish and generate enough ATP to be beneficial to the anaerobic host as well (Gray, 1992, Zimorski et al., 2014). In support of this theory, mitochondria have their own genome, with an alternative genetic code and DNA replication and repair machinery, which show significant similarity to those of the bacterial species *Rickettsia prowazekii* (Andersson et al., 1998). Mitochondria have their own ribosomes, which are more like those of bacteria than of eukaryotes (Manuell et al., 2007). Furthermore, mitochondria divide only by binary fission, which is also how bacteria

and archaea divide, and eukaryotic cells cannot generate *de novo* mitochondria (Margolin, 2005).

1.1.2 Mitochondrial structure

The mitochondrion has a double membrane comprising proteins and phospholipid bilayers. This creates 5 distinct mitochondrial compartments: outer membrane, intermembrane space, inner membrane, cristae (formed by folding of the inner membrane) and matrix (the space created between cristae) (Figure 1.1).

The mitochondrial outer membrane (MOM or OMM) has a protein:phospholipid ratio similar to that of the eukaryotic plasma membrane, and is largely composed of transmembrane porins, which allow free diffusion of small molecules between the cytoplasm and the mitochondrial intermembrane space (Checchetto and Szabo, 2018). Larger proteins can translocate into the mitochondria via binding of a signalling sequence on their N-termini to a multi-subunit mitochondrial translocase for active transport (Herrmann and Neupert, 2000). Disruption of the MOM allows intermembrane proteins to leak into the cytoplasm, resulting in cell death (Chipuk et al., 2006). As well as being crucial to mitochondrial integrity and function, the MOM can also associate with the endoplasmic reticulum (ER) (Hayashi et al., 2009).

The intermembrane space (IMS) is located between the outer and inner membranes of the mitochondria. Due to their free diffusion through the MOM, ions and other small molecules are at the same concentration as in the cytoplasm. However, the protein composition of the intermembrane space differs from the cytoplasm due to the need for specific signalling sequences to translocate. Cytochrome *c*, the last enzyme of the respiratory transport chain, is localised here, and its leakage into the cytoplasm is often used as a marker of cellular stress and/or death (Chipuk et al., 2006).

The inner mitochondrial membrane (IMM or MIM) is highly impermeable and has a membrane potential as a result of the electron transport chain. The MIM has a very high protein:phospholipid ratio, and incorporates enzymes involved in ATP synthesis, oxidative phosphorylation, metabolite transport, protein import, and mitochondrial fission and fusion. The MIM extends not only around the internal perimeter of the mitochondrion, but also invaginates to create numerous cristae, greatly increasing its available surface for ATP production; mitochondria in cells with greater energy-demands have greater numbers of cristae (Mannella, 2006).

The mitochondrial matrix fills the space between cristae and contains around 60% of all mitochondrial proteins, including enzymes required for pyruvate and fatty acid oxidation, as well as the citric acid cycle. Additionally, the matrix contains copies of the mitochondrial DNA genome, which encodes the machinery required to generate RNAs and proteins, including tRNAs and ribosomal components (Anderson et al., 1981).

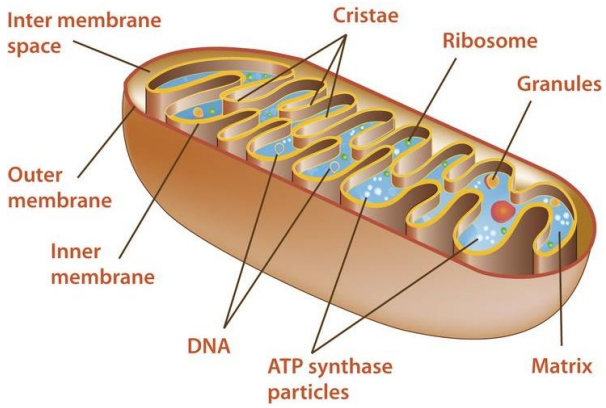

Figure 1.1 **Labelled schematic of a mitochondrion**. Mitochondria have an outer (MOM) and inner (MIM) membrane, separated by the intermembrane space (IMS). The MIM is highly folded, creating cristae, which increase the surface area for ATP production. The matrix sites between the cristae and is the site of various enzyme-catalysed reactions and the mitochondrial genome.

1.1.3 Organisation and distribution of mitochondria

In the vast majority of cells, mitochondria form extensive and dynamic networks, undergoing continuous cycles of fission (division) and fusion. This creates a highly adaptable and efficient energy transfer system, able to rapidly deliver ATP to where it is most urgently needed within the cell (Piquereau et al., 2013). Fused mitochondria (mitochondrial network/reticulum) facilitate delivery of ATP from the cell periphery to the core, whereas individual mitochondria can be trafficked rapidly, to meet localised increases in energy demand throughout the cell (Hom and Sheu, 2009, Skulachev, 2001). A growing body of work is uncovering an important role for mitochondria at ER contact sites, termed mitochondria-associated ER membrane (MAM) (Hayashi et al., 2009).

1.1.4 Mitochondrial function

The primary function of mitochondria is ATP production by aerobic respiration. Pyruvate and NADH, the main products of glucose glycolysis in the cytoplasm, are actively transported through the MIM and oxidised in a reaction that generates 13x more ATP than

anaerobic respiration (Rich, 2003). However, mitochondria also carry out numerous other functions.

Mitochondria can transiently store Ca^{2+} ions in the matrix, and can also rapidly release Ca^{2+}, allowing them to act as a cytosolic calcium buffer (Rossier, 2006). The ER is the primary site of Ca^{2+} storage, and the interactions between ER and MOM at MAM contact sites allow for significant Ca^{2+} exchange, and play an important role in Ca^{2+} signalling (Pizzo and Pozzan, 2007).

Other roles for mitochondria include intracellular signalling, for example via mitochondrially generated reactive oxygen species (ROS), which trigger the inflammatory response in pathologies including cardiovascular disease (CVD) (Li et al., 2013). Mitochondria are also sensitive and responsive to hormones, particularly via mitochondrial oestrogen receptors, which have been identified in mitochondria isolated from the brain and heart. Oestrogens have been shown to modulate several mitochondrial functions, including mitochondrial DNA transcription and oxygen consumption (Klinge, 2008). Mitochondrial fission and fusion proteins have also been shown to contribute to temporal regulation of mitochondrial metabolism and the cell-cycle (McBride et al., 2006). Additionally, mitochondria play a key part in activation of mammalian apoptosis. Bcl-2 proteins regulate the release of pro-apoptotic factors from the mitochondrial IMS to the cytosol, where they activate caspases responsible for apoptosis and phagocytosis (Wang and Youle, 2009).

1.1.5 Fission and fusion proteins

Mitochondria are constantly undergoing balanced cycles of fission and fusion to create an extensive reticulum that allows efficient energy transfer and can adapt quickly to meet changing energy demands, while also effectively disposing of damaged organelles. Fusion and fission events occur roughly every two minutes in a mitochondrion (Nunnari et al., 1997). These are both tightly regulated processes, effected by dynamins and dynamin-related proteins (DRPs). Mitochondrial fission will be the primary focus of this thesis.

1.1.5.1 Mitochondrial dynamics are controlled by Dynamins and DRPs

The 100kDa GTPase Dynamin was first identified in 1989 and was shown to be pivotal in fission of endocytic vesicles in both plant and animal cells (Shpetner and Vallee, 1989). Dynamin has the ability to self-assemble into helical polymers, which co-assemble with the neck of a budding vesicle and co-ordinate membrane severing. Structurally, Dynamin

comprises a GTPase domain, a long stalk made up of a four-helix bundle, a phosphoinositide-4,5-bisphosphate (PIP2)-binding pleckstrin homology domain (PH) to bind membranes, and a proline-rich domain (PRD). In mammals, three Dynamin isoforms (Dyn1-3) are expressed; Dyn2 is ubiquitously expressed and Dyn1 and -3 are neuron-specific (Antonny et al., 2016).

DRPs are also large GTPases that utilise GTP-dependent self-assembly and the resultant GTP hydrolysis-mediated conformational changes to remodel intracellular membranous structures (Faelber et al., 2013, Praefcke and McMahon, 2004). The mammalian DRP Drp1 (Dnm1 in yeast) drives fission of mitochondrial membranes, while DRPs Mfn1/2 (Fzo1 in yeast) mediate fusion of the MOM and Opa1 (Mgm1 in yeast) mediates fusion of the MIM (Hoppins et al., 2007).

1.1.5.2 Mitochondrial fusion

Mitochondrial fusion enables communication and contents-sharing between mitochondrial compartments. ATP can be rapidly trafficked through the reticulum, healthy mitochondrial components can be re-distributed, and damage to mitochondrial DNA can be diluted throughout the network, reducing the effects of genomic mutations. All of this is thought to buffer against transient defects in mitochondrial function, but fusion remains a relatively poorly understood mechanism (Chen and Chan, 2010). Currently, evidence supports a process in which MOM and MIM fusion occur in two separable stages, both of which require DRPs. The first stage is the tethering of membranes of two mitochondria and is mediated by the self-assembly of fusion DRPs (Song et al., 2009, Meeusen et al., 2004, Meeusen et al., 2006). The second stage is induced by DRP-dependent GTP hydrolysis and involves conformational changes. This is proposed to destabilise lipid bilayers of the tethered mitochondria and facilitate lipid mixing and ultimately mitochondrial fusion. Electron microscopy has been used to observed assembled fusion DRP structures, but it remains unclear if/how they contribute to active fusion complexes (Abutbul-Ionita et al., 2012, Rujiviphat et al., 2009).

1.1.6 Mitochondrial fission

Fission facilitates transport, distribution, quality control and degradation of mitochondria (Lackner and Nunnari, 2009). Individual mitochondria are far easier to traffic around the cell, allowing rapid response to localised changes in energy demands (Skulachev, 2001, Hom and Sheu, 2009). Additionally, unhealthy mitochondria are able to sequester damaged proteins/DNA into one daughter mitochondrion during asymmetrical fission. This allows one healthy daughter mitochondrion to function and divide normally, while the unhealthy one is simultaneously primed for degradation by the cellular quality control machinery (Twig et al., 2008a, Ni et al., 2015).

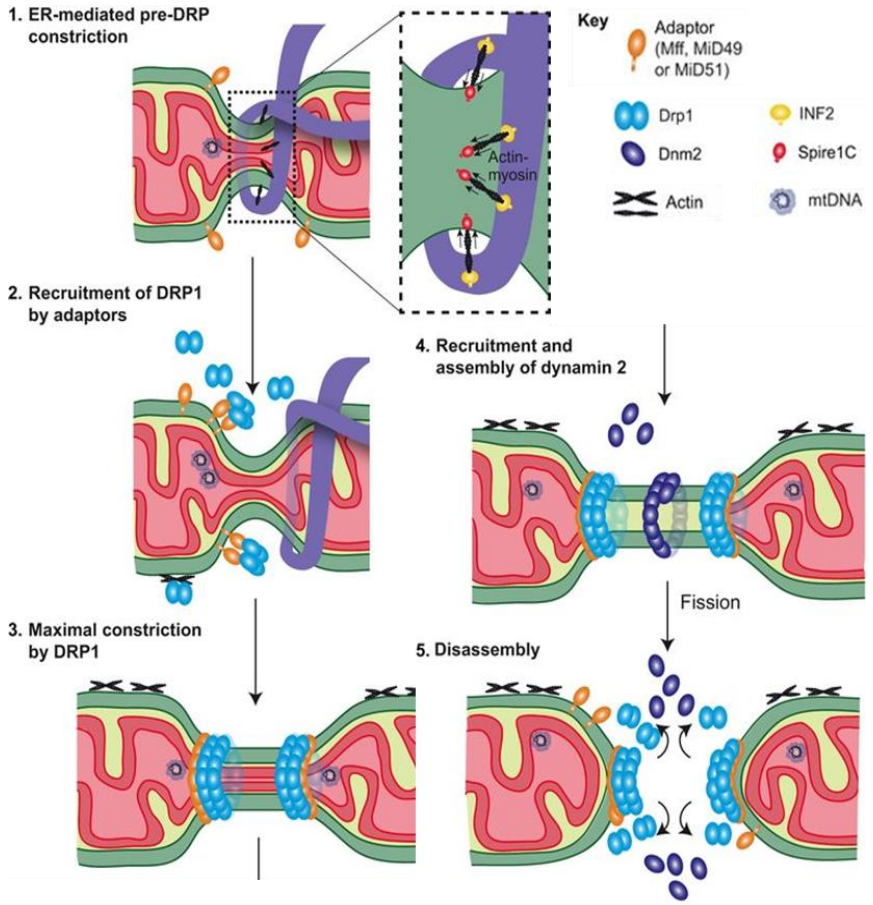

Figure 1.2 Schematic of mitochondrial fission. 1. Pre-Drp1 recruitment, contact between the mitochondrial membrane and ER constricts the mitochondrial membrane. 2. MOM adaptor proteins recruit Drp1. 3. Mitochondrial membrane is maximally constricted by Drp1-mediated GTP hydrolysis and oligomerisation. 4. Dyn2 (Dnm2) is recruited to the constricted neck. 5. Final scission of the mitochondrial membrane by Dyn2-mediated GTP hydrolysis. Figure adapted from *Kraus, F. and M. T. Ryan (2017). "The constriction and scission machineries involved in mitochondrial fission." Journal of Cell Science 130(18): 2953* (Kraus and Ryan, 2017).

1.1.6.1 Priming by ER-mediated constriction

The landmark discovery that ER-extensions physically wrap around mitochondria prior to their fission was relatively recent (Friedman et al., 2011). Friedman *et al* proposed their ER contact-determined model of fission following observation that mitochondria and ER have extensive points of contact (MAMs) and tightly coupled dynamics in both yeast and mammalian Cos-7 cells. They went on to show by electron microscopy and live cell-imaging that fission occurred at sites primed by ER tubule-mediated constriction, and suggested that this could provide a 'geometric hotspot' conducive to Drp1 polymerisation, with a dimeter of ~150 nm (Friedman et al., 2011). It was concluded that ER-dependent mitochondrial constriction occurs upstream and independently of Drp1-adaptor assemblies, as constrictive MAMs were observed even in cells devoid of Drp1 or its adaptors (Osellame et al., 2016, Friedman et al., 2011). At MAMs, actin and myosin filaments work together to generate a physical force, which drives initial membrane constriction (Figure 1.2, 1) (Hatch et al., 2014, Phillips and Voeltz, 2016). INF2, an ER-associated formin, has been shown to serve as a nucleation point to facilitate polymerisation of F-actin and recruitment of myosin to MAMs in mammalian cells (Korobova et al., 2014, Li et al., 2015). Spire1C serves as a mitochondrial actin nucleation centre, and binds to INF2 to promote actin polymerisation (Manor et al., 2015).

1.1.6.2 Maximal constriction by Drp1

For further constriction to proceed, the fission site must be demarcated for binding of Drp1. Unlike the archetypal Dynamin, Drp1 does not have a PH domain so cannot independently or directly bind membranes (Yoshida, 2018). It is therefore necessary for Drp1 recruitment to be primed by mitochondrial adaptor proteins (Figure 1.2, 2). Current hypotheses detail an important role for Mitochondrial Fission Factor (Mff) in recruitment of oligomerised Drp1. In addition, Mitochondrial Dynamics Proteins MiD49 and MiD51 have also been implicated in the assembly of Drp1 contractile oligomers, though other studies have asserted that they sequester inactive Drp1 away from Mff (Gandre-Babbe et al., 2008, Otera et al., 2010, Losón et al., 2013).

Once recruited to the MOM, Drp1 monomers self-assemble around the membrane into contractile ring structures (Fröhlich et al., 2013, Ingerman et al., 2005, Mears et al., 2011). GTP hydrolysis provides the energy to drive Drp1-helix conformational changes, resulting in the ring diameter being two-fold reduced and contributing to further membrane constriction (Figure 1.2, 3) (Mears et al., 2011, Koirala et al., 2013). Assembly

of Drp1 helices is mediated via the central stalk interface, with spirals nucleating from two adjacent starting points to form a two-start helix around the membrane (Fröhlich et al., 2013, Zhang and Hinshaw, 2001).

1.1.6.2.1 Drp1

Drp1 is a 70-80kDa cytosolic GTPase recruited to the MOM to facilitate fission. At steady state, ~3% of total Drp1 is associated with mitochondria (Smirnova et al., 2001). Cells lacking functional Drp1 exhibit highly elongated and interconnected mitochondria, particularly arranged in perinuclear clusters. This phenotype is consistent with a perturbed equilibrium between mitochondrial fission and fusion; fusion still occurring normally but fission being hindered. Similarly, cells devoid of Drp1 have severely elongated peroxisomes, indicative of a role for Drp1 in peroxisomal fission analogous to that of mitochondrial fission (Ishihara et al., 2009, Koch et al., 2003). Peroxisomes are ER-derived vesicles and are the site of oxidative degradation of hydrogen peroxide from the cell, as well as performing beta-oxidation of fatty acid chains (Hoepfner et al., 2005). During apoptosis, rates of mitochondrial fission are greatly increased, and coincide with cytochrome *c* release. Mutation or deletion of Drp1 delays release of cytochrome *c*, suggestive of a pro-apoptotic role for Drp1 (Munoz-Pinedo et al., 2006, Frank et al., 2001).

1.1.6.2.2 Drp1 adaptors

Without a PH domain to bind phospholipids, Drp1 requires adaptor proteins in the MOM for its recruitment, of which several have been characterised. In yeast, peripheral membrane receptors Caf4 and Mdv1 recruit and assemble Dnm1 (Drp1), with Fis1 acting as an adaptor on the MOM (Lackner et al., 2009). In metazoan species, however, there are no known homologues of Caf4 or Mdv1, and Fis1 has now been established as dispensable for mitochondrial fission (Otera et al., 2010, Osellame et al., 2016).

Mitochondrial dynamics proteins MiD49 and MiD51 are MOM proteins specific to higher eukaryotes (Palmer et al., 2011). It remains unclear if the MiD proteins facilitate mitochondrial fusion or inhibit mitochondrial fission; over-expression of either or both MiD proteins gives rise to fused mitochondrial tubules, but low-level expression of tagged MiD49/51 increases Drp1 colocalisation with mitochondria, indicative of a role in stabilising Drp1 at the MOM (Palmer et al., 2011). Both MiD proteins are capable of recruiting Drp1 to sites of mitochondrial fission, independently of each other and of Mff (Losón et al., 2013, Osellame et al., 2016, Otera et al., 2016, Richter et al., 2014). Unlike Mff, which remains

punctate at pre-constriction sites in the absence of Drp1, the MiD proteins diffusely localise throughout the MOM (Richter et al., 2014, Friedman et al., 2011, Otera et al., 2010).

Mff is found in all metazoans and is thought to be the primary adaptor for Drp1. The structure and domain architecture of Mff remain elusive, however the N-terminal domain of Mff is essential for its interaction with Drp1 (Otera et al., 2010). Mff knock out cell lines display grossly elongated mitochondria and tubular peroxisomes, consistent with a critical role for Mff in recruitment of Drp1, both to mitochondrial and peroxisomal membranes (Gandre-Babbe et al., 2008, Losón et al., 2013, Otera et al., 2010). Down-regulation of Mff inhibits mitochondrial Drp1 recruitment, whereas Mff over-expression induces excessive mitochondrial fission (Otera et al., 2010). While Mff and MiD51 have been shown to colocalise with Drp1 in MEF cells, suggestive of a functional complex (Osellame et al., 2016), *in vitro* studies have shown that incorporation of Mff into liposomes stimulates Drp1 GTPase activity, but incorporation of MiD51 inhibits it (Osellame et al., 2016, Macdonald et al., 2016). In HeLa cells, silencing of Mff with siRNA can partially rescue fusion defects caused by dominant negative mutants. Mff silencing also partially attenuates fragmentation upon mitochondrial uncoupling by CCCP treatment, and inhibits apoptosis in a similar way to Drp1-silencing (Gandre-Babbe et al., 2008). Mff, as the master regulator of Drp1 recruitment, has a crucial role in maintenance of the mitochondrial network. Its activity must be tightly regulated, as excessive or insufficient mitochondrial fission can have deleterious effects on mitochondrial function and cellular viability.

1.1.6.3 Final scission by Dyn2

Until recently, it was thought that Drp1 alone drove membrane constriction to full scission. However, a study by Lee *et al* revealed that siRNA-mediated silencing of Dyn2 created a highly elongated mitochondrial network phenotype, similar to that observed when Drp1 is silenced and indicative of a critical role for Dyn2 in fission (Lee et al., 2016). This study was consistent with a previous report that Drp1 could readily tubulate, but not sever, liposomes *in vitro* (Yoon et al., 2001).

Dyn2 (Dnm2) is a classical, PH domain-containing Dynamin, and directly binds to the MOM. Dyn2 is only recruited to restriction sites after Drp1, suggesting that it requires the narrower membrane diameter provided by Drp1-ring constriction to bind (Figure 1.2, 4). Unlike Drp1, which is found at ~80% of mitochondrial constriction sites, Dyn2 is recruited only transiently, and disassembles immediately after membrane scission (Figure 1.2, 5). A population of Drp1 remains on each of the daughter mitochondria after division,

suggesting that Dyn2-dependent scission occurs in the centre of the constriction site (Legesse-Miller et al., 2003, Lackner et al., 2009, Lee et al., 2016).

1.1.7 Mitochondrial dynamics: physiology and pathophysiology

Functional mitochondrial morphology is important in almost all cell types, with morphological defects having roles in many human diseases (Hom and Sheu, 2009). These include neurodegeneration, diabetes mellitus, liver diseases, cancers and myopathies (Wallace, 1999). Perturbations to mitochondrial fission can be lethal; a child born with a dominant negative mutation in Drp1 survived just 37 days (Waterham et al., 2007). Equally, disruptions to mitochondrial fusion can be lethal. Mutations of Mfn1 or Mfn2 are embryonic lethal in mice, while Mfn2 mutation in humans causes peripheral neuropathy-Charcot–Marie–Tooth subtype 2A (Pareyson, 2004, Züchner et al., 2004, Chen et al., 2003). Maintenance of functional mitochondrial networks is particularly critical in cell types with high energy demands, including neurons, skeletal muscle and heart.

1.1.7.1 Cardiac mitochondrial dynamics

Cardiac myocytes, in particular ventricular cells, are hugely enriched with mitochondria, which have been shown in electron micrographs to be compacted and highly ordered between contractile filaments. This begs the question: do adult ventricular mitochondria undergo the same continuous fusion, fission and movement as mitochondria from other cell types? This question has yet to be definitively answered (Hom and Sheu, 2009). Ventricular mitochondria are anchored by components of the myocyte cytoskeleton and surrounded by contractile proteins, which could suggest that there is no need or capacity for them to have similar dynamics to mitochondria in other cell types. However, mitochondria are limited by their lifespan, and their biogenesis, quality control and genomic integrity are all dependent on their ability to undergo fission and fusion, and to be motile (Twig et al., 2008b, Diaz and Moraes, 2008).

In support of fundamental requirements of mitochondrial dynamics in the heart, several studies have confirmed that all major fission/fusion proteins are expressed in the adult heart. Indeed, one study used Western blotting to screen various adult tissues for fusion DRP Mfn1 and Mfn2 expression and concluded that Mfn1 protein was expressed in greatest abundance in heart tissue. The same study also found mRNA encoding Mfn2 to be highly abundant in heart and muscle compared to other tissues (Santel et al., 2003). These data are supported by further studies confirming that Mfn1 and Mfn2 can be

detected by RT-PCR in rat and mouse heart tissue (Rojo et al., 2002, Bach et al., 2003). Similarly, high expression of mRNA encoding fission-mediating Drp1 has been detected by Northern blotting of adult human heart tissue (Imoto et al., 1998).

Presence of fission/fusion proteins in the adult heart does not confirm a functional role for them in the regulation of cardiac mitochondrial morphology, *per se*. Limitations in the spatial resolution of confocal microscopy make it difficult to distinguish subtle morphological differences between mitochondria that are so tightly packed as those in cardiac cells (Faulkner et al., 2014). However, electron micrographs dating back over 30 years demonstrate that perinuclear mitochondria differ in their morphology and distribution from those located between myofibrils or beneath the sarcolemma of ventricular myocytes. For example, perinuclear mitochondria are distributed in a more irregular manner and are more variable in shape and size, while interfibrillar mitochondria are generally elongated, similar in length to a sarcomere, and aligned in longitudinal rows. Some intrafibrillar mitochondria exhibit differing degrees of 'wrapping' around myofilaments, presumably allowing greater efficiency of ATP delivery to regions of high demand (Shimada et al., 1984, Palmer et al., 1985). The differences in distribution and morphology of mitochondria in different ventricular compartments suggest spatial and/or temporal heterogeneity in adult ventricular mitochondrial dynamics, but are indicative that at least some cardiac mitochondria regularly undergo fission, fusion and motility similar to the dynamics of other cell types (Hom and Sheu, 2009).

Due to their close proximity to the sarcoplasmic reticulum, many cardiac mitochondria are situated inside microdomains of high Ca^{2+} concentration and flux during the excitation-contraction coupling (EC-coupling) required to maintain the heartbeat (Sharma et al., 2000). This charges ventricular mitochondria with regulation of localised Ca^{2+} homeostasis and links energy metabolism to EC-coupling. Given the changeability of heart rate, mitochondrial generation of ATP must be effectively regulated to quickly adapt to changes in energy supply and demand. It has long been known that Ca^{2+} is used by mitochondria as a key regulator of metabolic activity; during cycles of EC, mitochondria sequester small concentrations of Ca^{2+} to activate ATP-generating enzymes and, in doing so, ensure bioenergetic homeostasis in the beating heart (McCormack and Denton, 1989, Matsuoka et al., 2004).

More recent studies have identified a role for Ca^{2+} in regulation of mitochondrial dynamics (Hom Jennifer et al., 2007). Breckenridge *et al* showed that caspase-mediated cleavage of ER protein BAP31 stimulates Ca^{2+}-dependent mitochondrial fission and

enhances release of cytochrome *c* during apoptosis (Breckenridge et al., 2003). Another study linked Ca^{2+} to kinesin-mediated mitochondrial motility, asserting that kinesin-1 is switched to an inactive state by Ca^{2+}-induced binding to MOM protein Miro, halting mitochondrial movement (Wang and Schwarz, 2009). A new role for Mfn2 has also been identified, in which it regulates mitochondrial Ca^{2+}-uptake by tethering the mitochondrial membrane to the ER (de Brito and Scorrano, 2008).

In instances of cardiac disease, including end-stage dilated cardiomyopathy, myocardial hibernation, and ventricular-associated congenital heart diseases, mitochondria have been shown to be abnormally organised and unusually small (Kalra and Zoghbi, 2002, Scholz et al., 1994, Schaper et al., 1991). Additionally, large, defective mitochondria have been shown to accumulate in senescent cardiac myocytes, in an age-correlated manner (Terman et al., 2006).

On reflection of the evidence discussed here, several aspects of adult ventricular mitochondrial dynamics can be proposed:

- The machinery required for fission and fusion appear to be expressed, and the requirement for mitochondrial regeneration, quality control and genomic stability indicate a demand for normal fission and fusion.
- Mitochondrial motility is probably minimal and may be limited to certain subcellular populations.
- Microdomain Ca^{2+} concentration and mitochondrial tethering to the sarcoplasmic reticulum may be critical to regulation of mitochondrial dynamics.

1.2 Myocardial ischaemia/reperfusion injury

The heart is an autonomous muscular organ and the epicentre of the circulatory system and, together with the blood and blood vessels, makes up the cardiovascular system. The proper functioning of all other organs is dependent on the heart, which pumps blood around the body, delivering oxygen and nutrients and removing carbon dioxide.

1.2.1 Structure and function of the heart

The heart is made up of 4 chambers: the left and right atria and the left and right ventricles. The right atrium receives deoxygenated blood via the *venae cavae*, which moves through the tricuspid valve into the right ventricle. The right ventricle feeds into

the left and right pulmonary arteries, which carry blood to the lungs to be re-oxygenated. The left atrium receives oxygenated blood back from the lungs via the pulmonary veins, which then passes through the mitral valve to the left ventricle. Oxygenated blood is pumped out to the rest of the body via the aorta.

The wall of the left ventricle is much thicker than that of the right ventricle, owing to the pressure required to pump blood around the entire body. The heart walls comprise 3 layers: the inner endocardium, myocardium, and the outer epicardium. The myocardium is the cardiac muscle tissue - involuntary striated muscle tissue within a complex collagen framework. Two types of cell make up the myocardium: highly contractile muscle cells (cardiomyocytes), which make up 99% of cells in the heart, and smaller pacemaker cells, which have limited contractibility. The pacemaker cells function in a similar way to neurons, firing synchronised action potentials to stimulate contraction of the entire heart (Lindskog et al., 2015).

1.2.2 Myocardial cells

Cardiomyocytes are relatively large cells, with an average volume 150x greater than that of a red blood cell. Healthy cardiomyocytes are cylindrical in shape, with a length of ~100µm and a 10-25µm diameter (Li and Liu, 2018). Their functional contractile unit, the sarcomere, comprises thick filaments of myosin which glide along thin actin filaments (Figure 1.3, green), arranged in parallel to give a striatal appearance (Bray et al., 2008, Mansour et al., 2004). The plasma membrane, or sarcolemma, periodically invaginates perpendicular to the long axis of the cardiomyocyte, forming an extensive tubular network referred to as the t-tubule system (Figure 1.3, red) (Göktepe et al., 2010). There are approximately 50 sarcomeres in a myofibril, and 50-100 myofibrils per cardiomyocyte (Sanger et al., 2000). Due to the incredibly high ATP demands of normal cardiac contractile function, cardiomyocytes are enriched with mitochondria, which account for around 35% of their total volume, as assessed by electron microscopy (Hom and Sheu, 2009).

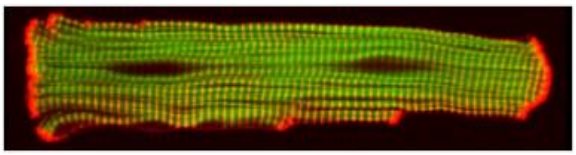

Figure 1.3 **Adult ventricular cardiomyocyte.** Transmission electron microscope image of human ventricular cardiomyocyte (stem-cell derived). Sarcomeric actin is labelled in green; t-tubule system is labelled in red. Image taken from *Göktepe, S., O. J. Abilez, K. K. Parker and E. Kuhl (2010). A multiscale model for eccentric and concentric cardiac growth through sarcomerogenesis. Journal of Theoretical Biology 265(3): 433-442.* (Göktepe et al., 2010).

1.2.3 Cardiac disease and dysfunction

Cardiovascular disease (CVD) refers to all diseases of the heart and circulatory system. This includes everything from heritable myopathies to developed conditions like coronary heart disease, atrial fibrillation, heart failure, and stroke. In all, CVD accounts for a quarter of all UK deaths, or one death every three minutes. It is estimated that 7 million people are living with CVD in the UK, with numbers set to increase with the aging population (BHF analysis of latest UK mortality statistics: ONS/NRS/NISRA (2016 data)).

1.2.3.1 Coronary heart disease

The most common form of CVD is coronary heart disease, also known as ischaemic heart disease (IHD). This occurs when atheroma (fatty deposits) builds up in the coronary arteries, narrowing them. Myocardial infarction (heart attack) can occur as a result of these blockages. Globally, IHD is the leading cause of death, primarily by induction of heart attacks. In the UK, one person is admitted to hospital because of a heart attack every three minutes (BHF analysis of latest UK mortality statistics: ONS/NRS/NISRA (2016 data)).

Ischaemia occurs when blood flow to the tissue is disrupted/blocked, resulting in cellular oxygen-deprivation (hypoxia) and glucose-deprivation. Hypoxia triggers a switch to anaerobic glycolysis, which rapidly acidifies the intracellular milieu (Marban et al., 1987). Within just a few minutes, the lack of oxygen severely depletes cellular ATP and causes contractile arrest (Sanada et al., 2011). After 15-30 minutes of ischaemia, cellular bulging and rupture of intracellular microstructures cause irreversible structural changes to the myocardium (Allen and Orchard, 1987).

1.2.4 Myocardial Ischaemia/Reperfusion injury is largely mitochondrial

Acute occlusion of blood flow to a dependent region of myocardial tissue causes localised ischaemia and defines the 'at risk area' for myocardial infarction should the occlusion be sustained. Cardiomyocyte death begins after around 20 minutes of ischaemia, spreading from the sub-endocardium toward the epicardium (Reimer et al., 1977). During an incident of tissue ischaemia caused by interrupted blood flow, common clinical practice is to restore the flow of blood as quickly as possible. Paradoxically, with the tissue already primed for damage, this can induce further damage through a phenomenon known as ischaemia/reperfusion (I/R) injury (Hausenloy and Yellon, 2013, Cadenas et al., 2010).

1.2.4.1 Pathophysiology of cardiac ischaemic injury

During ischaemia, abrupt biochemical and metabolic changes are brought about by the sudden restriction of oxygen and nutrients. Lack of oxygen terminates oxidative phosphorylation, which in turn causes depolarisation of the MIM and depletion of ATP, ultimately inhibiting contractile function. At the same time, attempts to maintain mitochondrial membrane potential by active pumping of protons (H^+) across the membrane require ATP hydrolysis, further depleting the limited ATP supply. Oxygen-deprivation triggers a switch in cellular metabolism to anaerobic glycolysis, causing acidification of the cell as H^+ accumulate and inhibiting opening of the mitochondrial Permeability Transition Pore (mPTP). The mPTP is a non-selective pore in the MIM which, when open, allows free passage of all molecules under 1.5kDa (Griffiths and Halestrap, 1995, Halestrap, 2010, Pasdois et al., 2013). This activates the Na^+-H^+ ion exchanger, which works to extrude intracellular H^+ coupled to uptake of Na^+. Na^+-overload is further exacerbated by the halted function of the ATP-dependent $3Na^+$-$2K^+$ transporter, which reverse-activates the $2Na^+$-Ca^{2+} ion exchanger, resulting in Ca^{2+}-overload (Figure 1.4, left) (Avkiran and Marber, 2002).

1.2.4.2 Pathophysiology of cardiac reperfusion injury

Clinically, rapid reperfusion of ischaemic tissue is required for several reasons: to salvage viable tissue, limit infarct size, preserve left ventricular systolic function, and prevent heart failure. Unfortunately, reperfusion can contribute to further myocardial damage and cell death (Braunwald and Kloner, 1985, Piper et al., 1998, Yellon and Hausenloy, 2007). There are four recognised forms of myocardial I/R injury: reperfusion-induced arrhythmias, myocardial stunning, microvascular obstruction, and lethal myocardial reperfusion injury. Of these, only the first two are reversible.

Lethal myocardial reperfusion injury refers to reperfusion-dependent death of cells that were still viable immediately following ischaemia and could be responsible for up to 50% of the final infarct size. Major contributing factors to lethal reperfusion injury are oxidative stress, Ca^{2+}-overload, opening of the mPTP and hyper-contracture (Yellon and Hausenloy, 2007).

Oxidative stress is brought about by several mechanisms but is particularly potent during the first few minutes of reperfusion, when a burst of reactive oxygen species (ROS) is produced by the sudden re-introduction of oxygen (Hearse et al., 1973, Zweier et al., 1987, Ambrosio et al., 1993). Intracellular overload of Ca^{2+} starts during ischaemia, but

disruption of the plasma membrane and mitochondrial re-energisation can exacerbate the problem at reperfusion. Recovery of the MIM potential upon mitochondrial re-energisation drives mitochondrial uptake of Ca^{2+} and induces opening of the mPTP. Once open, the mPTP allows equilibration of all small solutes across the MIM, leaving the mitochondrial matrix with high concentrations of proteins. This exerts osmotic pressure, drawing water into the matrix and causing a large increase in its volume, resulting in immense swelling of the mitochondrion (Halestrap, 1999, Crompton, 1999). The sudden restoration of physiological intracellular pH upon reperfusion, a result of lactate washout, also contributes to mPTP opening, as well as cardiomyocyte hyper-contracture (Figure 1.4, right) (Lemasters et al., 1996, Qian et al., 1997, Cohen et al., 2007).

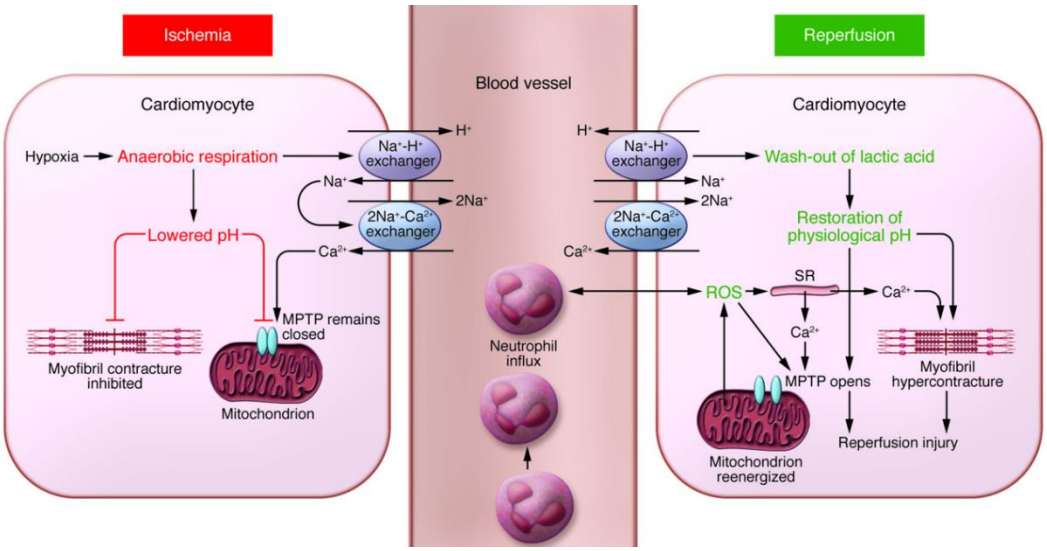

Figure 1.4 **Schematic of main proponents of acute myocardial I/R Injury**. Ischaemic pathways are shown in red, reperfusion in green, discussed above. Not discussed in the text is the inflammatory response, as it remains unclear whether this contributes to the pathogenesis of lethal myocardial reperfusion injury, or whether it is a reaction to the acute myocardial injury. Figure taken from *Hausenloy, D. J. and D. M. Yellon (2013). "Myocardial ischemia-reperfusion injury: a neglected therapeutic target." The Journal of Clinical Investigation 123(1): 92-100* (Hausenloy and Yellon, 2013).

1.3 Protein fate is determined by ubiquitin

Post-translational modifications (PTMs) refer to a large number of protein modifications that can be employed by the cell to alter protein function, stability, sub-cellular localisation, activity and interactions. There exists a wide range of PTMs, ranging from enzymatic cleavage of peptide bonds (as in propeptide processing), to addition of

small reactive groups such as phosphate, to covalent attachment of small modifier proteins like SUMO and ubiquitin.

1.3.1 Discovery of ubiquitin

Ubiquitination was the first discovered modification of a protein by covalent attachment of another protein (Ciechanover et al., 1980). Ciechanover *et al* had set out to find an explanation for the energy-requirement of mammalian intracellular proteolysis, which had first been shown by isotopic labelling of cellular proteins almost 30 years prior to this study; proteolysis of a peptide bond is an exergonic reaction, so thermodynamically the need for energy made no sense (Simpson, 1953). It was not until the late 1970s that hypotheses were set forward that the energy required was not for proteolysis *per se*, but rather some form of energy-dependent proteolytic regulation (Schimke, 1976). By 1980, Ciechanover *et al* had recognised that ubiquitin was a critical component of ATP-dependent proteolytic degradation, and made accurate predictions as to the exact mechanism, which were more conclusively demonstrated in the subsequent years (Hershko et al., 1980).

In the four decades since its discovery, ubiquitin and the ubiquitin-like family of modifiers have been implicated in virtually every cellular process, including regulating proteolysis, nuclear localisation, chromatin structure, genomic integrity, protein quality control and intracellular signalling (Schwartz and Hochstrasser, 2003, Wilkinson, 2005).

1.3.2 Evolutionary and subcellular distribution

As one of the most highly conserved eukaryotic polypeptides, ubiquitin was probably present in the last common ancestor of eukaryotes (Koonin, 2010). The "ubiquitin-fold" superfamily of proteins, to which ubiquitin belongs based on its structure, is an ancient group of proteins of widespread phylogeny (Iyer et al., 2006, Burroughs et al., 2012). Prokaryotic genomes do not encode ubiquitin, but do encode two, structurally unrelated, small modifying proteins that are conjugated to target proteins via isopeptide bonds (Maupin-Furlow, 2014). Actinobacteria synthesise prokaryotic ubiquitin-like protein (Pup), an intrinsically disordered polypeptide which is covalently attached to degradation targets via a distinct enzymatic mechanism called pupylation (Barandun et al., 2012, Burns and Darwin, 2010). Small archaeal modifier proteins (SAMPs), synthesised in archaea, are also ubiquitin-fold proteins, covalently attached to target proteins via a mechanism reminiscent of simplified ubiquitination in its requirement of an E1 activating enzyme, but not an E2 conjugating enzyme or E3 ligase (Darwin and Hofmann, 2010). The presence of ubiquitin-

like proteins and rudimentary conjugation systems in prokaryotes suggests that ubiquitination was not a newly acquired function of eukaryotes, but rather an amalgamation of several modification systems that had already undergone extensive diversification in prokaryotes (Koonin, 2010, Hochstrasser, 2009).

Ubiquitin is encoded by four genes: UbA52 and RPS27A encode monomeric ubiquitin moieties which remain fused to ribosomal subunits, whereas UbB and UbC encode polymeric ubiquitin precursors, from which free ubiquitin is cleaved by de-ubiquitinating peptidases (DUBs). UbC is believed to produce the majority of ubiquitin, with knock out MEFs having 40% reduced ubiquitin, despite compensatory upregulation of UbB mRNA (Heride et al., 2014). In HEK293 cells, ubiquitin makes up around 0.4% of total protein (w/w), of which ~23% is free ubiquitin, ~65% mono-ubiquitinated substrates and ~11% poly-ubiquitinated substrates (Kaiser et al., 2011).

1.3.3 Ubiquitin structure

Ubiquitin is a compact 76-amino acid polypeptide of around 8.5kDa (Komander, 2009). Almost 90% of its polypeptide chain contributes to its compact secondary structure via hydrogen-bonding. The main structural features are 3.5 α-helical turns and a 5-stranded mixed β-sheet. Between the α-helix and β-sheet is a hydrophobic core (Vijay-Kumar et al., 1987). Ubiquitin is conjugated to target proteins via lysine residues; an isopeptide bond is formed between the negatively-charged carboxyl-group of the ubiquitin peptide C-terminal glycine residue and the positively-charged amino-group on the target protein lysine residue (Johnson, 2004). Target proteins can be either mono-ubiquitinated or poly-ubiquitinated, the latter comprising ubiquitin chains (Hershko and Ciechanover, 1998). Ubiquitin itself has 7 lysine residues, all on different surfaces of the molecule and all of which can be ubiquitinated, resulting in differently branched ubiquitin chains, which have been linked to different molecular functions (Figure 1.5) (Komander, 2009).

1.3.4 Ubiquitin-like Modifiers (UBLs)

Ubiquitin-like modifiers (UBLs) are a family of small proteins, similar in structure to ubiquitin. With myriad functions, their conjugation to substrates can drastically modify target protein functions, and vastly enhances the complexity of the eukaryotic proteome. So far, around 16 ubiquitin-like modifiers have been identified in humans, including NEDD8, ISG-15, FAT10 and SUMO. Like ubiquitin, covalent attachment of these UBLs to substrates all rely on a C-terminal di-glycine motif in the UBL being conjugated to the ϵ-amino group of a lysine residue in the substrate protein, usually within a consensus motif.

1.3.4.1 NEDD8

NEDD8 (neural precursor cell expressed developmentally downregulated protein 8) is a predominantly nuclear protein, broadly expressed in most adult tissues (Kamitani et al., 1997a). Of all the known UBLs, it shares the greatest sequence identity to ubiquitin – 59% for the human orthologues (Whitby et al., 1998). Despite this, ubiquitin and NEDD8 are functionally non-interchangeable. The best understood role of NEDD8 is its neddylation of cullin RING Ligases (CRLs), which are the most abundant class of RING E3 ubiquitin ligases. Here, NEDD8 conjugation acts as a molecular switch, activating ubiquitin-transfer activity of the cullin RING ligase by altering its conformation (Duda et al., 2008).

1.3.4.2 ISG15

ISG15 (interferon stimulated gene 15) is a 15kDa protein, structurally resembling two tandem orientation ubiquitin folds (Daczkowski et al., 2017). Although constitutively expressed at low levels, transcription of ISG15 and its regulatory enzymes is upregulated by both interferon (IFN)-α and –β, ischaemic stress, DNA damage and aging, by binding of IFN-regulatory factors to IFN-stimulated response element-containing promoters (Sadler and Williams, 2008).

1.3.4.3 FAT10

Like ISG15, FAT10 (Human Leukocyte Antigen-F adjacent Transcript 10) also consists of two tandem array ubiquitin-like domains, of 29% and 36% homology to ubiquitin (Fan et al., 1996). Unlike ubiquitin, however, expression of FAT10 is generally limited to tissues of the immune system (Lukasiak et al., 2008). It is only upon IFN-γ and TNF-α stimulation that FAT10 transcription and translation is induced (Raasi et al., 1999). Unlike ubiquitin and other UBLs, the di-glycine motif of FAT10 is readily available for activation and conjugation, without the need for C-terminal pre-processing (Chiu et al., 2007). Like ubiquitination, conjugation of FAT10 to substrates also targets them for proteasomal degradation (Hipp et al., 2005).

1.3.4.4 SUMO

Small ubiquitin like modifier (SUMO, or SMT3 in *Saccharomyces cerevisiae*) refers to an ~11kDa protein with limited yet significant sequence homology to ubiquitin. Unlike ubiquitination, modification of substrates by SUMO (SUMOylation) does not generally result in their proteasomal degradation, and so far, has been shown to play roles in cell cycle regulation, chromatin remodelling, RNA processing, DNA damage repair,

transcriptional regulation, protein quality control and response to various cellular insults, including oxidative stress, proteasomal inhibition, heat shock, and viral infections. Given the immense range of functions, it is unsurprising that dysfunction of SUMO and its regulatory enzymes have been associated with various pathologies, including cancer (Kessler et al., 2012), neurodegenerative disorders (Cho et al., 2015, Krumova et al., 2011) and cardiovascular diseases (Kho et al., 2011, Wang et al., 2011b, Zhang and Sarge, 2008).

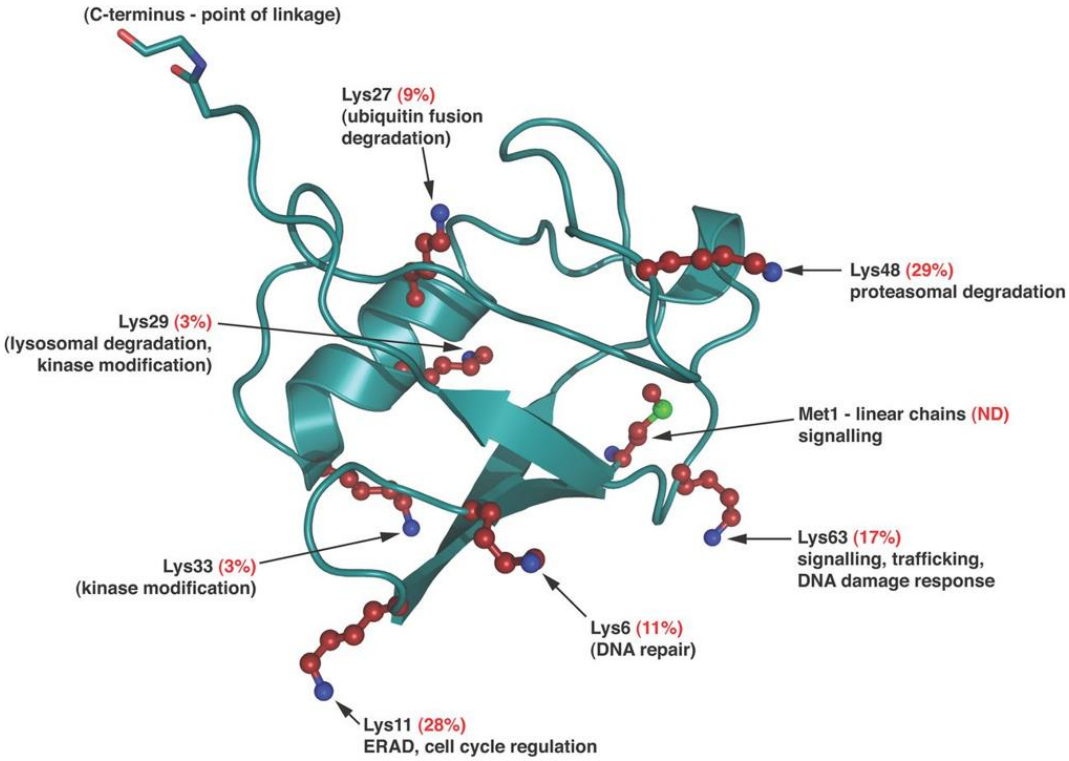

Figure 1.5 **Structure of Ubiquitin, with Lysine residues indicated.** The structure of ubiquitin (PDB code: 1UBQ) demonstrates that all seven lysine residues (red) reside on different surfaces of the molecule. The C-terminal Gly75-Gly76 motif involved in isopeptide bond formation is indicated. Relative abundance of chain linkages (in *S. cerevisiae*) and their tentative roles are indicated. Figure taken from *Komander, D. (2009). "The emerging complexity of protein ubiquitination."* Biochemical Society Transactions ***37****(5): 937* (Komander, 2009).

1.3.5 The ubiquitin cycle

Ubiquitination is a three-step cascade resulting in the covalent attachment of mature ubiquitin to a lysine residue of the target protein, in which the carboxyl group of the C-terminal glycine (Gly76) in ubiquitin forms a bond with the ε-amino group of a lysine residue in the target protein (Pickart, 2001). The sequential actions of an E1 activating enzyme, E2 conjugating enzyme and E3 ligase are required to complete the reaction. The E1 forms a thiol ester with the carboxyl group of ubiquitin Gly76, priming the ubiquitin C-

terminus for nucleophilic attack. The E2 then transiently carries the activated ubiquitin thiol ester on a cysteine residue, before the E3 transfers activated ubiquitin from the E2 to a lysine residue in the target substrate (Hershko et al., 1983). The same mechanism is utilised by all known ubiquitination reactions, regardless of the fate of the ubiquitinated substrate (Figure 1.6) (Pickart, 2001).

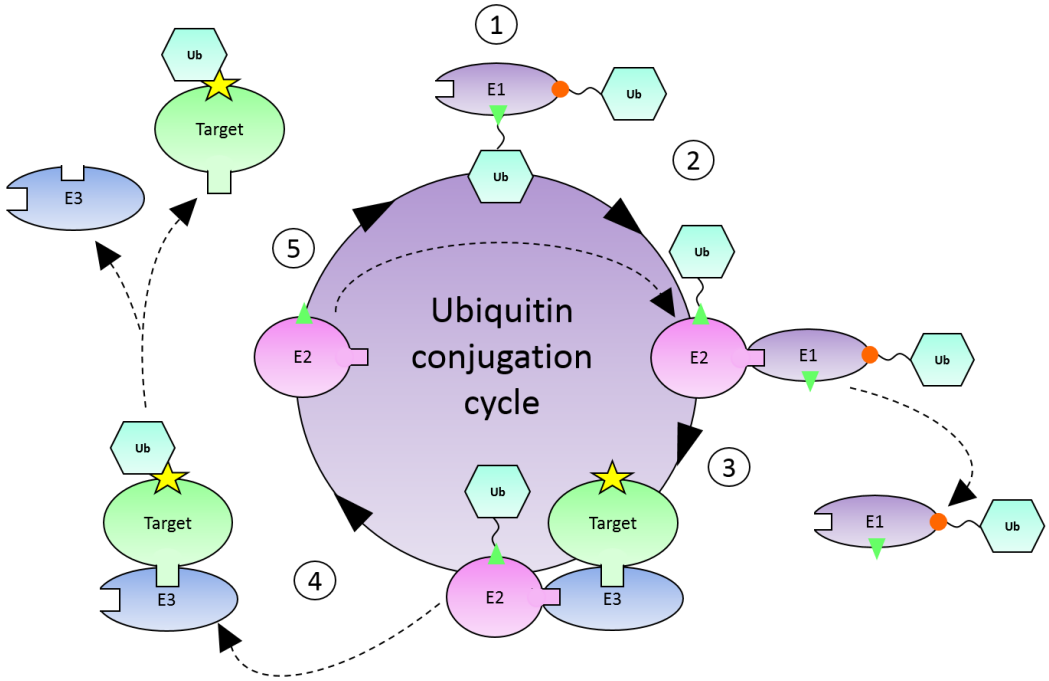

Figure 1.6 **Schematic representation of ubiquitination**. (1) An E1 ubiquitin-activating enzyme is loaded with two ubiquitin molecules: one at its adenylation domain (orange) and the other linked to a cysteine at its active site (green). (2) The activated ubiquitin is transferred to the cysteine in the E2 conjugating enzyme active site. (E3) The E2 dissociates from the E1 before it can engage with a cognate ubiquitin ligase (E3), which recruits substrates. (4) Once ubiquitin has been transferred to the substrate lysine (star), the E2 dissociates from the E3, and can be recharged with ubiquitin by E1 (5). ~ represents a thioester bond.

1.3.5.1 E1 activating enzymes

The human genome encodes two E1 enzymes, UBA1 and UBA6, which are around 40% identical (Jin et al., 2007). E1s serve to activate ubiquitin by C-terminal adenylation and thiol transfer, and subsequently charge cognate E2 enzymes (Schulman and Harper, 2009). The activation of ubiquitin is a two-step process. First, the E1 binds Mg-ATP and ubiquitin, and catalyses C-terminal adenylation of ubiquitin, creating a high-energy thioester bond. Next, the E1 enzyme catalytic cysteine residue nucleophilically attacks the ubiquitin-adenylate, forming the activated ubiquitin-E1 complex, bonded between the C-terminus of ubiquitin and the cysteine sulfhydryl group of the E1 (Schulman and Harper, 2009, Haas and Rose, 1982). The E1 subsequently catalyses adenylation of a further ubiquitin moiety, resulting in the enzyme being asymmetrically loaded with two ubiquitin

molecules; the first covalently bonded via a thioester bond to the catalytic cysteine, and the second non-covalently associated with the adenylation active site (Haas et al., 1982).

The two steps of E1-dependent activation are independently reversible; advance of the ubiquitination cascade is driven by release of PPi during adenylation and AMP during nucleophilic attack (Haas and Bright, 1988, Haas et al., 1988). The reason for E1 double-loading of ubiquitin is not yet fully understood. *In vitro* work has demonstrated that the singly-loaded E1-ubiquitin complex bound by a thioester bond is capable of transferring ubiquitin to an E2 enzyme, although the authors showed that the transfer is accelerated by Mg-ATP or ubiquitin-adenylate (Pickart et al., 1994). This suggests that the cascade is made more energetically or conformationally favourable by coupling of the second adenylation to ubiquitin transfer, or that the double-loading somehow prevents the E1 from becoming stuck in an unfavourable conformation (Schulman and Harper, 2009).

1.3.5.2 E2 conjugating enzymes

At least 38 E2 ubiquitin-conjugating enzymes are encoded by the human genome (Deshaies and Joazeiro, 2009). Due to their ability to recruit specific substrates, it was previously assumed that E3 ligases were the primary 'decision makers' of the ubiquitin cycle, while E2s had auxiliary 'carrier' roles. However, more recent studies have indicated that E2s play an active part in determining the length/structure of ubiquitin chains, thereby having an important role in determination of substrate fate (Ye and Rape, 2009). Active E2s contain a highly conserved ubiquitin-conjugating domain (UBC) at their core, which includes the catalytic cysteine residue and is the site of E1 interaction. The conserved UBC comprises four α-helices and a four-stranded anti-parallel β-sheet, with the catalytic cysteine sitting in a shallow groove (Lin et al., 2002, Eddins et al., 2006). E2s will generally only bind their cognate E1s with any significant affinity if the E1 is charged with ubiquitin (Schulman and Harper, 2009); ubiquitin binding to the E1 induces a conformational change that exposes E2-binding sites, facilitating formation of the E1-E2 complex and allowing transfer of ubiquitin (Huang et al., 2007, Lee and Schindelin, 2008).

To generate ubiquitin chains, the E2-E3 complex must distinguish between chain initiation and elongation, or ubiquitin conjugation to a substrate protein lysine or a ubiquitin lysine. This 'decision' is often made by the E2, and a handful of E2s dedicated to ubiquitin-conjugation in the context of initiation or elongation have recently been described (Ye and Rape, 2009). For example, the yeast anaphase-promoting complex uses E2 Ubc4 to modify substrate lysine residues, but Ubc1 to extend ubiquitin chains through lysine 48 (Rodrigo-Brenni and Morgan, 2007). In humans, several E2s, such as UBE2W and

UBE2E2, act in ubiquitin chain initiation with BARD1 (BRCA1-associated RING domain 1), while the E2 heterodimer UBE2N–UBE2V1 and UBE2K specifically promote ubiquitin chain elongation in the same system (Christensen et al., 2007).

1.3.5.3 E3 ligases

E3 ligases are engaged by ubiquitin-charged E2s to catalyse substrate ubiquitination (Ye and Rape, 2009). In humans, 600-1000 E3s are encoded, several of which can interact with each E2 (Deshaies and Joazeiro, 2009). So far, all characterised E2s recognise E3s via their N-terminal loops and α-helix, with subtle variations in this motif contributing to their E3-specificty (Zheng et al., 2000). The E2-E3 interaction is generally weak (micromolar dissociation constants) (Yin et al., 2009). Interaction with the E3 substantially increases the E2 active site rate of ubiquitin discharge; it is thought that the E3 induces an E2 conformational change, positioning an asparagine residue near the active site which stabilises an oxyanion intermediate of the transition state (Wu et al., 2003, Ozkan et al., 2005, Petroski and Deshaies, 2005b).

Ubiquitin E3 ligases generally fall into one of two groups, although variation and crossover do also occur (Figure 1.7). The two predominant types of E3 ligase are the Really Interesting New Gene (RING) ligases and the Homologous to the E6AP Carboxyl Terminus (HECT) ligases, described briefly below.

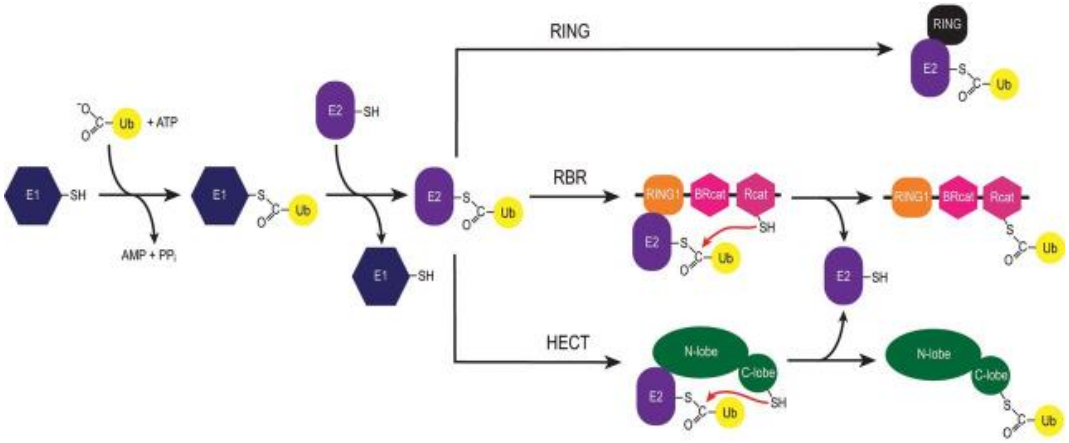

Figure 1.7 **Ubiquitination by different E3 ubiquitin ligases**. RING E3 ligases (top): E2-ubiquitin complex engages with E3 RING domain to optimally position ubiquitin for transfer to a substrate. HECT E3 ligases (bottom): engage E2-ubiquitin complex via their N-terminus and form a thioester bond between the C-terminus of ubiquitin and the conserved catalytic cysteine residue in the HECT E3. This HECT-ubiquitin intermediate is then poised for transfer of ubiquitin to a substrate. RBR E3 ligases (middle): use a 'RING–HECT' hybrid mechanism. RING1 engages with the E2-ubiquitin complex in a similar manner to RING E3s, and the Rcat (RING required for catalysis) acts in a similar fashion to the C-terminus of HECT E3s, forming a thioester bond between the C-terminus of ubiquitin and the catalytic cysteine of the Rcat domain of RBR E3. Figure taken from *Spratt D , E., H. Walden and S. Shaw G (2014). "RBR E3 ubiquitin ligases: new structures, new insights, new questions." Biochem J* ***458****(Pt 3): 421-437* (Spratt D et al., 2014).

1.3.5.3.1 HECT E3 ligases

The HECT E3 ligases are characterised by a C-terminal HECT domain, containing the conserved catalytic cysteine residue, and N-terminal extensions of varying lengths/architectures, that determine the E2-binding and substrate specificity of the E3 (Scheffner and Kumar, 2014, Kee and Huibregtse, 2007). These ligases directly engage in substrate ubiquitination by formation of a catalytic thioester intermediate between their catalytic cysteine and the C-terminal ubiquitin glycine (Maspero et al., 2011).

1.3.5.3.2 RING E3 ligases

The RING E3 ligases do not directly catalyse substrate ubiquitination, but rather act as scaffolds, orienting the substrate protein and E2-ubiquitin thioester to facilitate efficient ubiquitin transfer (Deshaies and Joazeiro, 2009, Metzger et al., 2014). They do this by co-ordinating two Zn^{2+} ions via a cross-brace formation of eight cysteine and histidine residues, which folds the E3 into a conformation that correctly positions conserved residues required for interaction with their cognate E2-ubiquitin, thus promoting ubiquitin transfer to the substrate protein (Plechanovova et al., 2012, Zheng et al., 2000, Pruneda et al., 2012).

1.3.5.3.3 SUMO-targeted ubiquitin ligases

A novel and relatively recently discovered class of ubiquitin E3 is the SUMO-targeted Ubiquitin Ligase (STUbL or E3-S). Over the last few years, a handful of STUbLs have been identified, either by their demonstrable binding to SUMO, possession of a SUMO-interacting motif (SIM), or by sequence similarity to other STUbLs (Uzunova et al., 2007, Sriramachandran and Dohmen, 2014). Presence of a SIM facilitates STUbL preference for SUMOylated substrates, with most of the currently identified STUbLs having multiple SIMs, mediating cooperative binding to several SUMO moieties and indicative of a preference for substrates with poly-SUMO chains (Weisshaar Stefan et al., 2008, Tatham et al., 2008). RNF4, the most extensively studied STUbL to date, contains at least three clear SIMs, which engage SUMO-1 and SUMO-2, and confer a preference for substrates with chains of at least three SUMO moieties (Tatham et al., 2008, Lallemand-Breitenbach et al., 2008, Sun et al., 2007). STUbLs often target their SUMOylated substrates for degradation via the ubiquitin-proteasome system (UPS), but can also contribute to a novel composite binding motif, that

can be recognised by tandem SIMs and ubiquitin-interacting motifs (UIMs) (Figure 1.8) (Sriramachandran and Dohmen, 2014).

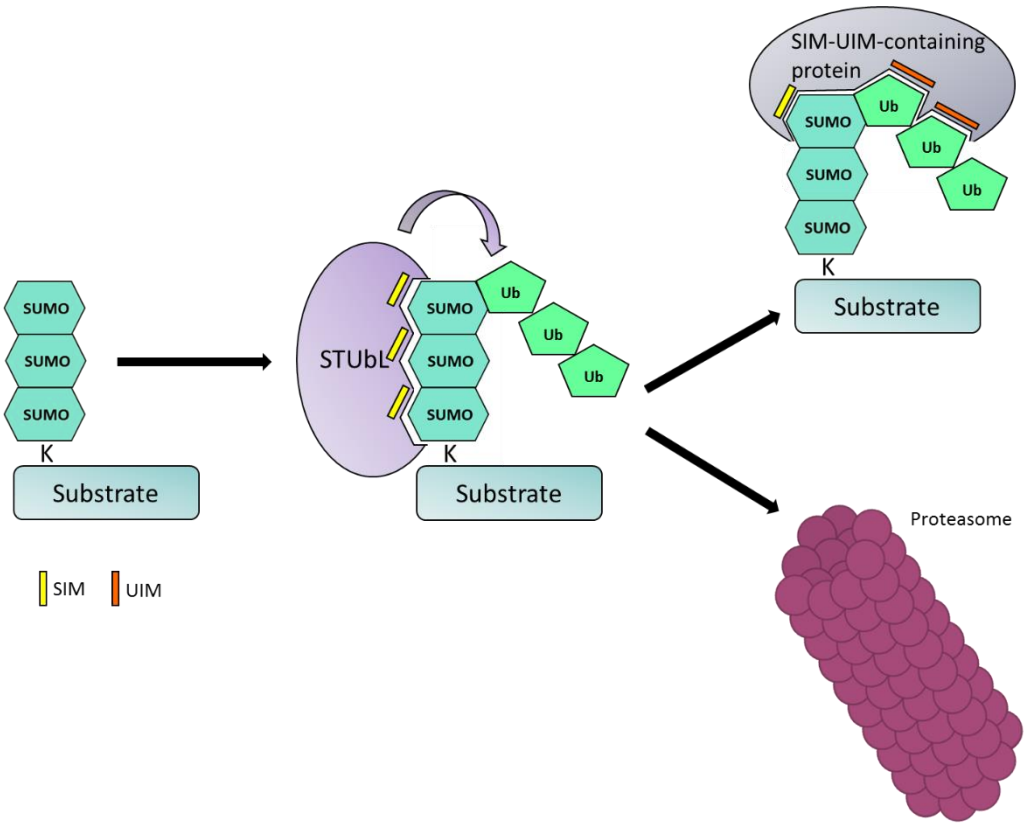

Figure 1.8 **Role of SUMO-ubiquitin hybrid conjugates in protein targeting.** Model illustrating SUMO-targeting ubiquitin ligation by a STUbL. Poly-SUMO is recognized by multiple SUMO-interaction motifs (SIMs) on the STUbL, a RING finger protein that, in conjunction with a ubiquitin-conjugating enzyme (E2) attaches additional ubiquitin (Ub) moieties to the SUMO-modified substrate. The ubiquitin modification may target the substrate to the proteasome (lower), or to a SUMO- and ubiquitin-interacting motif (SIM-UIM)-containing protein (upper).

1.3.5.4 De-ubiquitinating peptidases

De-ubiquitinating peptidases (DUBs) are responsible for generation of free ubiquitin by cleaving the poly-ubiquitin chain precursors encoded by ubiquitin genes UBB and UBC (Ozkaynak et al., 1987, Komander et al., 2009a). DUBs are also required in the recycling of ubiquitin necessary to maintain ubiquitin homeostasis. For this reason, the proteasome and lysosomal sorting machinery both have associated DUBs, which rescue ubiquitin from substrates committed to degradation (Clague and Urbe, 2006, Finley, 2009).

Around 80 active DUBs are encoded by the human genome, most of which fall into the category of ubiquitin-specific proteases (USPs). USPs, as well as most other DUB families, are cysteine-proteases (Clague et al., 2012). DUB-specificity is primarily

determined by preferences for ubiquitin chain linkages, via different ubiquitin binding domains, and sub-cellular localisation. Even within the same family, DUBs show high levels of discrimination for differing types of chain (Komander et al., 2009b, Bremm et al., 2010, Virdee et al., 2010, Licchesi et al., 2011).

1.3.6 Ubiquitin linkages dictate substrate fate

Protein ubiquitination is a very diverse modification. Substrates may be modified at one or multiple lysine residues, and substrate-bound ubiquitin can be further ubiquitinated at any of its seven lysine residues, resulting in complex chains and branching (Figure 1.9). As alluded to in Figure 1.5, different chain linkages target the substrate protein for different fates (Komander, 2009).

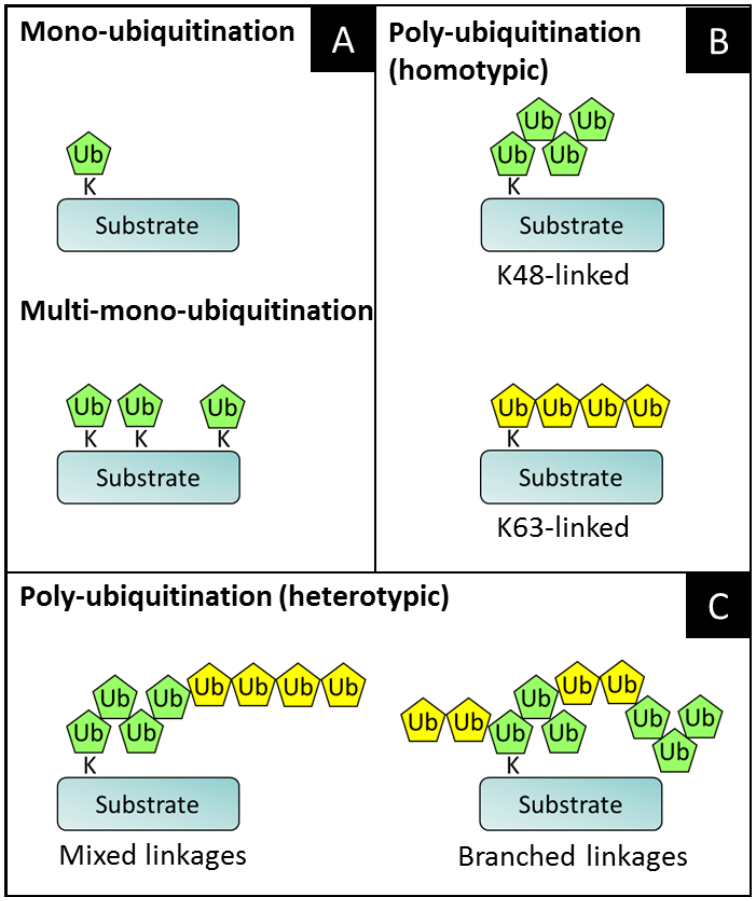

Figure 1.9 **Types of ubiquitin linkage**. Ubiquitin modification can be: (A) mono-ubiquitination (single-site), multi-mono-ubiquitination (multiple-sites, singly ubiquitinated) or (B) poly-ubiquitination (single-site, multi-ubiquitinated). Examples of Parkin-mediated homotypic poly-ubiquitination (Lysine-48- or -63-linked), where each chain contains a single type of linkage. Individual linkages result in different chain structures. Multiple homotypic ubiquitin chains of the same substrate are also possible. (C) Forms of heterotypic poly-ubiquitination. In mixed linkages, a ubiquitin chain has alternating linkage types. In branched or poly-ubiquitin chains, a single ubiquitin is extended at two or more lysine residues.

1.3.6.1 Mono-ubiquitination

Ubiquitin substrates can be singly ubiquitinated on a single lysine residue (mono-ubiquitination) or at multiple lysine residues (multi-mono-ubiquitination) (Komander, 2009). Nuclear mono-ubiquitination of histones and/or PCNA (proliferating-cell nuclear antigen) is a well-established part of the response to DNA-damage (Sigismund et al., 2004, Alpi et al., 2008). Both mono-ubiquitination and multi-mono-ubiquitination have been shown to trigger internalisation of cell-surface receptors, resulting in their lysosomal degradation or recycling (Haglund et al., 2003, Williams and Urbe, 2007).

1.3.6.2 Poly-ubiquitination

Each of the seven lysine residues in ubiquitin can be ubiquitinated in their own right, resulting in a complex landscape of differently linked chains, the roles of which are still being uncovered. Different types of chain can adopt different conformations, facilitating interactions with linkage-specific DUBs and UIMs (Komander, 2009). Chains can also be mixed, involving more than one type of linkage, and branched, when a single ubiquitin moiety is ubiquitinated at more than one site. Furthermore, other ubiquitin-like modifiers, like SUMO, can be incorporated into ubiquitin chains. Established roles of the different chain linkages are discussed briefly below.

1.3.6.2.1 Lys^{6}-linked chains

The physiological function(s) of this type of linkage remain elusive, although it might have a role in DNA repair (Sobhian et al., 2007). Lys^{6}-linked poly-ubiquitination is mediated by a heterodimeric RING-type E3 comprising BRCA1 and BARD1, which are localised at sites of DNA damage. Mutations in BRCA1 predispose individuals to early-onset ovarian and breast cancer (Venkitaraman, 2002).

1.3.6.2.2 Lys^{11}-linked chains

Lys^{11}-linked chains have long been established as potent signals for proteasomal degradation (Baboshina and Haas, 1996, Jin et al., 2008). However, there is mounting evidence for roles in diverse cellular processes, including the endoplasmic-reticulum-associated degradation (ERAD) pathway (Xu et al., 2009), and the APC/C E3 assembles Lys^{11}-linked chains in its regulation of the mammalian cell cycle (Jin et al., 2008).

1.3.6.2.3 Lys$^{27, 29 \& 33}$-linked chains

Due to their proximity, Lys^{27}-, Lys^{29}- and Lys^{33}-linked chains are difficult to distinguish by mass spectrometry, as the tryptic digest yields such small fragments. This makes it difficult to assign their specific roles (Komander, 2009). Lys^{27}-linked chains have no known cellular function, despite accouting for ~10% of ubiquitination (Xu et al., 2009). Lys^{29}-linked poly-ubiquitination has been associated with three different HECT E3 ligases: KIAA10, Itch and Ufd5. *In vitro*, KIAA10 mediates predominantly Lys^{29}-linked ubiquitination, along with Lys^{6}- and Lys^{48}-linked ubiquitination (You and Pickart, 2001). Itch assembles Lys^{29}-linked chains on the Notch-signalling regulator Deltex, resulting in its lysosomal degradation (Chastagner et al., 2006). Ufd5 assembles Lys^{29}-linked chains as part of the ubiquitin fusion degradation (UFD) pathway, in which ubiquitin chains are extended from a ubiquitin moeity on the substrate N-terminus, which has been fused with a non-cleavable linear linkage, effciently resulting in their degradation (Johnson et al., 1995, Licchesi et al., 2011).

1.3.6.2.4 Lys^{48}-linked chains

Lys^{48}-linked poly-ubiquitin chains are the canonical form of poly-ubiquitin, and the most-associated with protein degradation. Ubiquitin tetramers with Lys^{48}-linkages make up the minimal recognition motif for the proteasome – a Lys^{48}-linked substrate is typically degraded within minutes in the cell (Thrower et al., 2000). Lys^{48}-linkages are also assembled by Ufd5 as part of the UFD pathway (Johnson et al., 1995).

1.3.6.2.5 Lys^{63}-linked chains

Lys^{63}-linked ubiquitin chains are associated with a plethora of non-degradative roles, the best-understood of which is in cytokine signalling. Activation of IKK, responsible for the phosphorylation of IκB required to activate NF-κB in response to pro-inflammatory cytokines, is dependent on Lys^{63}-linked poly-ubiquitin by TRAF (TNF receptor-associated factor) E3 ligases (Deng et al., 2000). Many cell-surface receptors are poly-ubiquitinated with Lys^{63}-linked ubiquitin prior to their endocytosis, recognised by the ESCRT (endosomal sorting complexes required for transport) machinery (Williams and Urbe, 2007). AMSH, an endocytosis-regulating DUB, has intrinsic Lys^{63}-linkage-specificity (Sato et al., 2008). Lys^{63}-linked poly-ubiquitin is also heavily implicated in several aspects of the DNA-damage response (Hofmann and Pickart, 1999, Moldovan et al., 2007, Mailand et al., 2007, Doil et al., 2009).

1.3.6.3 Diversifying ubiquitin chains

Ubiquitination in itself is already diverse in the ways it can modify proteins. However, it is also possible for other post-translational modifications to become involved in ubiquitin chains. This gives rise to an almost infinite number of distinct modifications (Swatek and Komander, 2016).

While STUbLs are now well-established as ubiquitin ligases of SUMO chains, ubiquitin has also recently been shown in proteomics studies to be a target of SUMOylation, although a ubiquitin-targeted SUMO ligase ('UbTSL') has yet to be identified. Of the seven ubiquitin lysine residues, five can be SUMOylated – Lys6, 11, 27, 48 and 63 (Galisson et al., 2011, Lamoliatte et al., 2013, Hendriks et al., 2014). The physiological roles of SUMO-ubiquitin chains have not yet been established, although it has been reported that SUMOylation of Lys6 and Lys27 of ubiquitin is up-regulated during the heat shock response, or as a result of proteasome inhibition (Hendriks et al., 2014).

With ubiquitin SUMOylation established, it is conceivable that NEDD8 or other ubiquitin-like modifiers (UBLs) could also modify ubiquitin chains. Indeed, NEDDylated ubiquitin can be easily detected upon NEDD8 over-expression, although it remains unclear to what, if any, extent ubiquitin NEDDylation occurs under physiological conditions (Singh et al., 2012, Hjerpe et al., 2012).

It has been known for some time that small chemical groups including phosphate, methyl, and acetyl groups can modify ubiquitin and other UBLs, but the physiological relevance of this has only recently started to be investigated. For example, phosphorylation of ubiquitin at Serine 65 by PINK1 (PTEN-induced protein kinase 1) has been shown to recruit and activate Parkin during mitophagy (Caulfield et al., 2015, Wauer et al., 2015b).

1.4 SUMO

1.4.1 Discovery of SUMO proteins

The discovery of SUMO in the 1990s heralded a new way of thinking about post-translational modifications by small proteins. The gene encoding SUMO (SMT3) was first identified over twenty years ago in a genetic screen of *Saccharomyces cerevisiae* (Meluh and Koshland, 1995). Two research groups later independently verified that SMT3 encoded an as-yet uncharacterised peptide involved in covalent modification of RanGAP1

(Matunis et al., 1996, Mahajan et al., 1997). Ran, a nuclear Ras-like GTPase, is required for bidirectional transport of proteins and ribonucleoproteins across the nuclear pore complex (NPC). RanGAP1 (Ran-GTPase-activating protein) is a key regulator of the Ran GTP/GDP cycle (Bischoff et al., 1994). Both groups, Matunis *et al* and Mahajan *et al*, identified the novel modification as being structurally similar to ubiquitin, and went on to characterise its role in the subcellular partitioning of RanGAP1, targeting it to the NPC. The protein was found to colocalise with RanGAP1 at the NPC, and also to be present in the nucleus. Initially, the ubiquitin-like protein was referred to as GMP1 (GAP modifying protein 1) (Matunis et al., 1996). The subsequent paper showed that conjugation of the novel protein was ATP-dependent, and was required for association of RanGAP1 with RanBP2, a Ran–GTP-binding protein, at the NPC. It was from this study that SUMO (small ubiquitin-related modifier) took its name (Mahajan et al., 1997).

1.4.2 SUMO structure

Despite sharing only 18% sequence homology with ubiquitin (Mahajan et al., 1997), the structure of SUMO is very similar to that of ubiquitin, with the addition of an unstructured N-terminal extension (Bayer et al., 1998, Martin et al., 2007). Bayer *et al* used nuclear magnetic resonance (NMR) spectroscopy to solve the structure of SUMO-1 and found it to have the same protein fold ("ubiquitin-fold") as ubiquitin. Sequence alignment and structural representations of SUMO and ubiquitin are shown in Figure 1.10 (Martin et al., 2007). Residues highlighted in red and green are identical or conservatively changed; residues identical in the three SUMO paralogues are highlighted in blue.

The ubiquitin fold is one of 9 "superfolds" (Orengo et al., 1994). This consists of a five-stranded β-sheet, made up of parallel strands, except for β4, which is twisted against the main plane. Helix α1 is rotated approximately 45° relative to the first β-sheet (Figure 1.10, B). the ubiquitin superfold is found not only in ubiquitin and ubiquitin-like modifier such as SUMO, but also in unrelated proteins including ferredoxin and the Ras-binding domains of Raf kinase (Tsukihara et al., 1990, Nassar et al., 1995).

1.4.3 SUMO paralogues

All eukaryotes express one or more SUMO paralogues. Lower eukaryotes including *Saccharomyces cerevisiae* and *Drosophila melanogaster* express only the single SUMO paralogue (referred to as Smt3), whereas most mammals express 3 SUMO paralogues (Zhou et al., 2004, Smith et al., 2012). A fourth paralogue, SUMO-4, has more recently been described in humans, but is non-conjugatable due to a unique Proline 90 residue

preventing its maturation, and has no known function (Bohren et al., 2004, Owerbach et al., 2005). *Arabidopsis thaliana*, the most commonly used model plant organism, expresses up to eight SUMO paralogues (Miura et al., 2007).

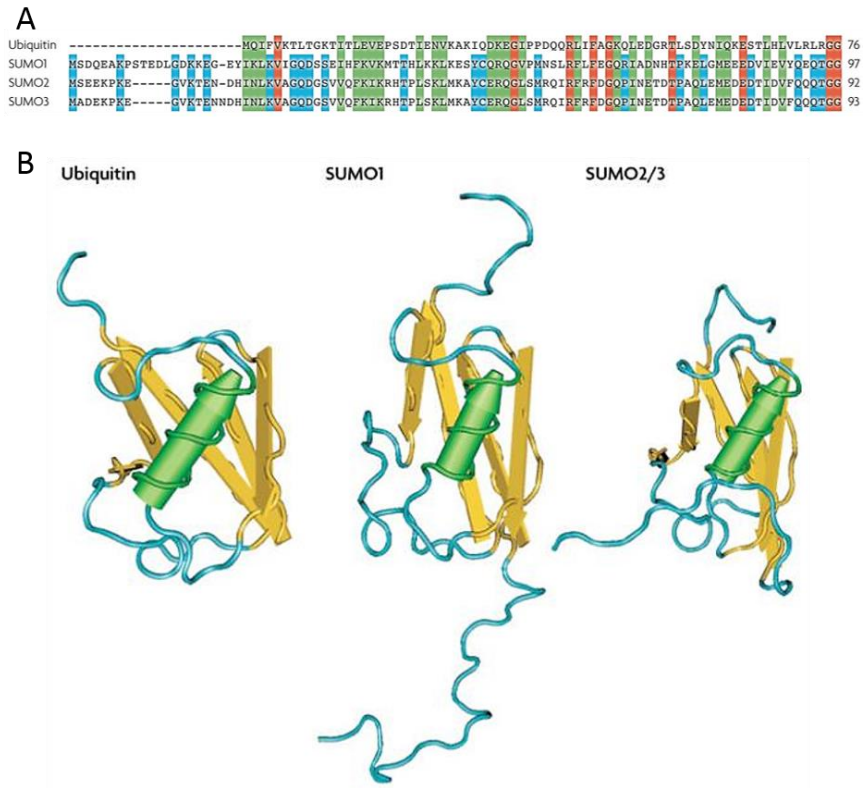

Figure 1.10 **Human ubiquitin and SUMO.** (A) Sequence alignment of ubiquitin and SUMO isoforms; identical residues are red, conservative changes are green, SUMO-only identical residues are blue. Alignment performed using ClustalW. (B) Ribbon diagrams of NMR structures of ubiquitin (Uniprot 1D3Z) and SUMO (Uniprot 1A5R and 2AWT). Figure adapted from *Martin, S., Wilkinson, K. A., Nishimune, A. and Henley, J. M. (2007). Emerging extranuclear roles of protein SUMOylation in neuronal function and dysfunction. Nature reviews. Neuroscience. 8(12): 948-959.* (Martin et al., 2007).

Mammalian SUMOs share around 45% sequence homology with yeast Smt3 (Wang and Dasso, 2009). Mature human SUMO-2 and SUMO-3 share 97% sequence homology, making them indistinguishable by Western blotting, and are therefore referred to as SUMO-2/3; SUMO-1 shares only 50% sequence homology with SUMO-2/3 (Wilkinson and Henley, 2010). Owing to their sequence and structural similarities, SUMO-1 and SUMO-2/3 can modify an overlapping group of proteins and are activated and conjugated by the same enzymes, which do not significantly discriminate between paralogues. In mammalian cells, SUMO-1 exists almost entirely in its conjugated form, whereas free SUMO-2/3 predominates. However, SUMO-2/3 is the preferred modifier, and is expressed 10x more than SUMO-1 (Saitoh and Hinchey, 2000). Owing to the higher intracellular levels of SUMO-2/3 and indiscriminate modifying enzymes, SUMO-2/3 conjugation is strongly

favoured (Flotho and Melchior, 2013). To balance this, cleavage of SUMO-2/3 conjugates is significantly faster than for SUMO-1 (Kolli et al., 2010).

1.4.4 Evolutionary importance of SUMO

SUMOylation has been established as an essential PTM for development and/or survival of almost all eukaryotes. The only currently known organisms whose SUMO-null mutants exhibit only a minor phenotype are the yeast *Schizosaccharomyces pombe* and the fungus *Aspergillus nidulans* (Tanaka et al., 1999, Wong et al., 2008). Inhibition of SUMO-conjugation by replacement of Ubc9 (required for SUMOylation) with a loss-of-function mutant caused defective cell division, accumulated chromosomal damage and apoptotic cell death in cultured DT40 chicken cells (Hayashi et al., 2002). Additionally, Ubc9-null murine embryos *in vivo* display severe chromosomal condensation and segregation defects, as well as aberrant nuclear envelope morphology, disruption of nucleoli, and die at the early post-implantation stage (Nacerddine et al., 2005). These studies demonstrating chromosomal and nuclear defects, *in vitro* and *in vivo*, in response to loss of SUMOylation are supportive of previous works that identified SUMOylation as a primarily nuclear PTM (Kamitani et al., 1997b).

It remains unclear if individual SUMO paralogues are necessary. Several studies of SUMO-1 knockout mice have shown them to be viable and fertile but with various phenotypes; some have cleft lip and palates whereas others display increased anti-inflammatory responses, cardiac defects and impaired adipogenesis (Alkuraya et al., 2006, Venteclef et al., 2010, Mikkonen et al., 2013). The same mice also have normal testis development and function, despite SUMO-1 mRNA being highly expressed in testes (Zhang et al., 2008). Collectively, these studies indicate that, while SUMO-1 can be compensated for by SUMO-2/3 in most circumstances, there are SUMO substrate proteins with paralogue-specific requirements.

1.4.5 SUMO distribution

The study by Kamitani *et al* showed by Western blotting that the majority of SUMOylation occurs in the nucleus (Kamitani et al., 1997b). More recent proteomics studies have confirmed this, identifying SUMO substrates with roles in DNA repair, transcription and replication (Jackson and Durocher, 2013, Wei and Zhao, 2016).

Nonetheless, cytoplasmic SUMO has also been detected and shown to modify extranuclear proteins (Geiss-Friedlander and Melchior, 2007). SUMOylated proteins have been shown to occur in the mitochondria by Western blotting of subcellular fractions and

by immunofluorescence, and have been implicated in maintenance of the fission/fusion equilibrium of mitochondria; Drp1 is a SUMO substrate and overexpression of SUMO1 or depletion of SENP5 results in mitochondrial fragmentation (Guo et al., 2013, Guo et al., 2017, Luo et al., 2017, Harder et al., 2004, Zunino et al., 2007). Protein-tyrosine phosphatase-1B was the first identified ER-associated SUMO substrate. It's SUMOylation is enhanced at the ER-outer membrane and directly inactivates the enzyme, suggesting a positive role for SUMO in receptor tyrosine kinase signalling (Dadke et al., 2006). At the plasma membrane, SUMO has been linked to the regulation of channels and receptors. The voltage-gated potassium channel Kv1.5, which has crucial roles in tightly regulated electrical responses throughout the cardiovascular system, is a SUMO substrate (Benson et al., 2007). Additional SUMO substrates at the neuronal plasma membrane are the metabotropic glutamate receptor-8 (mGluR8) and the GluR6 subunit of kainate receptors, the latter of which is SUMOylated upon kainate stimulation and is required for kainate-induced endocytosis of the receptor (Tang et al., 2005, Martin et al., 2007).

1.4.6 The SUMO cycle

Like ubiquitination, SUMOylation is a three-step process resulting in the covalent attachment of mature SUMO to a lysine residue of the target protein (Figure 1.11). While ubiquitin has several E2 enzymes and hundreds of E3 enzymes, SUMO has a specific and limited set of enzymes analogous to those required for ubiquitination. These comprise a single E1 activating dimer (SAE1/2), a single E2 conjugating enzyme (Ubc9), and a handful of known E3s, which are not essential but are thought to contribute to substrate specificity (Gareau and Lima, 2010).

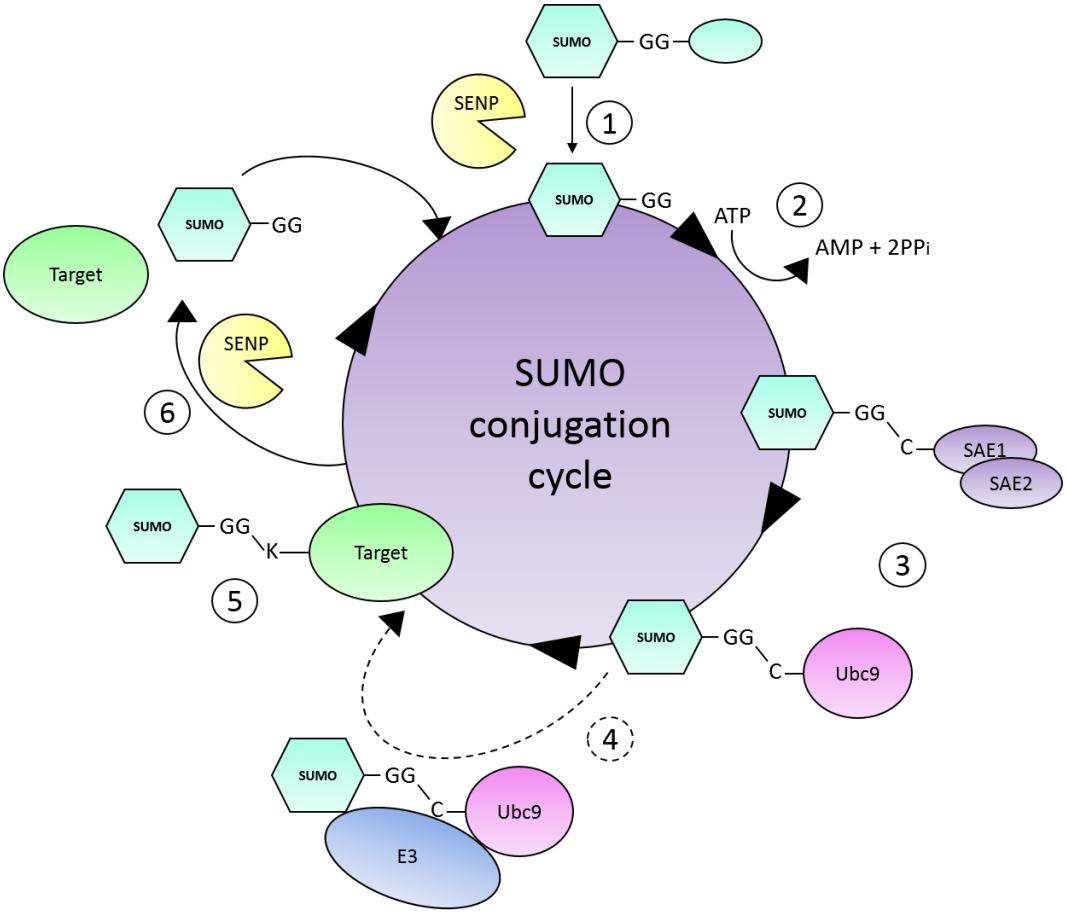

Figure 1.11 SUMO conjugation cycle. SUMO is transcribed and translated as an inactive precursor, which is cleaved by SENPs to expose a C-terminal di-glycine motif (1). This mature SUMO can then enter the SUMO conjugation cycle, where it is activated by ATP-dependent thioester bond formation with the active site of the E1 enzyme, a heterodimer of SAE1 and SAE2 (2). Activated SUMO is passed to the active cysteine of the E2 conjugating enzyme, Ubc9 (3), which catalyses transfer of SUMO to the target protein (5). This may be assisted by an E3 ligase (4). De-SUMOylation is mediated by SENP family proteases (6), releasing the unmodified target protein and free SUMO, which can re-enter the conjugation cycle.

1.4.6.1 SUMOylation consensus motifs

A SUMOylation consensus motif is defined as ψ-K-x-[D/E], where ψ is (usually) an amino acid with a large hydrophobic group and x can be any amino acid (Sampson et al., 2001). However, proteomics analyses by several groups have shown that more than half of all SUMO substrates do not contain a SUMO consensus motif (Zhu et al., 2008, Blomster et al., 2009). Interestingly, many proteins that contain the consensus SUMOylation motif are not detectably SUMOylated *in vivo* (Matic et al., 2010). SUMOylation motifs (both consensus and non-consensus) are described in more detail in Chapter 5.

1.4.6.2 SUMO-interacting motifs

The SUMO-interacting motif (SIM) is highly variable, and is the site of non-covalent binding between SUMO and a target protein (Kerscher, 2007). At its most basic, the SIM comprises a hydrophobic core, consisting of 3-4 aliphatic amino acid residues, which interact with a hydrophobic groove in SUMO (Song et al., 2005). The SIM hydrophobic core is often, but not necessarily, found in juxtaposition with a cluster of acidic residues (Hannich et al., 2005, Hecker et al., 2006). SIMs are described in more detail in Chapter 5.

1.4.6.3 SUMO maturation and activation

SUMO proteins are synthesised as inactive precursors and undergo proteolytic cleavage by sentrin-specific proteases (SENPs) to expose the C-terminal di-glycine motif required for conjugation (Johnson, 2004). Mature SUMO is then activated by the SUMO E1 enzyme heterodimer comprising SUMO activating enzyme (SAE)1 and SAE2, which have significant N- and C-terminal sequence homology to their ubiquitin E1 counterpart (Johnson et al., 1997, Gong et al., 1999). The SAE1/SAE2 complex activates SUMO protein in a two-step, ATP-dependent reaction in which a cysteine residue of SAE2 forms a thioester bond with SUMO (Olsen et al., 2010). The ubiquitin fold domain of SAE2 then interacts with the SUMO E2 enzyme, ubiquitin conjugating enzyme 9 (Ubc9), and SUMO is thiol-transferred to a conserved cysteine residue on Ubc9 (Yunus and Lima, 2006).

1.4.6.4 SUMO conjugation

SUMOylation requires formation of an isopeptide bond between the negatively-charged, exposed carboxyl-group of the mature SUMO peptide C-terminal glycine residue and the positively-charged amino-group on the target protein lysine residue (Johnson, 2004). Unlike ubiquitination, which requires an E3 ligase for the final step in substrate-conjugation, SUMOylation can occur in an E3-independent or -dependent manner; *in vitro*, SAE1/SAE2, Ubc9 and ATP are sufficient to conjugate SUMO to a substrate (Bernier-Villamor et al., 2002).

The E2 conjugating enzyme, Ubc9, can directly SUMOylate substrate proteins via two different mechanisms. Firstly, Ubc9 can recognise a consensus SUMOylation motif on a substrate protein and directly conjugate SUMO to the lysine residue. The structure of the Ubc9-RanGAP complex has been shown to contain a continuous interface, within which interactions are present between the consensus RanGAP1 SUMOylation motif (LKSE) and four surfaces of Ubc9, including its catalytic cysteine (Bernier-Villamor et al., 2002). Secondly, Ubc9 can directly SUMOylate SIM-containing substrate proteins. SIMs can

promote protein SUMOylation by non-covalently binding to the same SUMO moiety as Ubc9, thus bringing SUMO into proximity with their SUMO-acceptor lysine residue. As SIMs can have SUMO paralogue preferences, SUMOylation via a SIM in an E3-independent manner confers greater SUMO-specificity than E3-, consensus motif-dependent SUMOylation, which has not been shown to discriminate (Zhu et al., 2008).

Alternatively, SUMOylation can occur via an E3 ligase, as is the case for the majority of SUMO substrates. Unlike ubiquitin, for which hundreds of E3 ligases have been identified, only a handful of SUMO E3s have yet been described. While they are not necessary for SUMO conjugation, SUMO E3 ligases are believed to greatly enhance substrate specificity by forming multiple interactions with target proteins (Reverter and Lima, 2005). The SUMO conjugation cycle is graphically depicted in Figure 1.11.

1.4.6.5 SUMO deconjugation

Deconjugation of SUMO is the hydrolysis of the isopeptide bond between the C-terminal carboxyl group of SUMO and the lysyl amino group of the acceptor protein (Wang and Dasso, 2009). The main group of enzymes that deSUMOylate mammalian proteins are the SENP family of SUMO proteases, the same family that facilitate SUMO maturation.

SUMO proteases were first identified in 1999 in the yeast species *Saccharomyces cerevisiae*, where they were shown to have a crucial role in cell-cycle progression at the G2/M phase (Li and Hochstrasser, 1999). Since then, 6 SUMO proteases have been discovered in mammals (SENPs1-3 and 5-7) and 7 identified in the model plant organism *Arabidopsis thaliana* (ULP1a-d, ESD4, ULP2a/b) (Mukhopadhyay et al., 2006, Yeh et al., 2000, Colby et al., 2006).

Unlike the SUMO conjugating machinery, SENPs have some level of SUMO paralogue-specificity. SENPs 1 and 2 have roles in the maturation and deconjugation of both SUMO-1 and SUMO-2/3, whereas SENPs 3 and 5-7 preferentially interact with SUMO-2/3. As previously discussed, intracellular levels of SUMO-2/3 far exceed SUMO-1, and modifying enzymes are largely indiscriminate, resulting in SUMO-2/3 conjugation being strongly favoured (Flotho and Melchior, 2013). The larger number of SENPs acting to deconjugate SUMO-2/3 therefore contributes to the greater rate of SUMO-2/3 deconjugation required to maintain the balance of SUMO-1- and SUMO-2/3-ylation (Kolli et al., 2010, Gong and Yeh, 2006).

Owing to the large proportion of nuclear SUMOylation, the SENPs are predominantly found in and around the nucleus (Kamitani et al., 1997b). SENP1 and SENP2 mainly localise to the nuclear envelope, with SENP1 also able shuttle to the cytoplasm (Bailey and O'Hare,

2004, Hang and Dasso, 2002). SENP3 and SENP5 localise predominantly with the nucleolus (Di Bacco et al., 2006), although both have also been shown to have activity at the mitochondrial outer membrane (Guo et al., 2013, Luo et al., 2017, Zunino et al., 2007). SENP6 and SENP7 are mainly localised to the nucleoplasm, with SENP6 also exhibiting a significant cytoplasmic presence (Kolli et al., 2010, Li et al., 2018).

More recently, proteases outside of the SENP family have been shown to specifically deconjugate SUMO. DeSI1 and 2 (deSUMOylating isopeptidases) are part of the family of permuted papain fold peptidases of dsRNA viruses and eukaryotes, and were initially thought to be party of the ubiquitin pathway (Iyer et al., 2004). USPL1 (ubiquitin-specific protease-like 1) has significant homology to the family of ubiquitin-specific proteases, but preferentially cleaves SUMO over ubiquitin, both *in vitro* and *in vivo* (Schulz et al., 2012). A list of SUMO conjugation and deconjugating enzymes is given in Table 1.1.

Table 1.1 Overview of SUMO proteins.

Protein	Mammalian identity	Role(s)
SUMO	SUMO-1	Substrate modification
	SUMO-2/3	Substrate modification
SUMO E1	SAE1/SAE2	SUMO activation
SUMO E2	Ubc9	SUMO conjugation
SUMO E3 (examples)	PIAS1, RanBP2	SUMO conjugation, specificity
SUMO proteases	SENP1/2	SUMO-1 and -2/3 maturation and deconjugation
	SENP3/5	SUMO-2/3 deconjugation
	SENP6/7	PolySUMO chain editing
	DeSI1/2	SUMO deconjugation
	USPL1	SUMO deconjugation

1.4.6.6 Regulation of SUMOylation

SUMOylation is a highly dynamic modification and, as such, must be tightly regulated. The majority of SUMO substrates undergo rapid cycling of SUMO conjugation and deconjugation, essential in maintaining steady-state SUMOylation (Mukhopadhyay and Dasso, 2007). The proportion of substrate proteins that are SUMOylated at any given time is regulated on a number of levels. The amount of free SUMO available within the cell

dictates potential SUMOylation levels, as does the rate of substrate deSUMOylation. Additionally, SUMO proteases add specificity by having defined localisations and SUMO paralogue preferences (Flotho and Melchior, 2013).

Oftentimes, substrates are SUMOylated in response to intracellular stimuli, including DNA damage, cell-cycle phases and signal transduction. It is thought that 3 mechanisms regulate stimulus-dependent SUMOylation:

i. Activity of SUMO E1-3 enzymes and SUMO proteases can be manipulated. For example, hydrogen peroxide-dependent low-level oxidative stress has been shown to reduce global SUMOylation in two different ways:
    a. Via reversible inhibition of SAE2 and Ubc9 by formation of a disulphide bond between their catalytic cysteine residues (Bossis and Melchior, 2006).
    b. Via increased specific SUMO-2/3 deconjugation by stabilisation of SENP3. It has been speculated that SENPs may act as redox sensors (Huang et al., 2009, Xu et al., 2008).
ii. Phosphorylation can enhance substrate binding to Ubc9. Phosphorylation of a serine or threonine residue(s) up- or downstream of the substrate SUMO acceptor lysine creates a negative charge, similar to that provided by the D/E residue in a consensus SUMOylation motif (ψ-K-x-D/E), required to stabilise the Ubc9-substrate interaction. An example of this is GluK2, a kainate receptor subunit, in which phosphorylation at serine 868 enhances SUMOylation at lysine 886, resulting in kainate receptor endocytosis (Konopacki et al., 2011).
iii. The addition to or removal from the SUMO acceptor lysine of competing PTMs, including ubiquitin, acetyl and methyl groups, can inhibit/enhance SUMOylation (Ulrich, 2005).

1.4.7 Roles of SUMOylation

SUMO modification can have several different outcomes, which are outlined in Figure 1.12 (Everett et al., 2013). Mono-SUMOylation by SUMO-1 or SUMO-2/3 can change the substrate protein conformation or create/disrupt allosteric binding sites. SUMO-2/3 can form poly-SUMO chains through sequential SUMOylation of an internal consensus motif, which is missing from SUMO-1 (Matic et al., 2008). Poly-SUMO chains

can facilitate interactions between SUMO substrate proteins and SIM-containing proteins (Kung et al., 2014).

Interestingly, hybrid SUMO-Ubiquitin (SUMO-Ub) chains also occur, the synthesis of which is reliant on SUMO-targeted ubiquitin ligases (STUbLs), which specifically bind to and ubiquitinate poly-SUMO chains on substrate proteins. Originally, SUMO-Ub chains were detected on proteins targeted for proteasomal degradation, recognised by ubiquitin receptors (Tatham et al., 2008, Kung et al., 2014). However, subsequent work has established that hybrid chains are recognised as a distinct modification by receptors containing tandem SUMO-interacting motifs and ubiquitin-interacting motifs (tSIM-UIMs) (Guzzo et al., 2012).

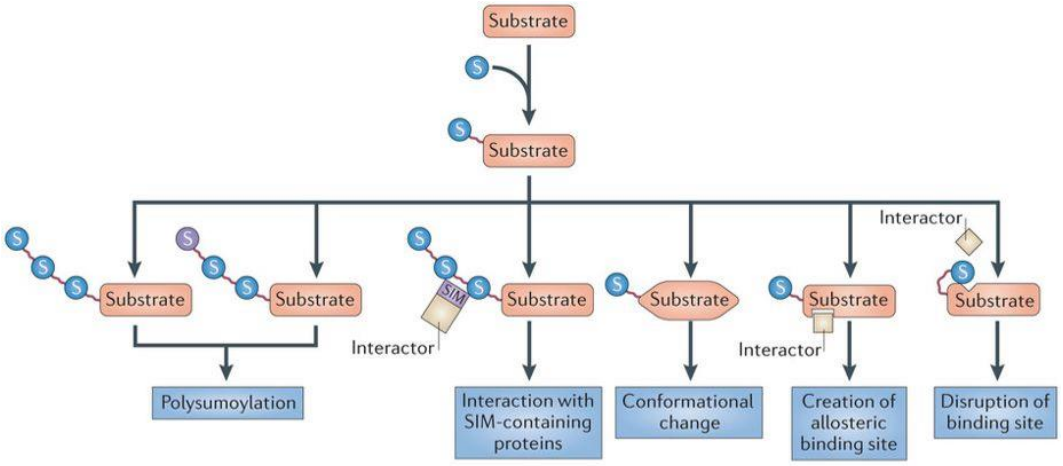

Figure 1.12 **Functional consequences of SUMOylation**. SUMO-1 or SUMO-2/3 can mono-SUMOylate substrates; targets can be poly-SUMO-2/3-ylated (blue S); poly-SUMO-2/3-ylated and terminated by SUMO1 (purple S). SUMOylated targets can be bound by SUMO interaction motif (SIM)-containing proteins; targets may change their conformation as SUMO disrupts structure. Allosteric binding pockets may be formed, or ligand-binding sites disrupted. Figure taken from *Everett, R.D., Boutell, C. & Hale, B.G., 2013. Interplay between viruses and host SUMOylation pathways. Nature Reviews Microbiology, 11(6), pp.400–411.* (Everett et al., 2013).

1.4.8 SUMO enigma

An interesting quirk of modification by SUMO is that only a tiny proportion of the available substrate pool need be SUMOylated at any given moment to achieve maximal effect. This is often referred to as the 'SUMO Enigma' (Hay, 2005). It remains a poorly understood paradox, yet elegant hypotheses have been put forward to explain the phenomenon, centring around the highly dynamic nature of SUMOylation and the rapid activity of SENPs, with the functional effects of substrate SUMOylation persisting beyond SUMO deconjugation (Martin et al., 2007).

SUMOylation is an ATP-dependent process, so the rapid SUMOylation, deSUMOylation and re-SUMOylation undergone by most SUMO substrates seems an unnecessarily energy-inefficient mechanism of modification. Why SUMO is so rapidly cycled on and off of substrate proteins is not yet understood, but it is proposed that having such a dynamic system allows for rapid responses to stimuli, and that the adaptability of the process makes it 'cost-effective' (Guo and Henley, 2014).

1.5 Parkin

Parkin is perhaps the best-known RING-between-RING (RBR) E3 ligase, notable for its significance in manifestation of early-onset Parkinson's disease. In contrast with traditional RING or HECT E3s, all of the currently acknowledged RBR E3s are complex, multidomain proteins (Spratt D et al., 2014). RBR E3s contain two Zn^{2+}-co-ordinating cysteine-rich domains that were once thought to loosely conform to the RING E3 consensus sequence, referred to as RING1 and RING2 (Marin and Ferrus, 2002, Marin et al., 2004). Between these domains, a third cysteine-rich domain referred to as the In-Between-RINGs (IBR), completes the recognisable RBR motif (Morett and Bork, 1999).

More recently, it has been shown that 'RING2' actually does not conform to the canonical RING E3 structure but is essential for RBR E3 ligase activity and is sometimes referred to as a Required for Catalysis (Rcat) domain. It has also been established that, unlike classical RING or HECT E3s, RBR E3s utilise an auto-inhibitory mechanism to regulate activity, which was first identified in Parkin (Chaugule et al., 2011). The E3 ligase activity of RBRs has now be shown to use a hybrid mechanism, combining aspects of RING and HECT E3 activity (Wenzel et al., 2011). Parkin modifies its substrates with a number of different ubiquitin chain linkages, the most common being K63, K48, K11 and K6 (Ordureau et al., 2014).

1.5.1 Structure and autoinhibition of Parkin

In recent years, high-resolution crystal structures of Parkin have revealed many intricacies of its regulation and function. The RBR E3 is now known to comprise an N-terminal ubiquitin-like domain (Ubl) and four Zn^{2+}-co-ordinating RING-like domains: RING0 (also referred to as the unique Parkin domain, UPD), RING1, IBR and RING2, collectively referred to as the RBR domain (Figure 1.13 (A)) (Trempe et al., 2013, Riley et al., 2013,

Wauer and Komander, 2013). The complex folded structure of Parkin is largely responsible for regulation of its activity (Figure 1.13 (B)).

The Ubl domain is required for substrate recognition, autoinhibition, association with the proteasome and regulation of Parkin activity and abundance. It also binds to the RBR domain *in cis*, inhibiting catalytic activity of Parkin (Chaugule et al., 2011, Finney et al., 2003). RING0 (UPD) contains a PINK1-interacting site (Xiong et al., 2009), while RING1 is responsible for E2-binding (Wauer and Komander, 2013). RING2 contains the catalytic cysteine residue C431 required for Parkin ligase activity. An additional structure, often referred to as the Repressor element (REP), connects the IBR and RING2 domains, and is responsible for holding Parkin in its inactive conformation in the cytosol by bringing RING0 (UPD) and RING2 together to occlude C431 (Seirafi et al., 2015, Wauer and Komander, 2013, Wauer et al., 2015b).

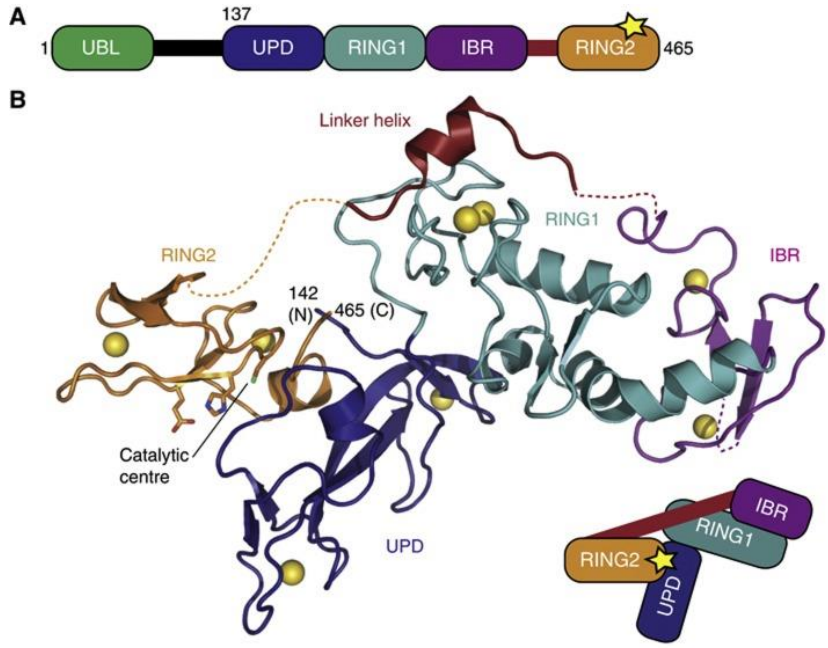

Figure 1.13 **Parkin structure.** (A) cartoon representation of linear Parkin structure, with N-terminal Ubl and C-terminal RING2 containing C431 (star). UPD = RING0. REP is shown in red, between IBR and RING2. (B) cartoon structures of UPD-RBR domains (Ubl not included in any high-resolution structures) in autoinhibited state. REP (linker helix) shown in red. C431 indicated (catalytic centre). Yellow spheres represent Zn^{2+}. Disordered stretches represented as dotted lines. Figure adapted from *Wauer, T. and D. Komander (2013). "Structure of the human Parkin ligase domain in an autoinhibited state." Embo j 32(15): 2099-2112* (Wauer and Komander, 2013).

1.5.2 PINK1-dependent activation

The majority of Parkin exists in an autoinhibited state in the cytosol and is recruited to mitochondria only during times of oxidative stress (Geisler et al., 2010). PTEN-induced

protein kinase 1 (PINK1) is targeted to the MOM by its N-terminal mitochondrial targeting sequence, but its kinase domain remains facing the cytosol and is known to physically interact with Parkin (Zhou et al., 2008, Kim et al., 2008b). Under basal conditions, PINK1 is degraded soon after mitochondrial import, but depolarisation of the mitochondrial membrane causes PINK1 to accumulate on the MOM. Here it phosphorylates mitochondrial ubiquitin and Mfn2, which serve as activator and receptor for Parkin, respectively (Chen and Dorn, 2013). Current data support a model for initiation of mitophagy in which PINK1-mediated phosphorylation of Mfn2 simultaneously facilitates mitochondrial Mfn2 to recruit Parkin, and functionally sequesters the mitochondrion by disturbing Mfn2-mediated mitochondrial fusion (Gong et al., 2015). PINK1 phosphorylation of ubiquitinated mitochondrial proteins activates Parkin and amplifies its mitochondrial activity by helping to retain its mitochondrial localisation (Ordureau et al., 2015). This mechanism thereby selectively recruits Parkin to dysfunctional mitochondria (Narendra et al., 2008, Narendra et al., 2010, Matsuda et al., 2010). In SH-SY5Y cells treated with mitochondrial uncoupler CCCP, endogenous PINK1 is able to co-immunoprecipitate more Parkin with longer treatments, compared to no treatment (Geisler et al., 2010).

Activation of Parkin requires the release of several 'safety belts' which hold it in its autoinhibited conformation (Figure 1.14) (Caulfield et al., 2015). PINK1-phosphorylated ubiquitin (pUb) binds to Parkin, forming an extensive interface along the RING1-IBR region of Parkin, and also interacting with side chains of RING0. This is proposed to destabilise the Ubl-RBR domain interaction by displacing IBR and reconfiguring the IBR-REP linker. With Ubl partially destabilised from the RBR domain, S65 is accessible for phosphorylation by PINK1 (Wauer et al., 2015b). PINK1 phosphorylates S65 of the Parkin Ubl, which sits within a cleft formed by the interface between Ubl and a flexible linker region, triggering a cascade of structural changes. Initially, the Ubl-linker cleft is opened up, eventually facilitating release of the Ubl from its close contact with RING1 and IBR. This opening further propagates more global conformational changes, all of which are required for full Parkin activity. The REP element loosens its interaction with RING1 (*in silico* modelling predicts an increased distance between Tyr391 and Cys238), exposing its binding site for a ubiquitin-loaded E2, and RING0 is released from its close contact with RING2, allowing increased hydration around the catalytic C431. It is thought that removal of these 'safety belts' is sequential (Caulfield et al., 2014).

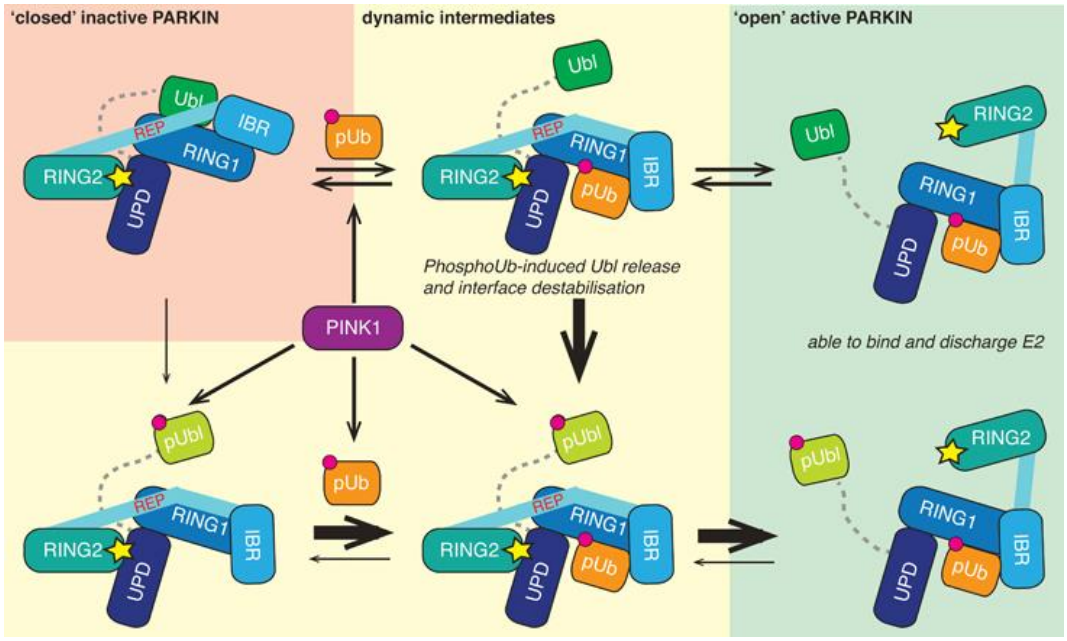

Figure 1.14 **Model of Parkin activation**. Multiple 'safety belts' hold Parkin in an autoinhibited state (top left). Inactive Parkin can interact with pUb, ultimately releasing Ubl and destabilising inhibitory interactions to 'open' Parkin (top row). Parkin is also phosphorylated by PINK1 at S65 of its Ubl, either directly (bottom left) or with greater efficiency after pUb binding (bottom middle). Phosphorylated Ubl undergoes a conformational change which probably prevents Parkin from reverting to an autoinhibited state. Phosphorylation of Ubl thereby stabilises an active and open Parkin conformation (bottom right). Figure adapted from *Wauer, T., M. Simicek, A. Schubert and D. Komander (2015). "Mechanism of phospho-ubiquitin induced PARKIN activation." Nature **524**(7565): 370-374* (Wauer et al., 2015b).

1.5.3 Parkin: mitochondrial roles and consequences

Through its interplay with PINK1 and pUb, the primary function of Parkin is the induction of mitophagy by heavily ubiquitinating proteins in the mitochondrial membrane and targeting the mitochondrion for degradation (Figure 1.15). However, Parkin has a number of other mitochondrial and non-mitochondrial roles. Established mitochondrial roles for Parkin are outlined briefly below.

- In relation to mitochondrial dynamics, Parkin has been shown to ubiquitinate a number of MOM proteins, including regulators of mitochondrial fusion, mitofusins and OPA1 (optic atrophy 1), and regulators of mitochondrial trafficking, such as Miro (Scarffe et al., 2014). This disrupts the equilibrium of mitochondrial fission and fusion, allowing isolation of dysfunctional mitochondria from the mitochondrial network prior to mitophagy.

- PINK1 and Parkin also co-operate in the repair of mildly damaged mitochondria that result from mild oxidative stress. By sequestering oxidised/damaged proteins in mitochondria-derived vesicles, which are then targeted for lysosomal degradation, the mitochondrion can be restored to function (Soubannier et al., 2012, McLelland et al., 2014).
- Complementing this, PINK1 and Parkin also contribute to the balancing of mitochondrial dynamics by promoting mitochondrial regeneration (Vincow et al., 2013). In SH-SY5Y cells, as well as other proliferating cell lines, over-expression of Parkin has been shown to increase mitochondrial transcription via interactions with TFAM (mitochondrial transcription factor A) (Kuroda et al., 2006, Rothfuss et al., 2009).

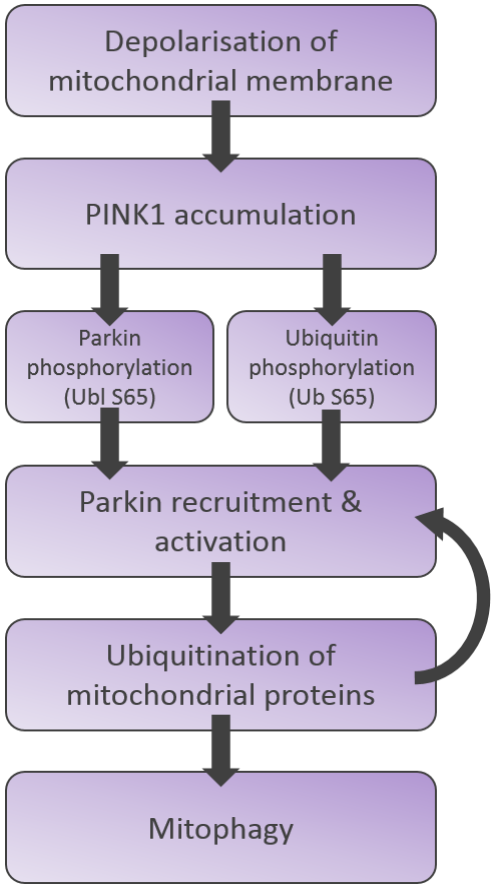

Figure 1.15 **How PINK1 and Parkin mediate mitophagy.** PINK1 accumulates on the membrane of damaged mitochondria, where it phosphorylates ubiquitinated MOM proteins and the Ubl of Parkin, activating the ligase activity of Parkin. Parkin ubiquitinates MOM proteins, which can then be PINK1-phosphorylated, contributing to further recruitment of Parkin. The heavily ubiquitinated mitochondrion is eventually targeted for degradation.

1.5.4 Parkin and pathology

Parkin is most commonly associated with the neurodegenerative disorder Parkinson's disease (PD). To date, more than 120 pathogenic Parkin mutations have been linked to PD (Seirafi et al., 2015). Clinically, PD is characterised by loss of dopaminergic (DA) neurons from the *substantia nigra* of the midbrain, often accompanied by presence of Lewy bodies in surviving DA neurons, resulting in motor deficits (Braak et al., 2003). DA neurons of the *substantia nigra* are generally very large, highly branched, highly active and under oxidative stress (as a result of dopamine oxidation), putting huge pressure on their mitochondria. Given the pivotal role of Parkin in mitochondrial homeostasis, it is understandable that Parkin dysregulation can lead to PD-associated DA neurodegeneration (Zhang et al., 2015). Indeed, mitophagy is defective in PD brains (Fiesel et al., 2015). Accumulating evidence is also implicating Parkin in the pathology of other neurodegenerative disorders, including Alzheimer's disease and Amyotrophic lateral sclerosis (Nemes et al., 2004, Lagier-Tourenne et al., 2012).

Beyond its mitochondrial functions, Parkin has been reported to have roles in cellular metabolism and regulation of the cell cycle, with at least 25 substrates or putative substrates described so far (Zhang et al., 2015). Through its non-covalent interactions with SUMO-1, Parkin has been shown to shuttle between the cytosol and nucleus, with its nuclear import increased by association with SUMO (Um and Chung, 2006). The zinc-finger protein PARIS (Parkin-interacting substrate) is a major transcriptional repressor of PGC (Peroxisome proliferator-activated receptor-γ coactivator)-1α expression and regulator of transcription of many metabolism-associated genes and has been identified as a target of Parkin-mediated degradation. Accordingly, studies of *post-mortem* brains showed that PARIS accumulates in brain tissue of Autosomal Recessive Juvenile Parkinsonism (ARJP) and sporadic PD patients. PARIS also was shown to accumulate in the ventral midbrain of mice in which Parkin had been conditionally ablated (Shin et al., 2011). Parkin has also been shown to interact with co-activators of the anaphase-promoting complex (APC/C), mediating APC/C-independent degradation of key mitotic regulators, with Parkin-deficiency resulting in mitotic defects, genomic instability and tumorigenesis (Lee et al., 2015). Additionally, Parkin dysfunction has been implicated in the progression of several types of cancer (Cesari et al., 2003, Tay et al., 2010, Yeo et al., 2012).

1.5.5 Parkin in the heart

Despite having been repeatedly shown to be expressed in cardiac tissue and cardiomyocytes, the role(s) of Parkin in the heart remains little-understood and often-debated (Wu et al., 2016, Bhandari et al., 2014, Dorn, 2016). Given the huge abundance of mitochondria in the mammalian heart, and the resulting need to prevent cardiotoxicity caused by damaged/senescent mitochondria, it is interesting that adult mouse hearts have so little Parkin (Dorn, 2013, Song et al., 2015). Current opinion is that Parkin plays little (if any) role in normal maintenance of homeostatic mitophagy in hearts, but that Parkin-mediated mitophagy is a critical stress-response and Parkin could be central in perinatal cardiac metabolic remodelling.

In *Drosophila melanogaster*, individual or combined knock out of Parkin and PINK1 provokes a Parkinson's-like phenotype, characterised by locomotor defects and skeletal myopathy associated with mitochondrial dysmorphology, indicative of impaired mitochondrial maintenance (Greene et al., 2003). Equally, cardiac-specific Parkin knock out in *Drosophila* heart tubes showed that Parkin is required for the maintenance of normal mitochondrial morphology and membrane polarisation, as well as the prevention of abnormal ROS production (Bhandari et al., 2014). However, orthologous germline gene-ablation in mice yields minimal phenotypes (Lee et al., 2012b). This could be the result of upregulation of hundreds of cardiac-expressed mRNAs in the germline Parkin-null mice providing a developmentally-incurred opportunistic compensation for loss of Parkin, which is not observed in cardiac-specific ablation of Parkin in adult cardiomyocytes (Song et al., 2015, Bhandari et al., 2014).

In 2013, Gustafsson's group used germline Parkin knock out mice to carry out the first full phenotypic characterisation of Parkin-deficient hearts (Kubli et al., 2013b). Under normal conditions, these mice did not exhibit cardiac dysfunction or structural abnormalities. Echocardiographic analyses demonstrated that, at least up to 12 months, cardiac function of the Parkin-null mice was normal. Despite maintaining normal function, the cardiac mitochondria of Parkin-null mice were smaller and disorganised compared to those of WT mice, and over time developed aberrant electron-dense inclusions (Kubli et al., 2013a). Notably, Parkin-null mice were far more sensitive to myocardial infarction than WT, developing larger infarcts and having reduced survival rates. In WT mice, Parkin protein expression and mitophagy were increased around the border of the infarct within 8 hours, and sustained for at least 48 hours, whereas border cardiomyocytes of the Parkin-null mice had reduced mitophagy, leading to an accumulation of swollen, dysfunctional

mitochondria (Kubli et al., 2013b). The same group went on to show that over-expression of WT Parkin, but not Parkinson's-associated lack-of-function mutants, in isolated adult cardiac myocytes was protective against hypoxia-induced cell death, suggesting a critical role for Parkin in adapting to stress and/or mitigating stress-related damage (Kubli et al., 2013b, Kubli et al., 2013a).

Stress-related up-regulation of Parkin has been linked to pathophysiological mitochondrial dynamics; disruption of cardiac mitochondrial fission by cardiomyocyte-specific ablation of Drp1 concordantly and chronically increases Parkin mRNA and protein level (Song et al., 2015). Additionally, PINK1-deficient hearts exhibit markedly increased Parkin expression compared to WT (Kubli et al., 2015). Regardless of any observable cardiac dysfunction, these data indicate that Parkin is upregulated in response to mitochondrial stress in the heart.

Interestingly, several reports have established a role for Mfn2 as a mitochondrial receptor for Parkin. As discussed previously, Mfn2 mRNA is highly abundant in the heart (Santel et al., 2003). Later studies went on to report that Parkin localisation to mitochondria is defective in both cardiomyocytes and neurons following *in vivo* cell type-specific Mfn2 knock out, suggestive of a role for the Mfn2-Parkin interaction in mitochondrial Parkin recruitment (Chen and Dorn, 2013, Lee et al., 2012a). This finding is supported by later work that demonstrates PINK1-dispensibility in the mitochondrial recruitment of Parkin and mitophagy activation in cardiomyocytes (Kubli et al., 2015). While it is generally understood that PINK1-mediated phosphorylation of Parkin, ubiquitin and Mfn2 are required for Parkin activation, it is evident from these data that other kinases can compensate for PINK1-deficiency (Chen and Dorn, 2013).

While basal cardiac expression of Parkin is minimal, the data presented here demonstrate three conditions under which cardiac Parkin expression is increased:

- Following myocardial infarction (Kubli et al., 2013b)
- In cases of defective mitochondrial fission (Song et al., 2015)
- In cases of PINK1-deficiency (Kubli et al., 2015)

It is therefore evident that, under conditions of stress, Parkin plays a pivotal, albeit conditional, role in removal of defective cardiac mitochondria (Dorn, 2016).

1.6 Fbxo7

F-box protein 7 (Fbxo7) has a number of roles, most notably as a substrate recognition subunit in certain Cullin-RING ligase complexes (CRLs), but also independently of CRLs. Like Parkin, mutations in Fbxo7 have been demonstrated to cause early-onset PD (Shojaee et al., 2008, Di Fonzo et al., 2009) and have more recently been linked to defective mitophagy (Burchell et al., 2013, Zhou et al., 2015, Skaar et al., 2013).

1.6.1 Cullin-RING ligases

Ubiquitin E3 ligases are largely responsible for the spatiotemporal regulation of substrate-specific ubiquitination. A major family of E3 ligases are the CRLs, which mediate proteolysis of thousands of proteins across almost every cellular pathway (Petroski and Deshaies, 2005a). The CRLs are multi-protein complexes containing a RING E3 ligase and a cullin scaffold (collectively referred to as the E3 ligase module), as well as a variable substrate recognition subunit (SRS) that mediates the interaction with cognate substrates (Komander and Rape, 2012). There are 6 main types of CRL, along with at least 2 atypical CRLs, with cullin proteins used as the backbone in all cases (Figure 1.16) (Skaar et al., 2013). F-box domain containing proteins (FBXO), including Fbxo7, are one type of SRS module that interact with the Skp1 (S-phase kinase associated protein 1) adaptor to form Skp1-Cul1-F-box (SCF)-type CRLs (Ravid and Hochstrasser, 2008). The carboxyl-terminus of Cul1 recruits Rbx (a small RING protein) which acts to direct the E2 enzyme to the E3 complex, while the amino-terminus binds Skp1, which can then bind one of 69 F-box proteins (in humans) to dictate substrate-specificity (Petroski and Deshaies, 2005a, Skaar et al., 2009). CRLs are activated by NEDDylation of the cullin scaffold (Duda et al., 2008).

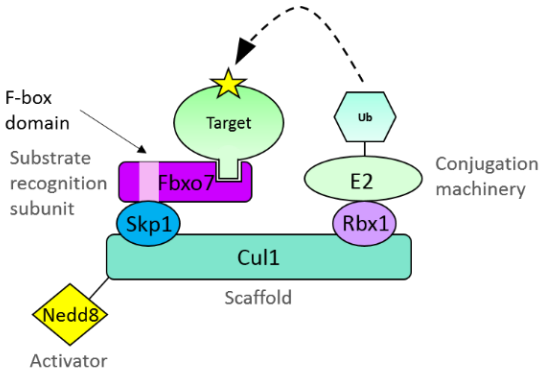

Figure 1.16 **Schematic of Fbxo7-containing SCF-type Cullin-RING ligase (CRL)**. Cullin protein 1 (Cul1) forms the complex scaffold, while Skp1 and an Fbxo7 act as substrate adaptors. Fbxo7 binds Skp1 via its F-box domain. RING-box protein 1 (Rbx1) recruits the E2 conjugating enzyme, which interacts with the E3 ligase (not shown) to ubiquitinate the target protein at a lysine residue (star). PTM Nedd8 activates the CRL.

1.6.2 Fbxo7 structure

Fbxo7 belongs to the family of F-box-containing proteins. An F-box is a ~40 amino acid protein motif which acts as a site of protein-protein interaction (Kipreos and Pagano, 2000). In the case of CRLs, the F-box motif links the FBXO to the rest of the E3 complex by binding Skp1. Two Fbxo7 isoforms are expressed in humans; isoform II is a truncated protein lacking the N-terminal Ubl of isoform I (Zhou et al., 2016). Isoform I comprises 5 functional domains: a Ubl domain, cdk6 domain, dimerization domain, F-box domain and a proline-rich domain (Figure 1.17) (Larsen and Bendixen, 2012, Ho et al., 2006). Isoform II of Fbxo7 could not be isolated from pig tissue, suggesting that it may be a very low abundance protein (Larsen and Bendixen, 2012). The dimerization (FP) domain is the site of Fbxo7 homo-dimerization and has also been shown to be present in PI31, a regulatory subunit of the proteasome which shares a similar structure and FP domain to Fbxo7. PI31 does not appear to be a substrate of SCF, as Fbxo7 knock down has no effect on PI31 expression, and it has been proposed that PI31 could act as an antagonistic regulator of SCF activity (Kirk et al., 2008, Bader et al., 2011). The proline-rich region (PRR) directly recruits substrates (Nelson et al., 2013).

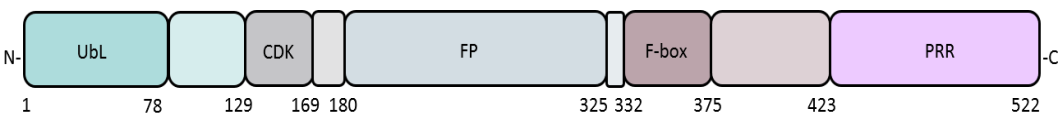

Figure 1.17 **Domain structure of human Fbxo7**. Full length isoform I comprises an N-terminal Ubl, a Cdk domain, a dimerization domain (FP), an F-box domain and a C-terminal proline-rich domain (PRR).

1.6.3 Fbxo7 and mitophagy

Fbxo7, like Parkin, has been linked to mitophagy (Burchell et al., 2013). In their 2013 study, Burchell *et al* demonstrated binding between the Fbxo7 Ubl and Parkin and significantly reduced localisation of Parkin to depolarised mitochondria in the absence of Fbxo7, together indicative of a role for Fbxo7 in Parkin recruitment. Like Parkin, mitochondrial recruitment of Fbxo7 was shown to be PINK1-dependent and over-expression of Fbxo7 was found to rescue, among other phenotypes, mitochondrial dysregulation in Parkin-null *Drosophila*. Knock down of Fbxo7 lead to a reduction in Parkin-dependent p62 recruitment, resulting in delayed lipidation of LC3-I and inhibition of autophagosomal recruitment, ultimately impeding CCCP-induced mitophagy in mammalian cells (Burchell et al., 2013).

The role for Fbxo7 in normal mitophagy was later confirmed by an independent study, in which the authors used mouse PC12 dopaminergic cells and showed that knock down of Fbxo7 impaired FCCP-induced mitophagy, while over-expression of Fbxo7 promoted mitophagy, even in the absence of mitochondrial stress (Zhou et al., 2015). Furthermore, Zhou *et al* showed that Fbxo7 accumulated under cellular stress and was found in aggregates in the *post-mortem* brains of PD and Alzheimer's disease (AD) patients, diseases which have been strongly linked to aberrant mitophagy. Disease-linked mutations in Fbxo7 also promoted its aggregation and inhibited mitophagy (Onyango et al., 2017).

1.6.4 Other roles for Fbxo7

Around 12% of FBXO proteins have so far been shown to have SCF-independent functions, with Fbxo7 being one of them. So far, demonstrable roles have included cell cycle-regulation, intracellular trafficking, transcription and mitochondrial dynamics (Nelson et al., 2013). The first-identified SCF-independent role of Fbxo7 was as a regulator of the cell cycle via its interactions with viral and cellular D cyclins, as well as cyclin-dependent kinase 6 (cdk6), which are regulators of cell cycle-progression (Laman et al., 2005). These interactions took place *in vivo* (U2OS mammalian cells) and *in vitro*, providing compelling evidence of direct, SCF-independent binding. The authors went on to show that Fbxo7 positively regulates these cell cycle proteins, acting as a proto-oncogene, and that Fbxo7 was upregulated in biopsies of human lung and colon cancers (Laman et al., 2005, Laman, 2006).

The capacity for Fbxo7 to bind with high affinity to PI31 via their FP domains has raised questions about the potential for Fbxo7 to have a regulatory role in the ubiquitin

proteasome system (UPS) (Kirk et al., 2008, Nelson et al., 2013). PI31 was initially characterised biochemically as a proteasome inhibitor, binding to the 20S barrel (Chu-Ping et al., 1992), but later *in vivo* work demonstrated that it does not inhibit proteasome activity, but rather regulates maturation of the inducible immunoproteasome (Zaiss et al., 2002). So far, there is no clear evidence for Fbxo7 and PI31 interacting to regulate mammalian proteasomal activity. However, work in *Drosophila melanogaster* (*Dm*) has shown that a partial orthologue of Fbxo7, Nutcracker, stabilises *Dm*PI31 to facilitate 26S proteasome function, and that abolishing *Dm*PI31 function results in defective protein degradation, cell cycle abnormalities and lethality. Of note, the authors observed that *Dm*PI31 binds Nutcracker via a mechanism conserved in the binding of mammalian PI31 and Fbxo7 (Bader et al., 2011).

1.7 Regulation of mitochondrial dynamics by post-translational modifications

1.7.1 Fission

The regulation of mitochondrial fission proteins utilises a diverse range of PTMs, including phosphorylation, ubiquitination, SUMOylation and nitrosylation (van der Bliek et al., 2013). The principal mediator of mitochondrial fission, Drp1, is the target of numerous PTMs.

Drp1 activity and subcellular localisation is largely regulated by its phosphorylation status. It has 3 phosphorylation sites, targeted by different kinases at different times. Serine 616 can be phosphorylated by protein kinase C (PKC) δ, Rock kinase, CDK1/Cyclin B or CAMK-Ia (Taguchi et al., 2007, Han et al., 2008, Qi et al., 2011, Wang et al., 2012c). Phosphorylation at S616 promotes Drp1 binding to other fission proteins, including Fis1, so is likely to activate mitochondrial fission (Chang and Blackstone, 2010, Han et al., 2008). Opposing this, phosphorylation of Drp1 by PKA at S637 inhibits fission by repressing GTPase activity and/or hindering mitochondrial translocation (Chang and Blackstone, 2007, Cribbs and Strack, 2007). S693 phosphorylation by GSK3β inhibits mitochondrial fission by inactivating Drp1 during apoptosis (Chou et al., 2012). It is thought that phosphorylation at this site affects GTP-hydrolysis or Drp1 oligomerisation (Chang and Blackstone, 2010).

Ubiquitination is known to regulate a number of mitochondrial dynamics proteins, including Drp1 and Fis1, which are both ubiquitinated by the MOM RING E3 ligase March5

(Nakamura et al., 2006, Yonashiro et al., 2006). Initially, ubiquitination of Drp1 was proposed to promote mitochondrial fusion (or inhibit fission), but a later study detailed evidence for ubiquitination of Drp1 promoting mitochondrial fission, potentially by mediating Drp1 trafficking to sites of mitochondrial division (Karbowski et al., 2007). In this study, Karbowski *et al* showed that expression of non-functional RING mutants of MARCH lead to abnormal mitochondrial assembly of Drp1 and aberrant mitochondrial morphology.

Drp1 was first demonstrated to be a SUMO substrate in 2004, but it was not until 2009 that its SUMO E3 ligase, mitochondria-associated protein ligase (MAPL), was identified (Harder et al., 2004, Braschi et al., 2009). The role of SUMO in Drp1 regulation remains unclear. It was initially proposed that SUMOylation of Drp1 was promoted by Bax/Bak during apoptosis and stabilised Drp1 at the mitochondria (Wasiak et al., 2007), a model which later evolved with the discovery of MAPL, which was found to function downstream of Bax/Bak and to promote stabilisation of ER/mitochondria contact sites by SUMOylating Drp1 (Prudent et al., 2015). However, other studies have found SUMOylation of Drp1 to have the opposite effect, demonstrating that SUMOylated Drp1 is sequestered in the cytosol, and that SENP3-mediated deSUMOylation facilitates its translocation to mitochondria to initiate cell death following ischaemia, probably by promoting the interaction between Drp1 and Mff on the MOM (Guo et al., 2013, Guo et al., 2017).

It has been proposed that Drp1 activity is also regulated by S-nitrosylation. Cho *et al* showed that mitochondrial fission was activated by nitric oxide (NO)-induced nitrosylation of Drp1 in AD patients, leading to neurodegeneration (Cho et al., 2009). In this study, the authors reported that NO-induced S-nitrosylation facilitated Drp1 dimerization and enhanced GTPase activity *in vitro*. However, this work was later disputed, with an independent publication finding no effect of S-nitrosylation on Drp1 GTPase activity (Bossy et al., 2010). Indeed, it has been previously established that Drp1 exists in a primarily tetrameric state under physiological conditions, so nitrosylated dimers may actually be a degradation/disassembly product (Shin et al., 1999, Zhu et al., 2004). Bossy *et al* went on to show that NO specifically induced Drp1 phosphorylation at S616, which facilitated its mitochondrial recruitment, and that nitrosylation was not specific to Drp1 nor to AD patients, with no difference in Drp1 nitrosylation between *post-mortem* brains of healthy and AD patients, and nitrosylated OPA1 also readily detected. A summary of Drp1 regulation by PTMs as described here is given in Figure 1.18 (A).

Mff, the primary receptor for Drp1, remains to be fully structurally annotated (Losón et al., 2013). There is currently little known of its domain architecture, apart from it having

an N-terminal Drp1-interacting domain and C-terminal single-pass transmembrane (TM) domain. So far, Mff has been annotated only as a target of post-translational phosphorylation at two sites, mediated by AMPK (Toyama et al., 2016). Figure 1.18 (B) depicts the Mff phosphorylation sites.

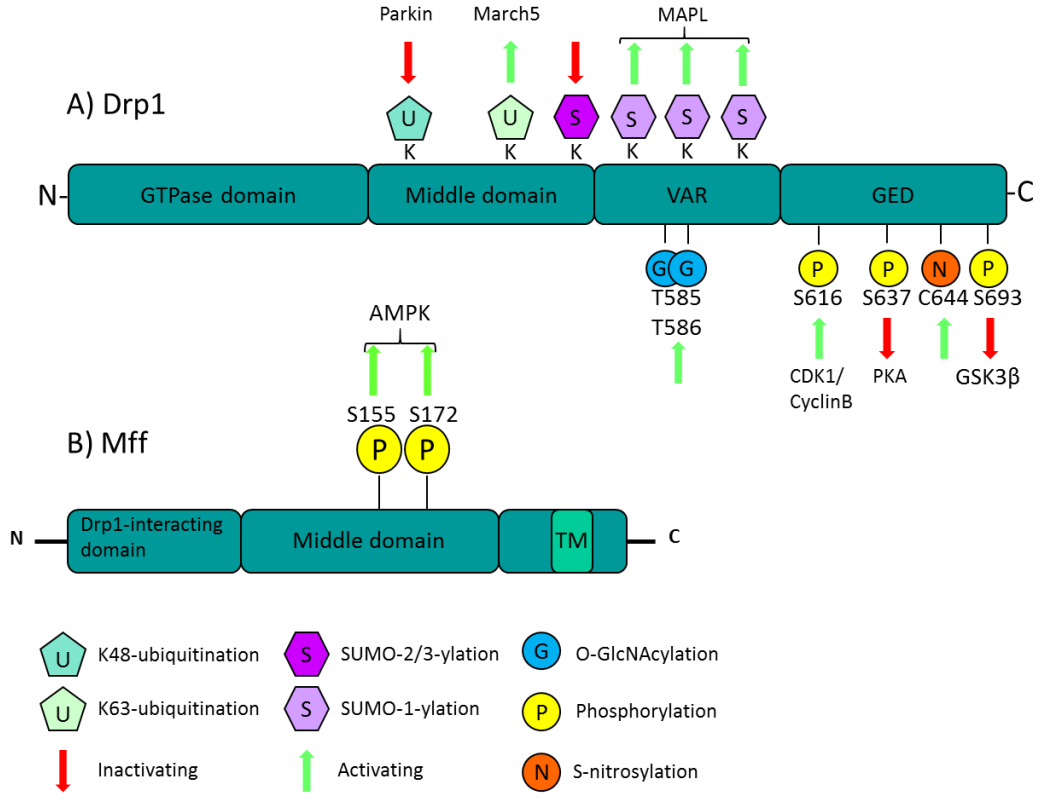

Figure 1.18 **Post-translational modifications of Drp1 and Mff.** (A) Drp1 has four domains: A N-terminal GTPase, middle domain, variable domain (VAR) and a C-terminal GTPase effector domain (GED). Parkin-mediated K48-linked ubiquitination targets Drp1 for degradation, while March5-mediated K63-linked ubiquitination stabilises the Drp1 pool. The sites of ubiquitination are not yet known. Drp1 can be SUMOylated at four residues between the middle and variable domains. SUMO-2/3-ylation is inactivating, sequestering Drp1 in the cytosol, while SUMO-1-ylation by MAPL stabilises Drp1 at mitochondria. O-linked-N-acetylglucosamine glycosylation at T585 and T586 activates fission. CDK1/Cyclin B-mediated phosphorylation at S616 activates Drp1 activity, whereas PKA-mediated phosphorylation at S637 inhibits mitochondrial translocation/GTPase activity and GSK3β-mediated phosphorylation at S693 inactivates Drp1. C644 S-nitrosylation of Drp1 is activating. (B) Mff is known to be phosphorylated at S155 and S172 by AMPK, promoting its function. Mff is characterised by an N-terminal Drp1-interacting domain and C-terminal mitochondrial anchoring region comprising a single TM domain.

1.7.2 Fusion

Proteolysis and ubiquitination are the primary post-translational regulators of mitochondrial fusion proteins; fusion dynamins of the MIM are largely regulated by

proteolytic cleavage, whereas MOM fusion dynamins are generally inactivated by ubiquitin-mediated degradation (van der Bliek et al., 2013).

The MIM fusion dynamins Mgm1 (yeast) and Opa1 (mammals) are regulated by proteolytic cleavage, but with differing effects. Here, I shall focus on the mammalian dynamin. Opa1, of which there are 8 mammalian isoforms, is cleaved in a complex pattern determined by the alternative splicing of mRNA (Olichon et al., 2007). Different isoforms are cleaved depending on the presence or absence of several short exons, which contain three distinct proteolytic cleavage sites, near the amino-terminus of Opa1; all isoforms contain the S1 cleavage site, while around half contain S2 and S3 sites. The S2 and S3 sites are constitutively cleaved in the intermembrane space by Yme1L, an AAA-protease, yielding short and long isoforms (Griparic et al., 2007, Song et al., 2007). The S1 site is only cleaved by the MIM Zn^{2+}-protease Oma-1 if the mitochondrion loses membrane potential, has low ATP levels or other quality control mechanisms are disturbed (Head et al., 2009, Ehses et al., 2009, Baricault et al., 2007). Under mitochondrial stress, this mechanism cleaves all isoforms of Opa1 within minutes, preventing inner membrane fusion well before the triggering of other stress-induced protective mechanisms like the PINK1-Parkin pathway (van der Bliek et al., 2013).

In mammals, MOM fusion dynamins Mfn1/2 are degraded via the UPS in a stress-induced manner. Upon loss of mitochondrial membrane potential, Mitofusins are degraded by the PINK1-Parkin ubiquitination pathway of mitophagy (Narendra et al., 2010). Following ubiquitination, the AAA+ protein p97, which accumulates on the surface of Parkin-positive mitochondria, excises Mfns from the MOM before they are degraded by the proteasome (Tanaka et al., 2010).

1.7.3 Mitophagy

Mitophagy is the ultimate form of mitochondrial quality control. Mitochondrial damage and/or depolarisation triggers Parkin recruitment and the ubiquitin proteasome system (UPS), resulting in ubiquitination and proteasomal targeting of MOM proteins for degradation. The remainder of the organelle is then removed via selective autophagy, known as mitophagy (Figure 1.19) (Kageyama et al., 2012, Youle and Narendra, 2011).

PINK1 is generally unstable in the mitochondrial intermembrane space (IMS) and is constitutively proteolytically degraded in healthy mitochondria (Jin et al., 2010), with a proteolytic C-terminal fragment released into the cytosol and degraded by the UPS (Yamano and Youle, 2013). Loss of membrane potential prevents PINK1 proteolysis and

allows its accumulation on the MOM, recruiting and activating Parkin (Narendra et al., 2008, Kim et al., 2008b). Parkin then poly-ubiquitinates MOM proteins with K48- and K63-linked chains, triggering their UPS-dependent degradation and reconfiguring the MOM protein composition, as well as changing the ubiquitination status of cytosolic domains of MOM proteins (Geisler et al., 2010, Sarraf et al., 2013). Mass ubiquitination on the surface of damaged mitochondria is thought to recruit ubiquitin-binding adaptors, including p62. These proteins can interact with the cellular autophagic machinery to mediate clearance of the damaged organelle (Ding et al., 2010, Lee et al., 2010, Geisler et al., 2010).

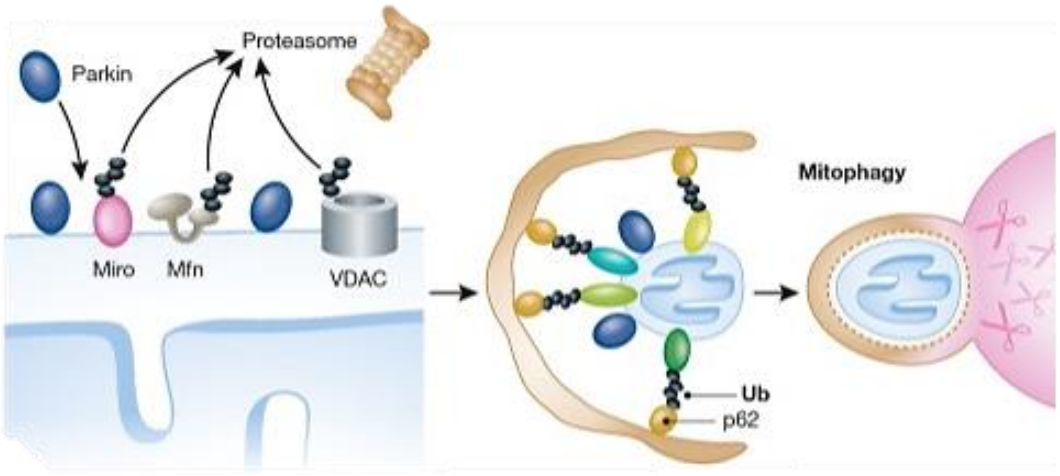

Figure 1.19 **Mitophagy of dysfunctional mitochondria is ubiquitin-dependent in mammals**. Recruitment of Parkin to the MOM of depolarised mitochondria causes ubiquitination and proteasomal degradation of MOM proteins including Miro, Mfns, and VDAC. This inhibits various processes, including mitochondrial transport (Miro) and fusion (Mfn1/2). It also triggers mitophagy by recruiting adaptors of the autophagic machinery, such as p62. Figure taken from *Escobar-Henriques, M. & Langer, T. 2014. Dynamic survey of mitochondria by ubiquitin. EMBO Rep, 15, 231-43* (Escobar-Henriques and Langer, 2014).

Parkin is largely regulated by PINK1 and its own structure, primarily existing in the cytosol in an autoinhibited state, as described in 1.5.1 and 1.5.2 (Wauer et al., 2015a). While PINK1-mediated phosphorylation of ubiquitin and of the UbL of Parkin are the major PTMs contributing to regulation of Parkin activity, further modifications have been described in the literature (Figure 1.20) (Chung et al., 2004, Rubio de la Torre et al., 2009, Vandiver et al., 2013, Imam et al., 2011).

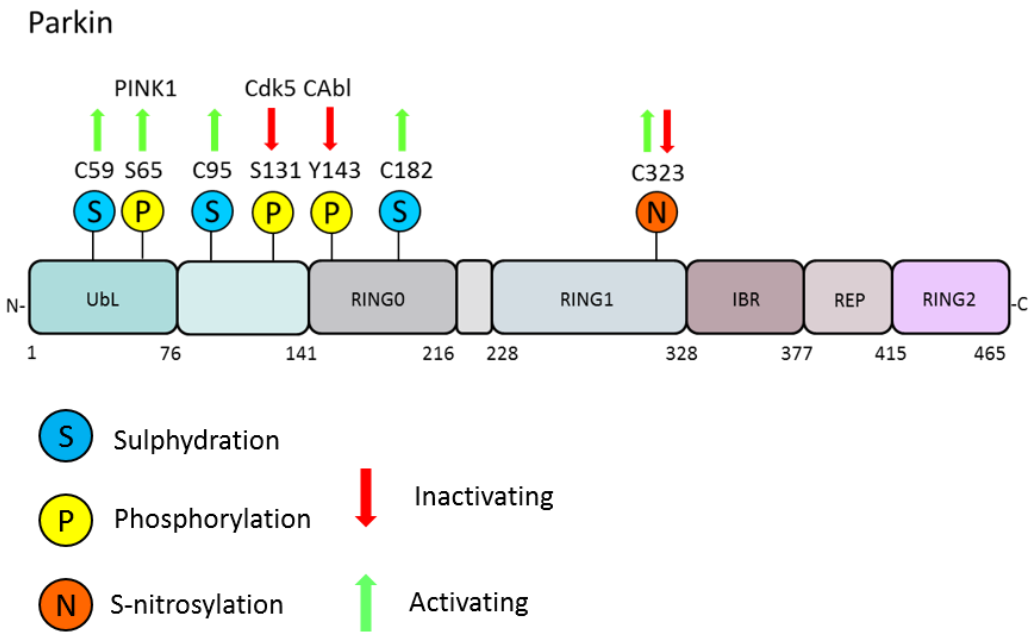

Figure 1.20 **Post-translational modifications of Parkin**. PINK1 phosphorylation of the UbL at S65 contributes to Parkin activation, along with sulphydration at C59, C95 and C182. Phosphorylation at S131 by Cdk5 or Y143 by CAbl inhibit Parkin activity. S-nitrosylation at C323 initially activates Parkin, but further S-nitrosylation (presumably at other sites) then becomes inhibitory.

1.8 Aims

The overarching aims of my PhD were to:

i. Identify mitochondria-associated proteins that are regulated by an *ex vivo* model of cardiac ischaemia/reperfusion (I/R) injury.
ii. Define the regulation of selected protein(s) in mitochondrial dynamics in cell culture models.

1.8.1 Profiling the ischaemia/reperfusion injury proteome

During ischaemia and reperfusion, the cellular proteome is vastly changed by stress-induced up- and down-regulation of protein expression. Mitochondrial dynamics and function are heavily perturbed by I/R injury, so the focus of this thesis was on regulators and post-translational modifications of these processes (Baines, 2010, Halestrap, 2010). I/R injury can be attenuated by ischaemic pre-conditioning (Kalogeris et al., 2014). Accordingly, mitochondrial regulators with differential pre-ischaemia/ischaemia expression were of particular interest. The aims of this part of my PhD project were to:

i. Use an *ex vivo* model of cardiac I/R injury to generate ischaemic damage in whole hearts.
ii. Generate a protein expression profile of mitochondrial dynamics proteins during I/R injury.
iii. Identify candidate proteins for further study, focussing on those whose mitochondrial recruitment/expression was altered by ischaemic pre-conditioning.

1.8.2 Investigating the interplay between Parkin, Fbxo7 and Mff

Levels of Parkin, Fbxo7 and Mff in the mitochondrial fraction were all altered in response to I/R injury. Parkin has previously been reported to ubiquitinate Mff (Gao et al., 2015) and to interact with Fbxo7 to mediate mitophagy (Burchell et al., 2013). I therefore wanted to investigate the interplay between these three proteins with regard to mitochondrial dynamics. In light of this, the aims of this part of the project were to:

i. Generate and/or validate knock down of Parkin and Fbxo7 in mammalian cells.
ii. Investigate the effects of Parkin/Fbxo7 knock down, focussing on Mff protein level and ubiquitination.
iii. Examine the roles of post-translational modifications in the interactions and activities of Parkin, Fbxo7 and Mff.

Chapter 2 Materials & Methods

2.1 Materials

2.1.1 Chemicals

All chemicals were obtained from Sigma-Aldrich Company Limited unless otherwise stated. Acids/solvents were purchased from Fisher Scientific unless otherwise stated.

2.1.2 Glass- and plastic-ware

0.5mL and 1.5mL microcentrifuge tubes were obtained from Eppendorf, 0.2mL and 0.5mL thin-walled PCR tubes from Starlabs, 15mL and 50mL conical Falcon tubes from Greiner, and 5mL Bijou and 30mL Universal tubes from Greiner. 14mL Cell Culture Tubes were from Bio-Rad. 10µL, 20µL, 200µL, 1000µL and 1250µL Gilson pipette tips and sterile filter tips were purchased from Starlabs. 5mL, 10mL and 25mL sterile serological pipettes were from Greiner. 24-well-, 12-well and 6-well cell culture plates, 35mm, 60mm and 100mm cell culture dishes and T25, T75 and T175 vented cell culture flasks were obtained from Greiner. Syringes and needles were from Terumo; syringe filters were from Sartorius.

2.1.3 Cell culture reagents

2.1.3.1 Cell lines

Human Embryonic Kidney (HEK293T) cells were obtained from The European Collection of Cell Cultures (ECACC). Stocks containing 1% (v/v) DMSO were stored in liquid nitrogen.

2.1.3.1.1 HEK293T Media and reagents

Dulbecco's Modified Eagle's Medium (DMEM), with Phenol Red, without Glutamine, 4.5g/L glucose, was acquired from Lonza (HEK293T cell culture) or Sigma (HEK293T viral production). Foetal Bovine Serum (FBS) was obtained from Sigma, as were Penicillin/Streptomycin and Poly-L-Lysine Hydrobromide. Phosphate-buffered Saline (PBS), sterile cell culture water, 0.05% Trypsin-EDTA and L-Glutamine were purchased from Gibco (Life Technologies). Lipofectamine 2000 transfection reagent was purchased from Invitrogen. Bortezomib (BTZ) was purchased from Cell Signalling.

2.1.4 Molecular Biology Reagents

2.1.4.1 Kits, enzymes and markers

RNeasy® RNA extraction kit was from Qiagen. RevertAid First Strand cDNA Synthesis Kit was from Thermo Fisher Scientific. KOD Hot Start DNA Polymerase kit for polymerase chain reaction (PCR) was purchased from Merck Millipore. Restriction enzymes were from New England Biolabs (NEB) and T4 DNA ligase from TaKaRa. GeneJET™ Mini- and Midi-prep kits and Gel Extraction kits were purchased from Thermo Scientific; DNA molecular weight marker (HyperLadder™ 1kB) was from Bioline.

2.1.4.2 Oligonucleotides

Lists of oligonucleotides (primers) generated and used as part of this work can be found in Table 2.1 (over-expression) and Table 2.2 (knock-down). All primers were purchased from Sigma-Aldrich.

2.1.4.2.1 Generating over-expression constructs

All primers used in the generation of over-expression constructs are listed in Table 2.1. Sequence validation of over-expression constructs was performed by Eurofins Genomics, either using primers listed in this table or using standard primers provided by Eurofins Genomics. All over-expression constructs encode the *Homo sapiens* protein (Parkin accession number: O60260). Oligonucleotide sequences are given in the 5'-3' direction, with any restriction sites underlined.

Table 2.1 Oligonucleotides used to generate mammalian over-expression constructs

Primer (cloning)	Sequence (5'-3')	Restriction site
Parkin fwd	GCGGAATTCATGATAGTGTTTGTCAGG	EcoRI
Parkin fwd	GCGAAGCTTGCCACCATGATAGTGTTTGTCAG GTTCAAC	HindIII
Parkin fwd	GCGGGATCCATGATAGTGTTTGTCAGGTTCA AC	BamHI
Parkin rev	GCGGGATCCCTACACGTCGAACCAGTG	BamHI
Parkin rev	GCGGGATCCCTACACGTCGAACCAGTGGTCC CC	BamHI
Parkin rev	CGCAAGCTTCTACACGTCGAACCAGTGGTCCC C	HindIII

Myc-Parkin fwd	GCGAAGCTTGCCACCATGGAGCAAAAGCTCA TTTCTGAG	HindIII

Primer (sequencing)	Sequence	Restriction site
Fwd Seq Parkin 250	GAGGCGACGACCCCAGAAACG	-
Fwd Seq Parkin 484	CTCAGGGTACAGTGCAGCACC	-
Fwd Seq Parkin 635	GTGGAGCACACCCCACCTCTG	-
Fwd Seq Parkin 1189	GCCGCCGAGCAGGCTCGTTGG	-

2.1.4.2.2 Generating knock-down constructs

All primers used in the generation of knock-down constructs (shRNAs) are listed in Table 2.2. Sequence validation of knock-down constructs was performed by Eurofins Genomics using standard primers. Parkin knock-down constructs were generated to target both *Homo sapiens* and *Rattus norvegicus* DNA sequences. Oligonucleotide sequences are given in the 5'-3' direction, with DNA target sequences underlined.

Table 2.2 Oligonucleotides used to generate knock-down constructs

Primer (shRNA)	Sequence (5'-3')
Parkin fwd	GATCCCCACCAGCATCTTCCAGCTCAAGTTCAAGAGACTTGAGCTGGAA GATGCTGGTTTTTTC
Parkin rev	TCGAGAAAAAACCAGCATCTTCCAGCTCAAGTCTCTTGAACTTGAGCTGG AAGATGCTGGTGGG
Fbxo7 fwd	GATCCCCCCTTTGGGAAAGCTCATCATGTTCAAGAGACATGATGAGCTTT CCCAAAGGTTTTTC
Fbxo7 rev	TCGAGAAAAACCTTTGGGAAAGCTCATCATGTCTCTTGAACATGATGAG CTTTCCCAAAGG GGG

2.1.4.2.3 Bacterial expression of proteins

All primers used in the generation of bacterial expression constructs are listed in Table 2.3. Sequence validation of expression constructs was performed by Eurofins Genomics, using standard primers provided by Eurofins Genomics. All expression constructs encode the *Homo sapiens* protein (Parkin accession number: O60260). Oligonucleotide sequences are given in the 5'-3' direction, with restriction sites underlined.

Table 2.3 Oligonucleotides used to generate bacterial expression constructs

Primer	Sequence (5'-3')	Restriction site
His-Parkin fwd	GCGGGATCCATGATAGTGTTTGTCAGGTTCAAC	BamHI
His-Parkin rev	CGCAAGCTTCTACACGTCGAACCAGTGGTCCCC	HindIII

2.1.4.3 Plasmids

2.1.4.3.1 Mammalian over-expression plasmids

All plasmids used to over-express proteins in mammalian cells are listed in Table 2.4. Over-expression constructs all encoded the human sequence of the protein of interest and were used for over-expression of desired proteins in HEK293T cells. Accession numbers: Parkin - O60260, SUMO-1 - P63165, SUMO-2 - P61956, Mff - Q9GZY8.

Table 2.4 Plasmids generated to over-express mammalian proteins

Protein	Backbone	Tag	Cloning sites
Parkin	pcDNA3.1(+)	-	5' HindIII, 3' BamHI
Parkin	pcDNA3.1(+)	Myc	5' HindIII, 3' BamHI
Parkin	pET28a	His	5' BamHI, 3' HindIII
SUMO-1	pET28a	GST	5' BamHI, 3' HindIII
SUMO-2	pET28a	GST	5' BamHI, 3' HindIII
SUMO-1	pEYFP	YFP	5' KpnI, 3' BamHI
SUMO-1 ΔGG	pEYFP	YFP	5' KpnI, 3' BamHI
SUMO-2	pEYFP	YFP	5' KpnI, 3' BamHI
SUMO-2 ΔGG	pEYFP	YFP	5' KpnI, 3' BamHI
E1E2-SUMO1	pE1E2-SUMO-1	-	5' KpnI, 3' BamHI
E1E2-SUMO2	pE1E2-SUMO-2	-	5' KpnI, 3' BamHI
Mff WT	pECFP	CFP	5' KpnI, 3' BamHI
Mff K151R	pECFP	CFP	5' KpnI, 3' BamHI
Mff E153A	pECFP	CFP	5' KpnI, 3' BamHI
Mff S155A	pECFP	CFP	5' KpnI, 3' BamHI
Mff S155D	pECFP	CFP	5' KpnI, 3' BamHI

2.1.4.3.2 Mammalian knock-down plasmids

All plasmids used to knock-down proteins in mammalian cells are listed in Table 2.5. Knock-down constructs contained sequences targeted to either human and rat DNA or only human DNA, as indicated. esiRNA was purchased from Sigma-Aldrich and was targeted to only the human DNA sequence. XhoI and BglII restriction sites were used to clone into pSUPER.

Table 2.5 Plasmids generated to knock-down mammalian proteins

Protein	Target sequence (5'-3')	Backbone	Tag	Species
Parkin shRNA	ACCAGCATCTTCCAGCTCAAG	pSUPER	mCherry	Human, Rat
Parkin shRNA	ACCAGCATCTTCCAGCTCAAG	pXLG3	GFP	Human, Rat
Fbxo7 siRNA	esiRNA pool	-	-	Human
Fbxo7 shRNA	CCTTTGGGAAAGCTCATCATG	pXLG3	GFP	Rat
PINK1 siRNA	esiRNA pool	-	-	Human

2.1.4.3.3 Bacterial expression plasmids

All plasmids used to express proteins in bacterial cells (BL21 (DE3)) are listed in Table 2.6. All constructs encoded the human form of the protein of interest. Accession numbers: Parkin - O60260, SUMO-1 - P63165, SUMO-2 - P61956.

Table 2.6 Plasmids generated to express proteins in bacteria

Protein	Region	Backbone	Tag	Cloning sites
Parkin	UbL + RING0	pET28a	His	5' BamHI, 3' HindIII
Parkin	RING0 + RING1	pET28a	His	5' BamHI, 3' HindIII
Parkin	RING-1 + IBR	pET28a	His	5' BamHI, 3' HindIII
Parkin	IBR + RING2	pET28a	His	5' BamHI, 3' HindIII
SUMO-1	Full-length	pGEX-4T1	GST	5' BamHI, 3' XhoI
SUMO-2	Full-length	pGEX-4T1	GST	5' BamHI, 3' XhoI
GST	Full-tag	pGEX-4T1	GST	5' BamHI, 3' XhoI

2.1.5 Bacterial reagents

2.1.5.1 Escherichia coli (E. coli)

Table 2.7 Competent E. coli strains

Strain	Genotype	Supplier
DH5α	F^- endA1 glnV44 thi-1 recA1 relA1 gyrA96 deoR nupG purB20 ϕ80dlacZΔM15 Δ(lacZYA-argF)U169, hsdR17($r_K^-m_K^+$), λ^-	Thermo Fisher
XL1-Blue	endA1 gyrA96(nalR) thi-1 recA1 relA1 lac glnV44 F'[::Tn10 proAB+ lacIq Δ(lacZ)M15] hsdR17(rK- mK+)	Thermo Fisher
BL21 (DE3)	B F– ompT gal dcm lon hsdSB(rB–mB–) λ(DE3 [lacI lacUV5-T7p07 ind1 sam7 nin5]) [malB+]K-12(λS)	Stratagene

2.1.5.2 Bacterial growth media

Luria-Bertani (LB) Broth (1% (w/v) tryptone, 0.5% (w/v) yeast extract and 0.5% (w/v) NaCl) was used for cultivation of *E. coli* for plasmid propagation. 2xYT Broth (1.6% (w/v) bacto-tryptone, 1% (w/v) Bact yeast extract, 0.5% (w/v) NaCl, pH7.0) was used for expression of recombinant proteins in BL21 (DE3). LB Agar (LB Broth containing 1.5% (w/v) agar) was used to plate *E. coli* for single colony selection. 100μg/mL ampicillin, 25μg/mL kanamycin or 34μg/mL chloramphenicol were added to media to enable antibiotic resistance-dependent selection. Protein expression was induced by addition of Isopropyl β-D-1-thiogalactopyranoside (IPTG, Sigma Aldrich) to a final concentration of 0.2mM.

2.1.6 Protein Biochemistry

2.1.6.1 Cell/tissue lysis, immunoprecipitation

N- Ethylmaleimide (NEM) was purchased from Sigma Aldrich, cOmplete™ Protease Inhibitor Cocktail Tablets were purchased from Roche Diagnostics GmbH, and Phosphatase Inhibitor Cocktail 2 was purchased from Sigma Aldrich. Pierce® BCA Protein Assay Kit was purchased from Thermo Fisher Scientific. Glutathione Sepharose® 4 Fast Flow and Ni-NTA Sepharose® 4 Fast Flow were obtained from GE Healthcare Life Sciences. GFP-Trap® beads were bought from Chromotek.

2.1.6.2 SDS-PAGE and Western blotting

Prestained molecular weight marker PageRuler was purchased from Thermo Scientific. 30% (v/v) 37.5:1 acrylamide:bis-acrylamide mix was purchased from Geneflow Limited. Immobilon-PVDF membrane (0.45µm) and Whatman blotting paper (3CHR) were obtained from Millipore and GE Healthcare Life Sciences respectively. Non-fat milk powder was from The Co-operative (own brand) and Bovine Serum Albumin (BSA) was from Sigma-Aldrich. SuperSignal™ West-Pico and –Femto Chemiluminescence substrates were purchased from Thermo Scientific and Luminata™ Crescendo and Forte were purchased from Millipore. CL-Xposure™ X-ray film was obtained from Thermo Scientific and Hypercasettes™ were bought from Amersham Biosciences.

2.1.6.3 Antibodies

2.1.6.3.1 Primary antibodies

Primary antibodies were diluted in TBS-T (1x Tris-buffered saline, 0.1% (v/v) tween) containing 5% (w/v) milk, apart from phospho-ubiquitin, SENP3 and SUMO antibodies, which were diluted in 4% (w/v) BSA in TBS-T. A complete list of antibodies, dilutions and suppliers can be found in Table 2.8.

Table 2.8 Primary antibodies used for Western blotting

Antibody	Species	Dilution	Supplier	Cat. No.
β-actin	Mouse	1:10,000	Sigma-Aldrich	A5441
Cleaved Caspase 3	Rabbit	1:1000	Cell Signalling	5A1E 9664S
Drp1	Mouse	1:1000	BD Biosciences	611112
Dyn2	Mouse	1:1000	Sigma-Aldrich	SAB4200661
Fbxo7	Rabbit	1:5000	Aviva Systems Biology	ARP43128_P050
Fis1	Rabbit	1:1500	ProteinTech	10956-1-AP
FLAG	Mouse	1:10,000	Sigma-Aldrich	M2 F1804
GAPDH	Mouse	1:20,000	Abcam	6C5 Ab8245
GFP	Rat	1:10,000	Chromotek	3H9
GST	Goat	1:10,000	GE Healthcare	27-4577
HA	Mouse	1:1000	Sigma-Aldrich	H3663 HA-7
Hexokinase II	Rabbit	1:1000	Cell Signalling	C64G5 2867S
His	Rabbit	1:1000	Santa Cruz	H-15 sc-803
Lamin B	Goat	1:1000	Santa Cruz	C20 sc-6216

LC3 A/B	Rabbit	1:1000	Cell Signalling	D3U4C 12741S
MAPL	Rabbit	1:1000	Abcam	Ab155511
Mff	Mouse	1:2000	Santa Cruz	C11 sc-398731
Mitofusin II	Rabbit	1:1000	Cell Signalling	D2D10 9482S
c-Myc	Mouse	1:1000	Santa Cruz	9E10 sc-40
Parkin	Mouse	1:1000	Santa Cruz	PRK8 sc-32282
PINK1	Rabbit	1:1000	Novus Biologicals	BC100-494
PINK1	Rabbit	1:1000	Cell Signalling	D83G 6946
SUMO-1	Rabbit	1:1000	Cell Signalling	4930S
SUMO-2/3	Rabbit	1:1000	Cell Signalling	18H8 4941S
T7	Mouse	1:10,000	Novagen	69522
Ubiquitin	Mouse	1:1000	Cell Signalling	P4D1 3936S
VDAC-1/2/3	Rabbit	1:1000	Santa Cruz	FL-283 sc-98708

2.1.6.3.2 Secondary antibodies

Anti-goat, -mouse, -rabbit and –rat Horseradish Peroxidase (HRP)-conjugated IgG secondary antibodies were purchased from Jackson ImmunoResearch and diluted 1:10,000 in 5% (w/v) milk or 4% (w/v) BSA in TBS-T, depending on primary antibody.

2.1.6.4 Electrical Equipment

Sterile cell cultures hoods and cell culture incubators were from Holten LaminAir and RS Biotech, respectively. Bacterial incubators were from New Brunswick Scientific and LTE Scientific. Gel electrophoresis power packs were from Bio-Rad Laboratories. Centrifuges were from Beckman-Coulter and Jouan; benchtop microcentrifuges were from Eppendorf. PCR Thermocycler (PTC-2000) was from MJ Research. The automated medical X-ray film developer (SRX-101A) was from Konica. Cell imaging was performed on a SP5-II confocal laser scanning microscope attached to a DMI 6000 inverted epifluorescence microscope, both from Leica.

2.2 Methods

2.2.1 Eukaryotic Cell Culture

All cell culture techniques were performed using aseptic technique and under sterile conditions in a laminar flow hood (Holten LaminAir). Media and other reagents (unless otherwise stated) were pre-heated to 37°C in a water bath prior to use. Cells were incubated at 37°C in a humidified cell culture incubator (RS Biotech), supplied with 5% CO_2 and 95% O_2.

2.2.1.1 Culture of HEK293T cells

Aliquots of frozen HEK293T (Human Embryonic Kidney 293 with mutant version of the SV40 large T antigen, (Lebkowski et al., 1985)) cells were taken from the cryostore, thawed at 37°C in a water bath and transferred into a 15mL Falcon tube with 9mL Dulbecco's Modified Eagle's Medium (DMEM), supplemented with 2mM L-Glutamine, 10% (v/v) Foetal Bovine Serum (FBS) and 1% (v/v) Penicillin/Streptomycin ('complete DMEM'). The cell suspension was centrifuged at 1000 x g for 2 minutes at room temperature (RT). DMEM was aspirated (to remove DMSO) and the cells re-suspended in 1mL complete DMEM. This suspension was transferred to a T25 flask containing 5mL complete DMEM. This was incubated for 24 hours and then passaged into a T75 containing 20mL complete DMEM. HEK293T cells were subsequently cultured in a T75 flask with 20mL complete DMEM and passaged approximately twice per week.

2.2.1.1.1 Passaging of HEK293T cells

HEK293T cells were passaged upon reaching 80-90% confluency. Complete DMEM was aspirated from the flask and the cell monolayer was gently washed with 10mL 1x Phosphate Buffered Saline (PBS). PBS was then aspirated and 1mL Trypsin-EDTA was added to the cells and the flask returned to the incubator for 3 minutes. Individual cells were detached from the flask by gentle tapping before 9mL complete DMEM was added to quench the trypsin digest. The cell suspension was then centrifuged in a 15mL Falcon tube at 1000 x g for 2 minutes to pellet the cells. DMEM was then aspirated and the cells resuspended by gentle trituration in 10mL fresh complete DMEM. For maintenance of HEK293T stock flask, this suspension was diluted 1:20 in complete DMEM in a new T75. For transfection, cells were plated on 35mm (120-150µL cell suspension in 2mL DMEM) or 60mm (250-350µL cell suspension in 5mL DMEM) plastic cell culture dishes pre-coated with 0.1mg/mL poly-L-lysine.

2.2.1.1.2 Transfection of HEK293T cells

Cells were transfected 20-24 hours after plating (at around 70% confluency). Depending on construct expression levels, ≤3µg DNA was transfected in 35mm dishes and ≤8µg DNA in 60mm dishes. DNA was added to 100µL plain DMEM in a 1.5mL Eppendorf tube, and 1.5µL Lipofectamine 2000 per µg DNA were added to 100µL plain DMEM in another 1.5mL Eppendorf tube (e.g. 3µL Lipofectamine 2000 for 2µg DNA) and left to equilibrate at room temperature (RT) for 5 minutes. The Lipofectamine 2000 suspension was then added to the DNA suspension and mixed by inversion, then incubated at RT for a further 20 minutes to allow complex formation. During this time, cells were gently washed twice in plain DMEM and thereafter cultured in 'transfection DMEM' (DMEM supplemented with 2mM L-Glutamine and 10% (v/v) FBS). The transfection mix was then added drop-wise and cells incubated for 48-72 hours.

2.2.1.1.3 Poly-L-Lysine coating of dishes

For transfection of HEK293T cells, cell culture dishes were first coated with 0.1mg/mL poly-L-lysine (PLL), to promote cell adhesion. PLL was diluted to 0.1mg/mL in sterile cell culture water and used to coat the bottom of dishes. Dishes were incubated at 37°C for ≥ 1 hour, then washed 4 times with sterile cell culture water prior to cell plating.

2.2.1.2 Oxygen-glucose deprivation

Oxygen-glucose deprivation (OGD) was used as a cell model of ischaemia. Cells were transferred into an anaerobic chamber (95% N_2, 5% CO_2) at 37°C, washed once with de-oxygenated 1x PBS, and incubated in de-oxygenated, glucose-free media. Control cells were washed once in 1x PBS and incubated in fresh, oxygenated, glucose-containing media in a normal cell culture incubator at 37°C for the same period of time. Cells were lysed or fixed in the anaerobic chamber to prevent reperfusion.

2.2.2 Molecular Biology

2.2.2.1 RNA Extraction from cells

RNA was purified from cells using the RNeasy® kit (Qiagen), according to the manufacturer's protocol. RNA concentration was quantified using the NanoDrop™ ND-1000 (LabTech) and its corresponding software. Distilled water (dH_2O) was used for reference and absorbance was measured at wavelengths of 260 and 280nm to ascertain purity in accordance with the Beer-Lambert law.

2.2.2.2 cDNA synthesis

cDNA was synthesised from RNA using the RevertAid First Strand cDNA Synthesis Kit (Thermo Fisher Scientific), in accordance with the manufacturer's protocol. Oligo$(dT)_{18}$ primers were used to selectively bind to the poly(A) tail of mRNAs and generate a cDNA library. DNA concentration was quantified using the NanoDrop™ ND-1000 (LabTech) and its corresponding software. Distilled water (dH_2O) was used for reference and absorbance was measured at wavelengths of 260 and 280nm to ascertain purity in accordance with the Beer-Lambert law.

2.2.2.3 Polymerase Chain Reaction

Polymerase Chain Reaction (PCR) was used to amplify DNA fragments or interest using custom oligonucleotide primers synthesised by Sigma Aldrich. PCR reactions were mixed in 0.5mL PCR tubes using the high fidelity KOD Hot Start DNA Polymerase kit. Reactions were prepared as indicated in Table 2.9.

Table 2.9 PCR components

Component	Volume (µL)	Final Concentration
10 x Buffer	5	1x
dNTP mix (2mM each)	5	0.2mM
$MgSO_4$ (25mM)	3	1.5mM
DMSO	2.5	5%
Sense (5') primer (10µM)	1.5	0.3µM
Antisense (3') primer (10µM)	1.5	0.3µM
Template DNA (1ng/µL)	10	0.2ng/µL
dH_2O	20.5	-
KOD Hot Start Polymerase (1.0 U/µL)	1	0.02U/µL
Total Volume (µL)	**50**	

The PCR reaction was carried out in a thermocycler under the conditions outlined in Table 2.10 depending on size of required DNA fragment.

Table 2.10 PCR conditions

	Target Size			
Step	<500bp	500-1000bp	1000-3000bp	>3000bp
1. Polymerase activation	95°C for 2 minutes			
2. Double – strand denaturation	95°C for 20 seconds			
3. Primer annealing	55°C for 10 seconds			
4. Primer extension	70°C for 10 s/kb	70°C for 15 s/kb	70°C for 20 s/kb	70°C for 25 s/kb
5. Repeat steps 2-4	20-40 cycles			
6. Final extension	70°C for 5 minutes			
7. Cooling	10°C for 5 minutes			

2.2.2.4 Site-Directed Mutagenesis

Site-Directed Mutagenesis (SDM) was used to insert point substitution mutations into DNA constructs. Sense and antisense oligonucleotides including the mutated codon and 21bp either side were used in a standard, 20-cycle PCR reaction (as described in 2.2.2.3), with the extension time calculated for the full length of the plasmid. Wild-type (WT) DNA was removed by digest of methylated plasmid within the PCR products with DpnI (20U, 1 hour, 37°C). 5µL of the cleaned PCR product were then used to transform 50µL DH5α, which were then plated on LB agar plates containing 25 µg/mL kanamycin or 100 µg/mL ampicillin to obtain single colonies. Several colonies were screened for the mutation by DNA sequencing following DNA Mini-Prep.

2.2.2.5 Agarose Gel Electrophoresis

0.8 - 1.5% (w/v) agarose gels containing 0.5µg/mL ethidium bromide were used to resolve cleaned DNA products. 6x DNA loading dye (30% (v/v) glycerol, 0.25% (v/v) xylene cyanol, 0.25% (w/v) bromophenol blue) was diluted in the DNA sample to a final concentration of 1x. The gel was immersed in 0.5x TAE buffer (20mM Tris acetate, 0.5mM EDTA) in a Mupid-exU electrophoresis system (Mupid Co. Ltd) and samples loaded alongside HyperLadder™ 1kb molecular weight marker. Samples were run under constant voltage (135V) for 20 minutes, and bands visualised on a UV transilluminator (Ultra-Violet Products Ltd).

2.2.2.6 PCR Product Purification

DNA was cleaned up following PCR using the GeneJET Gel Extraction kit (Thermo Scientific) in accordance with the manufacturer's protocol and eluted in 50µL dH_2O.

2.2.2.7 Restriction Digest

Plasmid DNA (1µg) or cleaned PCR product (50µL) were incubated with 20U of the appropriate restriction enzyme at 37°C for 2 hours as indicated in Table 2.11, then re-purified and eluted in 25µL dH_2O.

Table 2.11 Restriction digest components

Component	Volume (µL)	Final Concentration
DNA	50 plasmid DNA (0.02µg/µL) or 50 PCR product	0.5µg/µL plasmid DNA
Restriction enzyme	2 (10U/µL)	0.2U/µL
NEB Buffer	10 (10x)	1x
dH_2O	38	-
Total Volume (µL)	**100**	

2.2.2.8 Sticky end Ligation

Equal volumes of digested and cleaned PCR product and plasmid DNA were resolved on 0.8 – 1.5% (w/v) agarose gels containing 0.5µg/mL ethidium bromide to approximate the insert:vector ratio. DNA was diluted appropriately in dH2O to obtain a

3:1 insert:vector molar ratio for efficient ligation. 1µL each of insert and vector DNA were added to 2µL TaKaRa T4 ligase Solution I (2x concentrate), mixed and incubated for 30-60 minutes at RT. A separate ligation with dH_2O in place of insert DNA was carried out to control for vector re-ligation.

2.2.2.9 *E. coli* Transformation

To amplify DNA constructs, 1µL mini-/midi-prep DNA or 4µL ligation mix were mixed with 10µL or 50µL, respectively, competent *E. coli*. XL-1 Blue *E. coli* were used for amplification of pXLG3 constructs. DNA/*E. coli* mix was incubated on ice for 30 minutes, heat shocked at 42°C for 90 seconds and placed back on ice for 2 minutes. In the case of kanamycin-resistant plasmids, 100µL plain LB broth were added to the mix and incubated at 37°C for 1 hour, to allow expression of the antibiotic resistance. *E. coli* cells were then plated on LB agar plates containing the appropriate selection antibiotic (100µg/mL ampicillin, 25µg/mL kanamycin or 34µg/mL chloramphenicol) and incubated overnight at 37°C. The following day, single colonies were picked for mini-prep and insert-screening (ligated DNA), or midi-prep (amplification of plasmid DNA).

2.2.2.10 DNA Mini-Prep and screening

Single bacterial colonies were picked from an agar plate the day after transformation. Colonies were streaked on a fresh agar plate containing the appropriate selection antibiotic (100µg/mL ampicillin, 25µg/mL kanamycin or 34µg/mL chloramphenicol) and dropped into a cell culture tube containing 2mL LB broth and selection antibiotic. Agar plates were incubated overnight at 37°C, and culture tubes were incubated overnight at 37°C in a shaking incubator. Plasmid DNA was isolated from the bacterial suspension culture using the GeneJET™ Plasmid Mini-Prep kit in accordance with the manufacturer's protocol. DNA was eluted in 50µL dH_2O and screened for presence of a correctly sized insert by restriction digest and agarose gel electrophoresis. DNA containing an appropriately sized insert was validated by DNA sequencing.

2.2.2.11 Plasmid DNA Sequencing

Prior to use in experiments, all DNA constructs were validated by DNA sequencing. This was carried out by Eurofins Genomics. Plasmids containing the correct sequence were amplified by midi-prep.

2.2.2.12 DNA Midi-Prep

The streak colony corresponding to mini-prep DNA validated by sequencing was picked and cultured overnight at 37°C in 100mL LB broth containing the appropriate selection antibiotic (100µg/mL ampicillin, 25µg/mL kanamycin or 34µg/mL chloramphenicol) in a shaking incubator. DNA was purified according to the manufacturer's protocol using the GeneJET™ Plasmid Midi-Prep kit. DNA was eluted in 350µL dH_2O, and its concentration and purity measured using a NanoDrop™ ND-1000 prior to transfection into cells.

2.2.2.13 shRNA Synthesis

Protein knockdown was achieved using shRNAs targeted to regions within the gene of interest. 5'-phosphorylated oligonucleotides (custom-made, Sigma Aldrich) were dissolved in TE Buffer (1M Tris pH8.0, 100mM EDTA) to a final concentration of 100µM. 2µL each of the sense and antisense oligonucleotides were mixed, heated at 95°C for 4 minutes to denature any secondary structures, and left at RT for 30 minutes to anneal. 1µg pSUPER was digested with restriction enzymes corresponding to restriction sites that would allow the target sequence to be in-frame and match the overhang of the annealed primers, as described in 2.2.2.7. The annealed primers were diluted 1:250 in dH_2O, then 1µL primer mix, 1µL cut vector and 2µL TaKaRa DNA Ligase T4 Solution I were mixed and incubated for 30 minutes at RT. The ligation mix was then transformed into 40µL competent DH5α, plated on agar containing 100µg/mL Ampicillin, and incubated overnight at 37°C. Single colonies were picked for screening as described in 2.2.2.10/11, and DNA amplified as described in 2.2.2.12.

2.2.3 Biochemical Methods

2.2.3.1 Cell Lysis

Cells were lysed on ice and in the presence of protease inhibitors (cOmplete™ Protease Inhibitor Cocktail Tablets, Roche) to minimise protein degradation. The cell monolayer was washed twice with ice-cold 1x PBS and lysed in 200µL (35mm dish) or 500µL (60mm dish) lysis buffer (25mM HEPES pH7.4, 150mM NaCl, 1% (v/v) Triton X-100, 0.1% (w/v) SDS, 1x protease inhibitors) and the lysate scraped into a 1.5mL Eppendorf tube. When SUMO-conjugates were of interest, N-Ethylmaleimide (NEM, Sigma Aldrich), a cysteine protease inhibitor which irreversibly inhibits SENPs, was added to a final

concentration of 20mM. Lysates were sonicated (5x 1-second pulses) and incubated on ice for 15 minutes. Lysates were then centrifuged at 16,000 x g at 4°C from 15 minutes to pellet insoluble debris. The cleared lysate was then added to an equal volume of 2x Laemmli sample buffer (4% SDS (w/v), 10% glycerol (v/v) 125mM Tris-HCl pH6.8, 0.004% bromophenol blue (w/v), 10% (v/v) 2-β-mercaptoethanol) to give a final concentration of 1x Laemmli sample buffer. Samples were heated at 95°C for 10 minutes and centrifuged at 16,000 x g for 1 minute prior to use for SDS-PAGE.

2.2.3.2 Immunoprecipitation by GFP-Trap®

60mm dishes of cells were lysed in 500µL lysis buffer (20mM Tris pH7.4, 137mM NaCl, 2mM sodium pyrophosphate, 2mM EDTA, 1% (v/v) Triton X-100, 0.1% (w/v) SDS, 25mM β-glycerophosphate, 10% glycerol (v/v), 1x cOmplete™ protease inhibitors, 20mM NEM) and the lysate scraped into a 1.5mL Eppendorf tube. Lysates were sonicated briefly (5x 1-second pulses) and incubated on ice for 30 minutes. Lysates were then centrifuged at 16,000 x g at 4°C from 15 minutes to pellet insoluble debris. 5µL GFP-Trap® bead suspension were aliquoted into a 1.5mL Eppendorf tube per sample and washed twice with 500µL wash buffer (20mM Tris pH7.4, 137mM NaCl, 2mM sodium pyrophosphate, 2mM EDTA, 1% (v/v) Triton X-100, 0.1% (w/v) SDS, 25mM β-glycerophosphate, 10% glycerol (v/v)). Washes were carried out by gently inverting tubes to mix and centrifuging at 1180 x g for 2 minutes to pellet beads. 20µL cleared lysate were kept on ice as an input sample, and the remaining lysate was added to the washed GFP-Trap® beads. The bead/lysate suspension was then incubated on a spinning wheel at 4°C for 90 minutes. Beads were pelleted and washed 3 times as before. Wash buffer was aspirated and 40µL 2 x Laemmli sample buffer added to the beads. 20µL 2 x Laemmli sample buffer were added to the input samples and all samples were briefly vortexed and heated at 95°C for 10 minutes. Samples were then centrifuged at 16,000 x g for 1 minute prior to use for SDS-PAGE.

2.2.3.3 BCA Assay

BCA assays were performed in duplicate in 96-well plate format. Albumin standards were prepared by serial dilution as described in the manufacturer's protocol. Sufficient working reagent for 200µL/well was prepared by mixing 50 parts BCA reagent A with 1-part BCA reagent B. 10µL each unknown sample and BSA standards were pipetted into the wells of a 96-well plate. 200µL working reagent were then added to each well and the plate shaken for 30 seconds, before being covered and placed in a 37°C incubator for 30 minutes. Absorbance was measured at 570nm using a VersaMax Microplate Reader

(Molecular Devices). The blank value was subtracted from all sample/standard values and a standard curve plotted as the average measurement from each BSA standard vs. its concentration (µg/mL). This was then used to determine the concentration in µg/mL of the unknown samples.

2.2.3.4 SDS-PAGE

Proteins were resolved according to their molecular weight (MW) using previously described methods (Laemmli, 1970) by Sodium Dodecyl Sulphate-Polyacrylamide Gel Electrophoresis (SDS-PAGE). 10-15% resolving gels (375mM Tris-HCl pH8.8, 10-15% (w/v) acrylamide, 0.1% (w/v) SDS, 0.1% (w/v) ammonium persulphate (APS), 0.01% (v/v) tetramethylethylenediamine (TEMED, Bio-Rad Laboratories Inc.)) were cast in 1.5mm glass plates according to the manufacturer's protocol (Bio-Rad). The resolving gel was overlaid with butan-1-ol and left at room temperature (RT) to polymerise. Following removal of butan-1-ol, the 4% stacking gel (125mM Tris-HCl pH6.8, 4% (w/v) acrylamide, 0.1% (w/v) SDS, 0.1% (w/v) APS, 0.01% (v/v) TEMED) was cast on top of the resolving gel and a 10- or 15-well comb inserted into the stacking gel, which was then left at RT to polymerise.

Polymerised gels were mounted into the electrophoresis tanks (BioRad Mini-Protean II) in accordance with the manufacturer's protocol. Running Buffer (25mM Tris base, 250mM glycine, 0.1% (w/v) SDS) was used to fill the central and bottom tank reservoirs. Protein samples in Laemmli buffer were loaded into the wells alongside 5µL molecular weight marker (PageRuler™ Prestained Protein Ladder, Thermo Scientific). SDS-PAGE was carried out at 80V until samples had cleared the stacking gel, and then at 180V until the dye front reached the bottom of the gel. Gels were then removed from the glass plates and used either for staining with Coomassie Brilliant Blue or transferred to membrane for immunoblotting.

2.2.3.5 Coomassie Brilliant Blue Staining

Proteins in acrylamide gels following SDS-PAGE were fixed and stained in Coomassie Brilliant Blue stain (50% (v/v) methanol, 10% (v/v) glacial acetic acid, 0.25% (w/v) Coomassie Brilliant Blue) for 1 hour at room temperature (RT), gently shaking. Excess stain was then removed by incubation overnight at RT, shaking, in De-staining solution (50% (v/v) methanol, 10% (v/v) glacial acetic acid), leaving only protein-bound stain.

2.2.3.6 Western Blotting

2.2.3.6.1 Wet Transfer

Following SDS-PAGE, proteins were transferred onto 0.45µm Immobilon-Polyvinyl Difluoride (PVDF, Millipore) by wet transfer. PVDF membrane was activated in methanol for 5 minutes and then equilibrated in Transfer Buffer (50mM Tris base, 40mM glycine, 20% (v/v) methanol) for 5 minutes. 6 sheets of filter paper (Whatman™) and 2 sponges per transfer were also soaked in Transfer Buffer. Bio-Rad Wet Transfer apparatus was used according to the manufacturer's protocol. The acrylamide gel was excised from the glass plates and laid carefully on top of 3 sheets of filter paper and a sponge, adjacent to the cathode. PVDF membrane was then laid over the gel, followed by a further 3 sheets of filter paper and another sponge, so that the membrane was adjacent to the anode. The Bio-Rad cassette was then placed back into the electrophoresis tank, which was filled with Transfer Buffer. Transfer was performed at 400mA for 70-90 minutes, with constant cooling and stirring of the buffer.

2.2.3.6.2 Immunoblotting

Following transfer, PVDF membranes were briefly washed in TBS-T (200mM Tris, 137mM NaCl, 0.1 (v/v) Tween-20, pH7.4). Membranes were then blocked at room temperature (RT) for 1 hour in 5% (w/v) non-fat dry milk or 4% (w/v) Bovine Serum Albumin (BSA) in TBS-T, shaking, according to manufacturer's directions for use of the antibody required. Primary antibodies were diluted to an appropriate concentration (1:1000-1:20,000), according to manufacturer's directions in 2.5% (w/v) non-fat dry milk or 2% (w/v) BSA in TBS-T and incubated with membranes at 4°C overnight, or RT for 1 hour, shaking. Excess primary antibody was removed from the membrane by washing 3 times (3 x 5-minute washes in TBS-T, shaking), and Horseradish Peroxidase- (HRP-) conjugated secondary antibody, diluted 1:10,000 in 5% (w/v) non-fat dry milk or 4% (w/v) BSA in TBS-T, incubated with the membrane at RT for 1 hour. The membrane was then washed again 3 times in TBS-T, as before.

2.2.3.6.3 Developing

Membranes were developed using enhanced chemiluminescence (ECL) as a substrate for the HRP-conjugated secondary antibody. Membranes were incubated face-down in ECL substrate for 2 minutes, then excess ECL substrate was removed and membranes sealed between two sheets of transparency film in a developing cassette

(Amersham). Signal was detected by exposing CL-Xposure™ X-ray film (Thermo Scientific) to the membrane in a dark room and processing in an automated X-ray film developer (Konica SRX-101A medical film processor). Up to 4 ECL substrates were used, depending on sensitivity required. These are listed in Table 2.12 in order of increasing sensitivity.

Table 2.12 Substrates for chemiluminescence

ECL Substrate	
SuperSignal® West-Pico (Thermo Scientific)	
Luminata™ Crescendo (Millipore)	↓ *Increasing sensitivity*
Luminata™ Forte (Millipore)	
SuperSignal® West-Femto (Thermo Scientific)	

2.2.3.6.4 Stripping blots

To re-probe the blot for further proteins, the membrane was stripped of bound antibody in Restore™ PLUS Western Blot Stripping Buffer (Thermo Fisher Scientific) at 60°C for 20 minutes. The membrane was then was 3 times in TBS-T, re-blocked in 5% (w/v) non-fat dry milk or 4% (w/v) BSA in TBS-T for 1 hour before incubation with the appropriate primary antibody.

2.2.3.6.5 Quantification of Immunoblots

Films were scanned, and blots analysed by scanning densitometry. Pixel intensity of bands was quantified using ImageJ software (NIH). Relative band intensity was reported as the area under each peak. Numerical values were exported to Microsoft Excel, where raw values were normalised to appropriate controls. These data were then exported to GraphPad Prism for statistical analysis. As appropriate, two-tailed unpaired Student's *t*-tests (with or without Welch's correction, depending on reported group variance), one-way analysis of variance (ANOVA) with Bonferroni's or Welch's correction for multiple comparisons or two-way ANOVA with appropriate correction were performed. Error bars represent Standard Error of the Mean (SEM). Unless otherwise stated, statistical significance is reported as: *p<0.05, **p<0.01, ***p<0.001, ****p<0.0001.

Chapter 3 *Ex vivo* modelling of Ischaemia/Reperfusion injury

3.1 Introduction

Cardiovascular diseases (CVD) are a primary cause of morbidity and mortality worldwide, with more than 7 million people living with CVD in the UK alone (Mittal et al., 2018). Of the CVDs, Ischaemic Heart disease (IHD) is the most common, and the leading cause of death worldwide (Mozaffarian et al., 2015). IHD occurs when build-up of atheroma narrows the coronary arteries. This can result in angina and, if the arterial occlusion is great enough, myocardial infarction.

3.1.1 Ischaemia/reperfusion injury is largely mitochondrial

Disruption of blood-flow to tissue causes oxygen- and glucose-deprivation (OGD), triggering a switch from aerobic to anaerobic respiration. This causes intracellular acidification, energy depletion and perturbations to ion homeostasis, leading to cardiac dysfunction and cell death. Low levels of residual oxygen during ischaemia also contribute to generation of reactive oxygen species (ROS) within the myocardium.

Paradoxically, rapid restoration of glucose and oxygen to the tissue may lead to greater damage, known as Ischaemia/reperfusion injury (I/R injury) (Kalogeris et al., 2014). I/R injury is multifactorial; however, mitochondrial dysfunction is thought to play a fundamental role, triggering a cascade of events which may ultimately result in cell death (Baines, 2010). A burst in ROS production, along with elevated levels of Ca^{2+} ions, lead to opening of the mitochondrial Transition Permeability Pore (mPTP). The mPTP is a non-selective channel which plays a crucial role in reperfusion injury. mPTP opening greatly increases the permeability of the mitochondrial membrane to solutes, resulting in release of cytochrome *c* from the mitochondrion and permanent loss of Adenosine Triphosphate (ATP), thus driving cell death (Halestrap, 2010). Some of the mitochondrial effects of I/R injury are illustrated in Figure 3.1 (Cadenas, 2018).

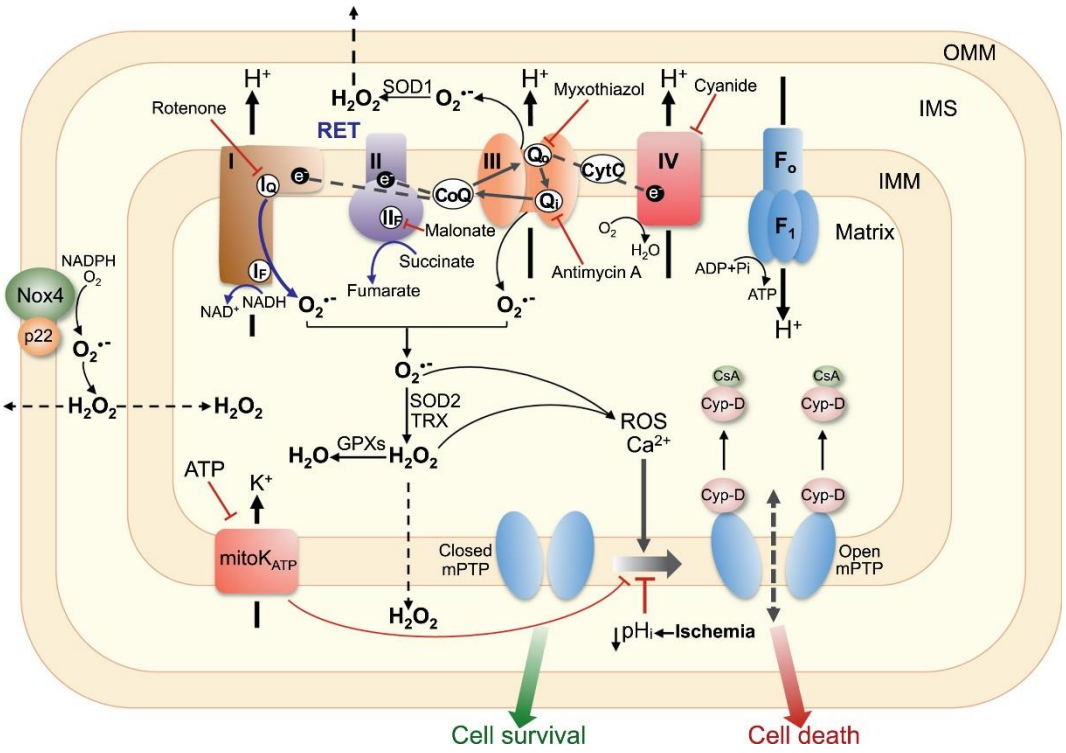

Figure 3.1 **ROS generation and mPTP opening during reperfusion.** Mitochondrial ROS are generated by electrons leaking from the electron transport chain, resulting in incomplete reduction of oxygen to superoxide (O2•-). During early reperfusion, reverse electron transport (driven by succinate) causes superoxide production. Mitochondrial NOX4 contributes to generation of H_2O_2. mPTP formation is promoted by ROS and Ca^{2+} but inhibited by acidosis. Ischaemia-effected low pH inhibits transition pore formation but, upon reperfusion, restoration of pH, Ca^{2+} overload and excessive ROS induce pore formation, leading to cell death. CyP-D enhances pore Ca^{2+}-sensitivity. Figure taken from *Cadenas, S. 2018. ROS and redox signaling in myocardial ischemia-reperfusion injury and cardioprotection*. *Free Radic Biol Med,* 117, 76-89 (Cadenas, 2018).

3.1.2 Ischaemic Preconditioning is protective against I/R injury

Interestingly, short bursts of ischaemia and reperfusion, termed ischaemic preconditioning (IPC), prior to prolonged ischaemia have a protective role against I/R injury, though the reasons for this are not yet fully understood (Pinheiro et al., 2016, Koch et al., 2014). IPC was first described by Murry *et al* and is among the most potent cardioprotective strategies that can be employed against I/R injury (Murry et al., 1986).

The protective effects of IPC have been demonstrated by a large number of separate studies and is not limited to cardiac tissue. Curiously, the protective effects of IPC can be conferred even when the site of preconditioning is distal to the site of ischaemic injury (Ren et al., 2009). IPC followed by I/R, compared to I/R insult alone, has been shown to decrease

cytolysis and lipid peroxidation, resulting in improved renal function in a study of ischaemic kidneys in rats (Mahfoudh-Boussaid et al., 2012). In the case of cardiac ischaemia, IPC has been shown to improve several different clinical outcomes of I/R injury. In a randomised controlled clinical trial of 180 cardiac bypass patients, the extent of perioperative myocardial injury was significantly reduced by remote IPC prior to surgery. In addition to reducing the magnitude of injury, IPC also decreased the incidence of post-operative atrial fibrillation and acute kidney injury and reduced the length of recovery required in an intensive care unit (Candilio et al., 2015). IPC alleviates cardiac contractile dysfunction upon reperfusion by preserving end-ischaemic ATP levels (Kaplan et al., 1994). It also prevents ventricular arrhythmia (Parratt and Vegh, 1994, Hagar et al., 1991). Most notably, infarct size is limited in IPC treated rat and pig hearts, both in cases of I/R injury and in cases where the subsequent ischaemia was lethal (Shintani-Ishida et al., 2006, Yellon et al., 1992, Schott et al., 1990).

3.1.3 Molecular mechanisms of IPC cytoprotection

Clinically, the effects of IPC are biphasic, with an early phase of protection occurring almost immediately post-IPC, and a second, late phase 12-24 hours later, although the late phase was not explored within this PhD. Early phase IPC has been linked ROS; whereas large-scale ROS production is detrimental to cellular viability, sub-lethal levels of ROS, such as those generated by IPC, may contribute to cardio-protection by acting as messengers in signal transduction to modify redox-sensitive proteins (Chen et al., 1995, Otani, 2004).

During ischaemia, fatty acid oxidation is replaced by glycolysis as the primary method of energy metabolism, allowing maintenance of cellular viability over a longer period. This metabolic switch is directly regulated by HIF (hypoxia-inducible factor), a redox-sensitive transcription factor (Cadenas, 2018). HIF is a heterodimeric protein comprising HIF-α and HIF-β; expression of the latter is constitutive, whereas accumulation of the former (comprising 3 subunits - HIF-1α, HIF-2α and HIF-3α) is oxygen-sensitive, with hypoxia inhibiting its degradation (Kim et al., 2006a).

Sub-lethal intracellular levels of ROS, such as those generated by short bursts of ischaemia and reperfusion during IPC, inhibit prolyl hydroxylases. Under normoxic conditions, prolyl hydroxylases are responsible for the hydroxylation of HIF-α, resulting in its ubiquitination and subsequent proteasomal degradation (Bruick and McKnight, 2001, Srinivas et al., 1999). During IPC, low levels of ROS facilitate HIF-α accumulation and translocation to the nucleus, where it dimerises with HIF-β. The HIF dimer can then bind

to hypoxia response elements, recruit the transcriptional co-activator CBP/p300 and induces gene transcription (Epstein et al., 2001, Lando et al., 2002, Mahon et al., 2001). HIF-induced transcriptional changes are responsible for initiation of various protective mechanisms, including endothelial/vascular remodelling and activation of the RISK (reperfusion injury signalling kinase) pathway (Holscher et al., 2011, Martin-Puig et al., 2015, Tsang et al., 2004).

Interestingly, there is accumulating evidence that IPC confers protection of cardiac mitochondria via cytosol-independent mechanisms. Sub-lethal I/R in isolated rat hearts reduced complex-I and -II-mediated respiration in sub-sarcolemmal (SS) mitochondria, but not interfibrillar (IF) mitochondria, an effect which was attenuated by IPC. Connexin-43 is a protein present in SS, but not IF, mitochondria, and is thought to modulate mitochondrial respiration via complex-I. Replacement of connexin-43 with connexin-32 abolished the protective effect of IPC, both in whole hearts and in isolated mitochondrial preparations (Ruiz-Meana et al., 2014, Rodriguez-Sinovas et al., 2018).

3.1.4 Mitochondrial dynamics are critical in I/R injury outcome

Because of its constitutive activity the heart has very high energy demands. To meet this requirement, cardiomyocytes are enriched with mitochondria, which account for 30-35% of their volume. Mitochondria are highly dynamic organelles, undergoing continuous, tightly regulated fission and fusion events, creating an adaptable and efficient energy transfer system, crucial to deliver ATP to where it is most urgently needed within the cell (Piquereau et al., 2013). Fused mitochondria (a mitochondrial network or reticulum) facilitate efficient delivery of ATP from the cell periphery to the core, whereas individual divided mitochondria can be trafficked rapidly to meet changing energy demands around the cell. Under conditions of oxidative stress, this fragile equilibrium is be perturbed, resulting in mitochondrial fragmentation, mitophagy, and apoptosis (Hom and Sheu, 2009, Skulachev, 2001).

To co-ordinate the tightly regulated processes of mitochondrial fission and fusion, a huge number of different proteins and pathways are required. However, stresses such as ischaemia and I/R injury can alter the expression, turnover and post-translational modifications of various fission and fusion proteins. My PhD work has focused primarily on changes to proteins associated with mitochondrial fission. There are a growing number of proteins known to be involved in mitochondrial fission, both under physiological and

pathophysiological conditions. Defining how these proteins are recruited and regulated is intrinsic to advancing our understanding of I/R injury and could lead to the identification of potential therapeutic targets. Brief introductions to the proteins assayed are given below, listed according to their primary function.

3.1.4.1 Mitochondrial fission proteins

Dynamin II (Dyn2) and Dynamin-related protein I (Drp1)

Mitochondrial fission is a tightly regulated process involving an ever-growing number of known proteins. Key players identified so far include dynamin II (Dyn2, also Dnm2) and dynamin-related protein I (Drp1). Knock out of Drp1, causes mass fusion of mitochondria and extended networks and is embryonic lethal, indicating a crucial role in development. However, cultured Drp1-knock out cells are viable and can divide, suggestive of a compensatory mechanism (Ishihara et al., 2009). It was previously assumed that final scission of the mitochondrial membranes during fission was achieved by Drp1-induced constriction forces. However, recent work has demonstrated that this task is actually carried out by the conventional dynamin Dyn2 (Lee et al., 2016). Electron microscopy and 3D tomography revealed that cells treated with siRNA targeting Dyn2 displayed stalled and elongated super-constricted mitochondrial membranes, which were not present in control cells (Lee et al., 2016). Drp1 is capable of constricting membranes of a greater diameter than Dyn2 but requires Dyn2 to constrict them far enough for scission. Lee *et al* proposed a model in which Drp1-dependent mitochondrial fission requires the sequential action of Drp1, which constricts the mitochondrial membrane to a diameter conducive to Dyn2 action, followed by recruitment of Dyn2 and complete membrane scission.

Mitochondrial Fission Factor (Mff) and Fission I (Fis1)

Mff has been previously identified as the main receptor for Drp1 (Lee et al., 2004, Alirol et al., 2006), and is discussed in greater detail in 1.1.6. It is a single-pass transmembrane protein with an N-terminal Drp1-interacting domain (Figure 1.18). Fis1 has previously been reported to bind Drp1 in an interaction which is at least partly stress-dependent (Joshi et al., 2018). Drp1-independent roles for Fis1, however, must also be considered, as knock down of Fis1 inhibits cell death significantly more than inhibition of Drp1, and Fis1 is not exclusively localised to sites of mitochondrial scission (Suzuki et al., 2003, Yoon et al., 2003).

Mitochondria-anchored protein ligase (MAPL)

MAPL (mitochondria-anchored protein ligase) is a SUMO-1 ligase and is currently the only known SUMO ligase that is mitochondria-bound (Neuspiel et al., 2008). MAPL has been shown to play a part in regulating mitochondrial fission via SUMOylation of Drp1, which is thought to stabilise the endoplasmic reticulum (ER)/mitochondrial interface that acts as a hotspot for constriction of the mitochondrial membrane, calcium flux, cristae remodelling and cytochrome *C* release (Braschi et al., 2009, Prudent et al., 2015).

3.1.4.2 Mitochondrial fusion proteins

Mitofusin II (Mfn2)

Mitochondrial morphology and integrity stems from a delicate balance of fission and fusion. Although fission was the main interest of this project, it was still important to consider any perturbations to mitochondrial fusion. We therefore also probed for Mitofusin II (Mfn2) in the mitochondrial samples. Stress-induced phosphorylation of Mfn2 by JNK, leading to ubiquitination and proteasomal degradation, has been shown to facilitate mitochondrial fragmentation and apoptosis (Leboucher et al., 2012). Conversely, it has recently been reported that Mfn2 plays a protective role in I/R injury by increasing the rate of autophagy; over-expression of Mfn2 was shown to ameliorate I/R injury by increasing formation of autophagosomes and promoting their fusion to lysosomes, whilst down-regulation of Mfn2 had the opposite effect (Peng et al., 2018).

3.1.4.3 Mitophagy proteins

PTEN-induced kinase I (PINK1)

PINK1 is a mitochondrial serine/threonine kinase that is constitutively cleaved from the mitochondrial membrane under physiological conditions, accumulating only upon mitochondrial membrane depolarisation (Geisler et al., 2010, Whitworth et al., 2008). PINK1 knock out has been shown to cause defects in mitochondrial morphology and increased sensitivity to several cellular stresses, including oxidative stress (Clark et al., 2006). However, mitochondrial dysfunction caused by lack of PINK1 can be compensated for by Parkin over-expression in *Drosophila melanogaster* (Park et al., 2006). This is thought to be because PINK1 loss-of-function causes not only abnormal mitochondrial morphology, but also altered mitochondrial membrane potential, which can be rescued by activation of autophagy by Parkin (Exner et al., 2007).

PINK1 is cytosolically synthesised as a 63kDa protein, which undergoes at least two cleavage events in the mitochondrial inter-membrane space (IMS), first by mitochondrial processing peptidase (MPP) to remove the mitochondrial targeting sequence, then by

presenilin-associated rhomboid-like protease (PARL) and m-AAA protease, resulting in 55kDa and 48kDa species (Greene et al., 2012). It has previously been shown that, upon dissipation of the mitochondrial membrane potential, the full-length PINK1 protein accumulates (Jin et al., 2010).

Parkin and F-box only protein 7 (Fbxo7)

Parkin is well established as playing an important role in mitophagy, through its selective recruitment to damaged mitochondria and dramatic changing of the ubiquitination status of the mitochondrial proteome (Sarraf et al., 2013, Chan et al., 2011). Parkin is a primarily cytosolic ubiquitin ligase, canonically recruited to depolarised mitochondrial membranes by accumulation of PINK1 (PTEN-induced putative kinase 1) (Matsuda et al., 2010, Narendra et al., 2010, Narendra et al., 2008) which has been previously reported to ubiquitinate Mff, promoting its association with the autophagic receptor p62 (Gao et al., 2015). Fbxo7, an adaptor protein of the Skp1-Cul1-Fbx Cullin RING ligase complex, has also been shown to play a part in mitophagy, in a role thought to be linked to its direct interactions with Parkin (Burchell et al., 2013). Further detail on Parkin and Fbxo7 is given in 1.5 and 1.6, respectively.

3.1.5 Aims

Several previous studies have identified increased SUMOylation as a protective mechanism against ischaemic stress, including that experienced by ground squirrels during torpor (Lee et al., 2007), neurons subjected to OGD (Guo et al., 2013, Guo et al., 2017) and HEK293T cells in a heavy metal-induced model of ischaemia (Luo et al., 2017). Additionally, a recent study has implicated the SUMO-protease SENP3 as a key influencer of myocardial infarct outcomes, showing that cardiac-specific knock down of SENP3 *in vivo* reduces infarct size, and over-expression of SENP3 increases infarct size upon induced I/R injury (Gao et al., 2018).

The aim of this part of my PhD was to investigate whether the global changes in SUMOylation observed by other groups studying ischaemic stress were also apparent in our model of cardiac ischaemia. Additionally, given the importance of mitochondria in I/R injury, potential SUMO target proteins and fission/fusion proteins at the mitochondrial outer membrane (MOM) were also of interest in this study.

3.2 Methods

3.2.1 Ex vivo retrograde perfusion

250-274g male Wistar rats were anaesthetised with isofluorane and killed by cervical dislocation in accordance with Schedule 1 Guidance on the Operation of the Animals (Scientific Procedures) Act, 1986. The aorta was cannulated *in vivo* and retrograde perfusion started immediately using Langendorff apparatus (Figure 3.2). Hearts were perfused under constant flow (12 mL/min) at 37°C with continuously oxygenated (95% O_2, 5% CO_2) Krebs Henseleit Buffer (KHS: 118mM NaCl, 4.7mM KCl, 1.2mM $MgSO_4$, 1.25mM $CaCl_2$, 1.2 mM KH2PO4, 25 mM NaHCO3, 11mM glucose) at pH 7.4. A ~15-minute stabilisation period allowed hearts to recover to physiological levels of function prior to commencement of perfusion protocols. Ischaemia was achieved by submerging the heart in de-oxygenated KHS and cessation of perfusion.

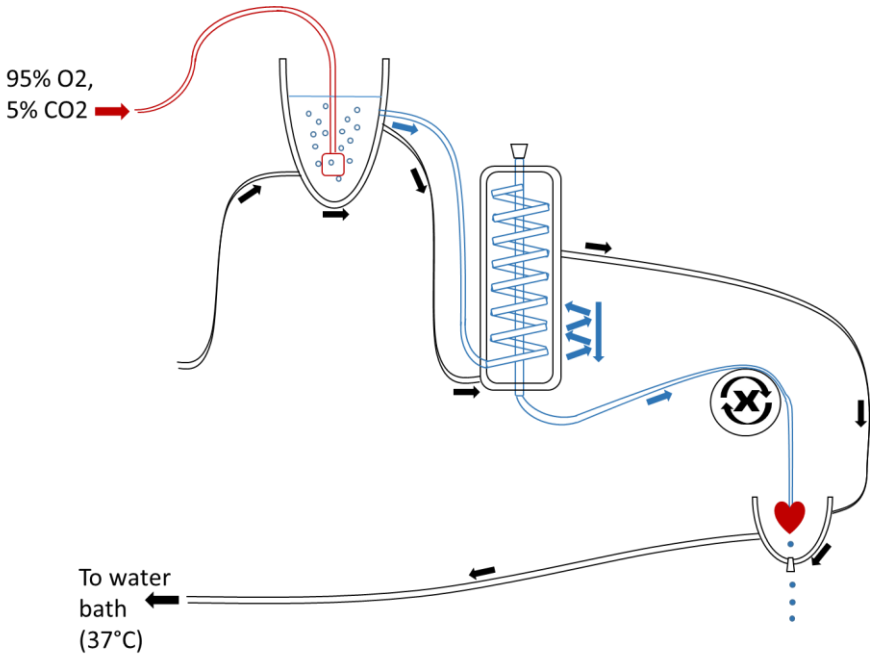

Figure 3.2 **Schematic of Langendorff retrograde perfusion apparatus.** Hearts were perfused under constant flow at 37°C with continuously oxygenated Krebs-Henseleit solution (KHS). Ischaemia was achieved by submerging the heart in perfusion buffer and cessation of perfusion. 37°C water was continuously circulated around the system (black arrows). KHS was perfused with a 95% O2, 5% CO2 mixture to maintain oxygen supply to cardiac tissue and pH of KHS (red arrow). Oxygenated KHS was driven through the Langendorff apparatus under constant flow by a pump (X and blue arrows).

The pre-ischaemic group was continuously perfused for 30 minutes. Ischaemia was performed by submersion in de-oxygenated KHS with no perfusion for 30 minutes, and the

ischaemia & reperfusion group was then perfused for a further 120 minutes. Ischaemic pre-conditioning consisted of 3 x 2-minute bursts of ischaemia, separated by 3 minutes reperfusion. This was followed by 30 minutes of ischaemia. The schematic in Figure 3.3 illustrates the 4 conditions used. An extended pre-ischaemia group (150 minutes of perfusion) was not significantly different from the 30 minutes pre-ischaemia group and was excluded from datasets for clarity. Left ventricular tissue was immediately subjected to subcellular fractionation. For each of the experimental conditions, 6 independent animals were used i.e. 6 hearts.

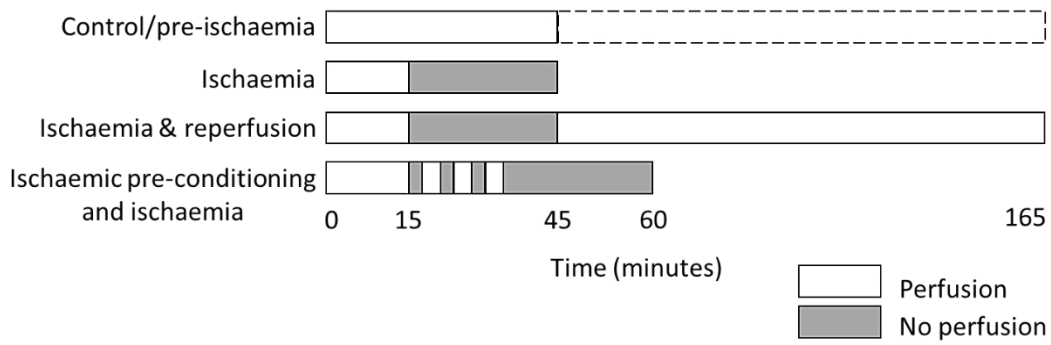

Figure 3.3 Schematic of retrograde perfusion protocols.

3.2.2 Subcellular fractionation of Left Ventricular tissue

The protocol for isolation of cellular fractions from rat left ventricular tissue was adapted from a previously published protocol (Pasdois et al., 2013) and performed at 4°C. A schematic of the protocol is shown in Figure 3.4.

Left ventricular tissue was immersed in 6mL ice cold isolation buffer (300mM sucrose, 3mM EGTA, 10mM Tris-HCl, pH7.1) supplemented with 20mM NEM, 1x complete protease inhibitors (Roche) and 1x phosphatase inhibitors. Tissue was rapidly chopped into fine pieces (Figure 3.4, 1) before homogenisation using a Polytron tissue disruptor (Kinematica) at 10,000rpm with 2 bursts of 5 seconds followed by 1 burst of 10 seconds. Tissue homogenate was diluted to 20mL total volume with isolation buffer supplemented with 1x complete protease inhibitors (2) and further homogenised by hand for 2 minutes using a glass Potter homogeniser and Teflon pestle (3). A small volume of homogenate was stored at -80°C as whole homogenate (4, A). The homogenate was centrifuged at 7500g for 7 minutes (5) and the soluble fraction (supernatant) stored at -80°C as a cytosol-containing fraction (B). The pellet was rinsed twice with 5 mL isolation buffer, resuspended

in 20mL isolation buffer and further hand-homogenised for 2 minutes (6). The homogenate was then centrifuged at 600g for 10 minutes (7) and the pellet resuspended in isolation buffer and stored at -80°C as a nucleus-containing fraction (C). The supernatant was centrifuged at 7000g for 10 minutes (8) to yield a crude mitochondrial pellet, which was resuspended in isolation buffer and stored at -80°C (D). All fractions were assayed for protein concentration using a standard BCA assay protocol prior to use for Western blotting.

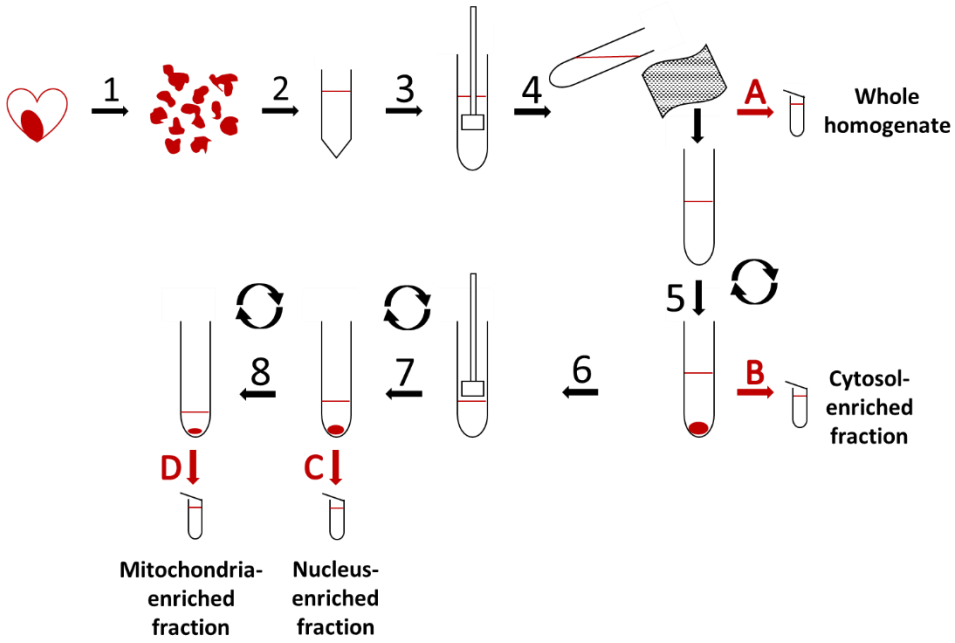

Figure 3.4 Schematic of cardiac tissue subcellular fractionation.

3.2.3 Lactate Dehydrogenase (LDH) Assay

The Pierce™ LDH Cytotoxicity Assay Kit was purchased from Thermo Fisher and used according to the manufacturer's protocol. Briefly, one volume each of perfusate and Substrate Solution were mixed in a 96 well plate, and incubated for 30 minutes at RT, protected from light. One volume Stop Solution was then added, and the absorbance read in a spectrophotometer at 490nm and 680nm. LDH activity was calculated by subtracting the 680nm reading (background) from the 490nm reading.

3.3 Results

3.3.1 Controls

Subcellular fractionation

To accurately assess protein levels within subcellular compartments, it was vital to ensure that the fractionation protocol followed yielded sufficiently clean fractions. Most importantly, due to the high proportion of SUMO proteins within the nucleus compared to the rest of the cell (Takahashi and Kikuchi, 2008), nuclear contamination of other cell compartments could significantly distort SUMO measurements from other compartments.

To assess the purity of mitochondrial samples, mitochondrial and total lysate samples were run side-by-side by SDS-PAGE, and Western blotted for markers of intracellular compartments (Figure 3.5). Lamin B is an integral structural constituent of the nuclear lamina, and its absence from mitochondrial fractions indicates that the nucleus has been largely excluded. GAPDH (Glyceraldehyde 3-phosphate dehydrogenase) is an enzyme involved in glycolysis partitioned to the cytosol, so its absence from the mitochondrial fractions is indicative of cytosolic exclusion. VDACs (Voltage-dependent anion-selective channels) are components of the outer mitochondrial membrane but are synthesised at endoplasmic reticulum (ER)-associated ribosomes.

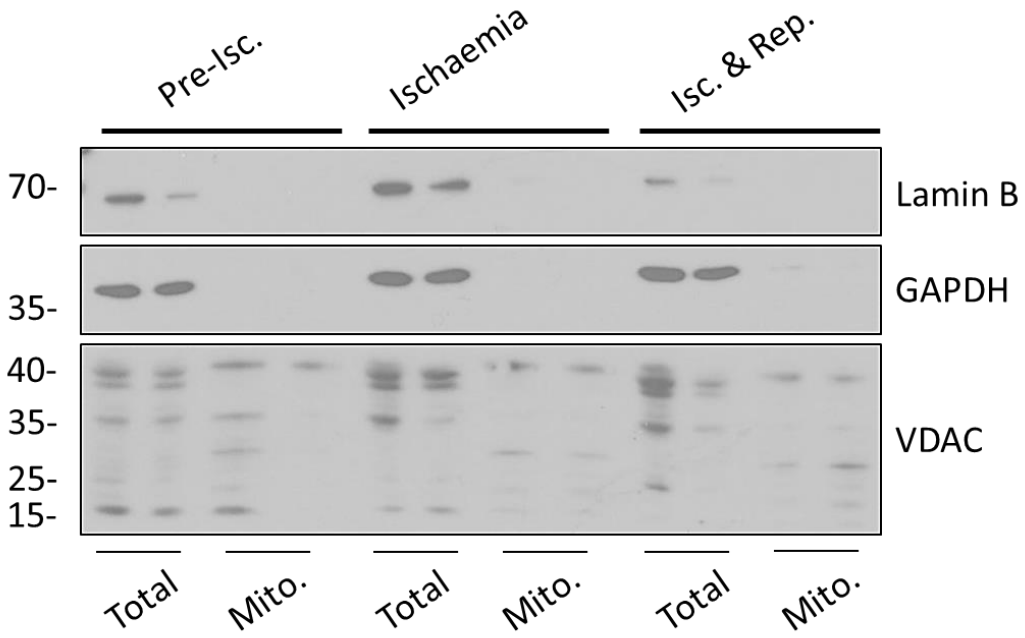

Figure 3.5 **Purity of mitochondrial fractions.** Following subcellular fractionation of perfused left ventricular tissue, total lysate (Total) and mitochondrial (Mito.) samples were subjected to SDS-PAGE and Western blotting side-by-side. Membranes were blotted for Lamin B (nuclear), GAPDH (cytosolic) and VDAC (mitochondrial). For each condition, two Total samples (independent hearts) were run alongside their mitochondrial fractions.

Langendorff apparatus ischaemia and reperfusion

It was also important to check that the ischaemia protocols in the Langendorff experiments were effective in damaging the cardiac tissue, thereby modelling true ischaemia/reperfusion (I/R) injury. To validate this, known cellular stress responses were examined by Western blotting. Cytosolic protein samples from the Langendorff perfused hearts were probed for cleaved Caspase-3 and Microtubule-associated protein 1A/1B-light chain 3 (LC3).

Caspase 3

The caspase protein family are a group of cysteine proteases with important roles in the regulation of apoptosis, broadly categorised as apoptosis initiator- and apoptosis executioner-caspases (of which Caspase-3 falls into the latter group) (Degterev et al., 2003). Their function must be tightly regulated to avoid inappropriate activation of the programmed cell death cascade, and as such, all of the 11 mammalian caspases are synthesised as inactive zymogens comprised of N-terminal pro-domain, a large subunit (p20) and a C-terminal small subunit (p17) (Yamin et al., 1996). Activation of the caspase only occurs via a series of cleavage events, with executioner caspases typically being processed and activated by upstream caspases. The appearance of cleaved caspase-3 within a cell therefore serves as an indicator of cellular stress and initiation of apoptotic pathways.

LC3

LC3 is the mammalian homologue of Atg8 (Autophagy-related protein 8). Post-translationally, LC3-I exists as cytosolic polypeptide, and its proteolytic cleavage yields LC3-II, which is membrane-bound at autophagosomes (Kabeya et al., 2000). An increase in the ratio of LC3-II to LC3-I (i.e. lower molecular weight to higher molecular weight LC3-reactive species) is therefore indicative of greater presence of autophagosomal membranes and autophagic activity (Aparicio et al., 2016).

In the Langendorff perfused hearts, cytosolic levels of cleaved caspase-3 were significantly increased ($p < 0.0001$) only during reperfusion, compared to pre-ischaemia and ischaemia (Figure 3.6 (A, C)). Similarly, the only significant ($p < 0.001$) increase in LC3-II/LC3-I ratio was also observed upon reperfusion (Figure 3.6 (A, B)). Taken together, these data confirm previous reports that the damage incurred as a result of I/R injury primarily occurs during reperfusion.

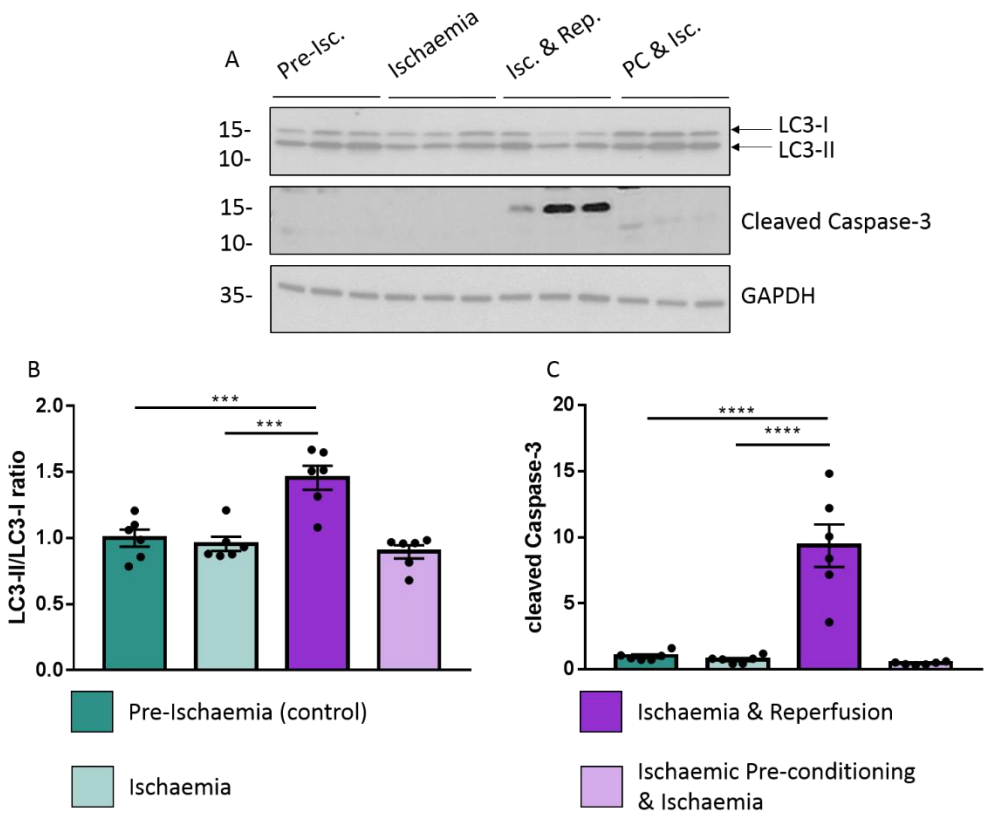

Figure 3.6 **Intracellular stress response during ischaemia and reperfusion.** Following subcellular fractionation of perfused left ventricular tissue, cytosolic samples were used for Western blotting. Samples were probed with LC3 and cleaved Caspase-3 antibodies. Blots performed by Nadiia Rawlings. N = 6 (blot shows 3 replicates of each condition). Analysed using ordinary one-way ANOVA with Sidak's correction for multiple comparisons with a pooled variance. Data presented as mean ± SEM. *** $p < 0.001$**** $p \leq 0.0001$.

In addition to probing cytosolic fractions for markers of intracellular stress, perfusate from the hearts was collected to measure extracellular stress responses. A lactate dehydrogenase (LDH) assay was used to quantify cytotoxicity by colorimetric measurement.

LDH is a cytosolic enzyme that converts lactate to pyruvate by reduction of NAD^+ to NADH in a reversible, coupled reaction (Everse and Kaplan, 1973). Cytotoxic conditions damage the plasma membrane, releasing LDH from the cytosol. LDH is then found in the perfusate collected during Langendorff perfusion. In an LDH assay, release of LDH can be quantified from a two-step reaction. LDH first reduces NAD^+ to NADH (coupled to deprotonation of lactate to pyruvate). Diapharose then uses NADH to reduce a tetrazolium salt to a formazan product, which is red and can be measured at a wavelength of 490nm by spectrophotometry. In this assay, formation of formazan is directly proportional to amount of released LDH, and thereby cytotoxicity.

During the Langendorff experiments, perfusate was collected at three different time points: after 30 minutes of normal perfusion (pre-ischaemia control), within the first minute of reperfusion following 30 minutes ischaemia (ischaemia), or within the first minute of the 3rd reperfusion of pre-conditioning (ischaemic pre-conditioning). As shown in Figure 3.7, only the perfusates collected immediately after 30 minutes of ischaemia had significant amounts of LDH, compared to the pre-ischaemic control or pre-conditioning group. We would expect that the largest LDH release would occur during reperfusion. However, by the end of 2 hours reperfusion, any extracellular LDH has been washed out and so cannot be collected in the perfusate.

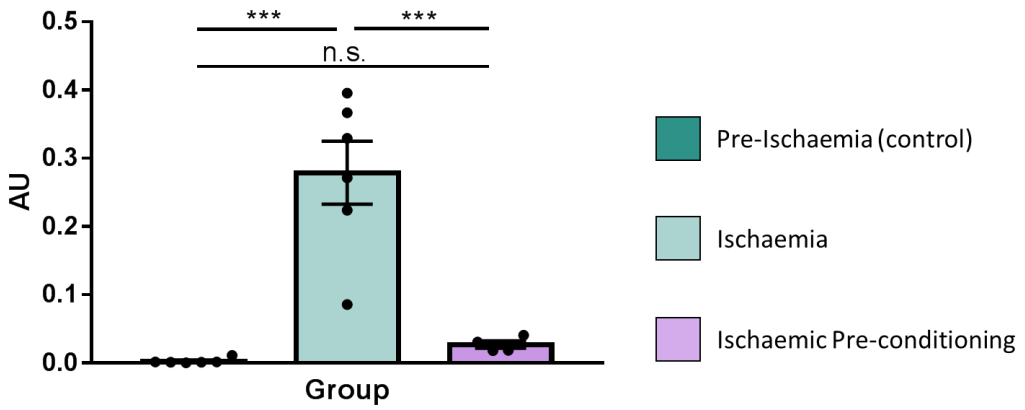

Figure 3.7 **Cytotoxicity during ischaemia.** Perfusate from the hearts was collected at various points during the ischaemia/reperfusion modelling and subjected to a lactate dehydrogenase (LDH) assay as a measure of cytotoxicity. The LDH assay provided a colorimetric readout of cytotoxicity, measured in absorbance units (AU). N = 4-6. Analysed using ordinary one-way ANOVA with Sidak's correction for multiple comparisons with a pooled variance. Data presented as mean ± SEM. *** $p < 0.001$.

3.3.2 Post-Translational Modifications

Post-translational modifications (PTMs) are a broad class of small molecular additions that can alter the subcellular location, efficiency, function, stability and activation status of target proteins. Under stress conditions, PTMs can rapidly and reversibly alter large portions of the proteome in an attempt to protect against cellular damage.

Global up-regulation of ubiquitination is a well characterised consequence of cellular stress that participates in triggering the Unfolded Protein Response (UPR) and targeting damaged proteins for proteasomal degradation *en masse* (Lindholm et al., 2017). It was therefore expected that this model of I/R injury would result in changes in total proteome ubiquitination. As shown in Figure 3.8, ischaemia resulted in a trend of decreased global ubiquitination, which became statistically significant with ischaemic pre-

conditioning. However, there was significant up-regulation of global ubiquitination upon reperfusion, consistent with the stress responses shown in Figure 3.6.

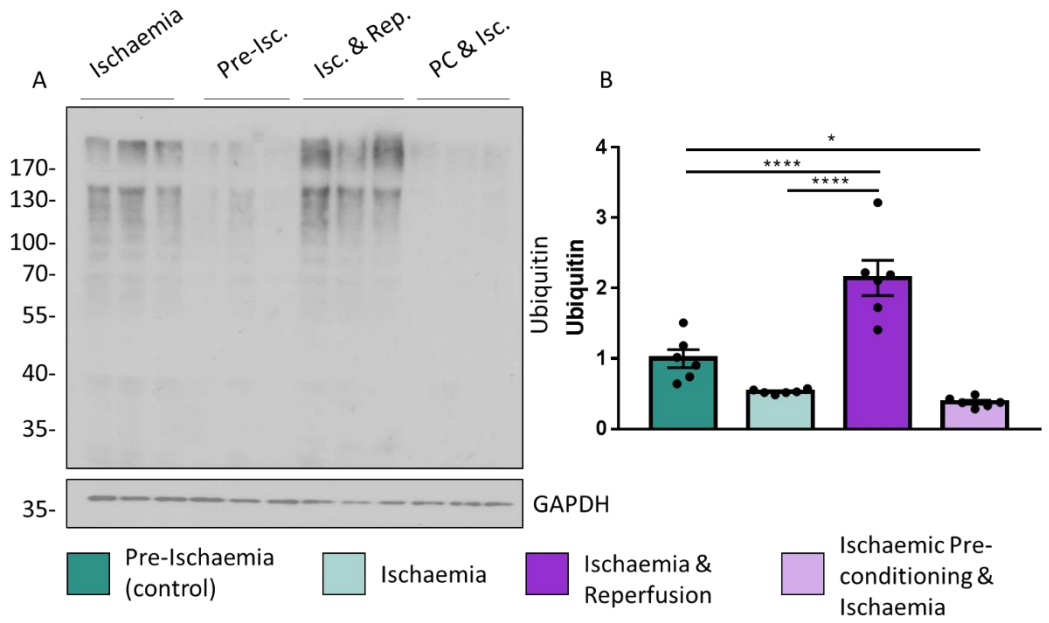

Figure 3.8 **Total Ubiquitination during ischaemia and reperfusion.** Prior to subcellular fractionation of perfused left ventricular tissue, whole homogenate samples were prepared to be used for Western blotting. Samples were probed with Ubiquitin antibody. Representative blots are of 3 samples per condition. N = 6. Analysed using ordinary one-way ANOVA with Sidak's correction for multiple comparisons with a pooled variance. Data presented as mean ± SEM. * $p < 0.05$, **** $p < 0.0001$.

Protein SUMOylation is globally upregulated during ischaemic stress in neurons and in embryonic anoxia (Guo et al., 2013, Meller et al., 2014). Therefore, it was hypothesised that a similar pattern might be expected in cardiac tissue having undergone ischaemia or ischaemia/reperfusion. I therefore assessed left ventricular tissue lysate by SDS-PAGE and Western blotting for SUMO-1 and SUMO-2/3 conjugated proteins. As shown in Figure 3.9, no global changes were detected in SUMO-2/3 conjugates (A, C) (analysis of whole lanes). However, a small but significant increase was seen in SUMO-1 conjugates when hearts were pre-conditioned prior to ischaemia, when compared to ischaemia alone (A, B).

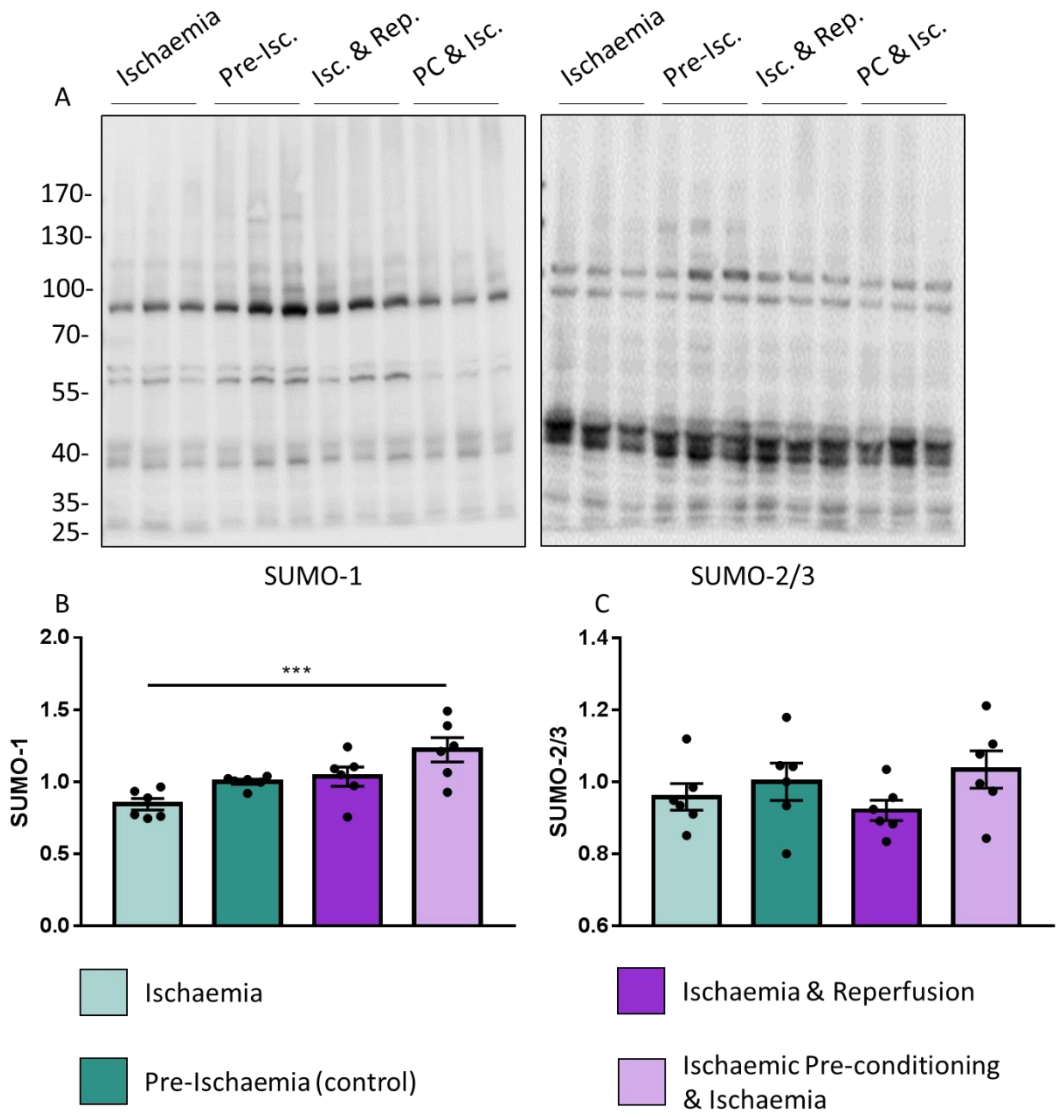

Figure 3.9 **Total SUMOylation during ischaemia and reperfusion.** Prior to subcellular fractionation of perfused left ventricular tissue, whole homogenate samples were prepared to be used for Western blotting. Samples were probed with SUMO-1 and SUMO-2/3 antibodies. Representative blots are of 3 samples per condition. Total protein stain was used as a loading control. Blots performed by Nadiia Rawlings. N = 6. Analysed using ordinary one-way ANOVA with Sidak's correction for multiple comparisons with a pooled variance. Data presented as mean ± SEM. *** $p < 0.001$.

Mitochondria are particularly susceptible to acute damage in I/R injury, largely due to localised oxidative stress (Jasova et al., 2017, Hassanpour et al., 2018). Changes in mitochondrial SUMOylation may have been masked in the total lysate by the presence of high levels of nuclear SUMO-conjugates (Takahashi and Kikuchi, 2008). I therefore separately assessed mitochondrial fractions for changes in SUMOylation. Additionally, the mitochondrial fractions were blotted for Ubiquitin-conjugates, to determine whether ubiquitination of mitochondrial proteins followed the same pattern as the total proteome.

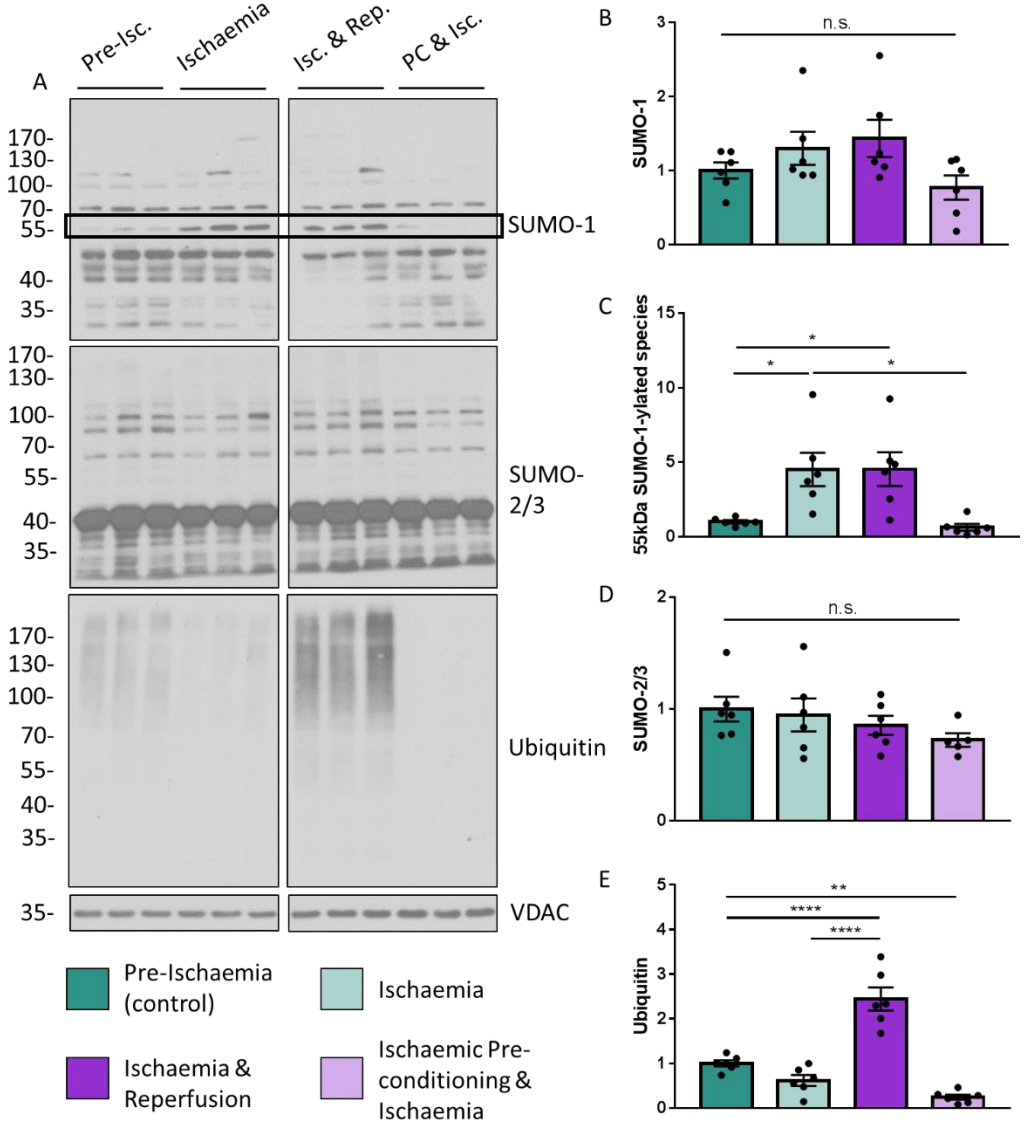

Figure 3.10 **Mitochondrial post-translational modifications during ischaemia and reperfusion.** Following subcellular fractionation of perfused left ventricular tissue, mitochondrial samples were used for Western blotting. Samples were probed with SUMO-1, SUMO-2/3 or ubiquitin antibodies. Representative blots are of 3 samples per condition. N = 6. Analysed using ordinary one-way ANOVA with Sidak's correction for multiple comparisons with a pooled variance. Data presented as mean ± SEM. * $p \leq 0.05$, ** $p < 0.01$**** $p \leq 0.0001$.

As shown in Figure 3.10, no significant changes were detected in global SUMO-1-ylation or SUMO-2/3-ylation of the mitochondrial proteome (A, B, D). This is not to say that subsets of the mitochondrial proteome did not have their SUMOylation status altered by I/R. For example, an approximately 55kDa SUMO-1-ylated species was significantly upregulated under ischaemia, compared to pre-ischaemia, but was not upregulated during ischaemia in tissue that had been pre-conditioned (A (highlighted), C).

The most notable change in mitochondrial PTMs was that of ubiquitin (Figure 3.10 (A, E)). As in the total lysate, ubiquitination of mitochondrial proteins was significantly increased during ischaemia and reperfusion, compared to ischaemia alone. This was consistent with Figure 3.6, in which significant cellular stress occurred primarily during reperfusion.

3.3.3 Mitochondria-associated proteins

Mitochondrial integrity is critical to the survival of cells following ischaemic insult or I/R injury (Ambrosio et al., 1993, Griffiths and Halestrap, 1995, Schaller et al., 2010). Proteins associated with mitochondrial structure and dynamics were therefore a primary focus in this study. Particular attention was paid to proteins involved in mitochondrial fission, both under physiological and pathophysiological conditions, especially those which appeared to be differentially expressed or recruited between ischaemia and ischaemic pre-conditioning groups, as this may provide some insight into the molecular mechanisms underpinning the cytoprotective effects of pre-conditioning.

Hexokinase II

Hexokinase II (HK2) catalyses the phosphorylation of glucose to glucose-6-phosphate (G-6-P), which is sequestered in the cytosol and primed for further metabolism (Halestrap et al., 2015). Despite its role in glycolysis, HK2 is found not only in the cytosol, but can also bind to the outer mitochondrial membrane (MOM), depending on the prevailing metabolic conditions; high (G-6-P) concentration favours dissociation of HK2 from the mitochondrial membrane (Pastorino and Hoek, 2008, Wilson, 2003, Murry et al., 1990). Bound HK2 inhibits opening of the mPTP and reduces mitochondrial membrane permeability to cytochrome *C*. This could be through stabilisation of mitochondrial-endoplasmic reticulum (ER)-contact sites and antagonization of pro-apoptotic Bcl-2 family members, potentially through association with VDAC (Pastorino and Hoek, 2008, Pastorino and Hoek, 2003). Glycogen metabolism during ischaemia produces G-6-P, and previous studies have shown that pre-ischaemic levels of glycogen in the heart determine the extent of reperfusion injury (Finegan et al., 1995, McNulty et al., 1996). No significant changes were detected in total HK2 under the conditions of this study, however a small loss of HK2 from the mitochondrial membrane was evident during ischaemia, with a statistically significant dissociation of HK2 upon ischaemia of the pre-conditioned group (Figure 3.11(B)).

Dynamin related protein 1 (Drp1) and Dynamin2 (Dyn2)

Given the mitochondrial fragmentation associated with ischaemia and reperfusion, we predicted an increase in association of proteins involved in fission (Chen et al., 2009). In our model of I/R injury, mitochondrial association of both Drp1 and Dyn2 was slightly, but not significantly, increased during ischaemia (Figure 3.11 (C, D)). Interestingly, association of Dyn2 during ischaemia was significantly reduced by IPC, suggestive of reduced ischaemic mitochondrial fission following IPC. The significant decrease in mitochondria-associated Drp1 during reperfusion was unexpected, as we would predict that the I/R-induced fragmentation of mitochondria depends on increased/dysregulated fission. However, we cannot rule out decreased mitochondrial fusion as the predominant driving force of fragmenting the mitochondrial network during I/R injury.

Parkin and Fbxo7

It has been widely reported that Parkin is recruited to mitochondria under conditions of oxidative stress, setting in motion a chain of events resulting in large-scale mitophagy (Matsuda et al., 2010, Vincow et al., 2013, Caulfield et al., 2015, Gong et al., 2015). Consistent with this, I observed that Parkin is heavily recruited to mitochondria during ischaemia, an effect which is partially offset by ischaemic pre-conditioning (Figure 3.11 (F)).

Intriguingly, recruitment of Fbxo7 to mitochondria during ischaemia was also attenuated by pre-conditioning (Figure 3.11 (E)), which could be indicative of a co-dependent mechanism of recruitment for Parkin and Fbxo7, as put forth in the publication by Burchell *et al* (Burchell et al., 2013). For this reason, Parkin and Fbxo7 were both chosen for further study in Chapter 4.

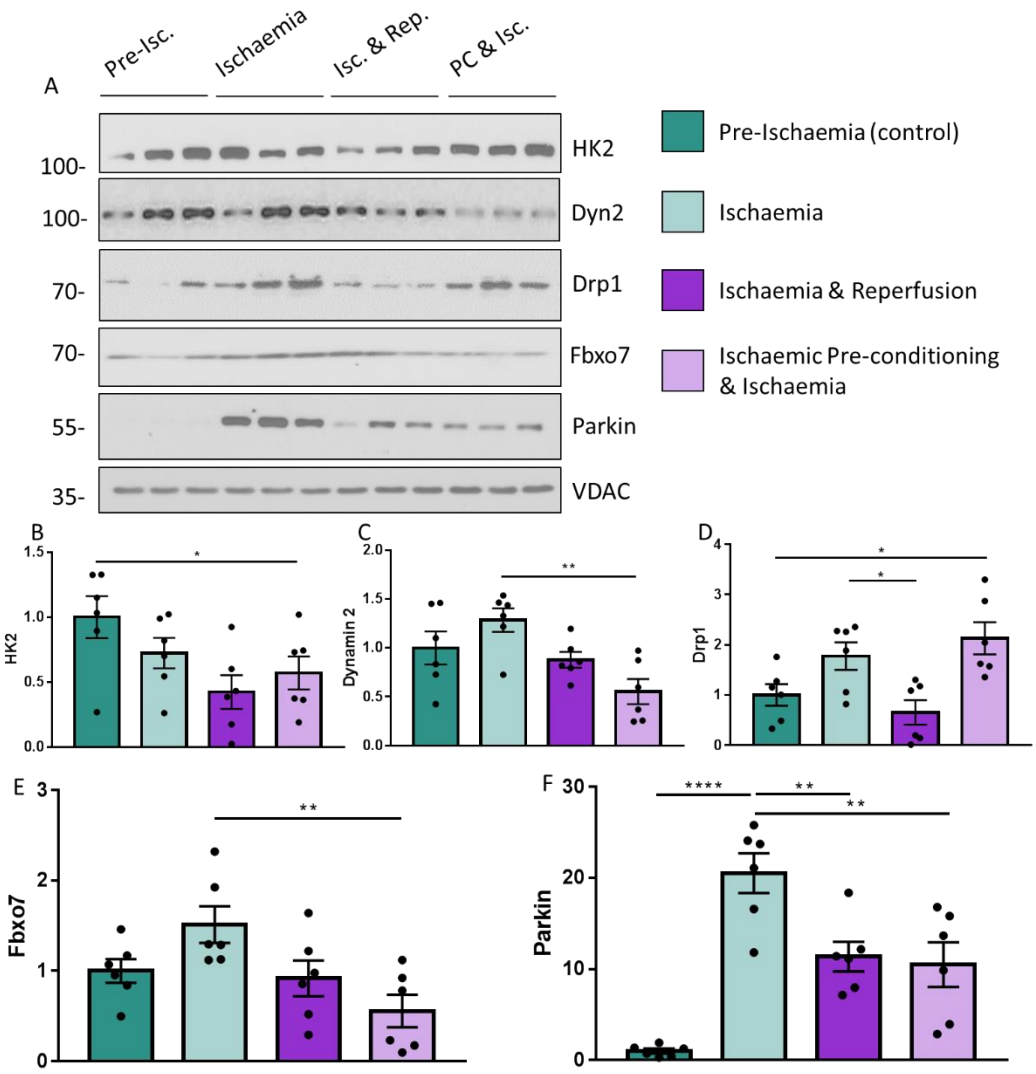

Figure 3.11 **Mitochondrial recruitment during ischaemia and reperfusion.** Following subcellular fractionation of perfused left ventricular tissue, mitochondrial samples were used for Western blotting. Samples were probed with HK2, Dyn2, Drp1, Fbxo7 or Parkin antibodies. Representative blots are of 3 samples per condition. N = 6. Analysed using ordinary one-way ANOVA with Sidak's correction for multiple comparisons with a pooled variance. Data presented as mean ± SEM. * $p < 0.05$, ** $p < 0.01$, **** $p < 0.0001$.

To determine if the apparent recruitment and dissociation of proteins to/from the mitochondrial membrane was due to changes in total levels of those proteins, the same proteins were also probed for in samples of the total lysates (Figure 3.12).

No significant changes were detected in total levels of HK2 (Figure 3.12 (B)), Dyn2 (C) or Parkin (F) over the course of ischaemia and reperfusion. These data suggest that changes of these proteins at the mitochondrial membrane were due to translocation, rather than changes to translation or degradation rates. In the case of Drp1, however, the

observed decrease in the mitochondrial fraction following reperfusion (Figure 3.11 (D)) likely stems from a decrease in its total abundance (Figure 3.12 (D)). Similarly, the presence of Fbxo7 at the mitochondrial membrane was decreased by ischaemic pre-conditioning, compared to ischaemia alone, an effect which is mirrored in the total level of Fbxo7 within cells, and which is suggestive of IPC-induced degradation of Fbxo7, rather than perturbations to its recruitment (E).

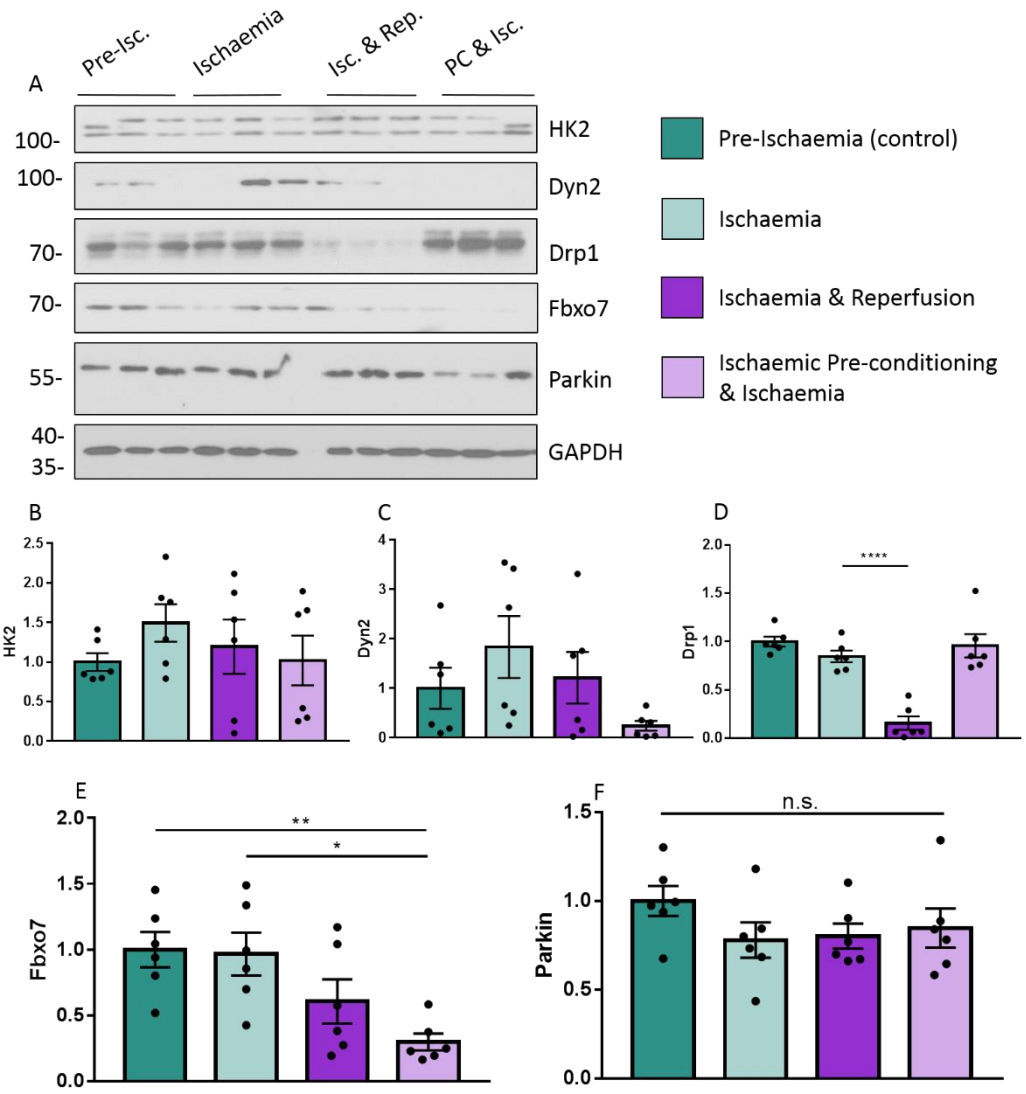

Figure 3.12 **Total changes to recruited proteins during ischaemia and reperfusion.** Prior to subcellular fractionation of perfused left ventricular tissue, total protein samples were collected, which were then used for Western blotting. Samples were probed with HK2, Dyn2, Drp1, Fbxo7 or Parkin antibodies. Representative blots are of 3 samples per condition. N = 6. Analysed using ordinary one-way ANOVA with Sidak's correction for multiple comparisons with a pooled variance. Data presented as mean ± SEM. * $p < 0.05$, ** $p < 0.01$, **** $p < 0.0001$.

3.3.4 Mitochondrial membrane proteins

Recruitment of predominantly cytosolic proteins to mitochondrial membranes is undoubtedly a critical aspect of mitochondrial fission pathways. In addition, changes to abundance of membrane resident proteins are also important. In the recruitment of Drp1, for example, several membrane-bound adaptor proteins play key roles (Kraus and Ryan, 2017).

3.3.4.1 Fission/fusion proteins

Unlike Dyn2 and other members of the conventional dynamin family, Drp1 does not contain a phospholipid-binding pleckstrin homology (PH) domain, so cannot directly bind to the MOM. To facilitate binding of Drp1, mitochondria present several known Drp1 adaptor (receptor) proteins on the outer surface of the membrane. Fission-associated Drp1 adaptors Identified so far include Mff, Fis1, Mid49 and Mid51. Due to a lack of reliable antibodies to the rat proteins, Mid49 and Mid51 were not included in this screen.

Mitochondrial fission factor (Mff)

As described in 1.1.6, Mff is the Drp1 adaptor thought to have the greatest role in mitochondrial fission (Lee et al., 2004, Alirol et al., 2006). We therefore reasoned that Mff abundance at the mitochondrial membrane would follow a similar pattern to mitochondrial recruitment of Drp1. However, a significant decrease was observed in Mff upon ischaemia (Figure 3.13 (D)). This appears to be at odds with the small increase in mitochondria-associated Drp1 under the same conditions. This could be due to increased Drp1-recruitment by other receptors (e.g. Mid49 and Mid51) which were not screened in this assay.

Fission 1 (Fis1)

A similar pattern was observed with Fission 1 (Fis1; Figure 3.13 (E)) as for Mff; a small decrease in abundance during ischaemia, which is furthered by reperfusion. However, the importance of these data is unclear, with Fis1 not currently thought to have any detectable role in mitochondrial fission (Otera et al., 2010, Osellame et al., 2016)

Mitofusin II (Mfn2)

As shown in Figure 3.13 (B), Mfn2 was significantly reduced upon reperfusion, but unchanged by ischaemia alone. This would indicate a decrease in total mitochondrial fusion; Mfns regulate MOM fusion, so their action is required prior to Opa1-mediated fusion of the MIM.

3.3.4.2 Mitochondrial modifying proteins

Mitochondria-anchored protein ligase (MAPL)

Although no total changes in mitochondrial SUMOylation were detected, the SUMOylation status of some individual proteins was altered (Figure 3.10). These proteins were not identified during this project, but it was predicted that their SUMOylation/deSUMOylation during ischaemia and/or reperfusion might be the result of changes to levels of SUMO ligases or SUMO proteases. No significant changes were

detected in MAPL abundance at mitochondria (Figure 3.13 (C)), although this does not rule out possible changes in activity.

PINK1

As shown in Figure 3.11 (F), Parkin was heavily recruited to mitochondria during ischaemia. Canonically, Parkin is only recruited to the membranes of depolarised mitochondria in a PINK1-dependent manner. Therefore, we reasoned that Parkin recruitment should align with PINK1 expression during ischaemia.

In these experiments (Figure 3.13), a significant increase of the 48kDa species (H) was seen during ischaemia, while a significant decrease of the 55kDa species (G) was observed upon reperfusion, while the 63kDa species remained unchanged (F). These data are difficult to interpret, as our fractionation protocol does not allow us to discriminate between proteins on the MOM of mitochondria, or in the lumen/IMS.

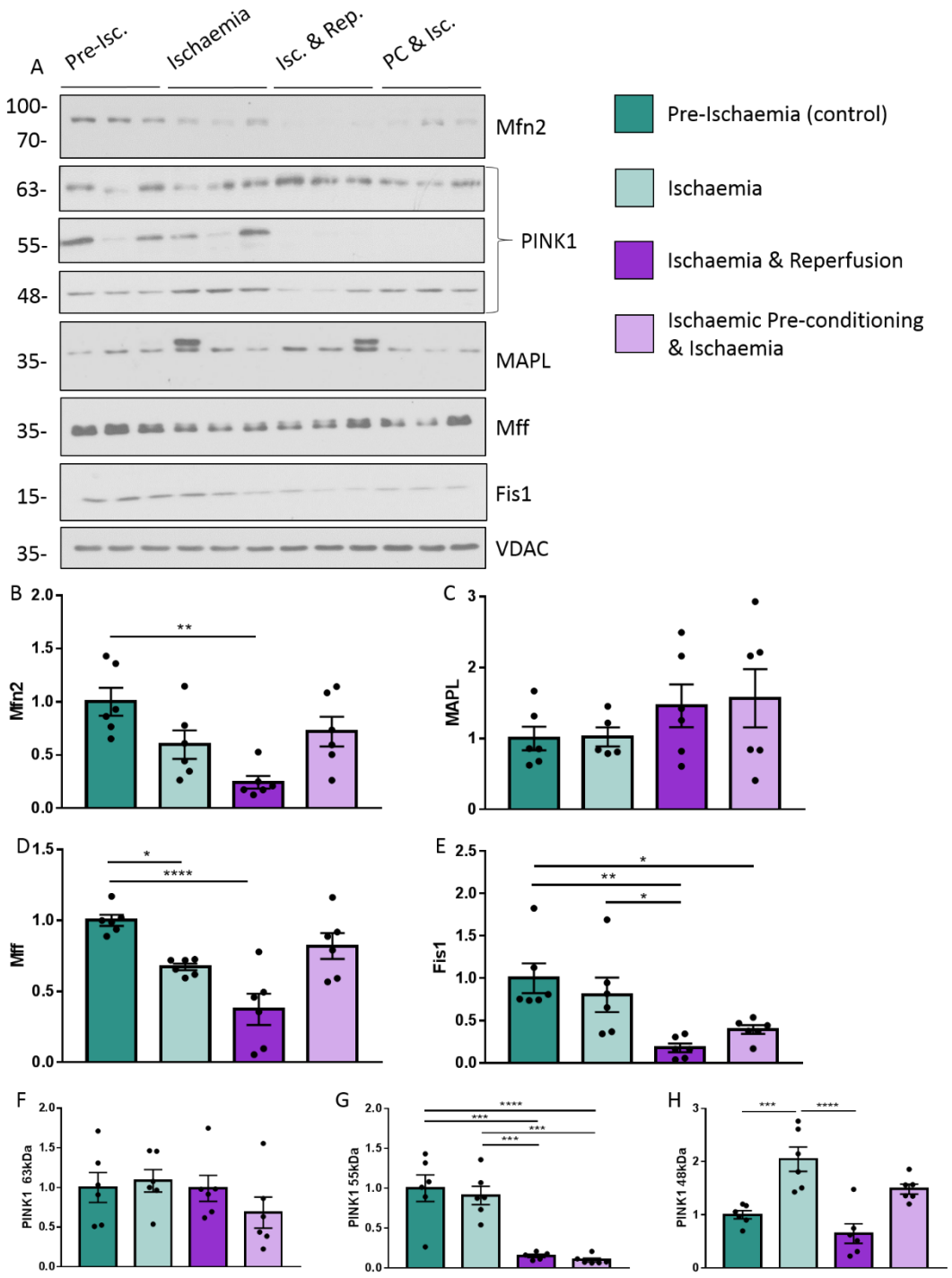

Figure 3.13 **Mitochondrial membrane proteins during ischaemia and reperfusion.** Following subcellular fractionation of perfused left ventricular tissue, mitochondrial samples were used for Western blotting. Samples were probed with Mfn2, PINK1, MAPL, Mff or Fis1 antibodies. Representative blots are of 3 samples per condition. N = 6. Analysed using ordinary one-way ANOVA with Sidak's correction for multiple comparisons with a pooled variance. Data presented as mean ± SEM. * $p < 0.05$, ** $p < 0.01$, *** $p < 0.001$, **** $p < 0.0001$.

3.3.4.3 Mff is a novel SUMO substrate

Of all mitochondrial membrane proteins studied in this project, Mff was of particular interest for two reasons. Firstly, during ischaemia, loss of Mff from the mitochondrial membrane coincided with recruitment of Parkin to mitochondria. This loss of Mff was also partially attenuated by ischaemic pre-conditioning, as was Parkin recruitment. Secondly, GFP-Trap immunoprecipitation of CFP-Mff from HEK293T cells revealed that Mff can be SUMOylated (Figure 3.14), both by SUMO-1 (A) and SUMO-2/3 (B). Mutation of lysine 151 of Mff to non-SUMOylatable arginine completely abolishes both SUMO-1- and SUMO-2/3-ylation of Mff, indicating that this is the only SUMO-modified residue. These same higher molecular weight species can also be observed in the CFP blot (C), indicating that it is Mff, rather than a co-immunoprecipitated protein, which is SUMOylated. Based on these observations we postulated that Mff SUMOylation, which has not been shown previously, could play a role in Mff stability and turnover.

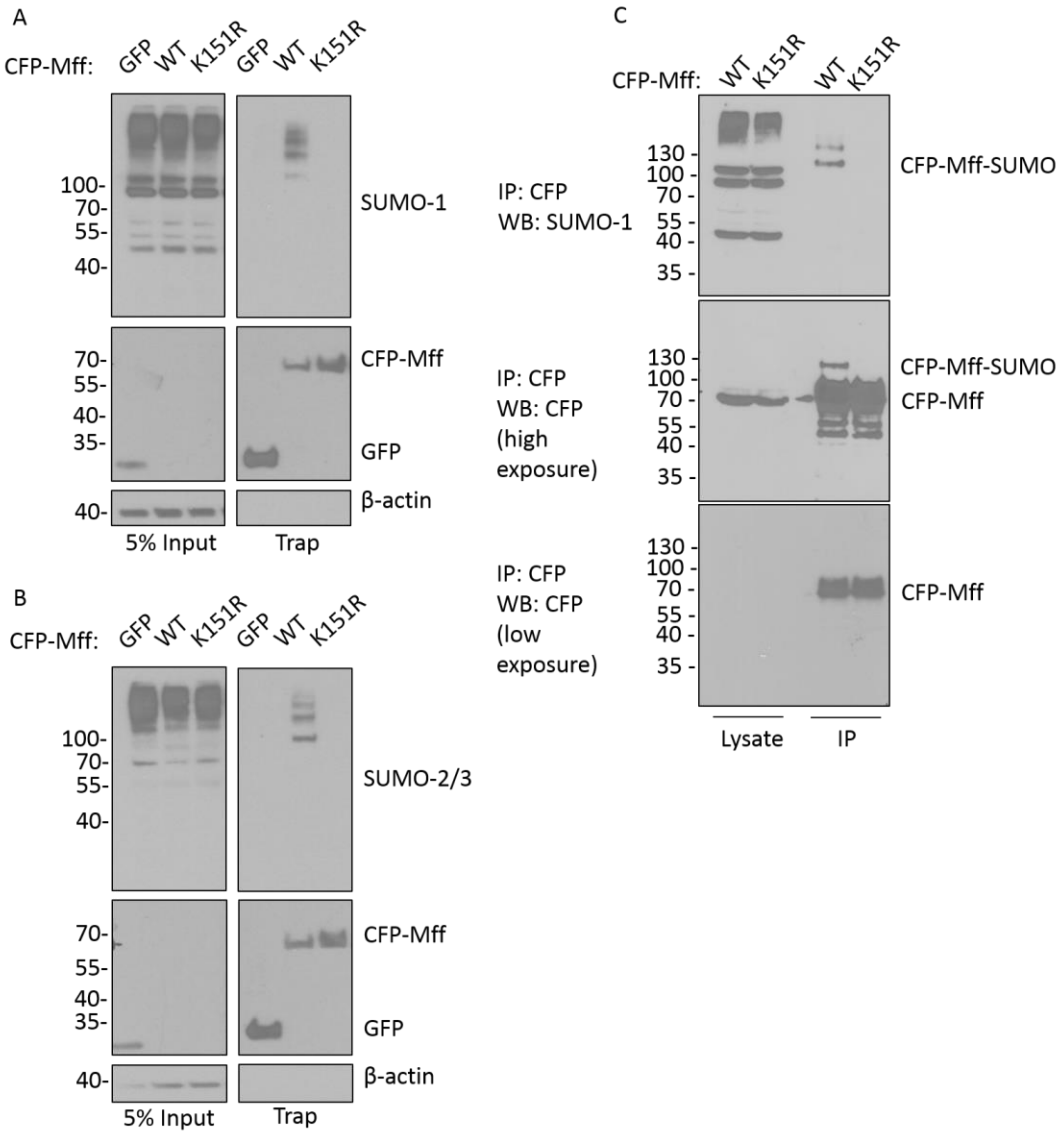

Figure 3.14 **Mff is SUMOylated at Lysine 151 only.** GFP-Trap immunoprecipitation and Western blotting of CFP-Mff reveals high levels of endogenous SUMO-1- (A) and SUMO-2/3-ylation (B). Mutation of Lysine 151 to Arginine (K151R) abolishes both SUMO-1- and SUMO-2/3-ylation of Mff. Over-exposure of the CFP blot from similar experiments reveals that the same higher molecular weight, SUMO-reactive bands are also CFP-reactive (C), indicating that we are observing SUMOylated CFP-Mff.

To validate the finding that Mff can be SUMOylated, further purification assays were performed, in the presence or absence of over-expressed deSUMOylating enzymes (SENPs). In these assays, GST or GST-Mff was transfected into HEK293T cells, with or without a tagged SENP. GST-tagged protein was then purified and probed for GST. By probing for the purified, tagged protein, the possibility of false-positive data as a result of covalent modification of another co-purified protein can be avoided. Additionally, the over-expression of a SENP allows us to distinguish genuine SUMO-modifications from any

SUMO cross-reactive species, as it is well characterised that SENPs are highly specific for SUMO (Reverter and Lima, 2004).

Figure 3.15 shows Western blots of GST-Mff purified from HEK293T cells co-transfected with FLAG-SENP2 (A) or GFP-SENP5 (B). In both cases, co-transfection with a SENP eliminates the higher molecular weight GST-reactive species that we believe corresponds to mono-SUMOylated GST-Mff (labelled GST-SUMO-Mff, ~100kDa) which is apparent in the absence of SENP.

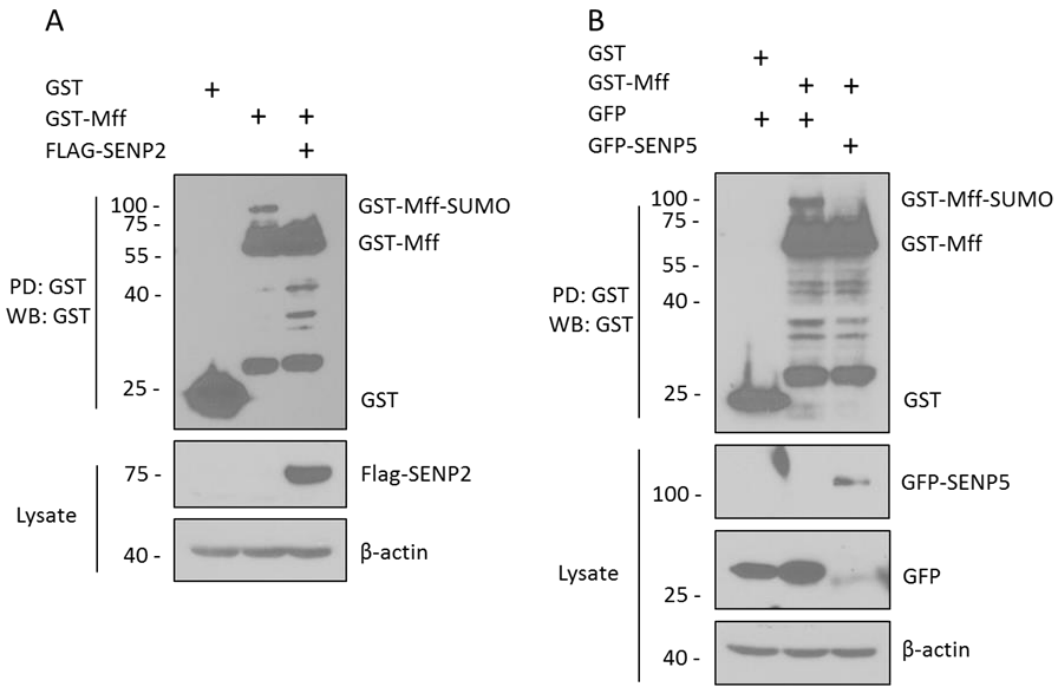

Figure 3.15 **Mff is a SENP substrate.** HEK293T cells were transfected with GST-Mff with or without FLAG-SENP2 (A) or GFP-SENP5 (B). GST-tagged protein was then purified using glutathione beads and the pull down (PD) probed for GST (WB). In the absence of SENP, GST-Mff exists at its unmodified molecular weight (~65kDa) and as a band-shifted species (~100kDa). In the presence of SENP, the 100kDa species is removed.

3.4 Discussion

3.4.1 Mitochondrial fraction was adequately clean

For the purposes of this study, highly purified mitochondrial fractions were neither necessary nor desirable; it has been shown previously that purified mitochondrial protein preparations are devoid of low affinity or fleetingly-bound associated proteins (Pasdois et al., 2013). Given that a number of proteins of interest are only transiently recruited to the MOM from the cytosol, crude mitochondrial fractions were used. However, owing to the large proportion of SUMOylation that is nuclear, it was important to adequately separate the nucleus-containing fraction from the mitochondria-enriched fraction, lest any mitochondrial changes in SUMOylation be contaminated and obscured by nuclear SUMO.

Sufficient purity of the mitochondrial fraction was determined by probing for cytosolic and nuclear markers. As shown in Figure 3.5, very little GAPDH (cytosolic) was detected by Western blotting of the mitochondrial samples, compared to the total ventricular lysate. Similarly, no Lamin B (nuclear) was detected in the same samples, indicating that purification had removed at least most traces of nuclear contaminants.

VDAC is typically considered to be a mitochondrial marker, being the most abundant protein of the MOM (Simamura et al., 2008). However, like most mitochondrial proteins, it is synthesised on ribosomes at the ER prior to its translocation and insertion into the MOM (Dubey et al., 2016). Interestingly, far more VDAC species were found to be present in the total lysate that the mitochondrial fraction (Figure 3.5). This suggests that the reasonable purity of the mitochondria-enriched fraction was achieved at the expense of mitochondrial yield. There are three isoforms of VDAC (VDAC-1, -2 and -3) in mammals, encoded on homologous genes, with VDAC-1 being the most abundant (Shoshan-Barmatz et al., 2010). All isoforms are subject to modification by phosphorylation and acetylation, resulting in the wide range of detected molecular weights species (Choudhary et al., 2009, Gauci et al., 2009, Kerner et al., 2012). The VDAC-1, -2, -3 antibody has been widely used in the literature, and has been previously validated (Zou et al., 2014, Quast et al., 2013, Plotz et al., 2012).

3.4.2 Reperfusion is the primary cause of cellular damage

It has long been known that reperfusion incurs greater cellular damage than the ischaemic insult itself. In particular, apoptotic mechanisms are almost exclusively brought about by reperfusion (Griffiths and Halestrap, 1995, Halestrap, 2010, Kalogeris et al., 2014). It was important that the *ex vivo* model of I/R injury employed in this study reflected this. To confirm this, various markers of cellular stress and/or cell death were probed.

As shown in Figure 3.6, no significant differences were observed in markers of apoptosis (cleaved Caspase 3) or autophagy (LC3-II/LC3-I ratio) between pre-ischaemic and ischaemic groups, indicating that little or no cell death was detectable during ischaemia alone. However, on reperfusion, both the cleaved Caspase 3 and LC3-II/LC3-I ratio were increased and were significantly different from both the pre-ischaemic and ischaemic controls, indicative of activation of apoptotic and autophagic mechanisms. As would be expected, IPC did not contribute to increase in either marker of cell death.

Although cell death brought on by I/R injury occurs almost exclusively on reperfusion, many of the mechanisms of cellular stress are set in motion during the ischaemic phase, often as a result of the accumulation of cytotoxic by-products of glycolysis, initiated under anoxic conditions. Lactate Dehydrogenase (LDH) catalyses the final step of anaerobic glycolysis, converting pyruvate to lactate via coupled oxidation of NADH to NAD+ (Everse and Kaplan, 1973). Damage to the plasma membrane, brought about by ischaemic stress, releases cytosolic LDH from the cell, where it can be collected from the perfusate.

Ischaemic pre-conditioning involves a series of short bursts of ischaemia. Ideally, this is not damaging to the tissue. However, too many or too long IPC cycles incur the same cellular damage as real ischaemic insult. To exclude the possibility that the IPC performed in this study contributed to cellular damage, perfusate was collected immediately after start of the final reperfusion dung IPC and subjected to LDH assay (Figure 3.7). The results of this were compared to perfusate samples taken before any ischaemic events, and to those taken immediately after start of perfusion following 30-minute ischaemic insult. As shown in Figure 3.7, LDH assay results from the IPC group were not significantly different from those of the pre-ischaemic group. The end-ischaemia group, however, had significantly higher LDH assay values than both the pre-ischaemic and IPC groups. These data indicate that the IPC protocol we used did not induce any detectable cellular damage.

3.4.3 Global ubiquitination, but not SUMOylation, changes during I/R Injury

Global protein SUMOylation has been reported to be upregulated as a result of hypoxia (Guo et al., 2013, Meller et al., 2014, Lee et al., 2007). Surprisingly, in this *ex vivo* study (Figure 3.9) very little change was observed in global conjugation of SUMO-1 or SUMO-2/3, although a small but significant increase was observed in SUMO-1-ylation of the IPC, compared to ischaemia alone. This could fit with the established narrative of SUMOylation as a cytoprotective modification (Guo et al., 2013, Guo et al., 2017, Lee et al., 2007, Luo et al., 2017), raising the possibility of SUMOylation as a protective influencer of IPC.

Nevertheless, a lack of global changes to the SUMOylated proteome does not preclude the possibility that the SUMOylation status of subsets of proteins may be altered under these conditions. Indeed, a clear example of this is the mitochondrial 55kDa SUMO-1-ylated species shown in Figure 3.10 (C). Whilst the total mitochondrial proteome mirrored the total proteome in lacking global changes to SUMOylation levels, this mitochondria-associated 55kDa species was significantly more abundant during ischaemia and after reperfusion compared to pre-ischaemia. Interestingly, IPC prevented this increase in abundance, potentially indicating that SUMO-1-ylation of this protein is in fact detrimental to recovery from I/R injury.

Much of the previous work on SUMOylation and ischaemia has made use of isolated cell cultures and cell lines (Guo et al., 2013, Luo et al., 2017). We speculate that cells in culture may be more receptive to stress/cytotoxicity due to the lack of supporting cells, extracellular matrix (ECM) and extracellular signalling pathways. One study showed that, in both a mouse model and infarct patients, extracellular vesicles of myocardial origin could be found in blood and tissues following myocardial infarct. In *in vitro* experiments, these vesicles could modulate endothelial function, indicative of an active role in post-ischaemic cardiac repair (Rodriguez et al., 2018).

Although no large-scale changes were observed in SUMOylation, this was not the case for ubiquitination. As shown in Figure 3.8 and Figure 3.10, global conjugation of ubiquitin was significantly increased upon reperfusion, compared to both pre-ischaemia and ischaemia alone. This is unsurprising, given the critical role of ubiquitin-targeted proteasomal degradation in the Unfolded Protein Response (UPR), triggered under cytotoxic conditions (Lindholm et al., 2017).

3.4.4 I/R recruits mitochondrial fission-associated proteins to the MOM

Due to their dynamic nature and the previously reported importance of mitochondrial fission in I/R injury cellular survival, proteins associated with fission were of particular interest (Ambrosio et al., 1993, Griffiths and Halestrap, 1995, Schaller et al., 2010).

Mitochondrial fission is a necessary part of cell division, maintenance of cellular integrity, and adaptability. In particular, due to their huge energy requirements, the mitochondria of cardiac myocytes undergo constant remodelling by fission and fusion, with networked mitochondria allowing efficient ATP transfer from the cell core to the periphery, and independent mitochondria being easily trafficked to more energy-demanding regions of the cell (Piquereau et al., 2013). Perturbation of the fission/fusion equilibrium as a result of ischaemia or reperfusion can drastically impact upon cellular recovery from I/R injury. By identifying differences in recruitment patterns between ischaemia and IPC groups, we hoped to identify potential protective proteins.

Drp1 and Dyn2

Drp1 is a key regulator of mitochondrial fission, facilitating membrane scission at ER junction sites (Prudent et al., 2015, Braschi et al., 2009, Lee et al., 2004). In addition, Dynamin II (Dyn2) has more recently been identified as another critical player in mitochondrial fission, without which organelle membranes become stuck at an elongated, pre-scission point (Kraus and Ryan, 2017, Lee et al., 2016). Both Drp1 and Dyn2 were probed for in the mitochondrial fractions from this study, as Dyn2 cannot act upon membranes not pre-constricted by Drp1 (Kraus and Ryan, 2017).

As shown in Figure 3.11, both Dyn2 and Drp1 appeared to be slightly more abundant on the MOM of ischaemic samples compared to pre-ischaemia, although this increase did not reach statistical significance. Interestingly, MOM levels of Drp1 were significantly increased by IPC, whereas Dyn2 abundance was significantly decreased by the same treatment. Taken alone, these data could be indicative of there being no net change in mitochondrial fission upon IPC, as the increase in one component of the fission machinery is counterbalanced by the decrease in the other. From these data it seems that other factors are also involved, and further investigation of fission-associated proteins would be required. For example, the primary Drp1 receptor, Mff, was unchanged by IPC, but this does not preclude the possibility that other, unidentified Drp1 receptors are not up- or down-regulated by IPC.

Parkin

Parkin is known to be recruited to depolarised mitochondrial membranes by accumulation of PINK1, where it sets in motion the various mechanisms of mitophagy (Berger et al., 2009, Clark et al., 2006, Exner et al., 2007, Geisler et al., 2010). It was therefore unsurprising that such a large increase in Parkin was detected at the MOM during ischaemia (Figure 3.11). With Parkin activated and in place at the MOM, damaged mitochondrial proteins can be marked for proteasomal degradation by Parkin-mediated poly-ubiquitination. One observation that was particularly intriguing was the decreased level of Parkin detected at the MOM of mitochondria subjected to IPC prior to ischaemia. This difference implicates the PINK1/Parkin pathway as a potential candidate for a role in IPC.

Fbxo7

With Parkin identified as a protein of interest, we reasoned that Parkin-related or functionally similar proteins might also prove interesting. We therefore tested if Fbxo7 co-localises with Parkin to the MOM in ischaemia. As shown in Figure 3.11, there was a hint that Fbxo7 abundance at the MOM was slightly increased by ischaemia, although this was not statistically significant. Interestingly, prior IPC did significantly reduce Fbxo7 mitochondrial presence compared to ischaemia alone, thereby marking it as another protein of interest for this study.

From the mitochondrial fractions alone, it is difficult to definitively discriminate between increased recruitment of proteins of interest to the MOM and increases in total expression. To that end, the total lysate was also probed for all candidate proteins. Although total levels of these proteins were often very variable between the different animals, no significant differences were detected in Dyn2 or Parkin over the course of I/R injury modelling (Figure 3.12). These data indicate that the large increase in Parkin at the MOM during ischaemia is attributable to enhanced recruitment rather than increased protein expression. In the case of Drp1, however, the significant decrease in abundance at the MOM on reperfusion seems to reflect a loss of total Drp1 from the cell, presumably a result of its degradation, given the short timeframe of the experiment. Similarly, the decrease in Fbxo7 at the MOM brought abought by IPC was also observed at the level of the total protein, so is likely due to a net loss of protein, rather than a translocation event.

3.4.5 The composition of the MOM is altered by I/R Injury

With various fission-associated proteins being recruited to the MOM over the course of I/R injury, it was proposed that the composition of the MOM itself could also be altered. Mff is the main fission-associated receptor of Drp1, so was an obvious candidate target (Guo et al., 2017). As shown in Figure 3.13, the Mff content of the MOM was decreased by ischaemia, and further decreased upon reperfusion. IPC appeared to oppose this loss. A secondary Drp1 receptor, Fis1, showed a very similar pattern, with a slight loss during ischaemia, exacerbated by reperfusion. Most interesting, however, was that loss of Mff from the MOM during ischaemia occurred over the same timescale as recruitment of Parkin. IPC blocked or partially blocked both of these events. It has been previously reported that Mff is a target of Parkin-mediated ubiquitination, and these complementary events support the previous findings, and also highlight the Parkin/Mff interaction as an interesting target in the study of ischaemia and IPC (Gao et al., 2015).

Moreover, we have shown for the first time that Mff is a target of modification by both SUMO-1 and SUMO-2/3. Taken together, the data presented in Figure 3.14 and Figure 3.15 provide compelling evidence for Mff as a *bona fide* SUMO substrate. We demonstrate that Mff presents not only at its unmodified molecular weight, but also as a higher molecular weight species, which is specifically removed in the presence of a deSUMOylating enzyme and can be ablated by point mutation of a lysine residue in Mff. In future, denaturing immunoprecipitation experiments could be performed to eliminate the possibility of the SUMO conjugates identified in Figure 3.14 being covalently attached to another Mff-interacting protein, although the data shown in Figure 3.14 (C), as well as Figure 3.15, in which the modified protein is CFP- or GST-positive, go a long way towards ruling out that possibility. The potential implications of this modification are currently being investigated, and it has been proposed that the SUMOylation status of Mff may be involved in its stability or activation.

Chapter 4 Regulation of Mff by Parkin and Fbxo7

4.1 Introduction

4.1.1 Drp1 requires adaptors for mitochondrial fission

As previously discussed, Drp1 is an intrinsic part of the mitochondrial fission machinery. In a coupled reaction, Drp1 hydrolyses GTP and oligomerises around the mitochondrial membrane, constricting the neck to a critical diameter at which Dyn2 can perform the final separation (Kraus and Ryan, 2017, Lee et al., 2004, Yoon et al., 2003). Receptor proteins expressed on the outer membrane of mitochondria are required to recruit Drp1, which cannot bind the mitochondrial outer membrane (MOM) directly due to its lack of PH domain (Losón et al., 2013) A brief overview of known Drp1 receptors is given below.

4.1.1.1 Mff

Mitochondrial Fission Factor (Mff) is thought to be the primary adaptor for Drp1-dependent fission, both of mitochondria and peroxisomes (Lee et al., 2004, Alirol et al., 2006, Gandre-Babbe et al., 2008). Consistent with this, Mff knock out cell lines exhibit greatly elongated mitochondria and peroxisomes (Osellame et al., 2016, Otera et al., 2010). Furthermore, Mff-deficient mice are smaller than their WT littermates and die at approximately 3 months due to enlargement and inefficiency of the heart (dilated cardiomyopathy) leading to heart failure (Gao et al., 2015). *In vitro*, incorporation of Mff into synthetic liposomes is sufficient to recruit and activate the GTPase activity of Drp1, whereas insertion of Mid51 is inhibitory (Osellame et al., 2016, Macdonald et al., 2016).

4.1.1.2 Fis1

Fis1 was identified in yeast as an adaptor of the MOM for Mdv1 and Caf4 peripheral membrane receptors (Lackner et al., 2009). These receptors can then recruit and form a complex with Dnm1, the yeast homologue of Drp1. In metazoans, however, there are no homologues of Mdv1 or Caf4, and it has more recently been shown that Fis1 is not required for fission (Osellame et al., 2016, Otera et al., 2010). Fis1 knock out murine embryonic fibroblast cells (MEF) do not exhibit notable morphological changes to the mitochondrial

or peroxisomal networks, casting doubt on the role of Fis1 as a true receptor of Drp1 (Osellame et al., 2016). However, they do have some resistance to apoptosis, implicating Fis1 in apoptosis-mediated fragmentation, stress—induced fission or mitophagy (Shen et al., 2013, Gomes and Scorrano, 2008, Wang et al., 2012a, Yamano et al., 2014).

4.1.1.3 Mid49/51

Mid49/Mid51 are chordate-specific mitochondrial proteins that can recruit Drp1 to the MOM independently of Mff and appear to modulate Drp1 function differently (Osellame et al., 2016, Macdonald et al., 2016). Whereas Mff is confined to foci associated with constriction sites, Mid49 and Mid51 become diffusely localised throughout the MOM in the absence of Drp1 (Richter et al., 2014). It is thought that Mid49 and/or Mid51 form part of a fission mechanism distinct from Mff-Drp1-mediated fission. Drp1-mediated fission via Mid49 and/or Mid51 is required for cristae opening and cytochrome *c* release following apoptotic induction, whereas Mff-Drp1-mediated fission is not (Otera et al., 2016). Despite this, Mff and Mid51 have been identified together and in proximity of Drp1 in mouse embryonic fibroblast (MEF) cells (Osellame et al., 2016). As well as acting to recruit Drp1 to the mitochondrial outer membrane, Mid proteins have been shown to assemble with Drp1 *in vitro*, and Mid49-Drp1 heteropolymer rings can constrict to a significantly smaller diameter than Drp1 homopolymers, indicating that Mid49 can enhance constriction of mitochondrial membranes by Drp1 (Koirala et al., 2013).

4.1.2 Drp1 activity is regulated by PTMs

Regulation of proteins by post-translational modifications (PTMs) has a pivotal role in most, if not all, cellular processes, including mitochondrial fission. Drp1 is heavily post-translationally modified, and this affects its activity as a fission- or fusion-promoting GTPase (Figure 1.18 (A)) (Gandre-Babbe et al., 2008). Phosphorylation of Drp1 by cyclin-dependent kinase 1 (Cdk1) serves to activate it during mitosis (Chang and Blackstone, 2007), while phosphorylation by cAMP-dependent protein kinase (PKA) inactivates Drp1 in quiescent cells and mitochondrial fission is triggered by reversal of PKA-dependent phosphorylation by calcineurin (Cribbs and Strack, 2007).

Drp1 was identified as a SUMO-1 substrate in 2004, by the first group to publish evidence of SUMOylation of the mitochondrial proteome (Harder et al., 2004). The same study showed that SUMO-1 is often detected at sites of mitochondrial fission, and that over-expression of SUMO-1 protects Drp1 from degradation and leads to an increase in mitochondrial fragmentation. Drp1 was later shown to be a substrate of all 3 SUMO

isoforms, despite its lack of consensus SUMOylation motifs, and it was suggested that SUMOylation of Drp1 was influenced by its subcellular localisation (Figueroa-Romero et al., 2009).

However, a later study by the Henley lab flipped this model around, proposing that SUMOylation of Drp1 actually regulates its subcellular localisation. In this study, it was proposed that SUMO-2/3 conjugation sequesters Drp1 in the cytosol, while and SENP3-mediated deSUMOylation allows Drp1 to translocate to the mitochondria. The authors showed that, in HEK293 cells, replacement of endogenous Drp1 with a non-SUMOylatable mutant, but not with WT Drp1, caused substantial release of cytochrome *c* from the mitochondria, indicating that Drp1 SUMOylation is a protective mechanism that reduces its ability to elicit cytochrome c release (Guo et al., 2013). Interestingly, Drp1 SUMO-2/3-ylation was increased by oxygen-glucose deprivation (OGD), providing further evidence that Drp1 SUMOylation may be a cytoprotective mechanism (Guo et al., 2013). It is important to note that the data from the McBride and Henley labs are not necessarily incompatible, as the two groups studied Drp1 modification by different SUMO isoforms.

The Henley lab later published work linking the SENP3-mediated deSUMOylation of Drp1 to increased cell death during OGD, by enhancing the interaction of Drp1 with Mff, but not Mid49, Mid51 or Fis1. They also showed that Drp1 binding to Mff is sufficient to induce cytochrome *c* release, and that preventing this interaction is cytoprotective during OGD and reperfusion (Guo et al., 2017).

4.1.2.1 Mff is regulated by Parkin

Despite its clear importance in maintenance of healthy mitochondrial function, as well as in pathophysiological pathways leading to apoptosis, Mff remains a relatively poorly characterised protein, with no published structure. Based on its sequence, it is predicted to have a single C-terminal transmembrane domain, and computer algorithms reported a region of Mff with high coiled coil-forming propensity, which was later shown to facilitate Mff dimerization *in vivo* (Gandre-Babbe et al., 2008). The Drp1 binding domain of Mff is at the N-terminus. In humans, there are five known isoforms of Mff (sequence alignment shown in Supplementary Figure 1), and a further four predicted, owing to numerous translation- start sites and splice-variants. The constructs used in this project encode isoform 1, the full length 342 amino acid protein (Friedman et al., 2011).

Parkin has previously been reported to ubiquitinate Mff (Gao et al., 2015). In their study, Gao *et al* showed that HA-Parkin could co-immunoprecipitate FLAG-Mff in HEK293 cells, and that carbonyl cyanide m-chlorophenyl hydrazine (CCCP)-induced mitochondrial

stress enhanced their interaction and induced mitochondrial ubiquitination. They showed that GFP-Parkin WT, but not a ligase-dead mutant (GFP-Parkin C431F), was able to ubiquitinate endogenous Mff and FLAG-Mff in HEK293 cells and went on to show that lysine 251 (corresponding to lysine 302 in the isoform used in this project) within the coiled-coil region was the only site of Parkin-induced ubiquitination on Mff. Neither CCCP treatment nor ubiquitination of K251 by Parkin were found to have any effect on Mff oligomerisation. However, a non-ubiquitinatable K251R mutant of Mff was unable to bind p62, which is recruited to damaged organelles during autophagy (Kim et al., 2008a), resulting in defective Parkin-induced mitochondrial clearance. The data presented by Gao *et al* thereby provide intriguing evidence that Mff is essential for Parkin-mediated mitophagy.

4.1.3 Fbxo7 mediates mitophagy

F-box domain-containing proteins act as adaptors to phosphorylated target substrates to SCF (Skp1-Cul1-F-box)-type E3 ubiquitin ligase complexes. This is usually achieved by substrate recruitment through a protein interaction domain and assembly of a functional ligase complex by recruitment of a Skp1 adaptor via the F-box domain (Skowyra et al., 1997). Fbxo7 has also been shown to have SCF-independent activity (Kuiken et al., 2012, Kirk et al., 2008).

Burchell *et al* provide evidence that the N-terminal ubiquitin-like domain (UbL) of Fbxo7 interacts with Parkin and PINK1, both in cells (U2OS osteosarcoma cells) and *in vitro* (Burchell et al., 2013). They also showed that carbonyl cyanide m-chlorophenyl hydrazone (CCCP)-mediated mitochondrial membrane depolarisation elicits Fbxo7 recruitment to mitochondria. Furthermore, knock down of Fbxo7 significantly reduced recruitment of Parkin to depolarised mitochondrial membranes, leading to their hypothesis that Fbxo7 functions upstream of Parkin in mitophagy. Like Parkin, Fbxo7 partitioning to mitochondria was PINK1-dependent, with recruitment of both Parkin and Fbxo7 significantly reduced by knock down of PINK1 (Burchell et al., 2013). Intriguingly, over-expression of Fbxo7 rescued several 'disease' phenotypes in Parkin-deficient *Drosophila*, including locomotor defects, dopaminergic neuron loss, muscle degeneration, and mitochondrial disruption. Knock down of Fbxo7 inhibited mitophagy, delaying the lipidation of LC3-I to LC3-II in the mitochondrial fraction by reducing Parkin-dependent recruitment of p62, the mitochondrial adaptor of LC3-II, thereby inhibiting LC3-II-dependent recruitment of the autophagosome to depolarised mitochondria (Burchell et al., 2013).

4.1.4 H9c2 cells

H9c2 cells are a clonal myoblast cell line isolated from embryonic rat ventricular tissue (Kimes and Brandt, 1976). This cell line was chosen for its ventricular origin, as the ex vivo fractionated heart samples were also ventricular; other cardiac cell lines, such as HL-1, are derived from atrial tissue (Rao et al., 2009). While H9c2 cardiac myoblasts cannot be induced to contract in culture, like HL-1 cells can, they are physiologically more similar to primary cardiac myocytes (Watkins et al., 2011). In culture, their electrophysiological properties, as well as their membrane morphology, are largely the same as those of primary cells (Sipido and Marban, 1991, Hescheler et al., 1991).

4.1.5 Aims

The aims of this part of the project were to investigate the interplay between Parkin, Fbxo7 and Mff, and their effects on mitochondrial dynamics. Specifically, these aims can be divided into three parts:

i. Knock down Parkin and Fbxo7, both individually and together, to study the effects on mitochondrial fission proteins Mff and Drp1.
ii. Parkin has been previously shown to interact with, and ubiquitinate, Mff (Gao et al., 2015). Therefore, I attempted to recapitulate and validate these findings. This is important because the functional study by Gao *et al* focused exclusively on over-expressed Parkin. E3 ligases are known to be promiscuous both in their target substrates and their preferred lysine residues (Kanner et al., 2017, Danielsen et al., 2011). For that reason, over-expression of E3 ligases can have off-target artefactual effects. For functional experiments, I focussed only on activity of endogenous Parkin.
iii. Fbxo7 has not been previously reported to ubiquitinate Mff, but we hypothesised that its functional relationship with Parkin and role in mitophagy made it a likely candidate regulator of Mff. Therefore, I investigated this possibility.
iv. Identify any gross morphological changes in mitochondrial networks as a result of manipulation of Parkin and/or Fbxo7.

4.2 Methods

4.2.1 Protein degradation assay

In order to measure rates of protein degradation in HEK293T cells, protein synthesis must be blocked. Protein translation elongation was inhibited by addition of a drug, cycloheximide (CHX). HEK293T cells were cultured and transfected as described in Chapter 2. Protein synthesis was blocked by addition of 25µg/mL cycloheximide (Sigma-Aldrich) for up to 24 hours prior to cell lysis. Western blotting was used to quantify rates of degradation.

4.2.2 Production of Lentivirus

4.2.2.1 Preparation of HEK293T cells

HEK293T cells were cultured only in DMEM from Sigma, supplemented with 10% FBS (Sigma), 2mM L-Glutamine and 1% (v/v) Penicillin/Streptomycin ('complete DMEM'). Once confluent, cells were counted and plated in 100mm cell culture dishes at 7,000,000 cells/dish. Cells were transfected 24 hours after plating.

4.2.2.2 HEK293T cell Transfection

10µg pXLG3 viral vector, 2.5µg pMD2.G (expression of VSV-G envelope protein) and 7.5µg p8.91 (helper vector) were mixed in a Bijou tube with 2.5mL plain DMEM. 60µL 1mg/mL Polyethylenimine (PEI) were added to 2.5mL plain DMEM in another Bijou tube and mixed by inversion. The DMEM-PEI mixture was sterile-filtered into a 15mL Falcon tube and incubated at RT for 3 minutes. The DMEM-PEI mixture was then mixed again by inversion and added to the DMEM-DNA mixture. This was inverted several times to mix, then incubated at RT for 30 minutes. Cells were gently washed once with 6mL warm plain DMEM. DMEM was aspirated, and the 5mL transfection mix gently added to the cells. Cells were incubated (37°C in a humidified cell culture incubator, supplied with 5% CO_2 and 95% O_2) for 4 hours, and then the transfection mix was aspirated and replaced with 7mL warm, sterile-filtered complete DMEM.

4.2.2.3 Harvesting Lentivirus

Virus was harvested 48 hours post-transfection. Virus-containing DMEM was centrifuged at 4000rpm for 10 minutes in a 15mL Falcon tube to remove cell debris. The supernatant was then filtered through a 0.45µm filter pre-wetted with complete DMEM.

Viral knock down efficiency was tested by adding a range of volumes to HEK293T or H9c2 cells in 35mm dishes and lysing 4-5 days later. Around 100µL was usually found to be sufficient to produce ≥80% protein knock down. Aliquots of lentivirus were stored at -80°C.

4.2.3 H9c2 cells

4.2.3.1 Cell culture

H9c2 rat cardiac myoblast cells were purchased from ATCC. Stocks containing 1% (v/v) DMSO were stored in liquid nitrogen. Aliquots of frozen H9c2 (subclone of the original myoblast clonal cell line derived from embryonic BD1X rat heart tissue (Kimes and Brandt, 1976)) cells were taken from the cryostore, thawed at 37°C in a water bath and transferred into a 15mL Falcon tube with 9mL 'complete media' (DMEM with phenol red, without Na-pyruvate, with stable glutamine, with 3.7 g/L NaHCO3 and 4.5 g/L D-glucose (Merck-Millipore) supplemented with 10% (v/v) FBS and 0.05% (v/v) Penicillin/Streptomycin. The cell suspension was centrifuged at 1000 x g for 2 minutes at room temperature (RT). The cells were re-suspended in 1mL complete media and transferred to a T75 flask containing 12mL complete media. Cells were cultured in T75 flasks and passaged upon reaching ~60% confluence. Cells were not used beyond passage 27.

4.2.3.1.1 Passaging of H9c2 cells

H9c2 cells were passaged upon reaching ~60% confluency. Complete media was aspirated from the flask and the cell monolayer was gently washed with 10mL 1x Phosphate Buffered Saline (PBS). PBS was then aspirated and 1mL Trypsin-EDTA was added to the cells and the flask returned to the incubator for 3 minutes. Individual cells were detached from the flask by gentle tapping before 9mL complete media was added to quench the trypsin digest. The cell suspension was then centrifuged in a 15mL Falcon tube at 1000 x g for 2 minutes to pellet the cells. Media was then aspirated, and the cells resuspended by gentle trituration in 10mL fresh complete DMEM. For maintenance of H9c2 stock flask, this suspension was diluted 1:10 in complete media in a new T75. For infection, cells were plated on 35mm (30,000 cells in 2mL media) plastic cell culture dishes pre-coated with laminin for biochemistry or live imaging, or on 13mm glass coverslips (pre-coated with laminin) in a 12 well dish at 12,000 cells/coverslip for fixed cell imaging.

4.2.3.1.2 Differentiation of H9c2 cells

To differentiate H9c2 myoblasts towards a more myocyte-like phenotype, cells in 35mm dishes or on 13mm coverslips were grown in complete media until they reached

confluency. At this point, media was replaced with complete media containing 1% (v/v) Horse serum in place of 10% (v/v) FBS ('differentiation media'). Cells differentiated to form multinucleated myotubes. H9c2 cells were kept in this condition for no more than 5 days.

4.2.3.2 Viral transduction of HEK293T cells and H9c2 cells using Lentivirus

Lentiviruses were generated to knock down Parkin and Fbxo7 in H9c2 cells. Lentivirus was tested in various volumes and for varying lengths of time (1-7 days) to optimise target protein knockdown. The appropriate volume of lentivirus (scrambled or knockdown sequence) was added to cells in penicillin/streptomycin-free media. Cells were lysed/fixed 4-5 days post-transduction.

4.2.3.3 Oxygen-Glucose Deprivation

Oxygen-Glucose Deprivation (OGD) is a widely used cellular model of ischaemia (Singh et al., 2009, Tasca et al., 2015). For OGD experiments, cells were placed in a temperature controlled anaerobic chamber at 37°C, in glucose-free DMEM. Media and 1xPBS (used to wash off glucose- and oxygen-containing DMEM) were left to de-oxygenate overnight in the chamber. A mixture of 95% N_2 and 5% CO_2 was used to remove oxygen and maintain carbonate-buffered pH of DMEM. Control cells were washed in oxygenated 1xPBS and maintained in oxygenated, glucose-containing DMEM in a normal cell culture incubator (95% O_2, 5% CO_2). To prevent reperfusion, cells were lysed inside the anaerobic chamber. Samples were then collected for Western blotting.

4.2.4 Fixed sample confocal imaging

Confocal images were acquired using a 63x HCX PL APO CS oil-immersion objective on a Leica SP5-II confocal laser scanning microscope attached to a Leica DMI 6000 inverted epifluorescence microscope. Images were acquired at 400Hz at a resolution of 1024x1024 pixels with 3.2x optical zoom. 3 independent experiments were performed, and 6 fields of view randomly imaged per coverslip. 1-4 cells were analysed per field of view; cells were chosen for analysis only if the nucleus was intact and in focus.

4.2.4.1 Preparation of coverslips

4.2.4.1.1 Sterilisation

13mm glass coverslips (VWR) were submerged in nitric acid overnight with gentle agitation. They were then washed 3 times with cell culture grade water and submerged in

70% ethanol overnight with gentle agitation. Coverslips were washed a further 3 times in cell culture grade water before being placed in 12 well plates.

4.2.4.1.2 Laminin coating

Laminin (Sigma-Aldrich) was diluted to 50 µg/mL in 1xPBS and used to pre-coat glass coverslips (100µL diluted laminin/13mm coverslip) at 37°C for ≥ 1 hour, then washed 4 times with sterile cell culture water prior to cell plating.

4.2.4.2 MitoTracker staining

Mitochondria were stained live using MitoTracker Deep Red (Thermo Fisher Scientific). Mitochondria were stained for 30 minutes prior to the experiment. MitoTracker Deep Red was added to the cell culture media to a final concentration of 100nM and cells returned to the incubator. After 30 minutes, cells were washed 3 times to remove excess stain.

4.2.4.3 Preparation of glass slides

After the experiment, coverslips were washed 3 times in 1xPBS and cells fixed in pre-chilled acetone for 10 minutes at -20°C. Acetone was then removed, and the coverslips washed twice in 1xPBS. Prior to mounting, coverslips were dipped in cell culture grade water. Coverslips were mounted on glass microscopy slides (Thermo Fisher Scientific) using 30µL Fluoromount-G with DAPI (Thermo Fisher Scientific). Slides were allowed to dry overnight at room temperature and then stored at 4°C.

4.2.5 Mitochondrial network analysis

MiNA (Mitochondrial Network Analysis) is a freely available pair of macros that work in conjunction with existing plugins in ImageJ to provide semi-automated analysis of mitochondrial networks (Valente et al., 2017). This software greatly simplifies analysis and quantification of mitochondrial numbers and networks in an efficient and unbiased way, compared to manually assigning morphological features. The toolset includes optional pre-processing steps which remove the need to manually enhance, sharpen and apply filters to images prior to analysis.

Sharp images with high contrast and minimal background noise are necessary for accurate analysis of mitochondrial networks. The pre-processing steps within the MiNA macros first apply Unsharp Masking to enhance image sharpness, thus contributing to deconvolution of the image by subtracting a blurred version of the image from the original.

The resulting image is then subjected to CLAHE (contrast limited adaptive histogram equalization) to equalize the histogram by adjusting pixel intensities and limiting the amount of local change that is allowed, to limit over-amplification of background. Median filtering is then applied to reduce the "salt and pepper" noise, common in fluorescent images, which can be amplified by Unsharp Masking and CLAHE.

Prior to analysis, the image is converted to binary form by thresholding. This assigns foreground pixels the maximum value of 255, and background pixels 0, the minimum value. This binary image is then converted to a skeleton, representing the features of the original image with a wireframe, the lines of which are just one pixel in diameter. MiNA then requires manual verification that the skeleton is an accurate representation of the original image before proceeding.

Finally, every pixel within the approved skeleton is assigned one of three categories: end point pixel, slab pixel, or junction pixel. The AnalyzeSkeleton ImageJ plugin then uses the definition and spatial relation of pixels to measure the number of branches and branch lengths within each network.

4.3 Results

4.3.1 Parkin and Fbxo7 regulate expression of mitochondrial fission proteins

To knock down Parkin in HEK293T cells, an shRNA sequence was designed to target human Parkin. Figure 4.1 (A) shows the open reading frame (ORF) of human Parkin, taken from the NCBI database (https://www.ncbi.nlm.nih.gov/nuccore/AB009973.1). Four different target sequences were selected for shRNA design, highlighted in (A). The Human (Berger) target sequence has been previously published (Berger et al., 2009). The other three target sequences were selected as they met published criteria for optimal knock down. These included a 5' A- or AA-, GC-content of <50%, and avoiding repeats of four or more A or T nucleotides (Elbashir et al., 2001, Yu et al., 2002). All sequences were also checked for off-target effects by BLAST search of the human genome. Of the three novel shRNA target sequences, one was designed to target only human Parkin, and two designed to target both the human and rat Parkin sequences. All four target sequences were generated as shRNAs in pSUPER alongside a scrambled shRNA negative control. A preliminary experiment showed that the Berger sequence and the Human/Rat 1 sequences both knocked down endogenous Parkin in HEK293T cells (Figure 4.1 (B)). It was anticipated

that future experiments would be performed in rat H9c2 cells, so the shRNA targeting both human and rat Parkin was selected for further use. Sequence alignment shown in (E) demonstrates that this shRNA should target human and rat Parkin. (C, D) shows the Parkin knock down construct almost completely ablates total Parkin (94% knock down) compared to a scrambled shRNA control in HEK293T cells 72 hours post-transfection.

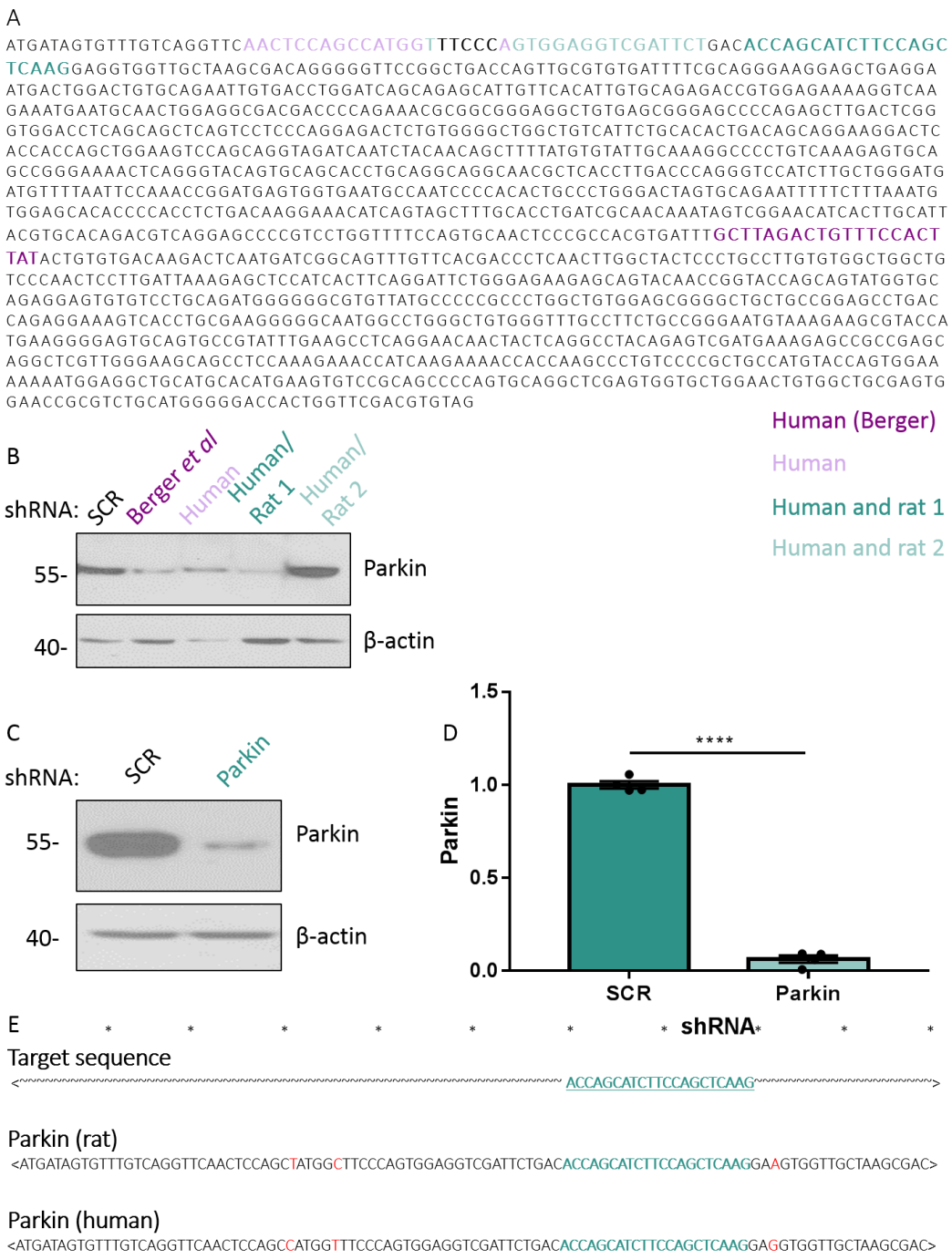

Figure 4.1 **Parkin sequence alignment and shRNA design.** (A) The full coding sequence (open reading frame) of the human Parkin gene. A panel of 4 shRNAs were designed to knock down Parkin in HEK293T cells (coloured). The Human (Berger) target sequence was previously published (Berger, A. K. *et al*, 2009); the other sequences were chosen as they met various criteria for optimal shRNA target sequences. HEK293T cells transfected with the 4 shRNA constructs targeted to the human Parkin sequence were lysed after 72 hours and Western blotted for Parkin. 2 of the 4 tested shRNAs successfully knocked down endogenous Parkin (B). The 'Human/Rat 1' shRNA knockdown was quantified and shown to significantly reduce endogenous Parkin after 3 days compared to a scrambled shRNA control (94% knockdown, C, D). N=4. Analysed using unpaired two-tailed students' t-test. Data presented as mean ± SEM. $p \leq 0.0001$. (E) shows a sequence alignment of the shRNA target sequence with human and rat Parkin. Base mis-matches are highlighted red.

HEK293T cells were transfected with the Parkin-targeted shRNA described in Figure 4.1 or a scrambled (SCR) control and lysed 72 hours post-transfection for Western blot (Figure 4.2). Parkin knockdown resulted in significant reduction of total Drp1 (Figure 4.2 (B)) and increase of total Mff (D). Both Drp1 and Mff have previously been reported to be targets of Parkin-mediated degradation, so while the increase in Mff was expected, the decrease in Drp1 was not (Gao et al., 2015, Wang et al., 2011a). Interestingly, Fbxo7 was also significantly reduced by knock down of Parkin (C), suggestive of a role for Parkin in stabilisation of Fbxo7 or Fbxo7-containing CRLs.

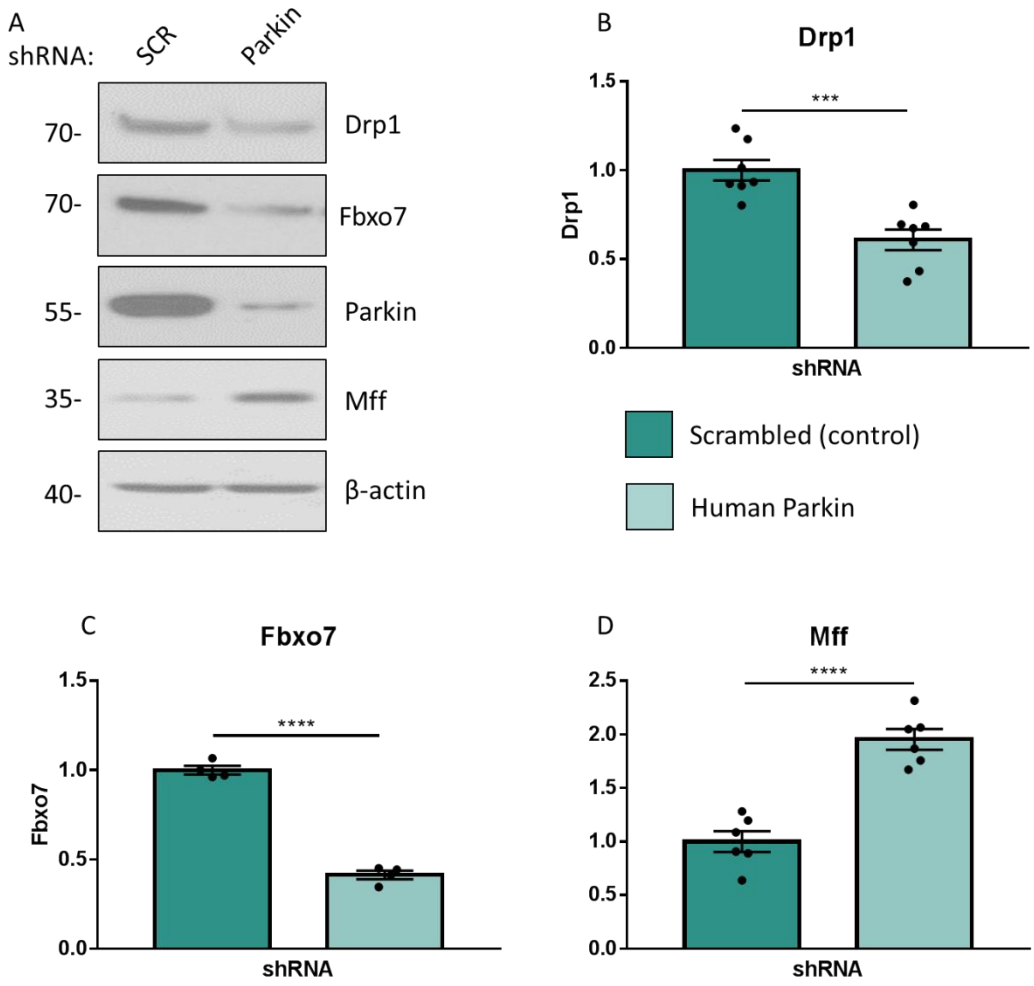

Figure 4.2 Knockdown of Parkin in HEK293T cells. Cells were transfected with either shRNA targeting human Parkin or a scrambled control (SCR). Cells were lysed 72 hours later for analysis. (A) Western blots for Drp1, Fbxo7, Parkin, Mff and β-actin. N= 4-7. (B-D) Quantitative analysis of Drp1, Fbxo7 and Mff levels using Student's unpaired t-test. Data presented as mean ± SEM. *** $p < 0.001$, **** $p < 0.0001$.

Canonically, Parkin is recruited to depolarised mitochondria via a PINK1-dependent pathway. Phosphorylation of S65 within the Ubiquitin-like domain of Parkin by PINK1 contributes to its activation and ubiquitination of mitochondrial proteins during mitophagy (Berger et al., 2009, Xiao et al., 2017).

To test whether the effects of Parkin knockdown on Drp1 and Mff were PINK1-dependent, PINK1 was knocked down in HEK293T cells using a commercially available siRNA (Figure 4.3). Compared to a negative control (siRNA targeting Firefly luciferase), the PINK1 siRNA significantly reduced total PINK1 in HEK293T cells by 72 hours post-transfection, as assessed by Western blot (Figure 4.3 (A, B)). Knock down of PINK1 had no significant effect on total cellular levels of Drp1, Fbxo7 or Parkin (Figure 4.3 (C, D, E)), indicating that the stability of these proteins is not PINK1-dependent. Similar to Parkin knock down, however, knock down of PINK1 significantly increased total Mff (F), suggestive of an upstream role for PINK1 in Parkin-mediated Mff degradation.

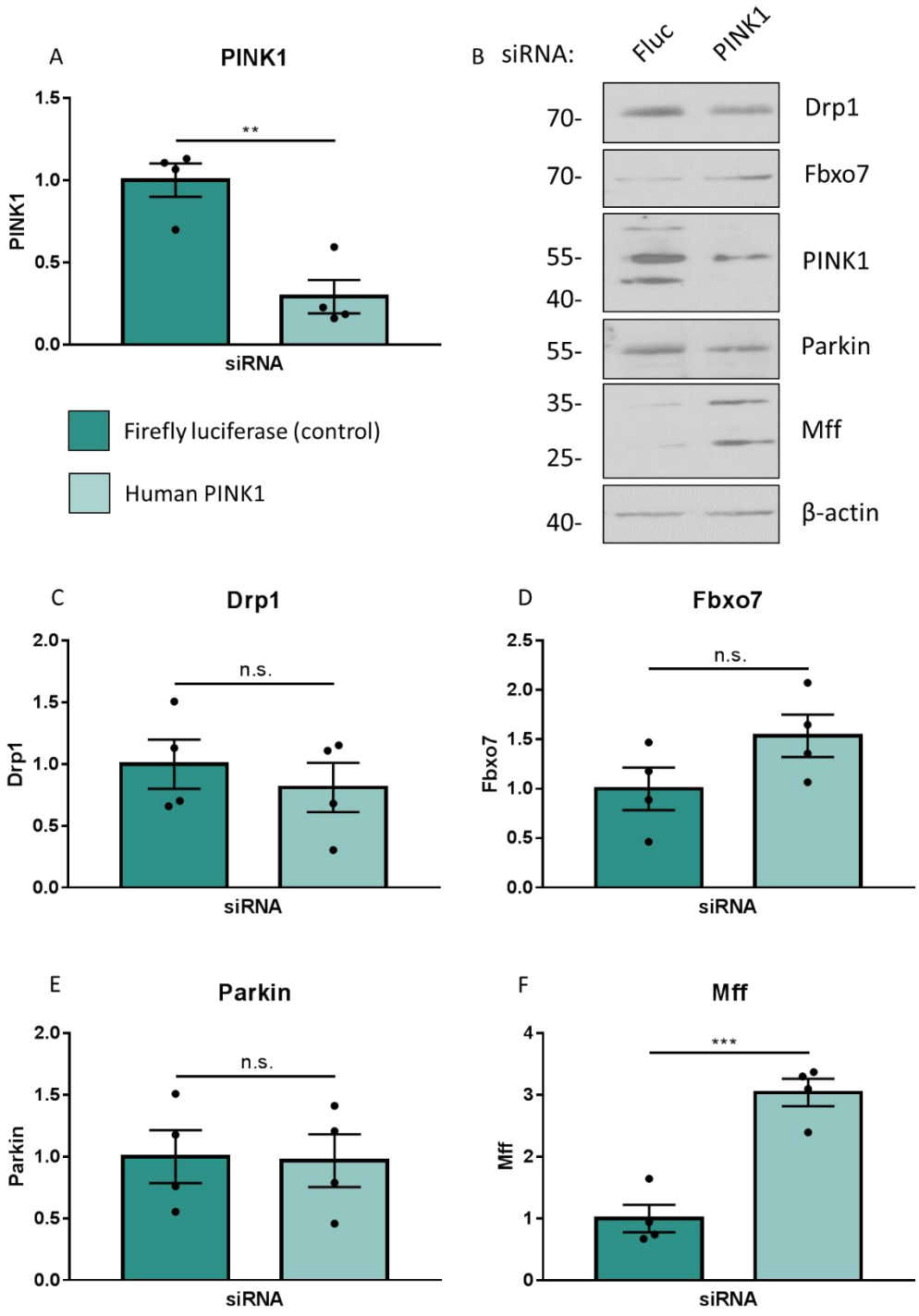

Figure 4.3 **Knockdown of PINK1 in HEK293T cells.** Cells were transfected with siRNA targeting either Firefly luciferase (control) or human PINK1. Cells were lysed 72 hours later. (B) Western blots for Drp1, Fbxo7, PINK1, Parkin, Mff and β-actin. N=4. (A, C-F) Quantitative analysis of blots using Student's unpaired t-test. Data presented as mean ± SEM. ** $p < 0.01$, *** $p < 0.001$.

Fbxo7 has been previously reported to be involved in mitophagy via its interactions with Parkin (Burchell et al., 2013). To examine whether this might be through regulation of Mff, Fbxo7 was knocked down in HEK293T cells using a commercially available siRNA (Figure 4.4). Compared to a negative control (siRNA targeting Firefly luciferase), the Fbxo7 siRNA significantly reduced total cellular Fbxo7 by 72 hours post-transfection (Figure 4.4 (A, B)). Knock down of Fbxo7 had no significant effect on total Drp1 or Mff (C, E). Interestingly, I observed that different Mff-reactive species responded to Fbxo7 knock down in different ways, with a significant reduction in the higher molecular weight species and significant increase of the lower molecular weight species (Figure 4.4 (F, G)). From these data, the lower molecular weight Mff species cannot be definitely labelled as isoforms or degradation products (further discussed in 4.4.1). It is also notable that knock down of Fbxo7 resulted in a significant reduction of cellular Parkin (D). This would be consistent with a model in which Fbxo7 and Parkin stabilise one another, perhaps forming a stable complex, but also confounds the interpretation of these data, as the effects on Mff could be ascribed directly to Fbxo7 knock down, or indirectly to Fbxo7 knock down via depletion of Parkin.

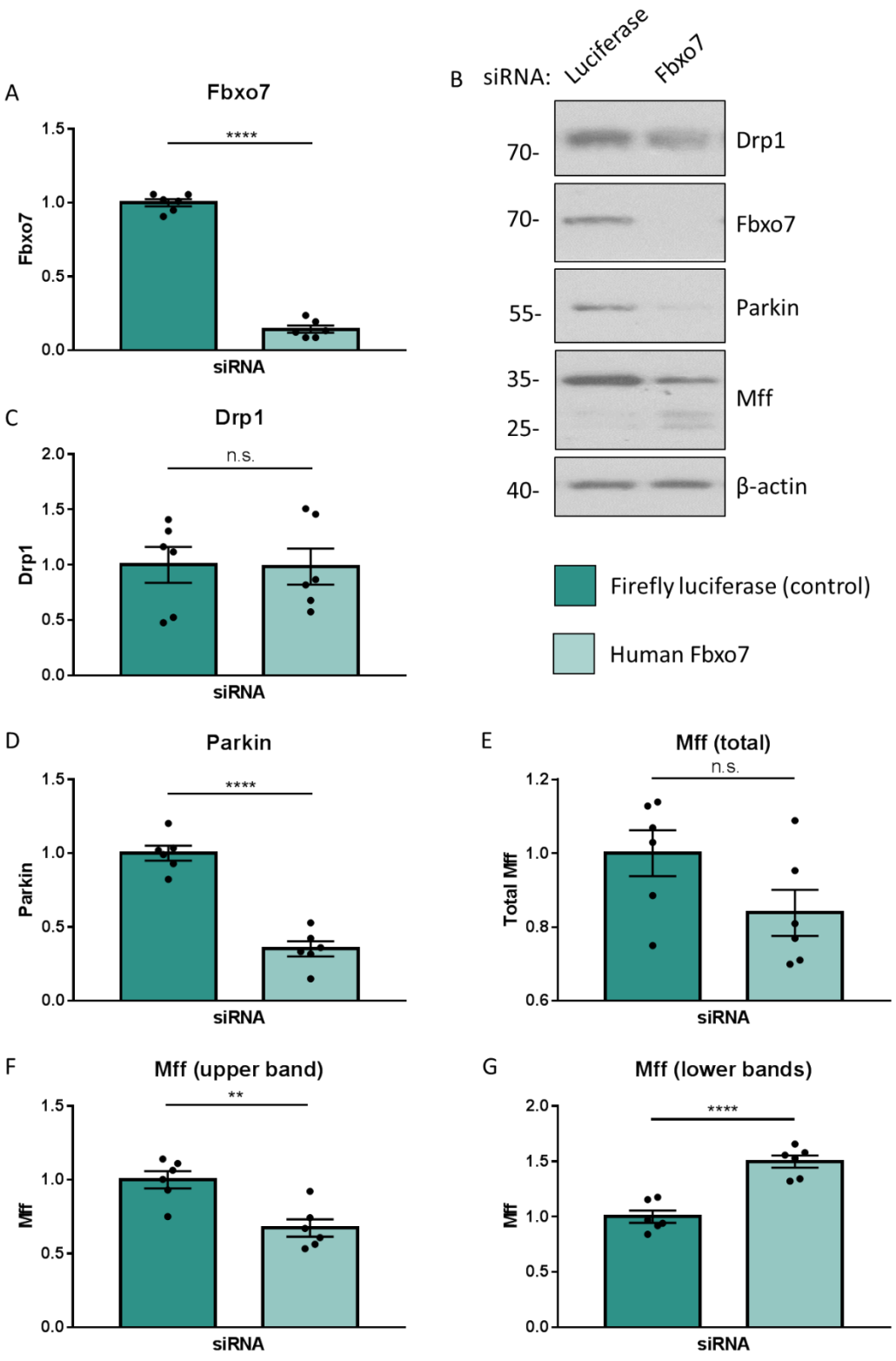

Figure 4.4 **Knockdown of Fbxo7 in HEK293T cells.** Cells were transfected with siRNA targeting either Firefly luciferase (control) or human Fbxo7. Cells were lysed 72 hours later. (B) Western blots for Drp1, Fbxo7, Parkin, Mff and β-actin. N=6. (A, C-G) Quantitative analysis using Student's unpaired t-test. Data presented as mean ± SEM. ** $p < 0.01$, **** $p < 0.0001$.

Given that Parkin and Fbxo7 have both previously been linked to mitophagy, and that Parkin has been linked to both Mff and Fbxo7 (Gao et al., 2015, Burchell et al., 2013), it was important to investigate how knock down of both Parkin and Fbxo7 affects total levels of Drp1 or Mff. Simultaneous knock down of Parkin and Fbxo7 (using shRNA targeted to Parkin and siRNA targeted to Fbxo7) significantly reduced total cellular levels of Drp1 and significantly increased total Mff (Figure 4.5 (D, E)) compared to a negative control (scrambled shRNA and Firefly luciferase-targeted siRNA). These data follow the same trend as knock down of Parkin alone, potentially indicating some functional redundancy of Parkin and Fbxo7.

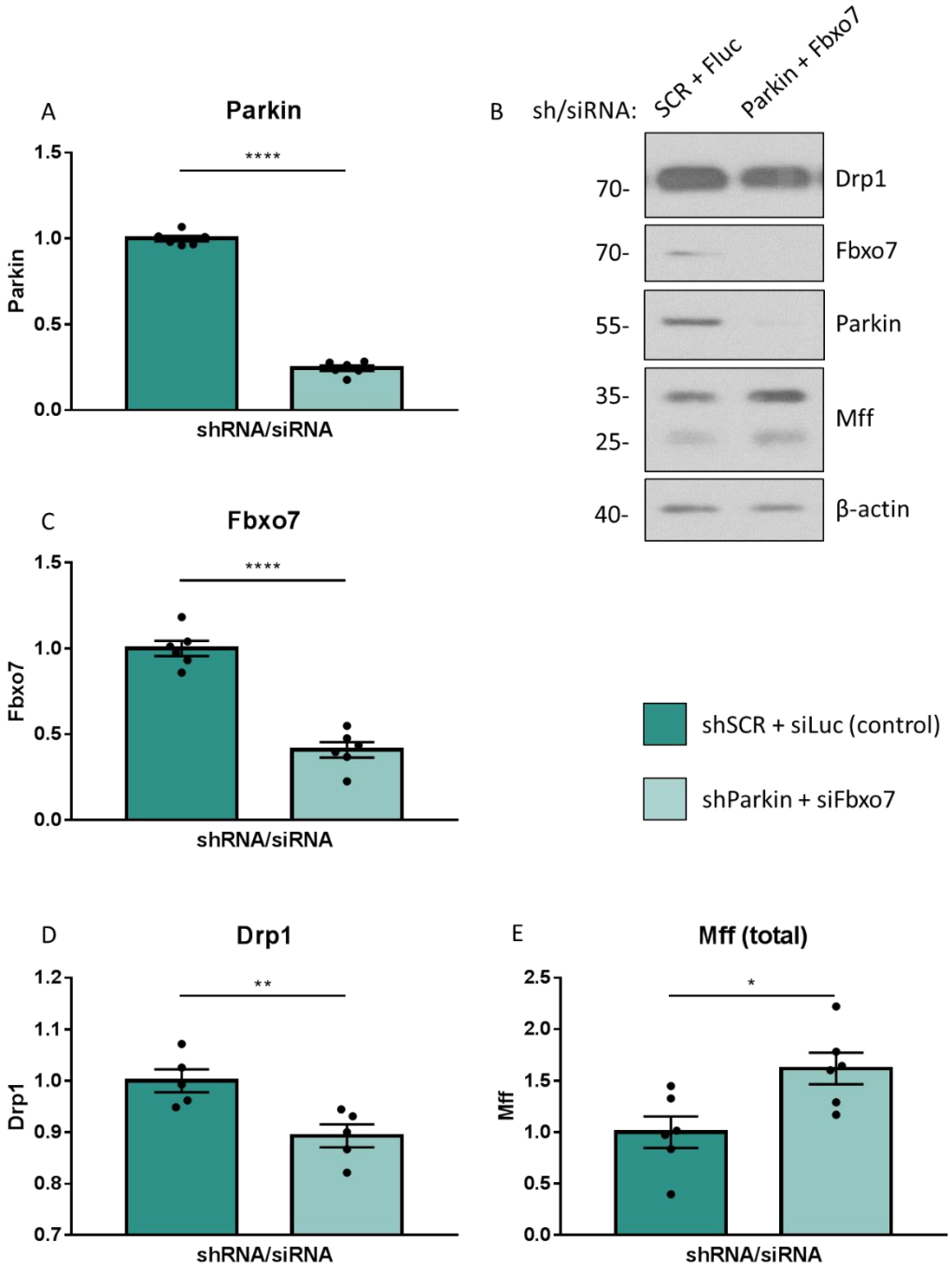

Figure 4.5 Knockdown of Parkin and Fbxo7 in HEK293T cells. Cells were transfected with either scrambled shRNA and luciferase siRNA or Parkin shRNA and Fbxo7 siRNA. Cells were lysed 72 hours later. (B) Western blots for Drp1, Fbxo7, Parkin, Mff and β-actin. N=6. (A, C-E) Quantitative analysis using Student's unpaired t-test. Data presented as mean ± SEM. * $p < 0.05$, ** $p < 0.01$, **** $p < 0.0001$.

4.3.2 Parkin and Fbxo7 mediate degradation of Mff

Next, I wanted to determine whether the loss of Mff from mitochondria during ischaemia, which coincides with Parkin recruitment, is attributable to Parkin ubiquitin ligase activity. To test if Parkin binds Mff, CFP-tagged Mff or free GFP (control) were co-expressed in HEK293T cells with untagged Parkin. 48 hours post-transfection, cells were lysed and GFP or CFP-Mff was immunoprecipitated using GFP-Trap beads. Parkin was present in the CFP-Mff co-immunoprecipitation, but not the free GFP co-immunoprecipitation (Figure 4.6). These data indicate a specific, albeit not necessarily direct, interaction between Mff and Parkin.

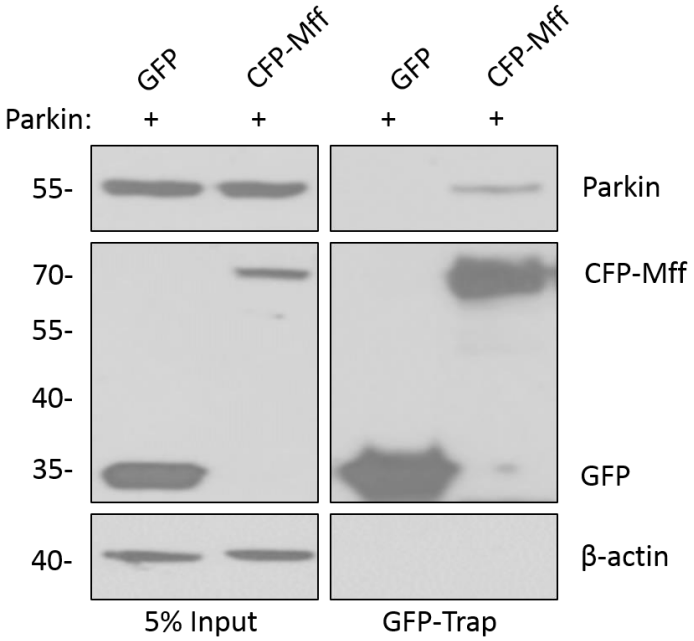

Figure 4.6 **Parkin specifically binds Mff in HEK293T cells.** Representative Western blot of GFP-Trap co-immunoprecipitation from HEK293T total cell lysates. Exogenously expressed untagged Parkin is co-immunoprecipitated with CFP-Mff, but not GFP alone. N=4.

HEK293T cells were co-transfected with GFP/CFP-Mff and shRNA (scrambled or Parkin-targeting). 72 hours post-transfection, GFP-Trap was used to immunoprecipitate free GFP or CFP-Mff. Post-translational modifications such as ubiquitination and SUMOylation are covalent and are therefore not lost under reducing/denaturing conditions used for immunoprecipitation and Western blotting. Immunoblotting of GFP-Trap samples revealed that CFP-Mff is highly endogenously ubiquitinated, compared to free GFP. Knock down of Parkin results in a significant ~50% reduction of ubiquitination (Figure 4.7), indicating that, at least in HEK293T cells, Parkin has a detectable functional role in Mff ubiquitination.

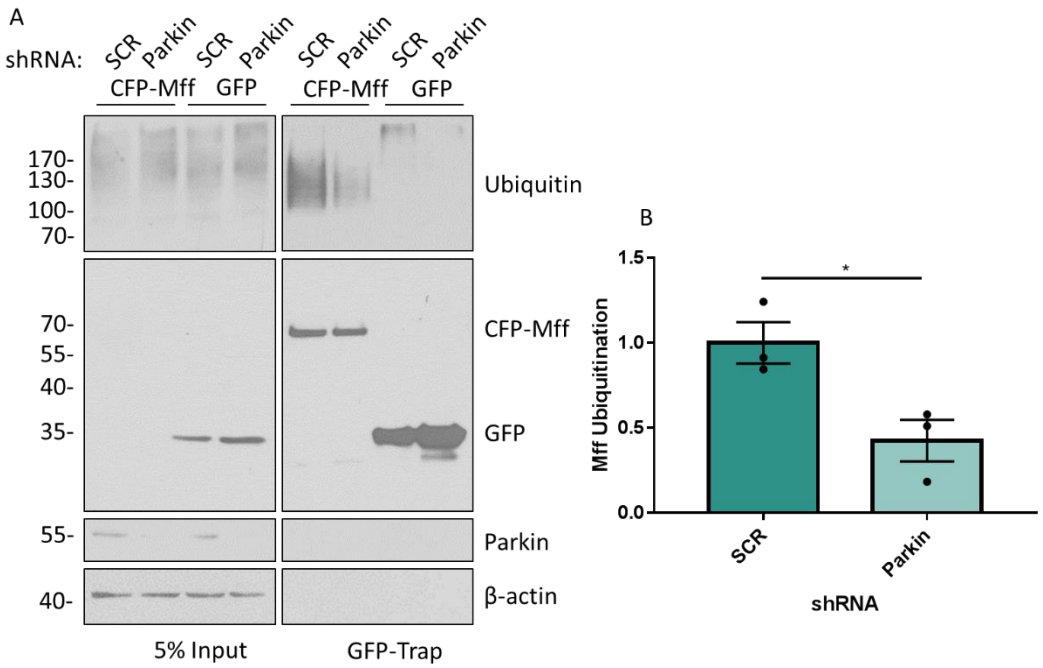

Figure 4.7 **Parkin ubiquitinates Mff in HEK293T cells**. (A) Western blots of GFP-pulldowns of exogenously expressed CFP-Mff in HEK293T cells reveal high levels of endogenous ubiquitination, which is significantly decreased by knockdown of Parkin (B). N=3. Analysed using unpaired two-tailed students' t-test. Data presented as mean ± SEM. $p < 0.05$.

My data demonstrate that Parkin recruitment to mitochondria coincides with the loss of Mff, and that knock down of Parkin results in an increase of Mff. Additionally, the GFP-Trap data show that Parkin can both bind Mff, and endogenous levels of Parkin ubiquitinate Mff.

I next assessed the time-course of Mff degradation ± Parkin or Fbxo7 in the presence cycloheximide (CHX), a drug that blocks protein synthesis by inhibiting translation elongation. The mechanism of translation inhibition remains largely unknown, but it has been proposed that CHX acts via direct binding to the E site of the 60S ribosome (Schneider-

Poetsch et al., 2010). By blocking protein synthesis, one can study the rate of protein degradation.

HEK293T cells were transfected with scrambled (control) or Parkin-targeted shRNA, or Firefly luciferase (control) or Fbxo7-targeted siRNA and treated with 25µg/mL cycloheximide for up to 24 hours prior to their lysis 72 hours post-transfection. Samples were prepared for Western blot and probed for endogenous Mff. As shown in Figure 4.8, knock down of Parkin (B) or Fbxo7 (D) significantly slows the degradation of Mff over 6 or 12 hours, but only knock down of Parkin significantly prevents loss of Mff by 24 hours, suggestive of a greater role for Parkin in Mff degradation than Fbxo7, or that this assay is more sensitive to manipulation of Parkin.

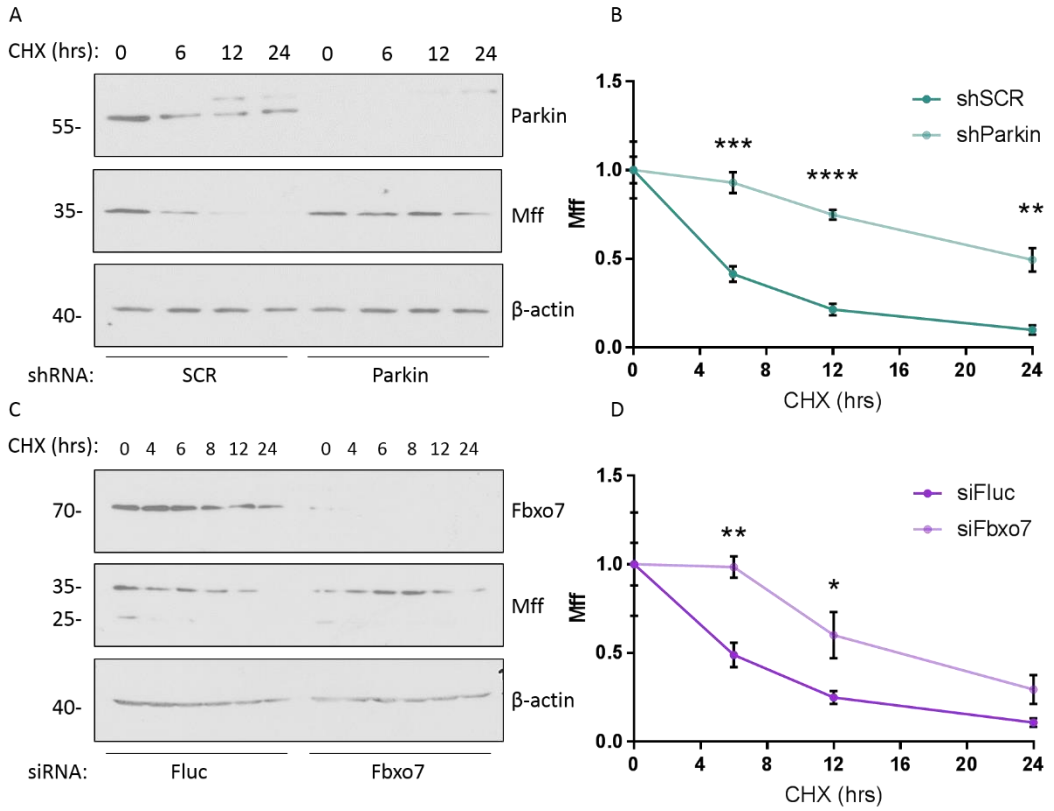

Figure 4.8 **Parkin and Fbxo7 contribute to Mff degradation.** HEK293T cells were transfected with either scrambled shRNA (control, SCR), Parkin shRNA, Firefly luciferase siRNA (control, Fluc) or Fbxo7 siRNA. Prior to lysis 72 hours post-transfection, cells were treated with 25µg/mL cycloheximide (CHX) for 0, 4, 6, 8, 12 or 24 hours (0-hour CHX received 6-hour DMSO treatment; 4 and 8-hour treatments were not included in sufficient replicates to be quantified). Lysates were then Western blotted for Fbxo7, Parkin, Mff and β-actin (A, C). (B, D) Quantitative analysis, data presented as mean ± SEM. Analysed using unpaired two-tailed Student's t-tests. N=4. * $p < 0.05$, ** $p < 0.01$, *** $p < 0.001$, **** $p < 0.0001$.

4.3.3 Parkin and Fbxo7 ubiquitinate Mff via independent mechanisms

Since Parkin knock down reduces cellular levels of Fbxo7, and *vice versa* (Figure 4.2, Figure 4.4), I anticipated knock down of Fbxo7, or of Parkin and Fbxo7 together, would have the same effect on Mff ubiquitination as Parkin knock down alone (Figure 4.7). To test this, HEK293T cells were co-transfected with CFP-Mff along with shRNA targeting Parkin, siRNA targeting Fbxo7, both, or a scrambled control. To ensure equal amounts of nucleic acids were transfected in all groups, empty pSUPER (shRNA vector) was used as a balance. 72 hours post-transfection, GFP-Trap was used to immunoprecipitate CFP-Mff, along with its post-translational modifications. Immunoblotting of GFP-Trap samples revealed that CFP-Mff ubiquitination was significantly reduced by knock down of either Parkin or Fbxo7 in this experiment. Surprisingly, simultaneous knock down of Parkin and Fbxo7 doubled this effect, suggesting that Parkin- and Fbxo7-mediated ubiquitination of Mff is additive and perhaps mediated via different pathways (Figure 4.9).

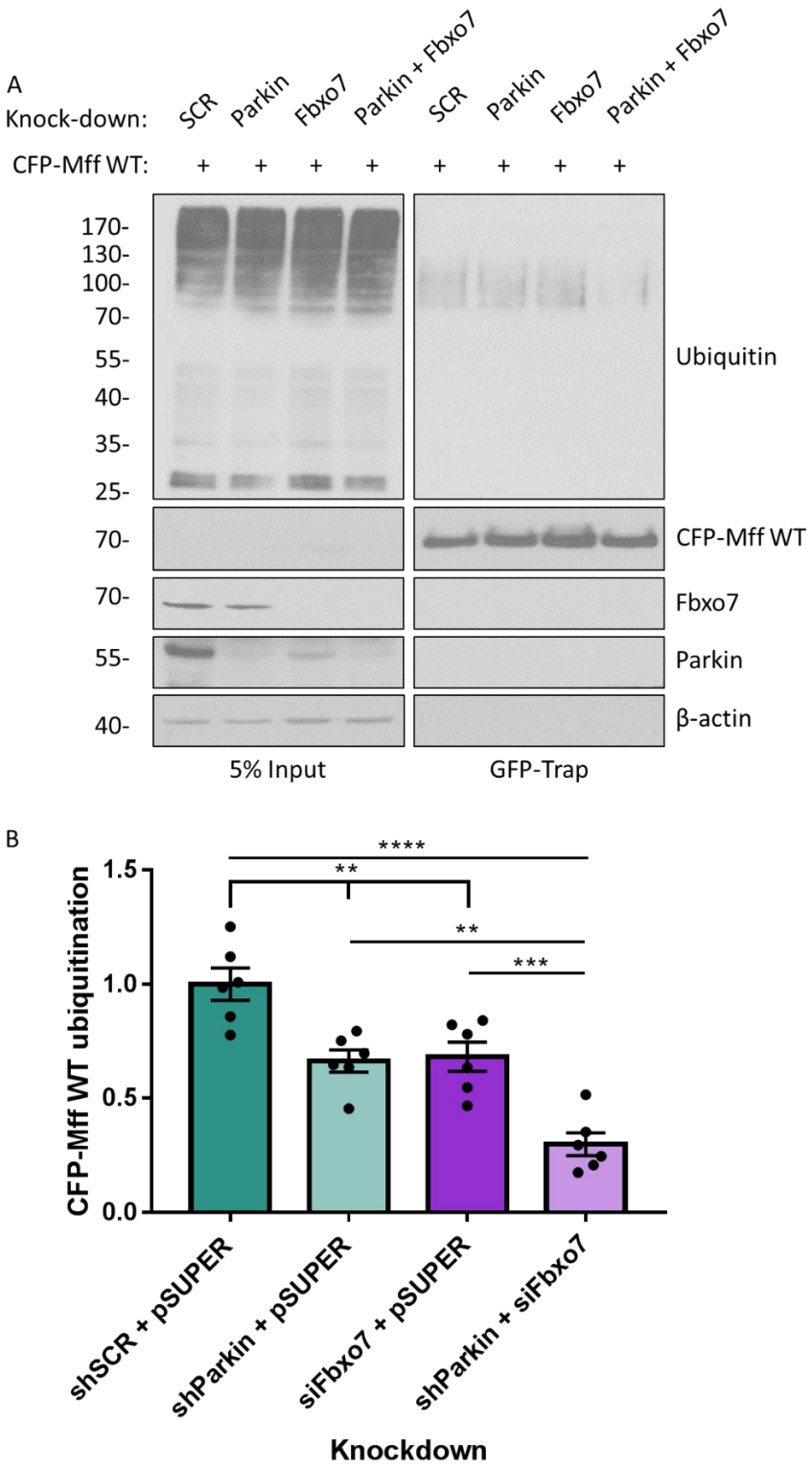

Figure 4.9 **Parkin and Fbxo7 ubiquitinate Mff independently.** (A) Western blots of GFP-pulldowns of exogenously expressed CFP-Mff WT in HEK293T cells reveal high levels of endogenous ubiquitination, which is significantly decreased by knockdown of Parkin (shRNA) or knockdown of Fbxo7 (siRNA), compared to a scrambled shRNA control, and is further reduced by knockdown of both Parkin and Fbxo7 (B). N=6. Analysed using ordinary one-way ANOVA with Tukey's correction for multiple comparisons with a pooled variance. Data presented as mean ± SEM. ** $p \leq 0.01$, *** $p \leq 0.001$, **** $p \leq 0.0001$.

4.3.4 Parkin and Fbxo7 regulate mitochondrial morphology during OGD

4.3.4.1 Parkin is recruited to mitochondria during OGD in H9c2 cells

The initial observations of this study were made in cardiac tissue. The most notable differences were observed in Parkin and Mff, so it was important to study the effects of their manipulation in a cardiac or cardiac-like cell type. In addition, Fbxo7 is of interest because it has been reported to interact with Parkin (Burchell et al., 2013) and it mediates ubiquitination of Mff (Figure 4.9). Due to their relative ease of culture and manipulation, I used the rat cardiac myoblast cell line H9c2. However, for H9c2 cells to be a viable model, they need to respond to ischaemic stress in a similar way to the cardiac tissue, particularly in the recruitment of Parkin to mitochondria, which was the most compelling change detected in the *ex vivo* experiments.

Figure 4.10 (A) shows Parkin in the whole cell lysate or mitochondrial fraction of H9c2 cell samples collected after different lengths of ischaemia. GAPDH was used as a total protein loading control, and VDAC as a mitochondrial loading control. VDAC is enriched and GAPDH is absent from the mitochondrial fraction indicating effective separation of subcellular compartments. Not all timepoints were repeated sufficient times to be quantified, but 2 hours of OGD was found to be sufficient to induce a significant ($p < 0.05$) 5-fold increase in mitochondria-associated Parkin (B), and was chosen as the length of OGD for future experiments.

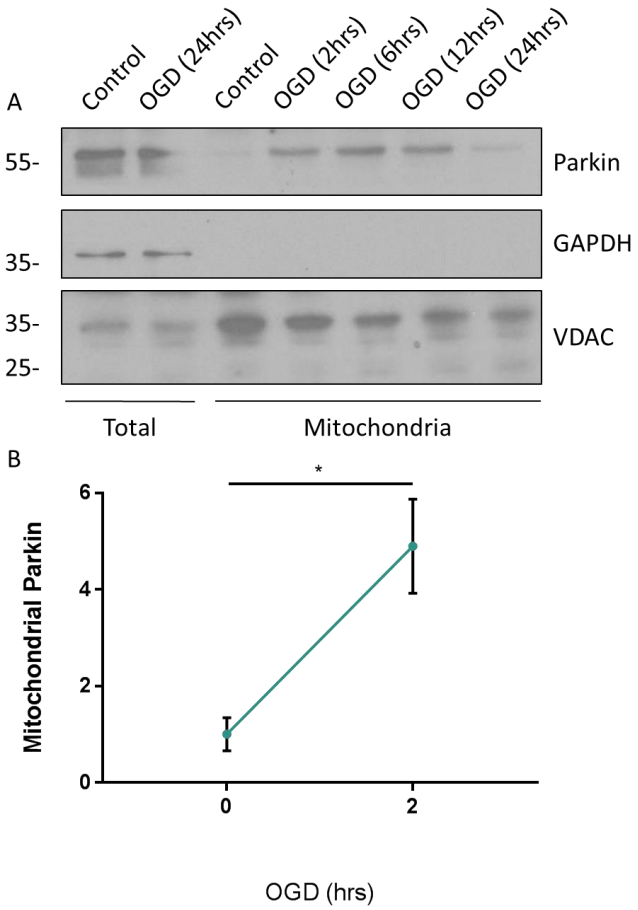

Figure 4.10 **Mitochondrial recruitment of Parkin during OGD in H9c2 cells.** H9c2 cells were subjected to oxygen-glucose deprivation (OGD) for 0-24 hours. Cells were lysed under OGD conditions and subsequently underwent subcellular fractionation. OGD was carried out in de-oxygenated, glucose-free DMEM in an anaerobic chamber (95% N2, 5% CO2). Control cells were maintained in a standard incubator (95% O2, 5% CO2) in glucose-containing DMEM. N=2-6 (2-hour time point n=3). (A) Western blots of Parkin, GAPDH and VDAC. (B) Quantitative analysis using unpaired two-tailed students' t-test. Data presented as mean ± SEM. $p < 0.05$. OGD and mitochondrial fractionation performed by Dr Nadiia Rawlings.

4.3.4.2 Validation of lentivirus

H9c2 cardiac myoblast cells have notoriously low transfection efficiency (Liu et al., 2011). I therefore used lentiviral infection to knock down Parkin and Fbxo7. A lentivirus containing shRNA to knock down rat Fbxo7 (target sequence: CCTTTGGGAAAGCTCATCATG) was already available (Dr Dan Rocca, unpublished work) but a Parkin knock down lentivirus had to be made.

Figure 4.11 (A) shows a sequence alignment of the Fbxo7 shRNA target sequence with rat Fbxo7. H9c2 cells were infected with lentivirus encoding this knock down and

were lysed for Western blotting 4 days later. Figure 4.11 (B) is a representative blot showing that endogenous Fbxo7 is knocked down.

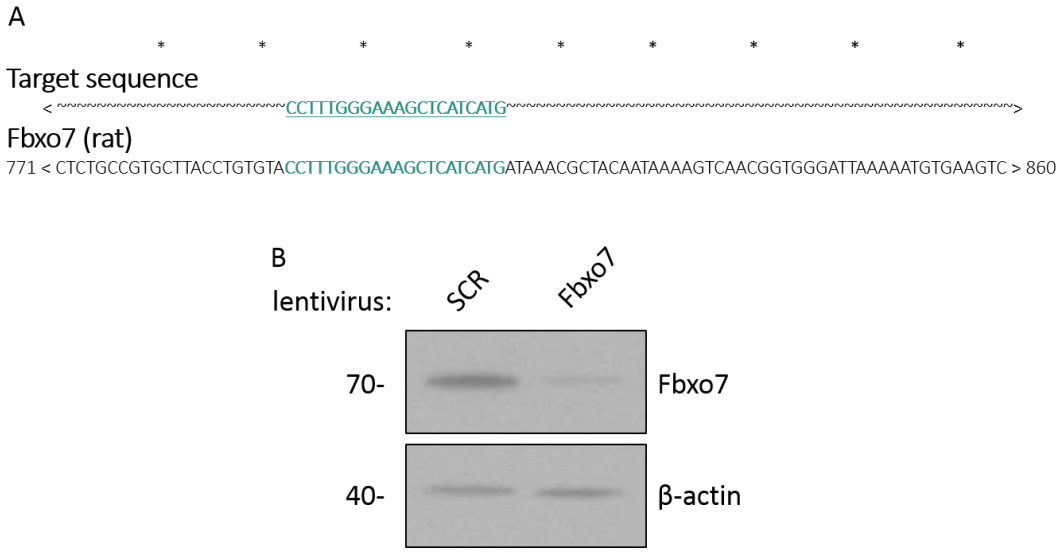

Figure 4.11 **Sequence alignment of Fbxo7 shRNA target sequence and rat Fbxo7 sequence.** The Fbxo7 shRNA targets a sequence starting at 793bp. The figure shows a partial sequence alignment of the relevant section of the rat Fbxo7 coding sequence and the shRNA target sequence. H9c2 cells were infected with lentiviral shRNA with the shown target sequence and lysed after 4 days for Western blot. (B) shows the successful knock down of Fbxo7, compared to a scrambled lentiviral shRNA control.

The knock down sequence for Parkin was designed to target both human and rat Parkin. A sequence alignment showing the start of the open reading frame of Parkin from human and rat, along with the target sequence, is shown in Figure 4.12(A). This sequence was used to create a lentiviral construct in pXLG3-GFP. H9c2 cells were infected with pXLG3-GFP-shParkin or –shSCR (control) and lysed 4 days post-infection. The Parkin knock down virus was highly effective and significantly reduced ($p < 0.0001$) total Parkin compared to the scrambled control (Figure 4.12 (B, C)).

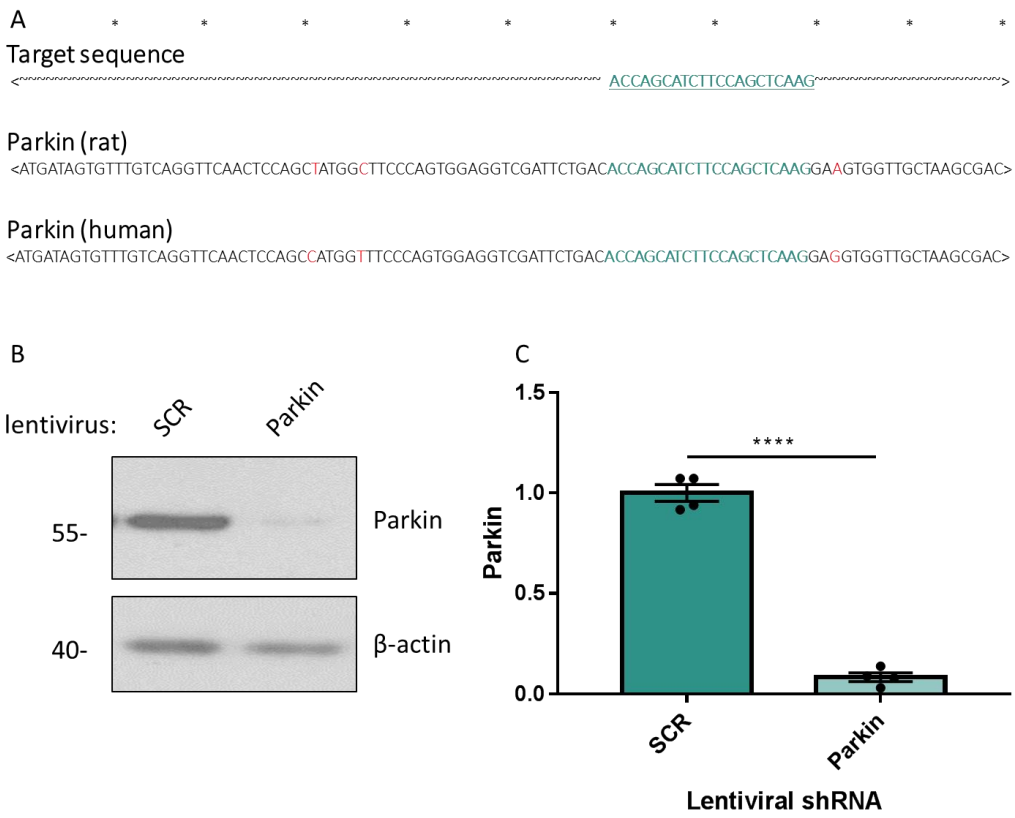

Figure 4.12 **Human and Rat Parkin sequence alignment and validation of Parkin knockdown lentivirus and lentiviral shRNA design.** The figure shows a partial coding sequence alignment from the start of the open reading frame of the *Rattus norvegicus* and *Homo sapiens* Parkin genes (A). Base mismatches are indicated (red). The shRNA target sequence, validated previously in HEK293T cells, is conserved in rat, and was therefore chosen as the target sequence of the lentiviral knockdown. H9c2 cells infected with lentiviral shRNA targeted to both human and rat Parkin sequences have significantly reduced endogenous Parkin protein levels after 4 days compared to a scrambled lentiviral shRNA control (B, C). N=4. Analysed using unpaired two-tailed students' t-test. Data presented as mean ± SEM. $p \leq 0.0001$.

Parkin is canonically only recruited to mitochondria under conditions of oxidative stress, whereupon PINK1 accumulates on the outer membrane of depolarised mitochondria ((Berger et al., 2009, Xiao et al., 2017). However, the previous experiments in HEK293T cells were all conducted under basal conditions, and Parkin still interacted with, ubiquitinated and degraded Mff. This demonstrates that even basally, there could is some constitutive activity of Parkin at the mitochondrial outer membrane, an effect which was expected, as mitophagy plays an important role in maintenance of the mitochondrial reticulum, with unhealthy mitochondria constantly requiring degradation even in healthy cells.

To gain a better understanding of the role Parkin might play in maintenance and/or regulation of mitochondrial morphology and the delicate balance between fission and

fusion, confocal image analysis was used. Any perturbation of the equilibrium between mitochondrial fission and fusion would have an effect on gross mitochondrial network size and structure (Sesaki and Jensen, 1999). H9c2 cells, being muscle cells, have high numbers of mitochondria, so an automated analysis tool was employed (Kuznetsov et al., 2015).

4.3.4.3 Mitochondrial networks and OGD

Parkin-targeted or Fbxo7-targeted lentivirus described in Figure 4.11 and Figure 4.12 were used to infect differentiated H9c2 cells. 4 days post-infection, mitochondria were stained with MitoTracker, and subjected to 2 hours of OGD (or 2 hours of normoxic culture). The cells were then fixed in acetone and used for confocal imaging (Figure 4.13).

Various mitochondrial network parameters were analysed, with control and OGD conditions compared for each knock down. As can be seen in Figure 4.13, the proportion of mitochondria that were involved in networks tended to decrease during OGD, compared to control conditions, although this was not significantly different for either of the knock downs (B). However, the average length of branches within mitochondrial networks was significantly decreased by OGD, compared to control, and this difference was exacerbated by knock down of Parkin, but not Fbxo7 (C). This could be interpreted as an increase in mitochondrial fission during OGD, which is increased in the absence of Parkin, but opposed by absence of Fbxo7. Interestingly, although there was a non-significant trend towards increases in mitochondrial network complexity during OGD (as measured by average number of branches within networks), this increase was amplified to statistical significance by knock down of Fbxo7, but not Parkin (D), which could indicate that absence of Fbxo7 inhibits mitochondrial fission or enhances fusion.

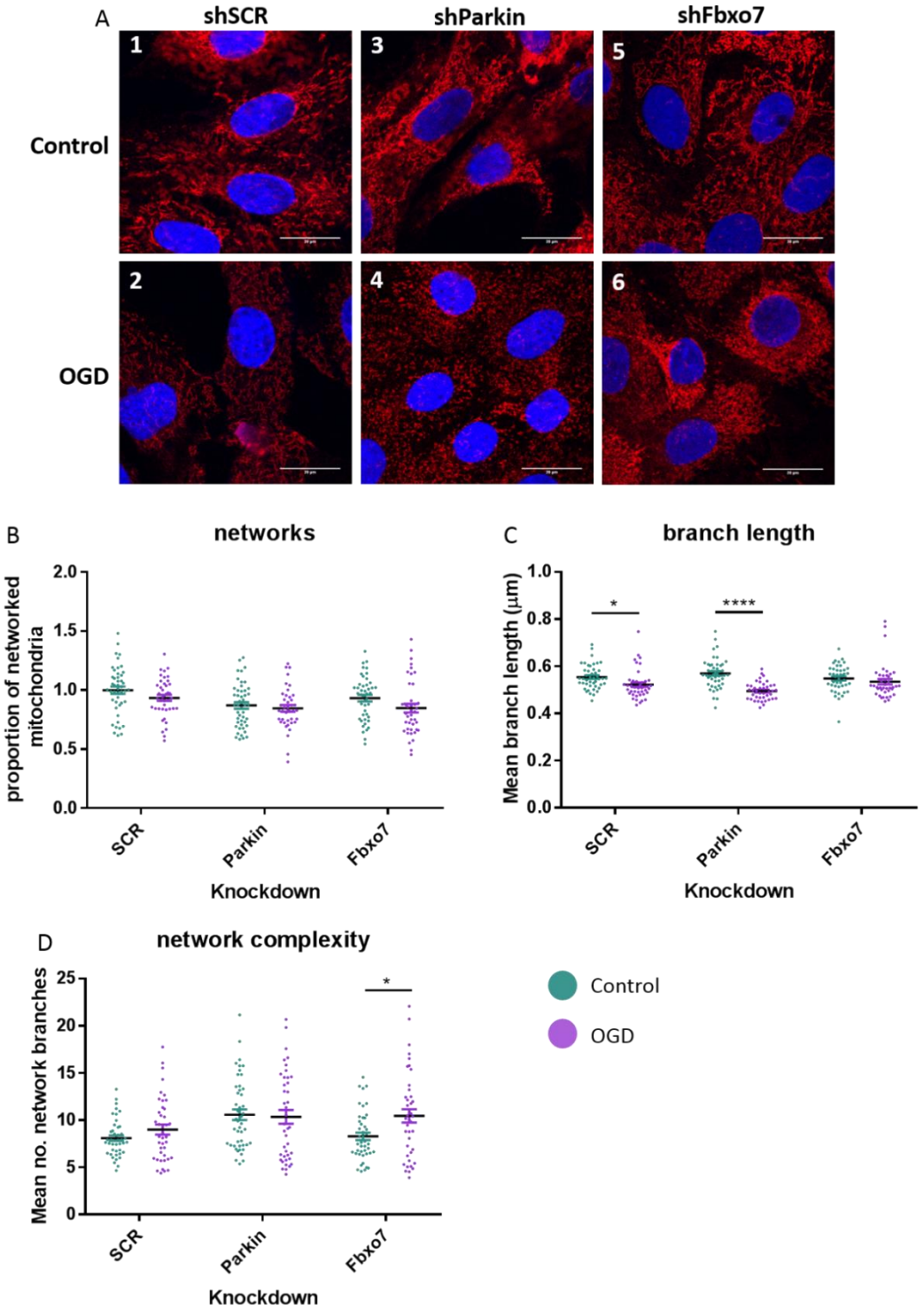

Figure 4.13 **Effects of Parkin or Fbxo7 knockdown on H9c2 mitochondrial networks under basal and OGD conditions.** H9c2 cells were infected with lentivirus encoding scrambled (control), Parkin or Fbxo7 shRNA. 4 days post-infection, cells were incubated with Mitotracker for 30 minutes. Control cells were washed and returned to normal incubator conditions; OGD cells were washed and placed in an anoxic chamber in de-oxygenated, glucose-free DMEM. After 2 hours, cells were washed and fixed in ice-cold acetone. Mitochondrial networks were evaluated using Fiji (ImageJ) with the MiNA macro. N=3 (40-47 cells per group for network analysis, 41-47 cells per group for branch length analysis, 41-46 cells per group for complexity analysis). Analysed using ordinary two-way ANOVA with Sidak's correction for multiple comparisons. Data presented as mean ± SEM. * $p < 0.05$, **** $p < 0.0001$. Scale bar = 20µm.

4.4 Discussion

4.4.1 Parkin and Fbxo7 differentially regulate mitochondrial fission proteins

4.4.1.1 Parkin

Knock down of Parkin in HEK293T cells was achieved using both a previously published (Berger et al., 2009) and a novel shRNA target sequence (Figure 4.1). The novel shRNA (target sequence: ACCAGCATCTTCCAGCTCAAG) produced the most complete Parkin knock down, at ~94%, and was used for subsequent experiments. The effects of Parkin knock down were then studied in HEK293T cells.

Consistent with a previous report that Parkin ubiquitinates Mff (Gao et al., 2015), knock down of Parkin significantly increased total expression of Mff (Figure 4.2 (D)). This was indicative of a role for Parkin in Mff degradation and complemented the findings from the *ex vivo* heart experiments in Chapter 3, in which Parkin recruitment to mitochondria coincided with a loss of Mff.

Parkin has previously been reported to ubiquitinate Drp1, contributing to its proteasomal degradation (Lutz et al., 2009, Tang et al., 2016, Wang et al., 2011a). It was therefore expected that knock down of Parkin would increase total Drp1. Surprisingly, however, the opposite effect was observed, with knock down of Parkin leading to a ~40% reduction in Drp1 (Figure 4.2 (B)). This would be consistent with Parkin having a protective role of Drp1, perhaps by contributing to degradation of another ubiquitin ligase involved in Drp1 degradation, or with the cells degrading Drp1 via a proteasome-independent mechanism to compensate for the increased Mff and maintain mitochondrial homeostasis.

Most published studies on Parkin activity rely on cellular stress models, such as ischaemia or chemical mitochondrial uncoupling. However, the experiments presented in this chapter were all performed under basal conditions. Basal mitophagy contributes to maintenance of healthy cells. While inducible stress will exaggerate the effects of Parkin, it is reasonable to expect that, at any given time, some cells will contain some dysfunctional mitochondria, perhaps a result of localised oxidative stress or ATP-depletion, which need to be cleared. In my functional experiments I only investigated manipulation of endogenous Parkin, and the knock down was almost complete. In contrast, the study by Wang *et al* relied heavily on Parkin over-expression in HeLa and HEK293T cells. It is notable that overexpression studies have been widely criticised for being an unreliable way of

identifying substrates due to enzyme promiscuity (Danielsen et al., 2011, Kanner et al., 2017). Wang *et al* also exogenously expressed ubiquitin, further contributing to potential off-target effects and/or physiologically irrelevant functional effects. Moreover, where a Parkin knock down was used in SH-SY5Y cells it was only partial (~50%), making it difficult to extrapolate the role of Parkin (Wang et al., 2011a). The work by Tang *et al* also used over-expressed Parkin to report on its degradation of Drp1, and a Parkin knock down performed in mouse N2a neuroblastoma cells was also partial (Tang et al., 2016).

Interestingly, knock down of Parkin also significantly reduced Fbxo7 (Figure 4.2 (C)). Although Parkin and Fbxo7 have been shown to interact (Burchell et al., 2013), it has not previously been reported that Parkin contributes to stability of Fbxo7. One possibility worthy of future investigation is that Parkin and Fbxo7 form part of a stable SCF-type E3 ubiquitin ligase complex, and that deletion of Parkin destabilises the other complex components. Consistent with this, knock down of Fbxo7 also significantly reduced total Parkin (Figure 4.4 (D)).

4.4.1.2 PINK1

It is widely-known that Parkin is recruited to mitochondria by PINK1 accumulation, triggered by membrane depolarisation (Clark et al., 2006, Geisler et al., 2010, Matsuda et al., 2010, Narendra et al., 2010). Therefore, PINK1 knock down using commercially available siRNA was performed, to examine whether the effects of Parkin knock down on mitochondrial proteins were PINK1-dependent. As shown in Figure 4.3, knock down of PINK1 had no significant effect on total levels of Drp1, Fbxo7 or Parkin (C-E), though this does not preclude effects on protein localisation. In the absence of PINK1, we would expect most, if not all, trafficking of Parkin to the MOM to be blocked. That PINK1 knockdown does not have the same effect on Drp1 or Fbxo7 levels as Parkin knockdown therefore indicates that regulation of Drp1 and Fbxo7 by Parkin occurs in the cytosol, and is independent of PINK1 and/or mitochondrial depolarisation. Unsurprisingly, a significant increase of Mff in the absence of PINK1 was observed (F), similar to the increase observed with knock down of Parkin, suggesting that Parkin-mediated degradation of Mff is PINK1-dependent, with PINK1 being required for mitochondrial recruitment and/or activation of Parkin to ubiquitinate Mff. To further verify this, a Parkin knockdown/replacement strategy could be used, replacing endogenous Parkin with WT or a PINK1-insensitive Parkin mutant (e.g. non-PINK1-phosphorylatable Parkin S65A (Ordureau et al., 2015)), to see if the effect of Parkin knock down on Mff can be rescued.

4.4.1.3 Fbxo7

Due to its known involvement in mitophagy and previously reported interaction with Parkin (Burchell et al., 2013), I tested if Fbxo7 could also play a role in regulation of mitochondrial fission proteins. No significant difference was detected in total Drp1 following knock down of Fbxo7 (Figure 4.4 (C)), indicating no substantial role for Fbxo7 in Drp1 degradation or protection. This was unsurprising, as there is no literature available on interplay between Drp1 and Fbxo7.

Knock down of Fbxo7 had no significant effect on total levels of Mff (Figure 4.4 (E)). However, different bands of Mff on the Western blots appeared to respond to Fbxo7 knock down in different ways. For that reason, the predominant higher molecular weight species and the lower molecular weight species were analysed independently. This revealed a significant decrease in the higher molecular weight species (F) and a significant increase in the lower molecular weight species (G). The Mff antibody used in this study recognises all five previously identified isoforms (Supplementary Figure 1), three of which have molecular weights between 25 and 28kDa, similar to the lower molecular weight bands shown in Figure 4.4 (Gandre-Babbe et al., 2008). This raises the intriguing possibility that, rather than affect total levels of Mff, Fbxo7 preferentially contributes to degradation of the smaller isoforms. The simultaneous decrease of the main Mff isoform could therefore be a compensatory mechanism to protect against excessive mitochondrial fission. However, we cannot rule out the lower molecular weight bands being Mff degradation products, which would also be interesting, as it would indicate that Fbxo7 may stabilise Mff, thereby opposing the degradative action of Parkin.

4.4.1.4 Parkin and Fbxo7

Given that knock down of Parkin also decreased cellular Fbxo7, and knock down of Fbxo7 similarly reduced Parkin, it was hypothesised that simultaneous knock down of both would have no further effect. However, knock down of Parkin and knock down of Fbxo7 had different effects on Drp1 and Mff, so it could be that they have an antagonistic relationship with regard to these two proteins.

Knock down of both Parkin and Fbxo7 resulted in significantly reduced Drp1 and significantly increased Mff (Figure 4.5 (D, E)). This follows the pattern of independent knock down of Parkin (Figure 4.2) and suggests that Parkin may be a more dominant regulator of Drp1 and Mff than Fbxo7, or that Fbxo7 functions upstream of Parkin in Mff regulation. However, given their demonstrable dependence on one another for stability,

it is not possible to dissect out any potential pathway. Moreover, the effects of Parkin and Fbxo7 on Mff are not opposing, so it is unlikely that they have an epistatic relationship. Interestingly, although still statistically significant, the effects of Parkin and Fbxo7 knock down on Mff and Drp1 were smaller than the effects of Parkin knock down alone; Drp1 reduction was ~50% with knock down of Parkin alone, compared to just ~10% with the double knock down, while Mff abundance was ~100% increased by the single knock down and only ~50% increased by the double knock down.

These data indicate that, at least in the cases of Mff and Drp1, the roles of Fbxo7 and Parkin are independent of one another, rather than through their possible roles in a common E3 ligase complex. The reduced effect of Parkin knock down with simultaneous Fbxo7 knock down is suggestive of Fbxo7 ablation being partially protective against the effects of Parkin knock down. However, it is possible that the effects are smaller simply because simultaneous Parkin and Fbxo7 knock downs are less complete than their individual knock downs, due to multiple transfections (Figure 4.5 (B, C)).

4.4.2 Parkin and Fbxo7 regulate Mff degradation

4.4.2.1 Parkin binds specifically to Mff

As outlined previously, Parkin has been reported to interact with and ubiquitinate Mff (Gao et al., 2015). Before this could be further explored, it was important to validate these findings. The co-immunoprecipitation data presented in Figure 4.6 use CFP-Mff, which can be immunoprecipitated using GFP-Trap beads. GFP was used as a control and differs from CFP by just a single amino acid: Y66W (Day and Davidson, 2009). As shown in the figure, Parkin was co-immunoprecipitated with CFP-Mff, but not GFP alone, providing strong evidence that the Parkin-Mff interaction is specific.

4.4.2.2 Mff is ubiquitinated by Parkin

The paper by Gao *et al* reported Parkin-dependent ubiquitination of Mff (Gao et al., 2015). In their study, Gao and colleagues expressed Myc-Mff and EGFP-Parkin in HEK293 Mff -/- cells, then performed immunoprecipitation with an anti-Mff antibody before Western blotting with anti-ubiquitin antibodies. For the data presented in Figure 4.7, the ubiquitination capacity of only endogenous Parkin was tested, going some way towards ruling out the possibility of enzyme promiscuity and false-positive data. As shown in Figure 4.7 (B), near complete knock down of Parkin resulted in a ~50% decrease in endogenous ubiquitin immunoprecipitated with Mff. This provides strong evidence that Mff is a true

substrate of endogenous levels of Parkin in HEK293T cells, as well as indicating that Parkin is not the only ubiquitin ligase to target Mff. This raised the question of a role for Fbxo7 in ubiquitination of Mff.

4.4.2.3 Parkin plays a greater role in Mff degradation than Fbxo7

Demonstrating binding between Mff and Parkin and Parkin-dependent ubiquitination of Mff does not conclusively provide evidence of a degradative role for Parkin. To assess rates of Mff turnover and their Parkin-dependence, endogenous Parkin was knocked down in HEK293T cells and cycloheximide (CHX), an inhibitor of protein synthesis, used to measure rates of Mff decay. As the role of Fbxo7 in Mff regulation remained unclear, the same experiment was also carried out using knock down of Fbxo7.

As shown in Figure 4.8 (A, B), Mff is degraded over the course of 24 hours to almost nothing by inhibition of protein synthesis, reducing by ~50% within around 4 hours. By contrast, knock down of Parkin preserves ~50% of initial Mff until the end of the experiment (24-hours CHX treatment). At 6-, 12- and 24-hours CHX treatment, the Parkin knock down cells still contain significantly more Mff than a scrambled control, indicating that knock down of Parkin both slows down Mff degradation, and protects from it, consistent with a role for Parkin in Mff degradation.

By contrast, knock down of Fbxo7 did not appear to protect Mff against degradation over 24 hours (Figure 4.8 (C, D)). As with the Parkin knock down experiment, the control cells (treated with siRNA targeted Firefly luciferase) have lost almost all initial Mff by 24 hours CHX treatment, but the Fbxo7 knock down cells did not have significantly higher residual Mff. However, the initial rate of degradation of Mff did appear to be slower in the absence of Fbxo7, with significantly higher Mff remaining after 6 and 12 hours of CHX treatment. Taken together, the results of the Parkin and Fbxo7 knock down could be indicative of roles for both proteins in degradation of Mff, but with Parkin being the dominant regulator of Mff turnover. Alternatively, partial ablation of Parkin as a result of Fbxo7 knock down would also explain the partial occlusion of degradation. To exclude this possibility, the experiment could be performed using Mff mutants that are insensitive to Parkin (to study Fbxo7-mediated degradation) or insensitive to Fbxo7 (to study Parkin-mediated degradation). However, there are caveats to this method as well. Degradation of over-expressed protein is unlikely to be representative of degradation of the endogenous, and the necessary involvement of different Mff mutants would confound data analysis.

4.4.2.4 Parkin and Fbxo7 ubiquitinate Mff independently

The data presented previously (Figure 4.7) show that Mff is ubiquitinated by Parkin at endogenous levels. Fbxo7 has not been previously reported to have a role in ubiquitination of Mff but has been shown to interact with Parkin in the mediation of mitophagy (Burchell et al., 2013). With Parkin-dependent ubiquitination of Mff having already been linked to mitophagy (Gao et al., 2015), we hypothesised that the role of Fbxo7 might also be linked to Mff. Given the ability of Fbxo7 over-expression to rescue phenotypes of Parkin-null *Drosophila*, we proposed a level of functional redundancy between the two proteins.

Figure 4.9 shows Western blot data of CFP-Mff immunoprecipitation. As shown previously (Figure 4.7), knock down of Parkin significantly reduced endogenous ubiquitination of Mff. Supportive of a functional redundancy hypothesis in which Parkin and Fbxo7 can both ubiquitinate Mff depending on their availability, knock down of Fbxo7 also significantly reduced Mff ubiquitination by the same amount. These data are suggestive of the two proteins being interchangeable or dependent upon one another in their regulation of Mff. Interestingly, however, simultaneous knock down of Parkin and Fbxo7 further reduced Mff ubiquitination, doubling the effect of individual knock down. This additive effect is indicative of separate, distinct roles for Parkin and Fbxo7 in Mff regulation, via independent pathways. In light of this, previous discussion that Fbxo7 functions upstream of Parkin within the same pathway is improbable (4.4.1.4). It will be intriguing to explore the mechanisms and consequences of this by studying the specific Mff ubiquitin-chain linkages Parkin and Fbxo7 mediate, as well as the site(s) that they target.

4.4.3 Parkin and Fbxo7 regulate mitochondrial networks during OGD

4.4.3.1 H9c2 cells are a suitable model for cardiac ischaemia

The data shown in Chapter 3, with Parkin recruitment to mitochondria during ischaemia coinciding with a loss of Mff, were informative, but the *ex vivo* model of heart perfusion cannot be readily genetically manipulated. As an alternative to *in vivo* viral infection and *ex vivo* experiments in whole heart I performed knock down experiments in the H9c2 cells, an extensively validated, immortalised rat cell line of cardiac myoblast–like cells (Hescheler et al., 1991, Watkins et al., 2011, Kuznetsov et al., 2015). H9c2 cells have been previously shown to be more similar to primary cardiac cell cultures than other lines,

for example HL-1, with respect to their energy metabolism patterns, including cellular ATP levels, bioenergetics, metabolism, function and morphology of mitochondria (Kuznetsov et al., 2015). As cardiac-like cells with high energy demands, they also have relatively large numbers of mitochondria, making them an ideal model to study mitochondrial networks and/or morphology.

Cells in culture can respond differently to stress compared to a whole organ it was necessary to establish that they would be reflective of the whole heart studies. The most striking effect observed during whole heart ischaemia was the recruitment of Parkin to mitochondria, so this was chosen as a bench-mark response to OGD. The data in Figure 4.10 show levels of Parkin in whole cell lysate and the mitochondrial fraction of control H9c2 cells and cells after varying lengths of OGD. As can be seen in (A), Parkin is recruited to and subsequently lost from the mitochondrial fraction over the course of 24 hours OGD. Recruitment of Parkin was significantly increased by 2 hours of OGD (B), so this was chosen as an appropriate time for future experiments.

Although H9c2 cells are relatively straight-forward to culture their transfection efficiency is very low (Liu et al., 2011). Despite numerous attempts, I was unable to transfect them with various commercially available reagents, so I used lentiviral infection to manipulate protein levels in these cells. A lentiviral knock down for Fbxo7 was already available in the lab. Figure 4.11 (A) shows a sequence alignment of the target sequence of the knock down with the relevant region of the rat Fbxo7 open reading frame. Figure 4.11 (B) shows that Fbxo7 was successfully knocked down within 4 days of transduction, compared to a scrambled lentiviral control.

The Parkin knock down previously used in HEK293T cell experiments was specifically generated to target both human and rat Parkin. Therefore, the functional part of the construct could easily be digested out of the mammalian vector and into the lentiviral vector. Figure 4.12 (A) shows a sequence alignment from the start of the open reading frames of both human and rat Parkin, along with the shRNA target sequence. As indicated in red, there are a few base pair mismatches between the human and rat sequences, but none are within the target sequence of the shRNA. It was therefore anticipated that this sequence would knock down Parkin as efficiently in rat H9c2 cells as it did in HEK293T cells. Figure 4.12 (B) and (C) show that this was the case, with an almost complete knock down achieved within 4 days of viral transduction.

The efficacy of Fbxo7 and Parkin knock downs, combined with the OGD-dependent mitochondrial recruitment of Parkin, and high mitochondrial content (Kuznetsov et al.,

2015) made H9c2 cells an ideal model to study protein manipulation and mitochondrial effects.

4.4.3.2 Analysis of mitochondrial networks

MiNA (Mitochondrial Network Analysis) was used for all analyses of mitochondrial networks (reticula) presented in this study. This pair of macros have been previously published and are freely available online (Valente et al., 2017). Analysis of mitochondria in this way circumvents many of the issues faced in manual analysis of mitochondria. Most previously published studies on mitochondrial morphology involved manual determination of structures, by categorising each mitochondrion as round-type or elongated-type. This is a very time-consuming method, and also can be very subjective, as mitochondria rarely fit neatly into one of two or three ideological categories. Performing analysis using the MiNA macros removes bias by being fully automated. It also allows a large number of cells to be analysed in a short time frame, allowing for larger numbers of replicates to be processed.

Using the MiNA analysis tools, the effects of knock down of Parkin or Fbxo7 were studied, under basal and OGD conditions. As previously described, 2 hours was chosen as an optimal time for OGD. Control cells were kept in normoxic conditions for the same period of time. To avoid the effects of reperfusion confounding the OGD data, cells were fixed in the anoxic chamber. Figure 4.13 (A) shows representative confocal images of H9c2 cells under all conditions, and various mitochondrial parameters are analysed in (B) – (D).

The cells selected for analysis were not all the same size, so the number of mitochondria, both total numbers and numbers of individual vs. networked mitochondria, are not comparable. However, this can be controlled for by instead calculating a ratio of networked to individual mitochondria within a cell (Figure 4.13 (B)). Somewhat surprisingly, this ratio was not changed by OGD for the control (scrambled) cells or either of the knock downs. However, the ratio not changing does not necessarily mean that mitochondrial numbers did not change.

OGD significantly decreased the average length of branches within the mitochondrial reticulum (Figure 4.13 (C)). This is indicative of an increase in mitochondrial fission, or a decrease in mitochondrial fusion. Interestingly, knock down of Parkin resulted in a greater decrease in average network branch length upon OGD (C). This could suggest that the shortening of branch length is a result of increased fission, as opposed to decreased fusion. Consistent with the data presented in this chapter, absence of Parkin would result in an increase of Mff, which could in turn facilitate excess fission.

Mitochondrial network complexity was measured as the average number of branches within the mitochondrial reticulum. As evident from Figure 4.13 (D), no significant change was observed in network complexity as a result of OGD. However, knock down of Fbxo7 did result in a significant increase in network complexity upon OGD.

The meaning of these data is not yet clear, and effects observed through knock down of Parkin or Fbxo7 cannot be definitively linked to Mff at this stage. What is clear, however, is that both Parkin and Fbxo7 play roles in the maintenance or regulation of the mitochondrial reticulum, perhaps by suppression of mitochondrial fission.

Chapter 5 SUMO regulates mitochondrial dynamics

5.1 Introduction

Evidence presented in Chapters 3 and 4 identified Mff as a target of Parkin-mediated ubiquitination and showed that Mff can be modified by conjugation of SUMO-1 and SUMO-2. A newly emerging group of ubiquitin ligases which identify substrates via SUMO chains is generating a lot of interest. These SUMO-targeted ubiquitin ligases (STUbLs) contain SUMO-interacting motifs to bind non-covalently to SUMO. It has been previously reported that Parkin can interact non-covalently with SUMO-1 (Um and Chung, 2006). I therefore wanted to explore the possibility that SUMOylation of Mff may play a part in regulation of its interactions with Parkin.

5.1.1 Identification of non-covalent SUMO interactions

Covalent attachment of one or more SUMO molecules (SUMOylation) to substrate proteins has been recognised as an important post-translational modification for more than 20 years (Mahajan et al., 1997, Matunis et al., 1996). However, non-covalent interactions of proteins with SUMO remain far less well-characterised (Li et al., 2000, Shen et al., 1996). Since the discovery of SUMO, two-hybrid assays have emerged as a convenient tool to differentiate covalent from non-covalent interactions with SUMO; proteins which interact with SUMO in the absence of the C-terminal di-glycine motif required for covalent conjugation are candidates for non-covalent interactors. Use of this approach has facilitated the identification of many SUMO-interacting proteins and the SUMO-interacting motifs (SIMs) which mediate the binding (Hannich et al., 2005, Hecker et al., 2006).

5.1.1.1 Two-Hybrid screen: initial identification of a SIM

The first specific SUMO-interacting proteins containing conserved SIMs were reported in 2000 (Minty et al., 2000). In their study, Minty *et al* used a two-hybrid approach to show that certain proteins were able to interact with SUMOylated p73 (a member of the p53 tumour suppressor family). A two-hybrid screen relies on the ability of most eukaryotic transcription factors (TFs) to still function when their two functional domains, the DNA-

binding domain (DBD) and the activating domain (AD), are proximal but not directly bound to one another (Fields and Song, 1989). Minty *et al* fused the DBD of TF LexA to p73α and used the resulting fusion protein as bait in a *Saccharomyces cerevisiae* (strain EGY48, containing LEU2 (required for synthesis of leucine (Storms et al., 1981)) under control of LexA promoters) based two-hybrid screen. The p73α-DBD fusion protein was transformed into the yeast and a cDNA library from two different cell lines (SK-N-AS neuroblastoma and U937 monocytic) was then introduced in plasmids encoding the LexA AD. Colonies were re-plated on agar lacking leucine, to allow selection of successful recombinants. Using this method, the authors isolated cDNA encoding, among others, SUMO-1, Ubc9, SAE2 and PIASX (Minty et al., 2000).

5.1.1.2 SIMs

With several newly identified SUMO-interacting proteins, Minty *et al* were able to interrogate their sequences for conserved motifs. A subset of their identified proteins contained an 11-amino acid motif, which they proposed to be a SUMO-1 interacting motif (SIM). At its core, the conserved motif comprised of a S-x-S triplet, in which x could be any amino acid. Flanking this core, the authors observed an N-terminal hydrophobic region and a C-terminal acidic region (Minty et al., 2000).

However, a study published a few years later disputed the requirement of the serine residues in SUMO-binding, arguing that the hydrophobic region was the principal component of the SIM (Song et al., 2004). The authors of this study used nuclear magnetic resonance (NMR) spectroscopy to investigate binding of SUMO-1 to a synthetic peptide comprising the previously described SIM of PIASX (PIASX-SIM) (Minty et al., 2000). The NMR data from Song *et al* revealed that the S-x-S and subsequent acidic residues were not directly involved in SUMO-1 binding and showed that the most significant chemical shift changes were induced by the hydrophobic residues Val-2 to Ile-9 in their synthetic PIASX-SIM peptide. The authors went on to validate this finding by synthesising a new peptide comprising just the hydrophobic part of the SIM, Val-2 to Glu-10, and found that this peptide induced almost identical chemical shift changes to those detected within the PIASX-SIM peptide, suggesting that both the full-length and the reduced synthetic SIM-containing peptides interacted with SUMO-1 in an identical way (Song et al., 2004).

Over the subsequent years, a SIM was identified in yeast that shared core characteristics of the previously described mammalian SIM, namely a hydrophobic core and flanking acidic residues (Hannich et al., 2005, Hecker et al., 2006). It emerged that this hydrophobic core, comprising 3-4 aliphatic residues, was an essential part of the SIM, and

that it was often juxtaposed to a cluster of acidic residues. Despite this, the SIM remains an enigmatic and highly variable motif. (Kerscher, 2007).

5.1.2 The SUMO-SIM interaction

5.1.2.1 SIM/SUMO hydrophobicity

NMR spectroscopy was used to solve the structure in solution of SUMO-1 bound to a SIM-containing synthetic PIAS peptide, revealing interactions between hydrophobic and aromatic residues (Song et al., 2005). In the case of both SUMO-1 and SUMO-2, these hydrophobic and aromatic residues were arranged in a SIM-binding groove between the beta-2 strand and alpha-1 helix of SUMO (Figure 5.1 (C)). In their study, Song *et al* showed that residues 2-8 of the PIAS peptide (V-D-V-I-D-L-T) embed, in an extended conformation, in the SIM-binding groove of SUMO.

The SIM-binding groove of SUMO identified by Song *et al* is the only concave surface of the molecule to comprise patches of hydrophobicity and aromatic residues (His-35, Ile-34, Phe-36, Val-38, Leu-47, and Tyr-51). The authors went on to show that mutation of Phe-36 to alanine, despite having no effect on the structural integrity of SUMO-1, reduced the affinity of the SIM-binding groove for the PIAS peptide to such an extent that interaction could no longer be detected, demonstrating the importance of hydrophobicity in SUMO-SIM binding (Song et al., 2005). These data were validated by independent studies that also noted the importance of key SUMO-1 hydrophobic residues involved in SIM-binding, Phe-36, Val-38 and Leu-47 (Hecker et al., 2006, Baba et al., 2005).

5.1.2.2 Charge clusters

Many SIMs contain not only a hydrophobic core, but also a juxtaposed cluster of acidic residues (Hannich et al., 2005, Hecker et al., 2006). These residues promote electrostatic interactions, with important roles in affinities, orientation and functionality of SUMO-SIM interactions (Hecker et al., 2006, Song et al., 2005). The binding surface of SUMO-1 has a positive electrostatic potential. In the PIAS peptide, two Asp residues are located to interact with Arg-54 and Lys-37 of SUMO-1, likely promoting the SUMO-SIM interaction. Mutation of the equivalent Asp residue in the RanBP2 SIM significantly reduced the SUMO-SIM binding affinity (Song et al., 2004).

Similarly, the hydrophobic core of many SIMs sits near serine and threonine residues. It has been shown that phosphorylation of these residues also regulates SUMO-SIM binding (Hecker et al., 2006). The authors in this case propose that phosphorylation

of a serine within the PIAS peptide SIM facilitates SUMO binding by introducing a negative charge, which Lys-39 of SUMO (conserved in the hydrophobic groove of all three mammalian SUMO homologues) can interact with to strengthen the interaction. Indeed, Hecker *et al* go on to show that the serine residue is phosphorylated *in vivo*. These data were later validated by an independent study, which showed that phosphorylation of serine residues adjacent to the SIM of PIAS1 favoured formation of a non-covalent ternary complex comprising PIAS1, SUMO and Ubc9, required for transcriptional repression (Mascle et al., 2013).

5.1.2.3 SUMO orientation

The hydrophobic core, as shown in Figure 5.1 (A), can be quite variable. Similarly, the cluster of acidic amino acids, if present, can be up- or downstream of the hydrophobic core (B). This allows the SIM to bind SUMO in a parallel or anti-parallel orientation (C). This has been shown in several studies; SUMO binds to the SIMs in thymine DNA glycosylase and RanBP2 in an anti-parallel manner, but to the PIAS protein-derived SIM in parallel (Baba et al., 2005, Song et al., 2005, Reverter and Lima, 2005).

5.1.2.4 SUMO preferences

As previously discussed, the crucial hydrophobic residues involved in SIM binding are conserved between the SUMOs. However, the different SUMO homologues may differ in the position of their hydrophobic groove. It has been shown by crystallographic analyses that the hydrophobic groove of SUMO1, SUMO2 and the yeast SUMO paralogue Smt3 is surrounded by basic residues, which act as 'prongs' to receive the SIM domain and its associated negative charges (Chupreta et al., 2005). However, the positioning of the hydrophobic groove relative to the basic residues differs between the SUMOs, indicating that the particular arrangement of hydrophobic and acidic residues within SIMs could allow them to discriminate between the different SUMO isoforms, which would be of potential importance in the case of STUbLs.

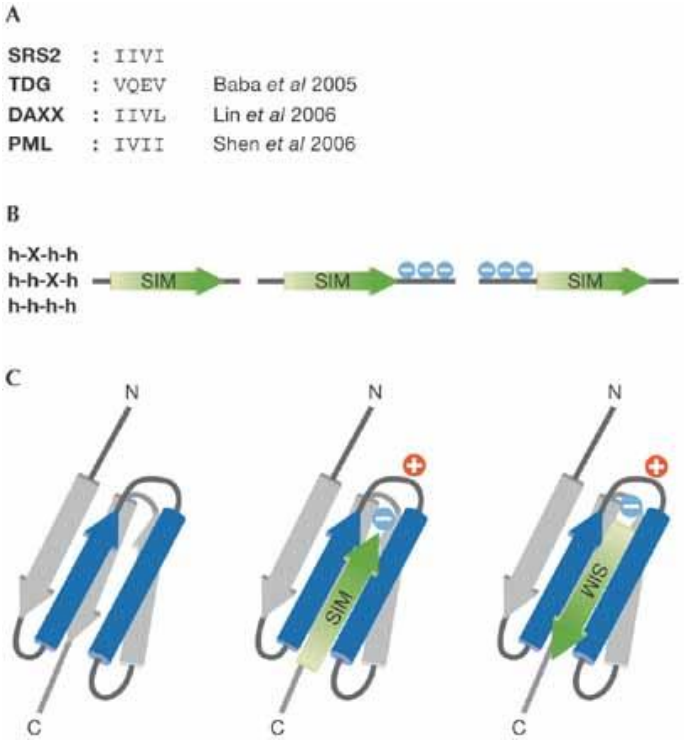

Figure 5.1 **SUMO interacting motifs are variable**. (A) illustrates the sequence variability between core hydrophobic components of SIMs from *bona fide* SUMO-interacting proteins. (B) possible combinations of hydrophobic (h) core and acidic/phosphorylated residues (blue minus symbol). X can be any amino acid. (C) SIM-SUMO binding can be parallel or anti-parallel, depending on arrangement of (h) to acidic residues. Positively charged lysine 78 of SUMO (red plus symbol) may be important in the orientation of phosphorylated SIMs. SUMO shown in blue, SIM-containing peptide in green. Figure taken from *Kerscher, O. (2007). "SUMO junction—what's your function? New insights through SUMO-interacting motifs."* EMBO Reports ***8****(6): 550-555* (Kerscher, 2007).

5.1.3 SUMOylation consensus motifs

SUMO is attached to a target protein via an ATP-dependent, enzyme-catalysed cascade, resulting in formation of an isopeptide bond between an ε-amino group on a lysine residue of the target protein and the C-terminal carboxyl group of the SUMO protein (Desterro et al., 1997). While all SUMOylation occurs at lysine residues, not all lysine residues can be SUMOylated (Matunis et al., 1998, Mahajan et al., 1998, Andre et al., 1996).

It was not until several targets of SUMOylation had been identified and their SUMO-conjugation sites mapped that a SUMOylation consensus sequence could be established. In 1999, Sternsdorf *et al* identified the SUMOylatable lysine residue of Sp100, a nuclear dot (ND) protein (Sternsdorf et al., 1999). Using this information, along with other published SUMOylation sites of IKappaB (Desterro et al., 1998), RanGAP (Matunis et al., 1998,

Mahajan et al., 1998) and PML (Kamitani et al., 1998), they predicted further SUMOylation sites in other ND proteins and ND-related proteins. Their predicted sites all fit a consensus sequence similar to one proposed by Desterro *et al* in 1998 (Desterro et al., 1998). The consensus SUMOylation motif, at its core, comprised 4 amino acids: (I/L)-K-x-E, where x could be any amino acid. This tetrapeptide consensus was later updated to recognise that the first position could be any large hydrophobic amino acid, rather than just isoleucine or leucine, giving the ψ-K-x-E motif still used in predictions of SUMOylation sites today (Sampson et al., 2001).

5.1.3.1 Non-consensus SUMOylation motifs

In a proteomics-based approach, Blomster *et al* used tryptic digestion of proteins followed by liquid chromatography-tandem mass spectrometry to perform an unbiased screen for identification of post-translational modification sites (Blomster et al., 2010). They identified 14 novel SUMOylated peptides, of which only 3 were SUMOylated at consensus SUMOylation motifs. This was in support of previous work carried out by them, and by other groups, which had suggested that a considerable proportion of SUMOylated proteins do not contain the consensus tetrapeptide SUMOylation motif (Blomster et al., 2009, Golebiowski et al., 2009, Hsiao et al., 2009, Zhu et al., 2008). Their previous study had identified 382 SUMO-2 targets, of which over half contained non-consensus SUMOylation motifs (Blomster et al., 2009).

5.1.3.2 Phosphorylation-dependent SUMOylation motifs

A recurrent phosphorylation-dependent SUMOylation motif (PDSM) was first reported in 2006 (Hietakangas et al., 2006). The authors of this study had previously shown that phosphorylation of HSF1, a stress-related transcriptional factor, was required for its SUMOylation (Hietakangas et al., 2003). Their 2006 paper identified a conserved motif among 48 human proteins, of which 71% were transcriptional regulators, that matched with the sites of phosphorylation and SUMOylation in HSF1. The proteins they identified included several known SUMOylation substrates, such as transcription factors GATA-1 and MEF2 (Collavin et al., 2004, Gregoire and Yang, 2005). The consensus sequence, Ψ-K-x-E-x-(x)-S-P, was termed PDSM (Hietakangas et al., 2006).

5.1.4 Aims

The data presented so far have established a role for Parkin in degradation of Mff during ischaemia and identified Mff as a novel target of SUMOylation. A previous study has reported that Parkin can associate non-covalently with SUMO-1 (Um and Chung, 2006). We therefore hypothesised a role for SUMO in Parkin-dependent regulation of Mff. The aims of this part of my PhD were to:

i. Validate a previous report of non-covalent interaction between SUMO and Parkin.
ii. Define the nature of the Mff SUMOylation site and determine if this can recruit Parkin.
iii. Investigate the role of SUMOylation in ubiquitination of Mff, in particular by Parkin.

5.2 Methods

5.2.1 *In vitro* co-immunoprecipitation

5.2.1.1 Fusion protein expression in BL21 (DE3) *E. coli*

BL21 (DE3) *E. coli* were transformed as described in Chapter 2 and plated on LB agar containing 100µg/mL ampicillin (pGEX-4T1 constructs: GST-fusions) or 25µg/mL kanamycin (pET28a: His-fusions) and incubated at 37°C overnight. A single colony was then picked and incubated in 100mL 2xYT Broth (1.6% (w/v) bacto-tryptone, 1% (w/v) Bact yeast extract, 0.5% (w/v) NaCl, pH7.0) containing appropriate selection antibiotic at 37°C overnight in a shaking incubator. Protein expression was induced by addition of Isopropyl β-D-1-thiogalactopyranoside (IPTG, Sigma Aldrich) to a final concentration of 0.2mM, and further incubation at 25°C, shaking, for 6 hours.

5.2.1.2 GST-fusion protein purification

Bacteria were pelleted at 4000rpm for 20 minutes at 4°C, the supernatant removed, and the pellet resuspended in 10mL lysis buffer (25mM Tris pH 7.5, 150mM NaCl, 10% (v/v) glycerol, 1% (v/v) Triton X-100, 1x protease inhibitors). Bacterial cells were lysed by sonication (6x 10 seconds, with cooling on ice in between) and left to solubilise on ice for 15 minutes. Lysates were then centrifuged at 20,000rpm for 25 minutes at 4°C to pellet

cell debris. For each GST-fusion protein, 200µL Glutathione Sepharose® 4 Fast Flow beads were washed twice with 10mL wash buffer (25mM Tris pH 7.5, 150mM NaCl, 10% (v/v) glycerol, 1% (v/v) Triton X-100) by gently mixing and pelleting at 2000rpm for 2.5 minutes. Wash buffer was then aspirated, and the cleared bacterial lysate added to the beads. Lysates were incubated on the beads for 2 hours at 4°C, on a spinning wheel. Beads were then pelleted as before and washed 4 times with 10mL wash buffer. After the final wash, beads were resuspended in a small volume (~1mL wash buffer), transferred to a 1.5mL Eppendorf tube and pelleted at 4000rpm, 4°C, for 2 minutes. The supernatant was aspirated, and the beads resuspended in 200µL elution buffer (25mM Tris pH 7.5, 150mM NaCl, 10% (v/v) glycerol, 1% (v/v) Triton X-100, 10mM reduced glutathione, pH 8.0). Tubes were incubated on a rocking platform for 5 minutes at RT, then the beads pelleted at 4000rpm as before. The eluate was removed, and the elution process repeated a further 2 times, giving a total of 600µL GST-fusion protein-containing eluate. 5µL of this were then run on an acrylamide gel alongside 1, 2.5, 5 and 10µg BSA standards, so that approximate concentration could be ascertained by Coomassie staining. Eluates were aliquoted and stored at -80°C.

5.2.1.3 His-fusion protein purification

His-tagged proteins were purified following the GST-fusion protein purification protocol, with the exception of buffer components and beads. Lysis buffer contained 25mM Tris pH 7.5, 150mM NaCl, 10% (v/v) glycerol, 1% (v/v) Triton X-100, 10mM imidazole and 1x protease inhibitors. Wash buffer was lysis buffer lacking protease inhibitors. Elution buffer contained 25mM Tris pH 7.5, 150mM NaCl and 250mM imidazole, pH 8.0. Ni-NTA Sepharose® 4 Fast Flow beads were used for purification.

5.2.1.4 Recombinant protein binding assay

In vitro recombinant protein binding assays were performed using GST-fusion proteins and Glutathione Sepharose® 4 Fast Flow beads to co-immunoprecipitate His-fusion proteins. Protein amounts stated are approximations based on BSA standards from a Coomassie gel.

1µg GST, GST-SUMO-1 or GST-SUMO-2 was mixed with 0.01µg His-Parkin in 500µL incubation buffer (50mM Tris pH 7.4, 150mM NaCl, 1% (v/v) Triton X-100, 0.1% (w/v) BSA and 1x protease inhibitors) in an Eppendorf tube. The protein suspension was incubated on a spinning wheel at RT for 1 hour. For each tube, 20µL Glutathione Sepharose® 4 Fast Flow beads were washed twice in 500µL wash buffer (50mM Tris pH 7.4, 150mM NaCl, 1%

(v/v) Triton X-100 and 1x protease inhibitors) by gently mixing and pelleting at 4000rpm, 4°C, for 2 minutes. Supernatant was aspirated from the beads and the protein suspension added. The protein/bead suspension was incubated on a spinning wheel at 4°C for 1 hour. Beads were then pelleted as before and washed 3 times in 500µL wash buffer by resuspension, 10-minute incubation of spinning wheel at 4°C and pelleting as before. After the final wash, supernatant was aspirated, and the beads resuspended in 40µL 2 x Laemmli buffer (4% SDS (w/v), 10% glycerol (v/v) 125mM Tris-HCl pH6.8, 0.004% bromophenol blue (w/v), 10% (v/v) 2-β-mercaptoethanol) and heated at 95°C, 1200rpm for 10 minutes. Samples were then subjected to SDS-PAGE and Western blotting, as described in Chapter 2.

5.2.2 Bacterial SUMOylation assay

5.2.2.1 Fusion protein expression and SUMOylation in BL21 (DE3) *E. coli*

BL21 (DE3) *E. coli* were transformed as described in Chapter 2 with either His-tagged protein only, or His-tagged protein and pE1E2-SUMO-1/SUMO-2 and plated on LB agar containing 25µg/mL kanamycin (single transformations) or 25µg/mL kanamycin and 34 µg/mL chloramphenicol (double transformations). Plates were incubated at 37°C overnight. A single colony was then picked and incubated in 3mL 2xYT Broth containing appropriate selection antibiotics (25µg/mL kanamycin or 25µg/mL kanamycin and 34 µg/mL chloramphenicol), at 37°C, shaking, overnight. Protein expression (and fusion protein SUMOylation) was induced by addition of IPTG to a final concentration of 0.2mM, and further incubation at 25°C, shaking, for 6 hours.

5.2.2.2 Assaying for *in vitro* SUMOylation

5.2.2.2.1 SUMOylation assay using crude bacterial lysate

Bacteria were pelleted at 4000rpm for 20 minutes at 4°C, the supernatant removed, and the pellet resuspended in 500µL 1x Laemmli buffer (2% SDS (w/v), 5% glycerol (v/v) 62.5mM Tris-HCl pH6.8, 0.002% bromophenol blue (w/v), 5% (v/v) 2-β-mercaptoethanol). The lysate was then sonicated (5x 5 second bursts) and heated at 95°C, 1200rpm for 10 minutes. Samples were then subjected to SDS-PAGE and Western blotting, as described in Chapter 2.

5.2.2.2.2 SUMOylation assay using His-fusion purification

SUMOylated, His-tagged fusion proteins were purified following a scaled down version of the protocol outlined in 5.2.1.3. Briefly, a 2mL IPTG-induced culture was pelleted at 16,000xg for 1 minute and the supernatant discarded. Each pellet was resuspended in 500µL lysis buffer (25mM Tris pH 7.5, 150mM NaCl, 10% (v/v) glycerol, 1% (v/v) Triton X-100, 10mM imidazole, 20mM NEM and 1x protease inhibitors) and sonicated with 2 bursts of 5 seconds. Insoluble material was removed by centrifugation at 16,000xg for 10 minutes. 2µL 2-β-mercaptoethanol was added to the cleared supernatant to quench unreacted NEM, before 30µL Ni-NTA Sepharose® 4 Fast Flow beads were added. The lysate was incubated with the beads at 4°C for 1 hour, on a spinning wheel. Beads were then pelleted (1180xg, 2 minutes) and washed 4 times with wash buffer (lysis buffer lacking protease inhibitors and NEM). Wash buffer was aspirated and the beads resuspended in 100µL 2 x Laemmli buffer. Samples were heated at 95°C, 1200rpm for 10 minutes, and then subjected to SDS-PAGE and Western blotting, as described in Chapter 2. This SUMOylation assay has been previously described (Wilkinson et al., 2008).

5.2.3 Protein degradation assay

In order to measure rates of protein degradation in HEK293T cells, protein synthesis must be blocked. Protein translation elongation was inhibited by addition of a drug, cycloheximide (CHX). HEK293T cells were cultured and transfected as described in Chapter 2. Protein synthesis was blocked by addition of 25µg/mL cycloheximide (Sigma-Aldrich) for up to 24 hours prior to cell lysis. Western blotting was used to quantify rates of degradation.

5.3 Results

5.3.1 Parkin interacts with SUMO-1 and SUMO-2

It was important to first ensure that the non-covalent Parkin-SUMO interaction identified previously by Um and Chung could be validated. In their study, Parkin was shown to interact specifically with SUMO-1 and could not be co-immunoprecipitated with SUMO-2 (Um and Chung, 2006). I co-transfected HEK293T cells with Myc-Parkin and YFP, YFP-SUMO-1 or YFP-SUMO-2, both full-length proteins and mutants lacking the C-terminal di-glycine motif required for their conjugation (ΔGG (Bayer et al., 1998)). 48 hours post-

transfection, GFP-Trap beads were used to immunoprecipitate YFP or YFP-SUMO, and samples were subjected to SDS-PAGE and Western blotting with an anti-Myc antibody to identify any co-immunoprecipitated Myc-Parkin. As shown in Figure 5.2, Myc-Parkin was effectively co-immunoprecipitated with both YFP-SUMO-1 (A) and SUMO-2 (B). Interestingly, co-immunoprecipitation of Myc-Parkin was significantly less efficient with both the SUMO-1 and SUMO-2 ΔGG mutants that cannot be covalently attached to substrates (B and D), indicative of a preference for binding to poly-SUMOylated substrates, rather than free SUMO.

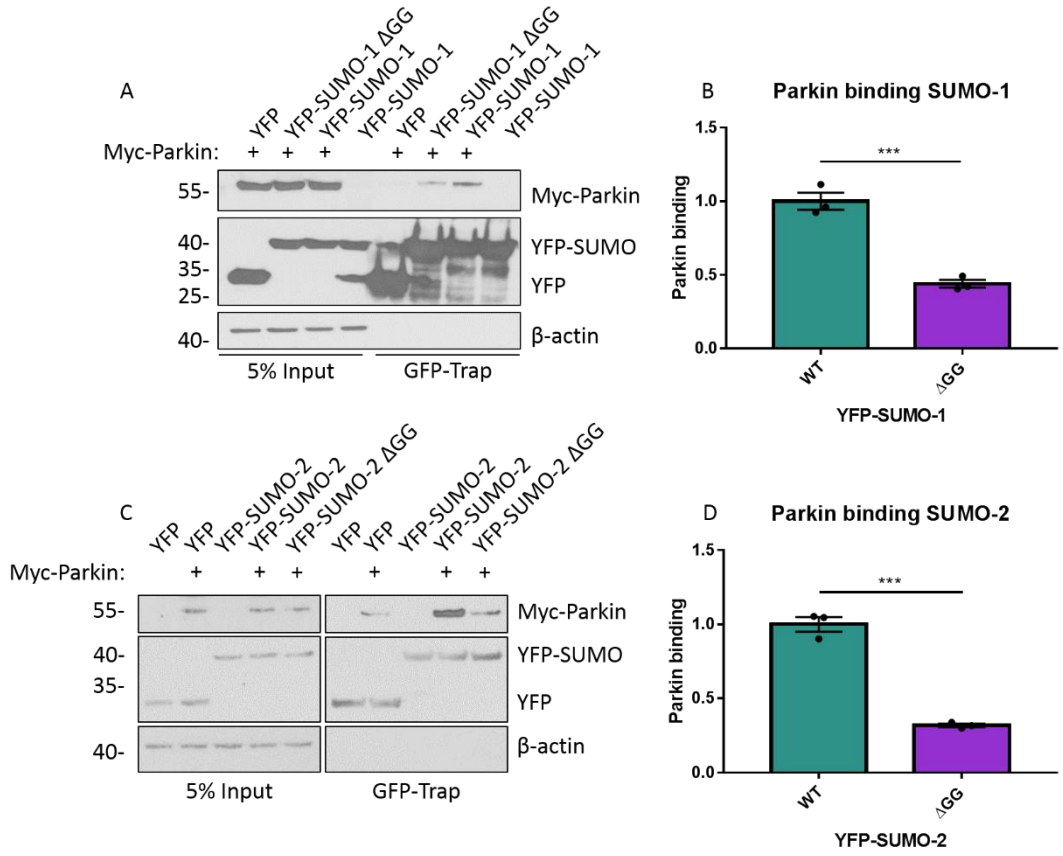

Figure 5.2 **Parkin binds SUMO-1 and SUMO-2 in HEK293T cells.** Exogenously expressed YFP-SUMO-1 or –SUMO-2 and, to a lesser extent, a non-conjugatable YFP-SUMO-1 or –SUMO-2 ΔGG mutant, co-immunoprecipitated Myc-Parkin by GFP-Trap from HEK293T lysate, whereas YFP alone could not. N=3. Analysed using unpaired two-tailed students' t-test. Data presented as mean ± SEM. *** $p \leq 0.001$.

5.3.2 Parkin may bind directly to SUMO-2

The data presented in Figure 5.2 demonstrate that Parkin can specifically and non-covalently interact with both SUMO-1 and SUMO-2. In a cell-based model, however, it cannot be determined whether or not this is a direct interaction, which would be required

if Parkin were acting as a STUbL. To examine the nature of this interaction, the proteins of interest need to be expressed within an isolated system.

His-tagged Parkin and GST-tagged SUMO were expressed in BL21 (DE3) *E. coli* and then purified using Glutathione Sepharose® 4 Fast Flow (GST-proteins) or Ni-NTA Sepharose® 4 Fast Flow (His-proteins).

Initially, GST- or His-tagged proteins were purified and subjected to SDS-PAGE, with Coomassie Blue used to stain the gel for total protein. Known amounts of BSA were loaded as a standard, to allow relative estimation of concentration of the purified proteins. As shown in Figure 5.3 (A), GST, GST-SUMO-1 and GST-SUMO-2 expressed well and were purified effectively. However, His-Parkin could not be detected. At this point, it was not known whether the bacteria had failed to efficiently produce His-Parkin, or if it had been lost at some point within the Ni-NTA Sepharose® 4 Fast Flow purification protocol. To troubleshoot this, the process was repeated using freshly transformed bacteria, with samples removed at various points throughout the purification. These samples were subjected to SDS-PAGE and Coomassie Blue staining as before (Figure 5.3 (B)). His-Parkin could not be identified within the total bacterial lysate, nor did it appear to be within any of the eluted fractions or still stuck to the beads, raising concern that the construct was not being efficiently expressed. However, when a 0.8% sample of the supposed purified His-Parkin eluate was transferred to PVDF membrane and blotted with a knock down-validated Parkin antibody, a band of the correct molecular weight (55kDa) was readily detected (Figure 5.3(C)). These results suggest that His-Parkin is expressed at much lower levels than the GST-tagged SUMO constructs and was not detected by Coomassie staining due to its relative insensitivity.

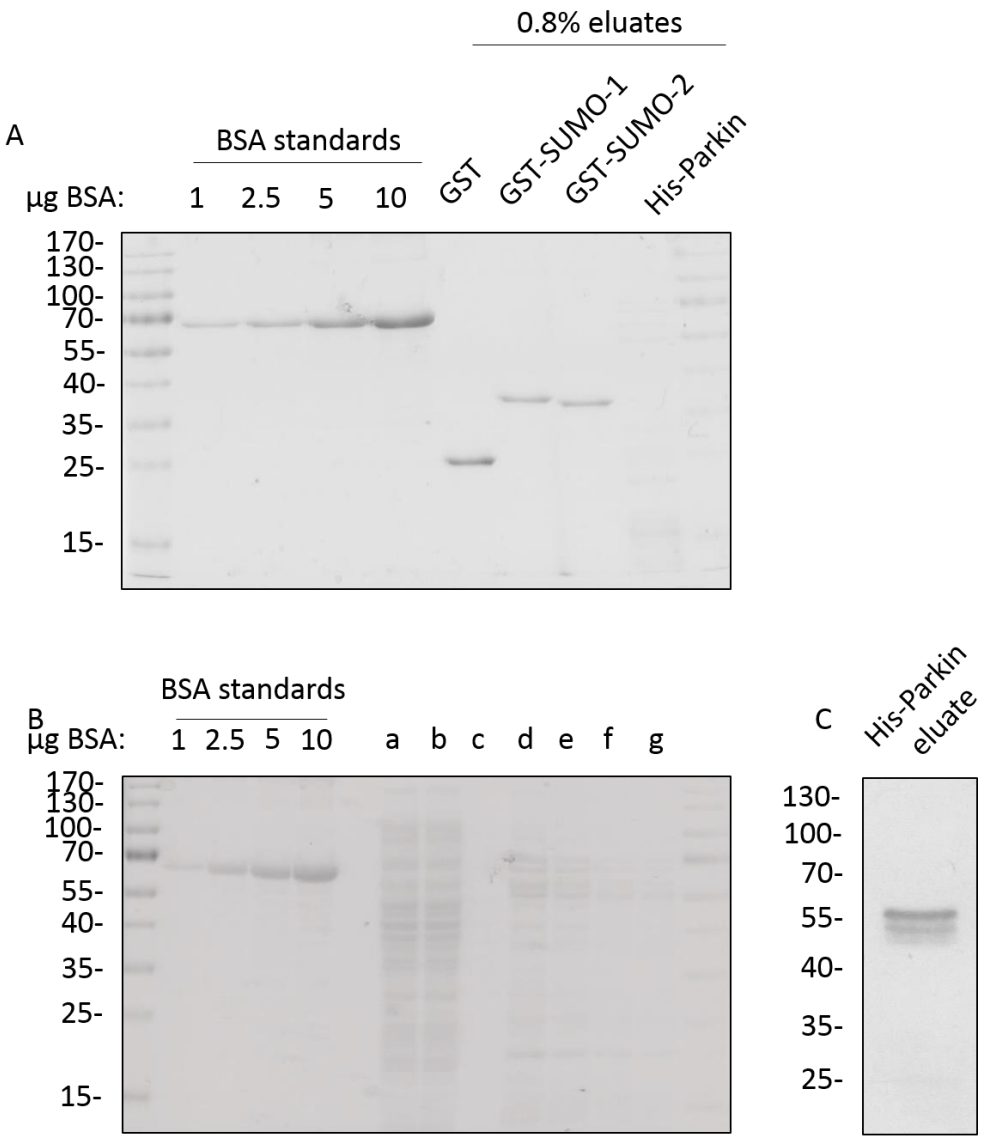

Figure 5.3 **Bacterial expression of GST-SUMO and His-Parkin.** GST, GST-SUMO and His-Parkin were expressed in BL21 (DE3) *E. coli* and purified with Glutathione Sepharose® 4 Fast Flow (GST-proteins) or Ni-NTA Sepharose® 4 Fast Flow (His-proteins). 0.8% samples of the eluate were then electrophoresed alongside known standards of BSA, and the gel stained with Coomassie (top panel). His-Parkin could not be detected in the eluate, so the purification was repeated, with samples taken at various steps (bottom left panel, a-g (a) Bacterial lysate, (b) unbound protein (pre-wash), (c) unbound protein (after wash), (d) eluate 1, (e) eluate 2, (f) eluate 3, (g) beads)). Coomassie was still not sufficient to visualise His-Parkin, however, when a 0.8% sample of the eluate was blotted with the Parkin antibody, a ~55kDa species was detected (bottom right panel).

Once pure recombinant proteins had been generated, *in vitro* binding assays were performed. Using the Coomassie staining of GST and GST-SUMO alongside BSA standards, protein concentration was estimated so that the volume required for approximately 1µg each could be calculated. This was then used in a binding assay with 0.01µg His-Parkin.

GST or GST-SUMO was then precipitated using Glutathione Sepharose® 4 Fast Flow, and the samples used for SDS-PAGE and Western blotting.

As shown in Figure 5.4, His-Parkin was co-purified with both GST-SUMO-1 and GST-SUMO-2 to a greater extent than GST alone, but this difference was only statistically significant in the case of SUMO-2 (B). Under these experimental conditions, it was not possible to fully displace the interaction between free GST and His-Parkin, so the data cannot be confidently interpreted. Nonetheless, the binding capacity of GST-SUMO for Parkin was between two (SUMO-1) and four (SUMO-2) times that of free GST, so a direct interaction cannot be ruled out based on this experiment.

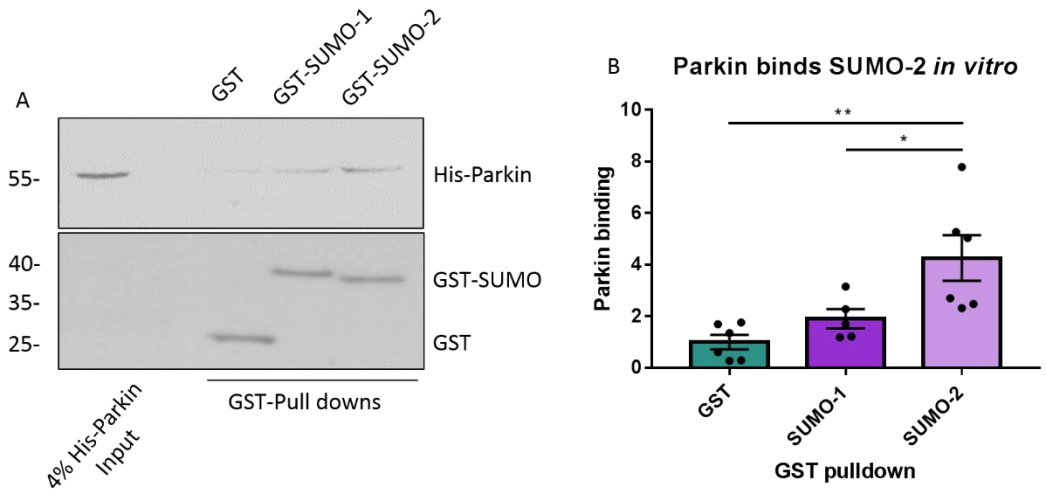

Figure 5.4 **Parkin interacts with SUMO *in vitro*.** GST-SUMO-2, but not GST-SUMO-1, was able to co-immunoprecipitate His-Parkin significantly more than free GST *in vitro*. N=6. Analysed using ordinary one-way ANOVA with Tukey's correction for multiple comparisons with a pooled variance. Data presented as mean ± SEM. * $p < 0.05$, ** $p < 0.01$.

5.3.3 Mff K151 is part of a stress-inducible PDSM

As was shown in chapter 3, Mff is modified by covalent conjugation of both SUMO-1 and SUMO-2. The single site of SUMO modification was identified as lysine 151. Upon closer inspection of the SUMOylation site, it became apparent that it is not a regular SUMO consensus motif, but rather part of a phosphorylation-dependent SUMOylation consensus motif (PDSM).

In a PDSM, phosphorylation of a nearby serine, in this case at reside 155, facilitates SUMOylation at the lysine, 151 in Mff, as shown diagrammatically in Figure 5.5. To test whether this conserved sequence within Mff does act as a PDSM, a series of mutants were

generated. In addition to the K151R non-SUMOylatable mutant already described, an E153A mutant was made to disrupt the SUMOylation consensus motif, whilst preserving the SUMOylatable lysine residue. In this mutant, Ubc9 binding is abolished, rendering the protein non-SUMOylatable (Sampson et al., 2001, Gareau and Lima, 2010). Mutations of the phosphorylatable serine were also generated: a phospho-null (S155A) and a phospho-mimetic, wherein aspartate mimics the charge (S155D). I then analysed the relative levels of SUMOylation of these mutants compared to the WT (Figure 5.6).

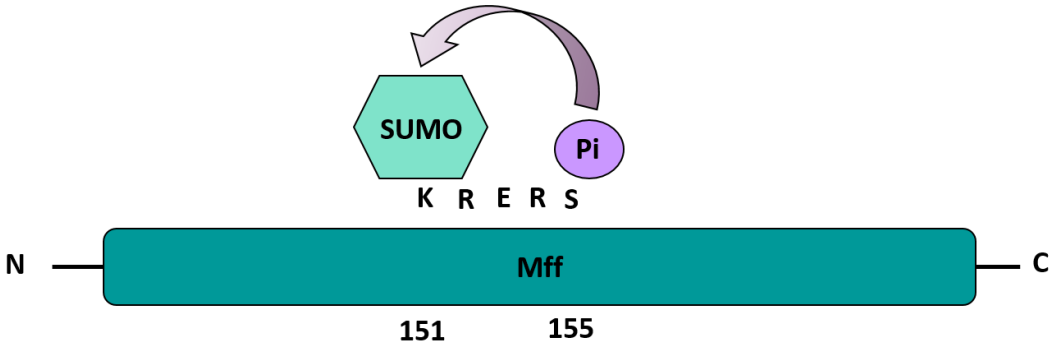

Figure 5.5 Schematic of Mff PDSM.

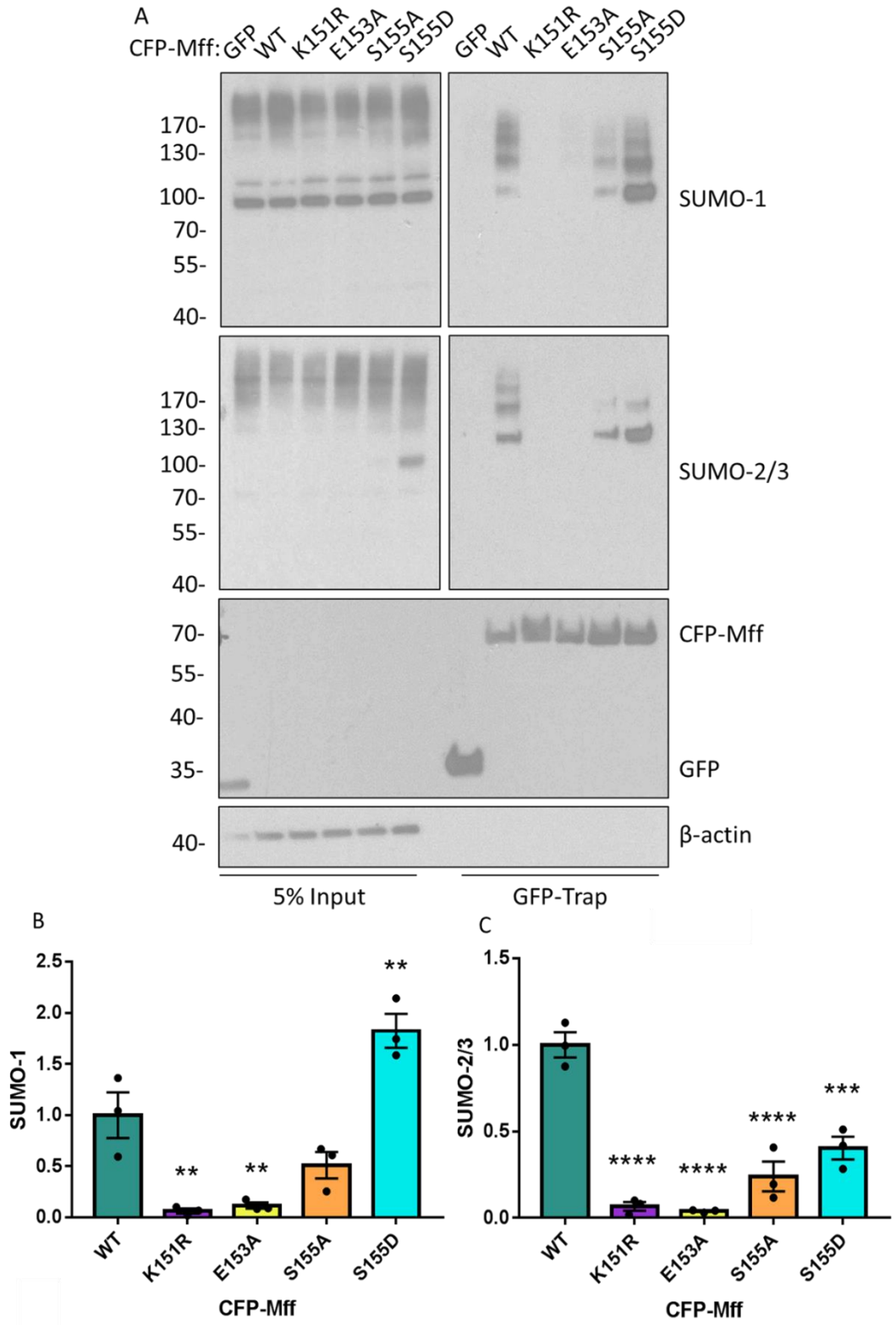

Figure 5.6 **Mff mutants are differentially SUMOylated in HEK293T cells.** CFP-Mff WT and mutants were exogenously expressed in HEK293T cells and immuno-precipitated with GFP-Trap. Samples were then blotted for endogenous SUMO-1 or SUMO-2/3. N=3. Analysed using one-way ANOVA (each mutant compared to WT) with Dunnett's correction for multiple comparisons. Data presented as mean ± SEM. ** $p < 0.01$, *** $p < 0.001$, **** $p < 0.0001$.

As shown in Figure 5.6, the various mutants of Mff were differentially SUMOylated, both by SUMO-1 and SUMO-2/3, compared to the WT (B, C). In the cases of SUMO-1 and SUMO-2/3, mutation of K151 or E153 abolished SUMOylation, whilst the phospho-null S155A mutation significantly reduced SUMO-2/3-ylation, as would be expected with the PDSM model. The phospho-mimetic mutation, S155D, behaved as expected for SUMO-1, resulting in a significant increase in SUMOylation of Mff (B). Curiously, this was not the case for SUMO-2/3, where a significant decrease in SUMOylation compared to WT was observed.

Phosphorylation often occurs as part of a stress response (Wang et al., 2012b, Auciello et al., 2014). In the case of Mff, and other PDSM-containing proteins, phosphorylation leads to increased SUMOylation. This raised the question: does cellular stress result increase Mff SUMOylation? In particular, we were interested in ischaemic stress, so we used oxygen and glucose deprivation (OGD) as a stressor.

HEK293T cells expressing GST-Mff WT were used for immunoprecipitation experiments with Glutathione Sepharose® 4 Fast Flow. Prior to lysis, cells were subjected to 2 hours of OGD in de-oxygenated, glucose-free media in an anoxic chamber at 37°C. Control cells were incubated in fresh, oxygenated, glucose-containing media in a normal cell culture incubator at 37°C for the same period of time. Western blots were then used to quantify endogenous SUMO-1-ylation of Mff. Figure 5.7 shows a representative blot and quantification of this experiment. Insufficient repeats have been performed so far to allow statistical analysis, but preliminary data indicate a ~100% increase in Mff SUMO-1-ylation during ischaemia (B), indicative of a mechanism whereby stress-induced phosphorylation of Mff promotes its SUMOylation.

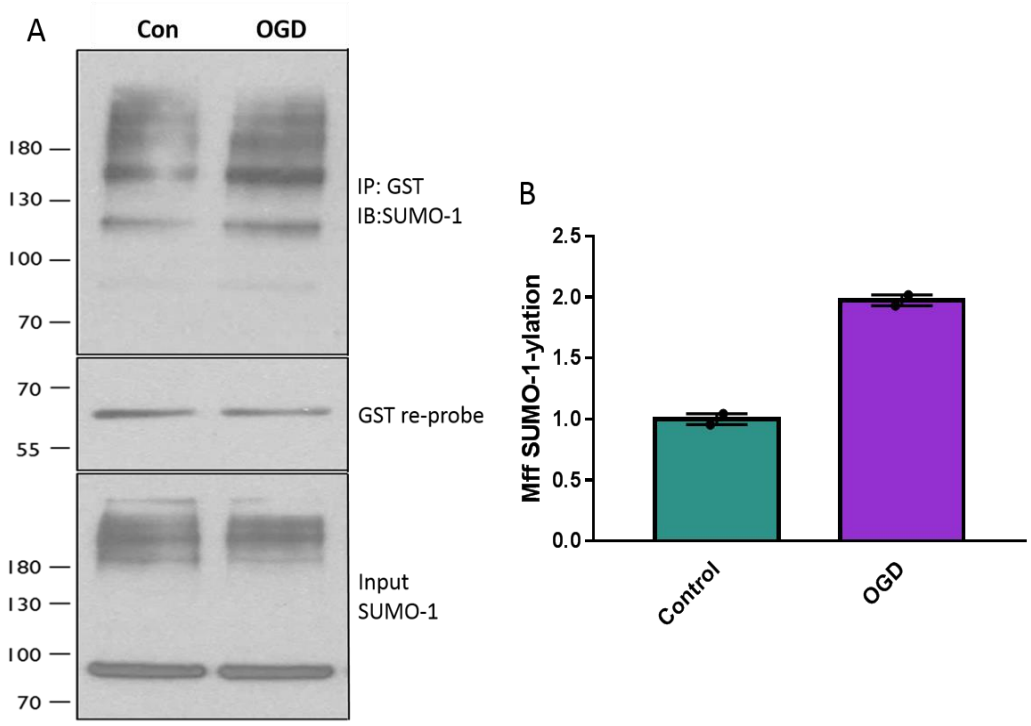

Figure 5.7 **Mff SUMOylation is increased during ischaemia.** HEK293T cells were transfected with GST-Mff (WT) and lysed 48-hours later. For 2 hours prior to lysis, cells were kept in either control or OGD conditions. Lysates were used for GST-immunoprecipitation (IP) and immunoblotted (IB) for endogenous SUMO-1. Data presented as mean ± SEM. N = 2. IP and Western blots performed by Richard Seager.

5.3.4 Parkin does not ubiquitinate Mff K151R

My data show that Parkin can bind to SUMO (Figure 5.2, Figure 5.4) and that Mff can be SUMOylated (Figure 3.14). Thus, this raised the question: does Mff SUMOylation regulate its interactions with Parkin? Specifically, does SUMOylation of Mff enhance Parkin-mediated ubiquitination? To test this hypothesis, HEK293T cells were co-transfected with CFP-Mff WT or K151R, along with scrambled (control) or Parkin-targeted shRNA. 72 hours post-transfection, cells were lysed, and the lysate used in GFP-Trap immunoprecipitation experiments, to identify Mff PTMs.

Figure 5.8 shows that the non-SUMOylatable Mff mutant K151R has significantly reduced ubiquitination compared to the WT (B). As shown previously, knock down of Parkin significantly reduces ubiquitination of WT Mff. However, knock down of Parkin has no significant effect of ubiquitination of Mff K151R, indicating that this mutant is insensitive to modification by Parkin.

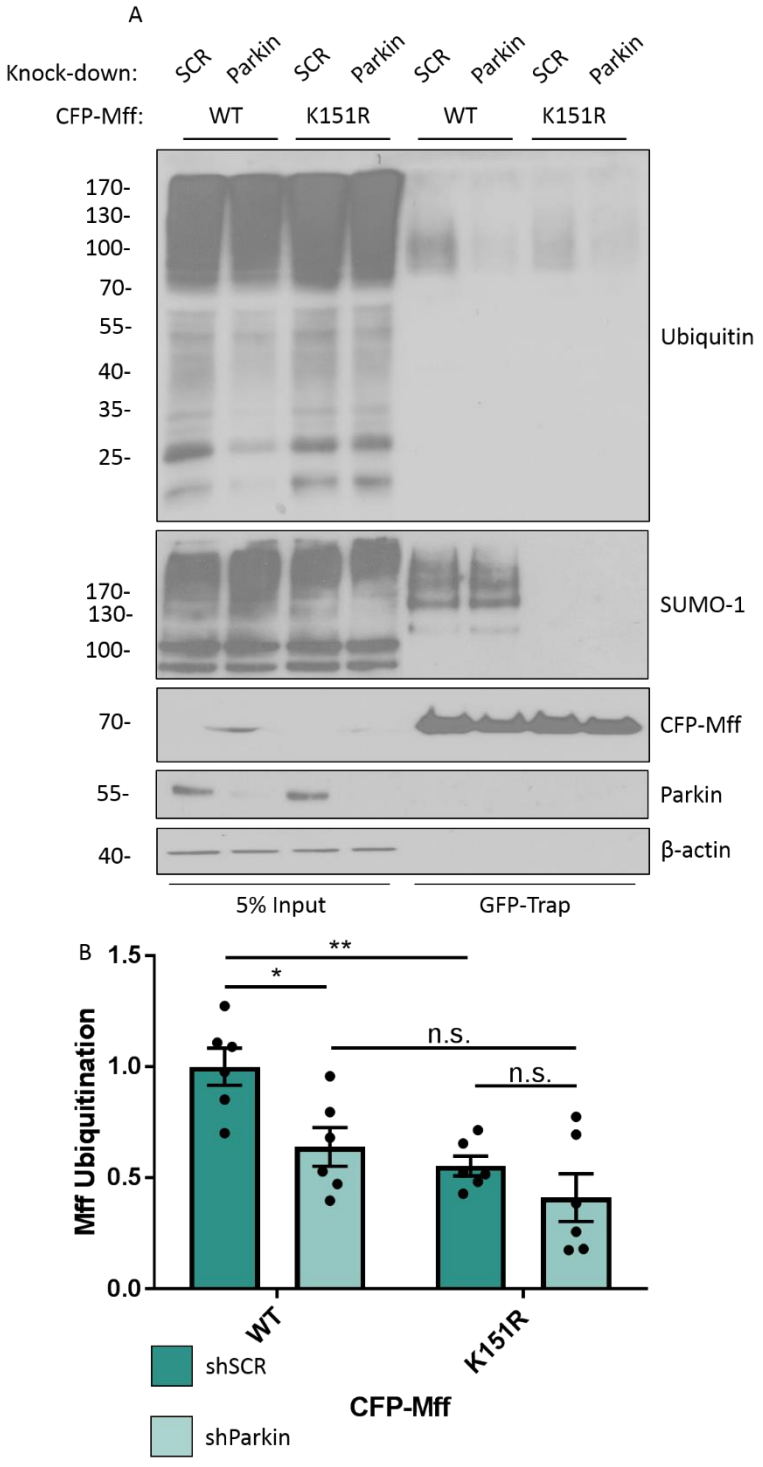

Figure 5.8 **Parkin ubiquitinates WT Mff, but not a non-SUMOylatable mutant of Mff.** GFP-pulldowns of exogenously expressed CFP-Mff WT or K151R in HEK293T cells reveal that the K151R mutant has significantly reduced endogenous ubiquitination compared to the WT. Knockdown of Parkin significantly reduces ubiquitination of WT CFP-Mff, but not CFP-Mff K151R. N=6. Analysed using ordinary two-way ANOVA with Tukey's correction for multiple comparisons with a pooled variance. * $p < 0.05$, ** $p \leq 0.01$.

5.3.5 Fbxo7 does ubiquitinate Mff K151R

In chapter 4, I demonstrated that Parkin and Fbxo7 contributed equally and independently to ubiquitination of Mff WT. There is no literature available on any interactions between Fbxo7 and SUMO, so I tested if Fbxo7 could ubiquitinate the non-SUMOylatable Mff K151R. HEK293T cells were co-transfected with CFP-Mff K151R, along with shRNA targeted to Parkin, siRNA targeted to Fbxo7, or both. GFP-Trap was again used to immunoprecipitate CFP-Mff, and samples were Western blotted for ubiquitin.

Consistent with Figure 5.8, Figure 5.9 shows that knock down of Parkin has no effect on ubiquitination of CFP-Mff K151R. However, knock down of Fbxo7 significantly reduces ubiquitination of CFP-Mff K151R (B). Knock down of both Parkin and Fbxo7 does not reduce ubiquitination significantly more than knock down of Fbxo7 alone. This suggests that Fbxo7-mediated ubiquitination of Mff is SUMO-independent and occurs at a site other than K151.

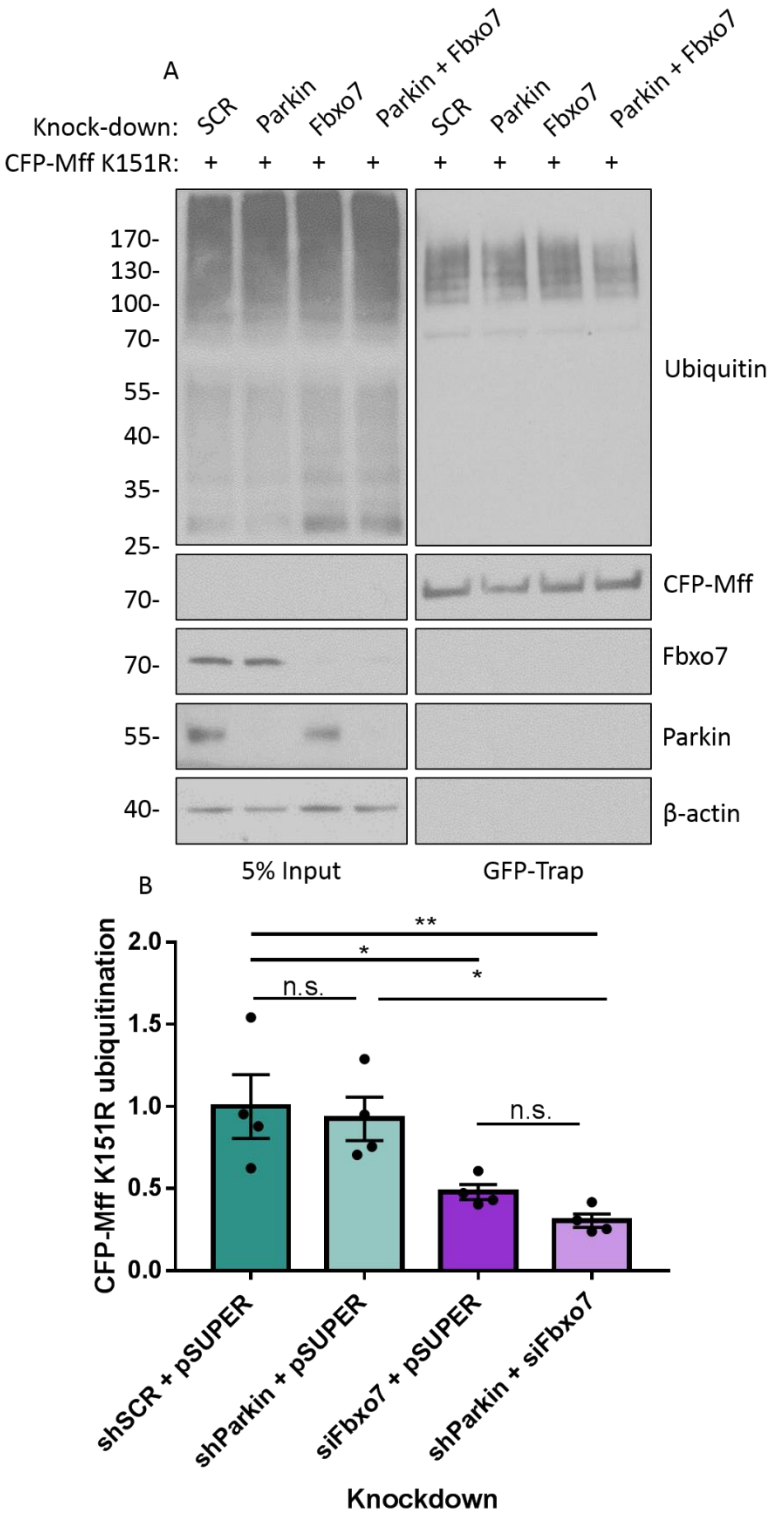

Figure 5.9 **Fbxo7, but not Parkin, ubiquitinates non-SUMOylatable Mff.** GFP-pulldowns of exogenously expressed CFP-Mff K151R in HEK293T cells with scrambled (control, SCR) shRNA, Parkin-targeted shRNA, Fbxo7-targeted siRNA, or both. N=4. Analysed using ordinary one-way ANOVA with Tukey's correction for multiple comparisons with a pooled variance. Data presented as mean ± SEM. * $p < 0.05$, ** $p \leq 0.01$.

Data presented so far have shown that Fbxo7 contributes to ubiquitination of both WT and K151R Mff, whereas Parkin contributes to ubiquitination of only WT Mff. This raised the question of whether Fbxo7 contributes equally to ubiquitination of WT and K151R Mff, or if Fbxo7 could have preference for non-SUMOylated Mff. To answer this question, the differences between WT and K151R ubiquitination with or without Fbxo7 knock down were compared. However, as can be seen in Figure 5.10, Fbxo7 did not show a preference for WT or K151R Mff, contributing equally to ubiquitination of both.

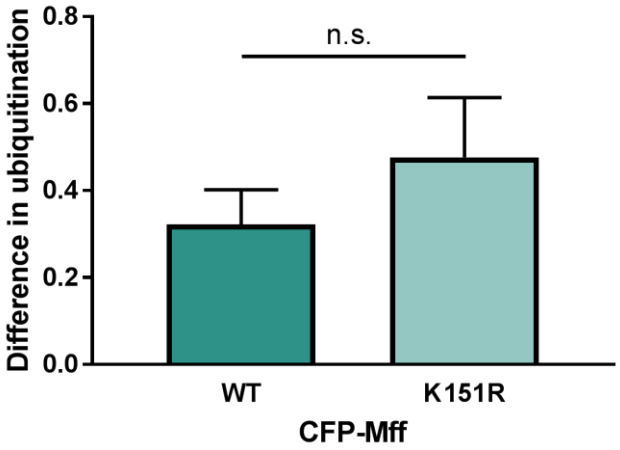

Figure 5.10 **Fbxo7 ubiquitinates WT and K151R Mff equally**. The average difference between scrambled control samples and Fbxo7 knock down samples for CFP-Mff ubiquitination, WT and K151R, were calculated and compared using an unpaired two-tailed Student's t-test. No significant difference was observed. N=4-6. Data presented as mean ± SEM.

5.3.6 Parkin as a proposed STUbL for Mff

Given the demonstrable interaction of Parkin with SUMO, and the insensitivity of a non-SUMOylatable mutant of Mff to Parkin ubiquitination, a model for Parkin as a SUMO-targeted ubiquitin ligase (STUbL) of Mff was proposed. A schematic of this model is shown in Figure 5.11. In this model, phosphorylation of Mff at serine 155 enhances/promotes SUMOylation at lysine 151. A SUMO-interacting motif (SIM) in Parkin recognises SUMOylated Mff, allowing recruitment of Parkin to Mff to catalyse its ubiquitination via the active cysteine, C431. The only published site of Parkin-mediated ubiquitination of Mff is lysine 302, as shown in this model (Gao et al., 2015). In their study, Gao *et al* demonstrated that K302 is the only ubiquitin-modified reside in Mff, showing that K302 mutation completely abolished Mff ubiquitination. However, this does not rule out the possibility that there are additional and/or alternative sites of Parkin-dependent ubiquitination.

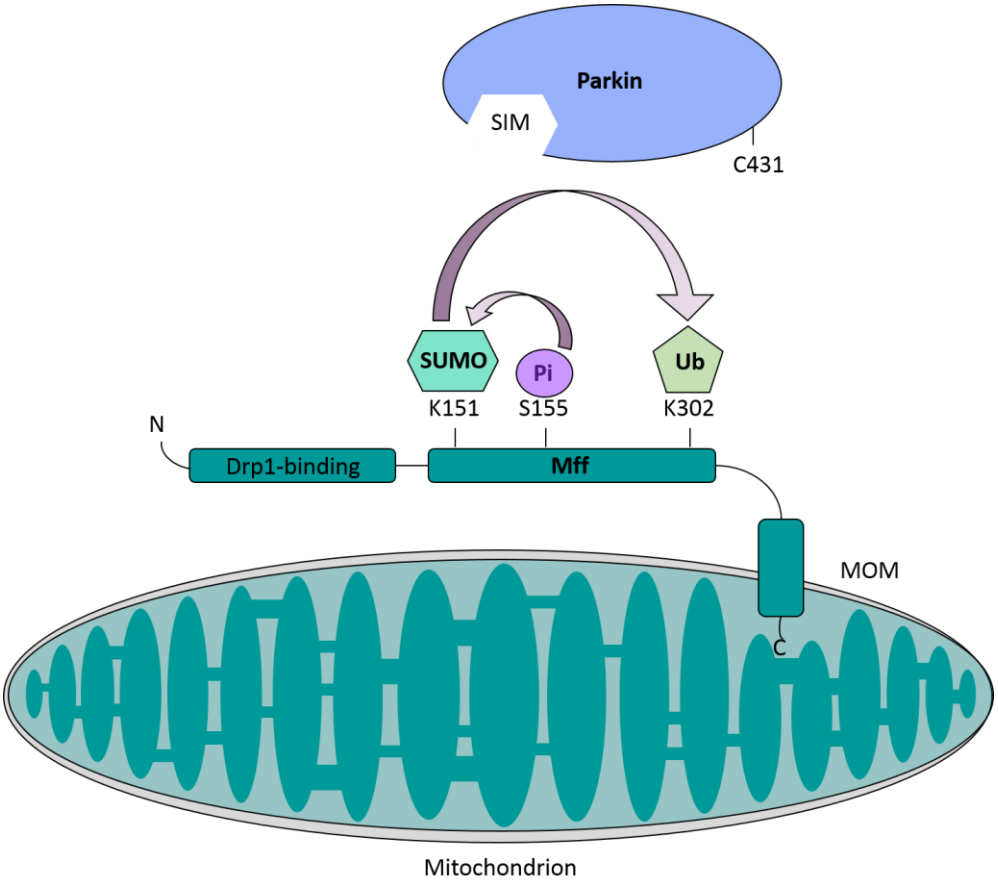

Figure 5.11 **Proposed model of Parkin as a STUbL for Mff (1).** Phosphorylation of S155 of Mff enhances SUMOylation of K151. SUMOylation of K151 of Mff facilitates recruitment and/or binding of Parkin via its SIM. Recruited Parkin can then ubiquitinate Mff at K302, via its catalytic site at C431. SUMOylation of Mff thereby promotes its Parkin-dependent ubiquitination.

To test this model, I performed a binding assay in HEK293T cells using expressed untagged Parkin and CFP-tagged Mff mutants. 48 hours post-transfection, GFP-Traps were used to immunoprecipitate CFP-Mff. Samples were then Western blotted to see which of the Mff mutants were able to co-immunoprecipitate Parkin. If this model is correct non-SUMOylatable K151R and E153A mutants would show reduced Parkin binding compared to the WT, and the SUMO-enhancing S155D mutant would be increased binding of Parkin. However, as can be seen in Figure 5.12, Parkin binding was not significantly different for any of the Mff mutants compared to the WT, suggesting that its phosphorylation and/or SUMOylation status has no effect on its ability to recruit Parkin .

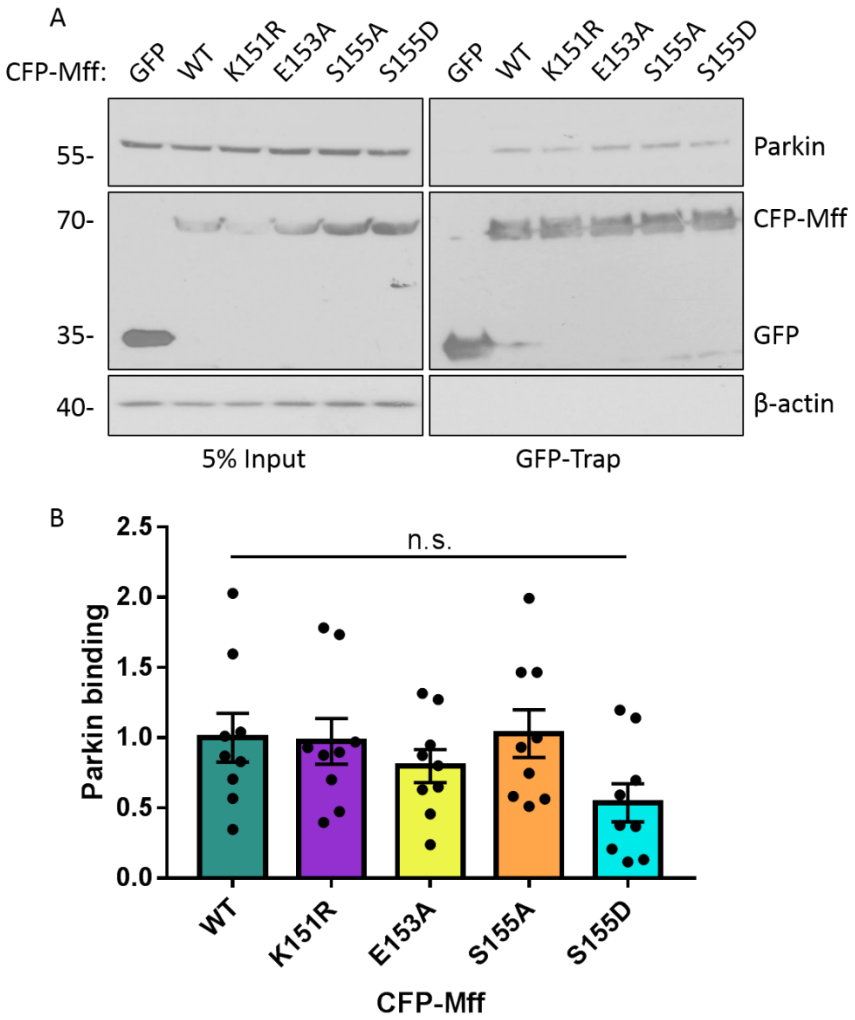

Figure 5.12 **Parkin binds equally to all CFP-Mff mutants in HEK293T cells.** Exogenously expressed CFP-Mff WT, K151R, E153A, S155A and S155D were all able to co-immunoprecipitate untagged Parkin from HEK293T cells using GFP-Trap. N=9. Analysed using one-way ANOVA (each mutant compared to the WT) with Dunnett's correction for multiple comparisons. Data presented as mean ± SEM.

Although the data presented in Figure 5.12, do not fit the proposed model of Parkin as a STUbL, previously shown data, namely Figure 5.8, have indicated that Parkin preferentially acts upon SUMOylatable Mff. It was therefore hypothesised that Parkin may not require Mff to be SUMOylated for binding, but SUMOylation of Mff might activate or enhance Parkin-dependent ubiquitination. I modified the model such that Parkin could bind to Mff directly, but in an inactive conformation, which required binding to SUMO to expose the catalytic site. This model is shown in Figure 5.13.

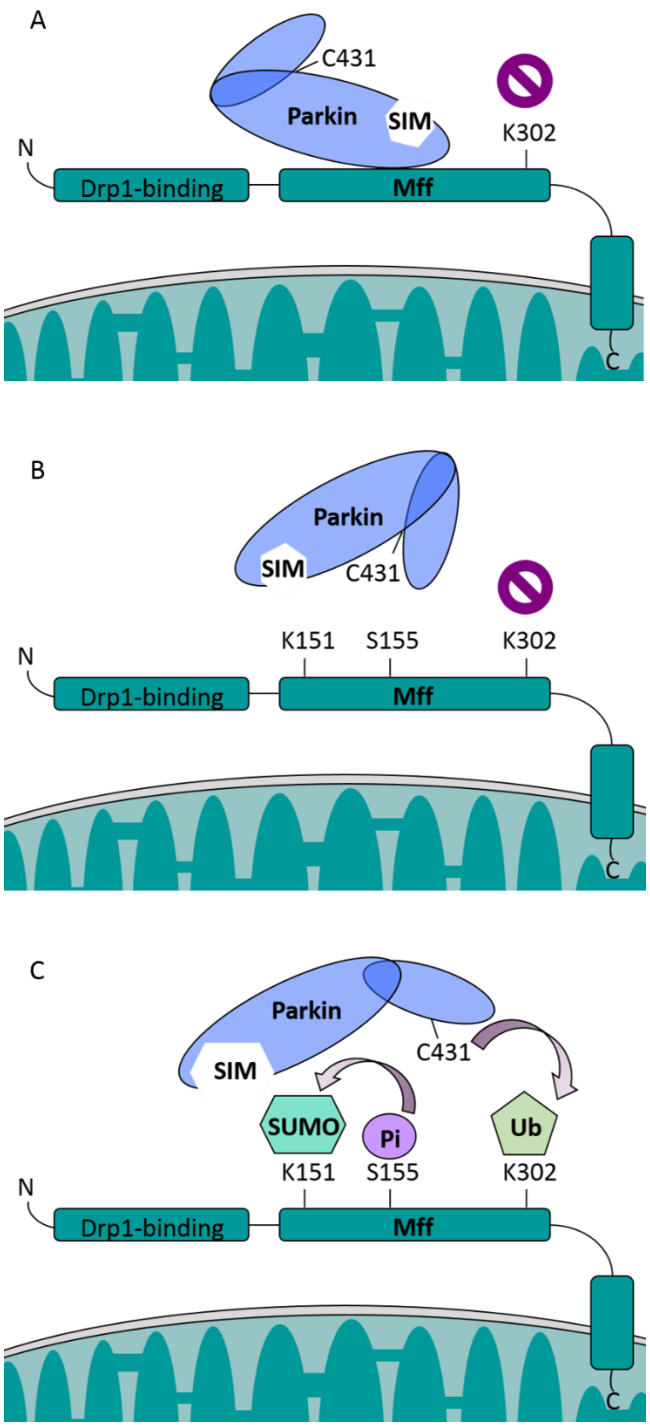

Figure 5.13 **Proposed model of Parkin as a STUbL for Mff (2).** Parkin can bind to Mff via a site other than its SIM. However, binding in this manner does not bring the catalytic site of Parkin into proximity with its ubiquitination site on Mff, K302 (A). When Parkin cannot bind to SUMO via its SIM, its conformation remains closed such that the catalytic site is inaccessible for efficient ubiquitination (B). Phosphorylation of S155 of Mff enhances SUMOylation of K151. Binding of Parkin to SUMO via its SIM induces a conformational change that exposes the catalytic site, allowing ubiquitination of Mff (C).

In this new model, binding of Parkin to Mff would be unaffected by the SUMOylation status of Mff, with Parkin binding via a site other than its predicted SIM. In this conformation, the active cysteine of Parkin is not only spatially sequestered away from the site of Mff ubiquitination, but also buried within an inaccessible cleft (Figure 5.13 (A)). Similarly, when Parkin is in close proximity to Mff, but not SUMO-bound, the conformation of Parkin remains such that the active cysteine is inaccessible (B). Binding of Parkin to SUMOylated Mff, via its SIM, induces a conformational change that opens up the active site of Parkin, making the active cysteine both accessible and spatially available to catalyse ubiquitination of Mff (C).

5.3.7 Ubiquitination and turnover of Mff

This modified model predicts that SUMOylation of Mff would enhance its ubiquitination by Parkin. To see if this was reflected in total ubiquitination of Mff, HEK293T cells were transfected with CFP-Mff mutants and lysed 48 hours post-transfection. GFP-Traps were used to immunoprecipitate CFP-Mff and its covalent attachments, including ubiquitination. Figure 5.14 shows, as previously shown in Figure 5.8, that the non-SUMOylatable K151R mutant of Mff has significantly reduced ubiquitination. This is also true of the non-SUMOylatable E153A mutant. However, the phospho-null (S155A) and phospho-mimetic (S155D) mutants do not show significantly different ubiquitination from the WT (B). In the absence of proteasome/autophagy blockers, we cannot rule out the possibility that some of these mutants are more heavily ubiquitinated, but then more rapidly degraded, resulting in the reduced ubiquitin signal observed.

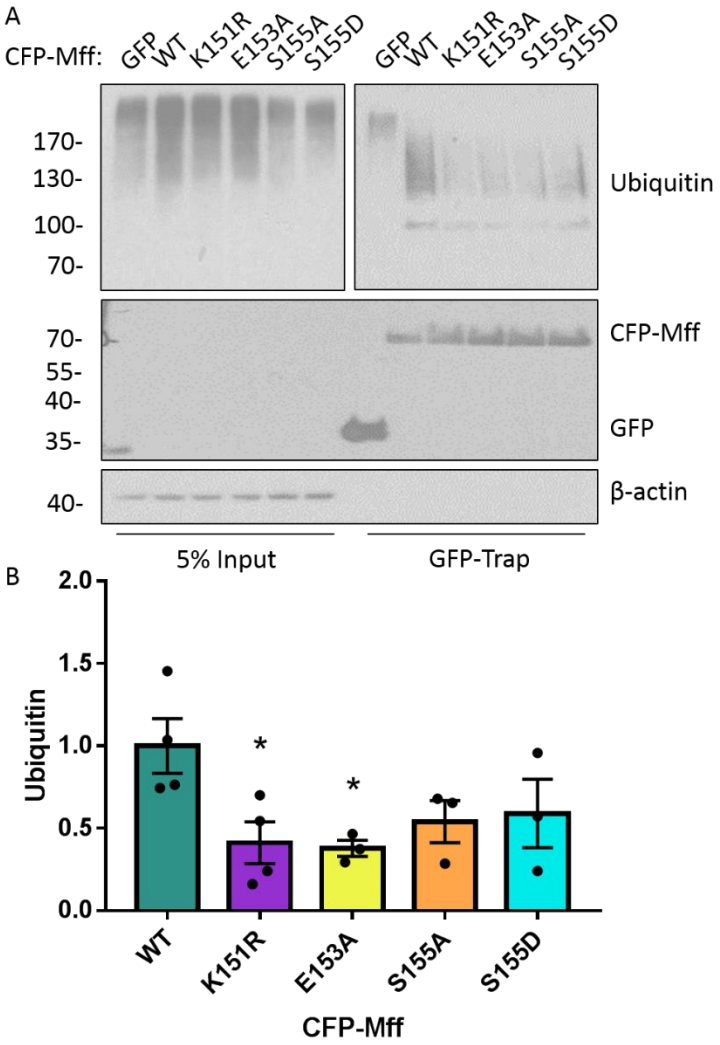

Figure 5.14 **Mff mutants are differentially ubiquitinated in HEK293T cells.** CFP-Mff WT and mutants were exogenously expressed in HEK293T cells and immuno-precipitated with GFP-Trap. Samples were then blotted for endogenous ubiquitin. N=3/4. Analysed using one-way ANOVA (each mutant compared to WT) with Dunnett's correction for multiple comparisons. Data presented as mean ± SEM. * $p < 0.05$.

Figure 5.14 shows that non-SUMOylatable mutants of Mff are significantly less ubiquitinated than WT Mff. We therefore hypothesised that non-SUMOylatable Mff could be more stable since they would be less susceptible to Parkin-mediated ubiquitin tagging and degradation. To test this, HEK293T cells transfected with either WT or non-SUMOylatable CFP-Mff (K151R) were treated with cycloheximide (CHX) to block protein synthesis. This allowed the rate of protein degradation to be measured. The results are shown in Figure 5.15. The experiment has not yet been performed enough times to be properly quantified or statistically tested, however, the data obtained so far suggest that CFP-Mff K151R is more stable than CFP-Mff WT over 24 hours (Figure 5.15 (B)).

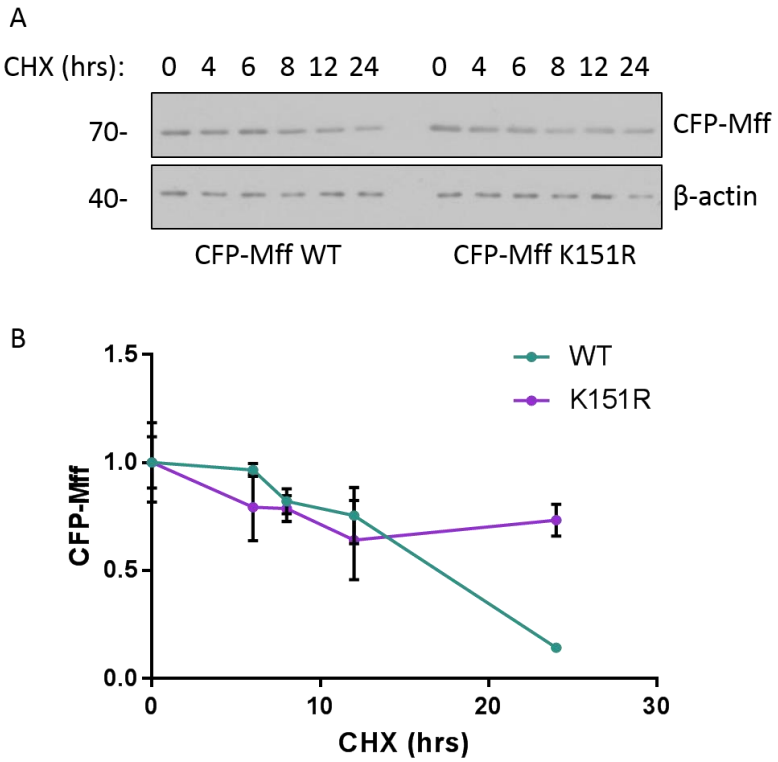

Figure 5.15 **Stability of WT vs K151R CFP-Mff.** HEK293T cells were transfected with either CFP-Mff WT or a non-SUMOylatable CFP-Mff K151R mutant. Prior to lysis 72 hours post-transfection, cells were treated with 25µg/mL cycloheximide (CHX) for 0, 4, 6, 8, 12 or 24 hours (0-hour CHX received 6-hour DMSO treatment). Lysates were then Western blotted for GFP (CFP-Mff) and β-actin. Data presented as mean ± SEM (where appropriate). N=2-4.

5.3.8 Parkin ubiquitinates Mff at K151

None of the data presented thus far preclude the possibility that Parkin may ubiquitinate Mff at the same residue as its SUMOylation site, lysine 151, perhaps competing with the SUMO ligase. If this were the case, it might be expected that knock down of Parkin would increase SUMOylation of Mff. To test this possibility, SUMOylation of WT Mff in the presence or absence of Parkin was compared.

HEK293T cells were co-transfected with CFP-Mff WT and shRNA targeted to Parkin, or a scrambled shRNA control. 72 hours post-transfection, cells were lysed, and the lysates used in GFP-Trap immunoprecipitations. SDS-PAGE was performed, and samples blotted for SUMO-1. As shown in Figure 5.16, no significant difference was detected in the intensity of the primary SUMO band (arrow, (C)). A significant decrease was observed in the higher molecular weight SUMO-reactive smear, consistent with this comprising SUMO and ubiquitin mixed chains (bracket, (B)).

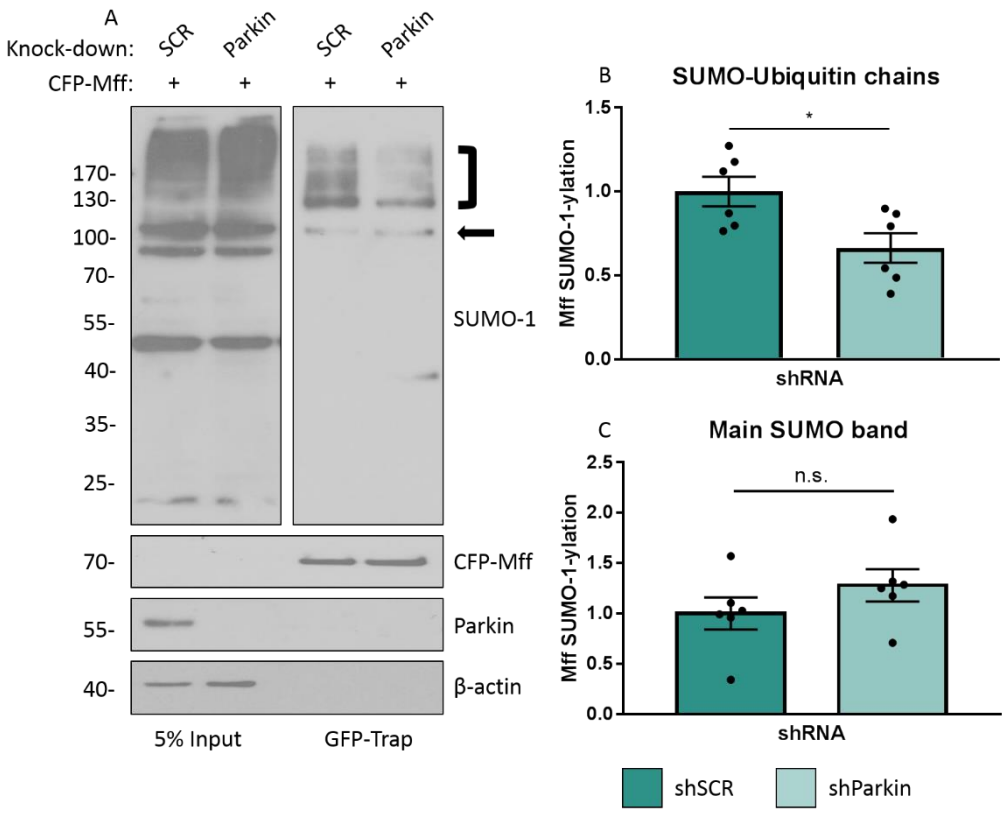

Figure 5.16 **Parkin knock down reduces CFP-Mff SUMO-Ubiquitin chains but not SUMOylation**. GFP-pulldowns of exogenously expressed CFP-Mff in HEK293T. (B) proposed mixed SUMO-Ubiquitin chains (bracket on (A)). (C) primary SUMOylation (arrow in (A)). N=6. Analysed using unpaired two-tailed students' t-test. Data presented as mean ± SEM. * $p < 0.05$.

The apparent lack of competition between SUMO and ubiquitin at K151 of Mff does not conclusively rule out the possibility that both modifications target the same residue. To explore this, HEK293T cells were co-transfected with WT, K151R or E153A CFP-Mff and scrambled- or Parkin-targeted shRNA. CFP-Mff E153A retains the SUMOylatable lysine residue, K151, but remains non-SUMOylatable due to disruption of the SUMO consensus sequence. It was shown in Figure 5.8 that CFP-Mff K151R is insensitive to Parkin knock down, indicating that Parkin does not ubiquitinate that mutant. However, this could be due to the lack of K151 or the absence of SUMO conjugated to K151.

Figure 5.17 shows representative Western blots of GFP-Trap immunoprecipitation experiments. As already demonstrated in Figure 5.8, knock down of Parkin significantly reduces ubiquitination of WT CFP-Mff, but does not affect CFP-Mff K151R. However, Parkin knock down also significantly reduces endogenous ubiquitination of CFP-Mff E153A (Figure 5.17), suggesting that it is the lysine residue, rather than its ability to be

SUMOylated, that is required for Parkin-dependent ubiquitination of Mff. Contrary to previous work, this suggests that K151 is modified by Parkin (Gao et al., 2015).

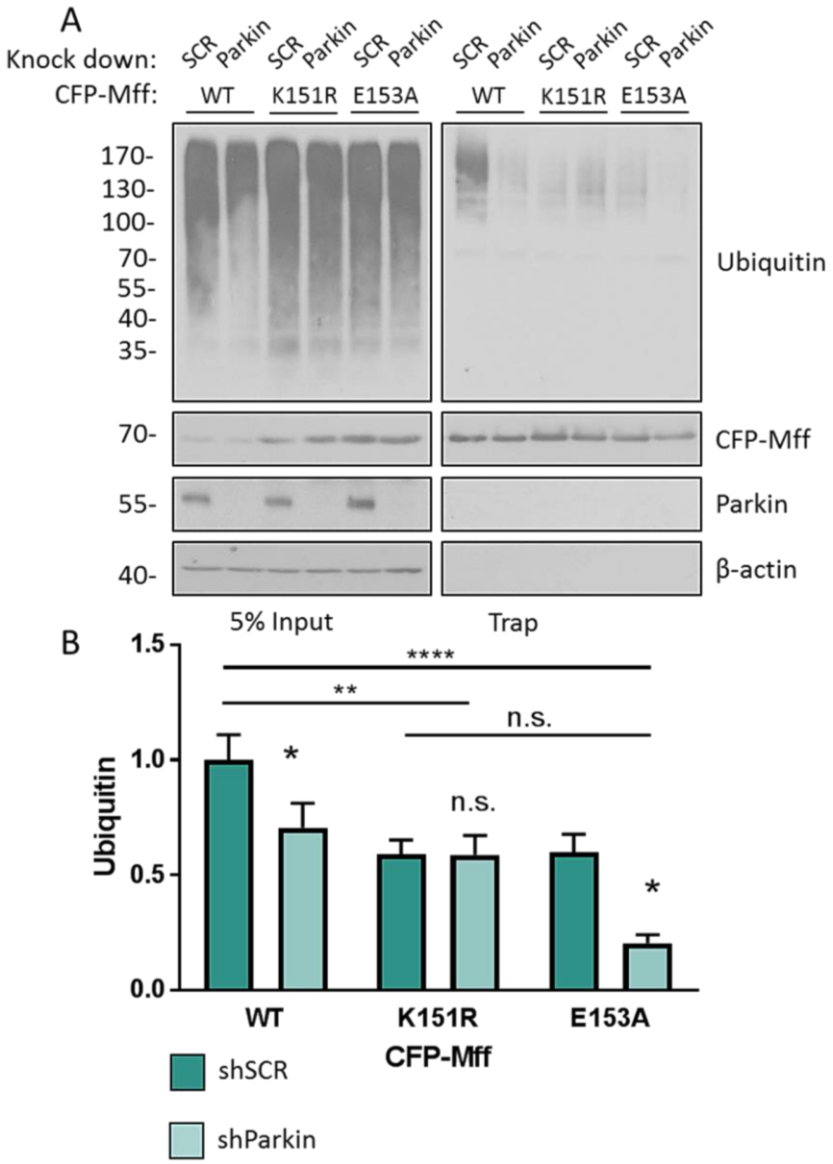

Figure 5.17 **Parkin ubiquitinates Mff at K151**. GFP-pulldowns of exogenously expressed CFP-Mff in HEK293T cells Total ubiquitination of CFP-Mff WT or CFP-Mff E153A is significantly decreased by knockdown of Parkin, but CFP-Mff K151R is not affected. N=8-10. Analysed using ordinary two-way ANOVA with Sidak's and Tukey's corrections for multiple comparisons with a pooled variance. Data represented as mean ± SEM. * $p < 0.05$, ** $p < 0.01$, **** $p < 0.0001$.

5.3.9 Parkin can be SUMOylated

Parkin is known to be subject to regulation by PINK1-mediated phosphorylation at serine 65, within its ubiquitin-like domain, and binding to PINK1-phosphorylated ubiquitin

(Chaugule et al., 2011, Riley et al., 2013, Trempe et al., 2013, Wauer and Komander, 2013). However, Parkin has not previously been shown to be a target of SUMOylation.

HEK293T cells were transfected with YFP-SUMO and Myc-Parkin and the lysates used for GFP-Trap co-immunoprecipitation experiments, as shown in Figure 5.2. For Figure 5.18, the non-covalently bound Parkin was allowed to saturate on the Western blots, revealing higher molecular weight, Parkin-reactive species, indicated by arrows. These bands were not present in samples containing non-conjugatable -ΔGG SUMO mutants, indicating that they represent covalently attached SUMO-1 and SUMO-2 (A and B, respectively).

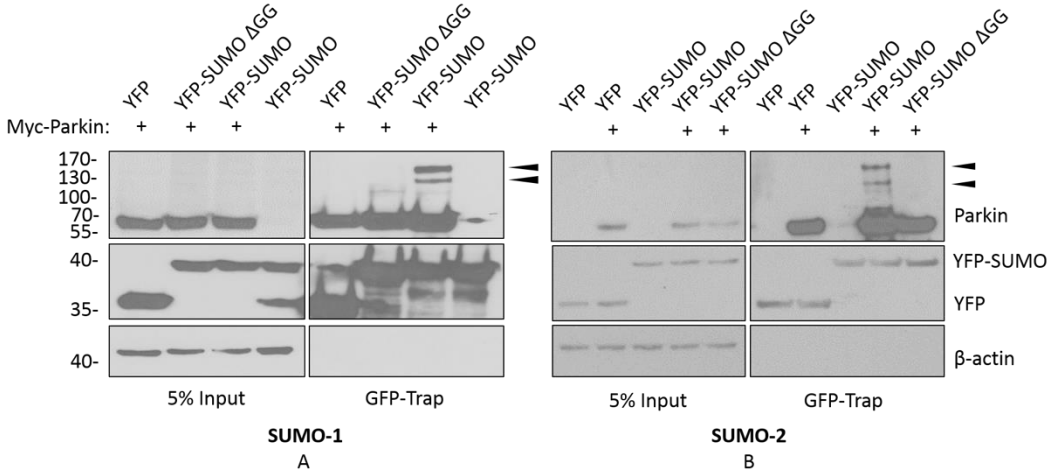

Figure 5.18 **Parkin can be SUMO-1-ylated and SUMO-2/3-ylated in HEK293T cells.** Exogenously expressed YFP-SUMO-1 and -2, but not non-conjugatable YFP-SUMO-1 and -2 ΔGG mutants, were able to co-immunoprecipitate Myc-Parkin at not only its unmodified molecular weight, but also higher (>100 kDa) Parkin- and YFP-reactive molecular weight bands by GFP-Trap from HEK293T lysate. N=4 (SUMO-1) and N=3 (SUMO-2).

As this has not previously been shown, it was important to validate the finding in more than one system. BL21 *E. coli* were transformed with DNA encoding His-T7-Parkin, either alone, or with a plasmid encoding SUMO-1 or SUMO-2, along with the SUMOylation machinery (E1E2-SUMO). The bacteria were then lysed, and the lysates used for Western blotting, using an anti-T7 antibody. T7 is a small peptide tag, encoded in between the His-tag and Parkin in the pXLG3 expression plasmid used.

Figure 5.19 shows a representative blot of the experiment. His-Parkin was detected as a 55kDa band using the T7 antibody in all samples. Also detected were bands of around 70kDa with the addition of E1E2-SUMO-1 or -SUMO-2, and two further bands around

100kDa with the addition of E1E2-SUMO-1, indicated by arrows. In particular, the bands at around 70kDa would be the right size to represent mono-SUMOylated Parkin.

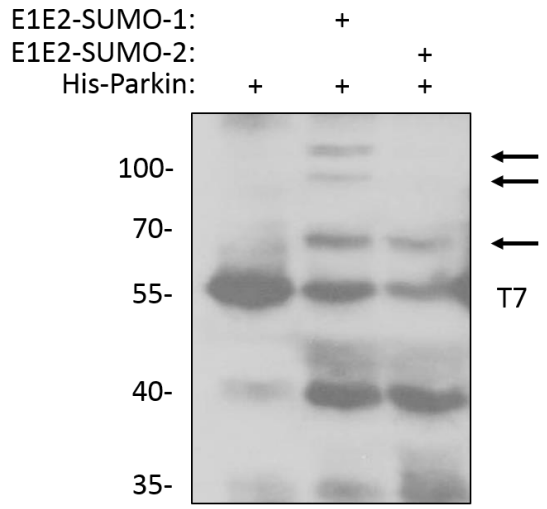

Figure 5.19 **Parkin can be SUMO-1-ylated and SUMO-2-ylated in bacteria**. Full length His-tagged Parkin was expressed in BL21 (DE3) *E. coli*, either alone, or with a vector encoding the SUMOylation machinery and either SUMO-1 or SUMO-2. Bacteria were lysed, and the samples used for Western blotting.

5.4 Discussion

The data presented in this chapter demonstrate a role for SUMO in both Parkin activity and Mff stability. However, it remains unclear if SUMO plays a part in the regulation of Mff by Parkin.

5.4.1 Parkin interacts non-covalently with SUMO

A 2006 study had reported that Parkin could form a non-covalent interaction with SUMO-1, but not SUMO-2, and that this interaction modulates Parkin function (Um and Chung, 2006). To validate these findings, Myc-Parkin and YFP-SUMO-1/-2 were co-expressed in HEK293T cells and GFP-Trap used to immunoprecipitate YFP-SUMO. As expected, based on the publication by Um and Chung, YFP-SUMO-1 was able to co-immunoprecipitate Myc-Parkin (Figure 5.2 (A)). Surprisingly, the same was true of YFP-SUMO-2 (C). In both cases, no/minimal binding was detected between Myc-Parkin and YFP, precluding the possibility of binding between Myc-Parkin and the GFP-Trap beads or YFP alone and indicating that the stringency of the experimental conditions was sufficient to exclude non-specific interactions.

In co-immunoprecipitation experiments with YFP-SUMO-1 and YFP-SUMO-2, Myc-Parkin favoured binding to WT SUMO over the non-conjugatable ΔGG mutant (Figure 5.2 (B, D)). As these experiments were performed in cells rather than in a reduced system, WT YFP-SUMO can be conjugated to substrate proteins by endogenous SUMOylation machinery. These results could therefore indicate that Parkin preferentially associates with SUMOylated proteins, rather than free SUMO.

While co-immunoprecipitations from HEK293T cells are sufficient to demonstrate specific binding between Parkin and SUMO, they cannot discriminate between direct and indirect binding on account of the presence of endogenous proteins. The original study by Um and Chung demonstrated Parkin-SUMO binding both in cell lines and in rat cortex, but not in a reduced system (Um and Chung, 2006). For this reason, it was decided that *in vitro* binding assays should be performed to determine the nature of the Parkin-SUMO interaction.

His-tagged Parkin and GST-tagged SUMO recombinant proteins were expressed and purified from BL21 (DE3) *E. coli.* These could then be used for *in vitro* binding assays. Glutathione Sepharose® 4 Fast Flow was used to pull down GST, GST-SUMO-1 or GST-SUMO-2 from an *in vitro* binding solution containing His-Parkin. As shown in Figure 5.4, GST-SUMO-1 did not bind significantly more His-Parkin than GST alone, whereas GST-SUMO-2 did. These data indicate that binding between Parkin and SUMO-2 is likely to be direct. However, the conditions used in these experiments were insufficiently stringent to discern direct binding between Parkin and SUMO-1 from non-specific binding of Parkin to GST. This could merely indicate that the experimental set-up was unsuitable, or that Parkin can bind directly to SUMO-2, but only indirectly to SUMO-1, either conjugated to a substrate protein or as part of a SUMO-chain. In future, alternative experimental conditions could be used to determine whether or not there is a significant binding of Parkin to SUMO-1 *in vitro* by removing non-specific Parkin-GST binding. This could include increasing detergent and/or salt concentration in the binding and wash buffers, increasing the length and/or number of washes, decreasing the concentration of proteins, reducing the incubation time of the binding reaction or decreasing the temperature of the binding reaction.

5.4.2 Phosphorylation and ischaemic stress regulate Mff SUMOylation

With K151 of Mff identified as the only SUMOylated residue, we explored the site in greater detail. The residues around K151 were found to conform to a phosphorylation-dependent SUMOylation consensus motif, or PDSM (Hietakangas et al., 2006). Figure 5.5 details the PDSM model, with phosphorylation of Mff at S155 enhancing SUMOylation at K151.

Once the nature of the SUMOylated residue had been identified as part of a PDSM, we sought to confirm that it acted as such. For this, a series of CFP-tagged Mff mutants were generated. These included two non-SUMOylatable Mff mutants, K151R and E153A, a phospho-null mutant, S155A, and a phospho-mimetic mutant, S155D (Dr Kevin Wilkinson and Richard Seager). CFP-Mff E153A retains the SUMOylatable lysine residue, K151, but cannot be SUMOylated due to disruption of the SUMOylation consensus motif precluding binding of the SUMOylation machinery. The S155A phospho-null mutant replaces phosphorylatable serine with non-phosphorylatable alanine, blocking phosphorylation at that site; the S155D phospho-mimetic mutant equally cannot be phosphorylated at that site, but mimics the charge of a phosphate group by replacement of serine with aspartic acid.

The CFP-Mff mutants were transfected into HEK293T cells, and the CFP-Mff immunoprecipitated using GFP-Trap 48 hours later. Western blotting was used to quantify the endogenous SUMOylation of the mutants relative to the WT. Figure 5.6 shows representative blots and quantifications of SUMO-1-ylation and SUMO-2/3-ylation. As expected, both the K151R and E153A mutant have no detectable SUMO-1- or SUMO-2/3-ylation (B, C). This is consistent with data shown in Chapter 3 indicating that K151 is the sole SUMOylated residue of Mff. If the region surrounding K151 does conform to a functional PDSM, it would be expected that replacement of the phosphorylatable serine, S155, with a non-phosphorylatable residue would decrease or abolish SUMOylation at K151. As shown in (C), SUMO-2/3-ylation of CFP-Mff S155A is significantly reduced compared to the WT. A similar pattern is evident for SUMO-1-ylation (B), though this is not statistically significant, possibly due to the greater variance in WT SUMO-1-ylation compared to SUMO-2/3-ylation observed in the experiments.

It was unclear whether replacement of S155 with aspartic acid would result in enhanced SUMOylation at K151. While the charge of a phosphate group can be mimicked using a charged residue, as in the case of S155D, the replacement does not truly mimic the

electrostatic or structural qualities of phosphoserine. Furthermore, phosphorylation *in vivo* is a transient modification, often only occurring in response to certain stimuli, which takes place only post-translationally. A phospho-mimetic mutant is permanently 'stimulated,' and may therefore not be particularly informative about the role of protein phosphorylation. Incorporation of the charged mimic residue during protein translation could also result in protein misfolding, further confounding its study (Stateva et al., 2015).

Nonetheless, it would be expected that the phospho-mimetic CFP-Mff S155D mutant would have increased SUMOylation compared to the WT, in keeping with its role as part of a PDSM. As evident from Figure 5.6, SUMO-1-ylation of Mff was significantly increased by the S155D mutation, compared to the WT (B) but SUMO-2/3-ylation, interestingly, was significantly decreased compared to the WT (C). This could be due to an occlusion mechanism, whereby the increased SUMO-1-ylation of Mff at K151 out-competes SUMO-2/3 and hinders Mff SUMO-2/3-ylation. However, this is unlikely due to the 10-fold greater expression of SUMO-2/3 in mammalian cells, compared to SUMO-1 (Saitoh and Hinchey, 2000). Another explanation could be the far greater off-on rate of SUMO-2/3 compared to SUMO-1 (Flotho and Melchior, 2013, Kolli et al., 2010). This makes SUMO-2/3-ylation far less stable than SUMO-1-ylation and may therefore make it more easily lost during immunoprecipitation or more difficult to detect by Western blotting.

With Mff now shown to have a PDSM, and up-regulated phosphorylation being a known marker of cellular stress, we proposed that Mff SUMOylation might also increase under conditions of stress (Auciello et al., 2014, Wang et al., 2012b). Data from *ex vivo* modelling in the whole heart, presented in Chapter 3, identified a ~55kDa SUMO-1-reactive species that was significantly increased during ischaemia. We speculated that this species could represent SUMOylated Mff. Using a cellular model of ischaemia, OGD, the experiment detailed in Figure 5.7 sought to determine if Mff SUMOylation could be a stress response.

Although the data presented in Figure 5.7 cannot yet be statistically analysed due to insufficient repeats, it appears that OGD does lead to a 2-fold increase in SUMO-1 conjugation to Mff (B). In the future, it would be pertinent to see if this increase in SUMOylation is indeed due to an increase in phosphorylation. We know that the kinase responsible for phosphorylating Mff at S155 (and S172) is adenosine monophosphate (AMP)–activated protein kinase (AMPK), which is activated under conditions of low intracellular ATP, usually associated with cellular stress, by binding of AMP (Toyama et al., 2016). In future, Western blotting of OGD samples for activation of AMPK, measured as an

increase in phosphorylated AMPK, would help to define this pathway. Samples taken at different timepoints in OGD should reveal a spike in AMPK phosphorylation, followed by the increase in Mff SUMOylation. It would also be interesting to test if SUMOylation of the phospho-null Mff mutant, S155A, can be increased by OGD; if it cannot, this would indicate that the upregulation of SUMOylation is dependent on upregulation of phosphorylation as a result of ischaemic stress.

5.4.3 Fbxo7 ubiquitinates Mff at a site other than K151

Data shown in Chapter 4 indicated that Parkin and Fbxo7 independently ubiquitinate Mff WT, with their simultaneous knock down having an additive effect on depletion of Mff ubiquitination. Additionally, data shown in this chapter (Figure 5.2, Figure 5.4) and previously published work have detailed a specific SUMO-binding capacity for Parkin (Um and Chung, 2006). We postulated that SUMOylation of Mff could be regulating its ubiquitination, by recruitment of one or more SUMO-targeted ubiquitin ligases (STUbLs).

Parkin knock down was performed in HEK293T cells expressing either WT or K151R CFP-Mff. 72 hours post-transfection, cells were lysed, and GFP-Trap used to immunoprecipitate CFP-Mff. These samples were then used for Western blotting and probed with a universal ubiquitin antibody. Figure 5.8 shows a representative blot and quantification. As shown in Chapter 4, knock down of Parkin significantly decreases ubiquitination of WT Mff. However, there was no significant effect on ubiquitination of the non-SUMOylatable mutant, K151R. This could indicate that SUMOylation of Mff is required to recruit Parkin, or that Parkin ubiquitinates Mff at K151. However, given the Parkin-SUMO binding data, it seemed likely that the former could be true, with Parkin acting as a STUbL for Mff.

Parkin and Fbxo7 contribute independently and equally to ubiquitination of WT Mff (Chapter 4). With Parkin not able to target CFP-Mff K151R, it was hypothesised that Fbxo7 might compensate, not least because over-expression of Fbxo7 has been previously shown to rescue the phenotype of Parkin-null *Drosophila melanogaster* (Burchell et al., 2013). We proposed that Parkin may target only SUMOylated Mff, while Fbxo7 could preferentially ubiquitinate non-SUMOylated Mff. HEK293T cells were co-transfected with CFP-Mff K151R and control sh/siRNA, Parkin-targeted shRNA, Fbxo7-targeted siRNA, or both. As shown in Figure 5.9 (and Figure 5.8), the non-SUMOylatable Mff mutant was insensitive to Parkin knock down. However, knock down of Fbxo7 significantly reduced its ubiquitination ((B)).

These data support a role for Fbxo7 in ubiquitination of Mff that is independent of K151 and suggest that Fbxo7 targets a different site(s) of Mff.

If Fbxo7 were to compensate for loss of Parkin-dependent ubiquitination of Mff K151R, it would stand to reason that Fbxo7 would favour this non-SUMOylatable mutant over the WT. To test this, the differences in Mff ubiquitination upon knock down of Fbxo7 for WT and K151R were compared (Figure 5.10). Disappointingly, there was no significant difference in reduction of Mff ubiquitination upon Fbxo7 knock down between the WT and K151R mutant. The most likely reason for this is that, in the case of Mff, Parkin and Fbxo7 are neither complementary nor compensatory, but rather they act independently to target different lysine residues.

5.4.4 Parkin as a proposed STUbL

So far, the only study to have identified a specific lysine residue of Mff targeted for ubiquitination showed a single site to be the only Parkin-targeted, and the only ubiquitinatable, residue. In their study, which used a shorter Mff isoform, the authors identified K251, which corresponds to K302 in the full-length isoform used in our work (Gao et al., 2015). We therefore proposed a model whereby SUMOylation of Mff at K151 acts to recruit Parkin, which then ubiquitinates Mff downstream at K302 (Figure 5.11). There remains no experimentally derived structure for Mff, so the spatial feasibility of this model cannot be commented upon. Additionally, the site of SUMO-binding within Parkin has not yet been identified, so it is unclear whether this SIM is sufficiently far from the active cysteine (C431) of Parkin for this model to be achievable.

In the first proposed model, SUMOylation at K151 of Mff is required for binding of Parkin, through its as-yet unidentified SIM. To test this, Parkin binding to Mff was experimentally measured. Free GFP, CFP-Mff WT, K151R, E153A, S155A or S155D were co-transfected into HEK293T cells with untagged Parkin. In line with the proposed model, we expected that Mff K151R and E153A would be unable to co-immunoprecipitate Parkin, and that Mff S155A might have a reduced Parkin-binding capacity. Similarly, we expected Mff S155D to have equal or greater Parkin-binding capacity to WT Mff. However, as shown in Figure 5.12, this was not the case; no significant differences in binding were detected between any mutant and the WT Mff. This indicates the neither SUMOylation nor phosphorylation of Mff plays a part in Parkin recruitment/binding.

In light of this, a new model was proposed in which SUMOylation of Mff K151 is not required for binding of Parkin but is required for activation/enhancement of its Parkin-

dependent ubiquitination (Figure 5.13). In this newer model, Parkin can bind to Mff via a site other than its proposed SIM but cannot efficiently ubiquitinate Mff. This could be due to the spatial arrangement of the proteins, meaning that the active site of Parkin is too far away from its target lysine on Mff to efficiently ubiquitinate, or it could be that binding of Parkin to SUMO induces a conformational change that makes its active site more readily accessible. In this way, binding of Parkin and Mff is unaffected by the SUMOylation status of Mff, but ubiquitination of Mff, at least by Parkin, is enhanced by SUMOylation at K151.

5.4.5 SUMOylation of Mff enhances its ubiquitination and rate of turnover

Under the newly proposed model, ubiquitination of Mff would depend at least in part on its SUMOylation. We therefore expected that the non-SUMOylatable mutants and phospho-null mutant of Mff would have reduced ubiquitination compared to the WT, and that the phospho-mimetic would have more. CFP-Mff WT and mutants were expressed in HEK293T cells and GFP-Trap used to immunoprecipitate them 48-hours post-transfection. Figure 5.14 shows a representative blot and quantification of endogenous ubiquitination of the mutants. As was expected, CFP-Mff K151R had significantly reduced ubiquitination compared to the WT (B). On its own, this result does not definitively discriminate between reduced ubiquitination as a result of replacement of a ubiquitin-targeted lysine residue, or reduced ubiquitination due to abolished SUMOylation of K151. However, the E153A mutant also had significantly reduced ubiquitination compared to the WT. This mutant retains the availability of K151 for potential ubiquitination but cannot be SUMOylated (Figure 5.6). This suggests that SUMOylation is required for or enhances ubiquitination of Mff, indicating that one or more ubiquitin ligases for Mff could be STUbLs.

Interestingly, neither the S155A phospho-null nor the S155D phospho-mimetic mutant had significantly different ubiquitination compared to the WT. The phospho-null mutant has significantly reduced SUMOylation compared to the WT but is not devoid of SUMO. Given the highly transient nature of SUMO modification, it could be that even this reduced level of Mff SUMOylation is sufficient to recruit any STUbL of Mff, due to the mass action model outlined in Chapter 1 (The SUMO enigma). It was expected, in keeping with its higher levels of SUMOylation, that the phospho-mimetic mutant might have greater levels of ubiquitination. It is possible that this is not the case due to the nature of the mimetic as described previously (5.4.2) and its inability to truly mimic transient phosphorylation. It is also important to note that these experiments were carried out in

the absence of any proteasomal inhibitors, so the ubiquitination detected reflects the steady-state levels. This set-up does not account for higher turnover rates of more heavily ubiquitinated proteins, so we cannot rule out the possibility that CFP-Mff S155D actually does get more heavily ubiquitinated but is then more rapidly degraded.

Having identified that lack of SUMOylation results in less ubiquitination, it remained to be determined if this had any physiological relevance. We proposed that, owing to its reduced ubiquitination, the K151R mutant of Mff may be more stable than the WT. To interrogate this hypothesis, HEK293T cells were transfected with CFP-Mff WT or K151R and lysed 72-hours post-transfection. Prior to lysis, cells were treated with the protein synthesis-blocking drug cycloheximide for up to 24 hours, as indicated in Figure 5.15 . This allows the rate of protein degradation to be measured. Unfortunately, owing to time constraints and logistical problems with the experimental set-up, this experiment was not repeated sufficient times to apply statistical analyses. However, over the 24-hour course of the experiment, CFP-Mff K151R does appear to be more stable than the WT, being only ~25% reduced within 24 hours, compared to a ~80% reduction of the WT (Figure 5.15).

While these data are encouraging, the set-up of this experiment was not ideal. The time-course was insufficient to determine protein half-life and in future would need to be longer. Additionally, degradation rates of over-expressed proteins are unlikely to truly reflect the degradation of endogenous levels of the protein, especially in light of their N-terminal CFP tags, which will undoubtedly affect their degradation via the N-end rule (Bachmair et al., 1986). However, as both the WT and K151R Mff constructs have the same N-terminal tag, we can assume that their half-lives will be equally affected by this. So, despite this experiment not necessarily reflecting the true half-life of Mff WT and K151R, it can still inform us about the effect of the K151R point mutation, compared to WT. Another problem is the use of transiently over-expressed proteins; without a stably expressing cell line, there can be no guarantee that all of the conditions had the same level of expression of CFP-Mff to begin with, but this must be assumed during quantification. In future work, this experiment would be repeated over a longer time-course, using stable knock-down replacement cell lines expressing endogenous levels of WT or K151R Mff.

5.4.6 K151 of Mff is ubiquitinated by Parkin

None of the data discussed thus far preclude the possibility that K151 of Mff is the target of Parkin ubiquitination. We reasoned that if both SUMO and ubiquitin could be

conjugated to the same residue, this would likely be competitive. Therefore, reduction of one modification might result in an increase of the other. As shown in Chapter 4, knock down of Parkin results in a ~50% decrease in endogenous ubiquitination of Mff. We hypothesised that, in the event of PTM competition, this could induce a similar increase in SUMOylation of that site.

Figure 5.16 shows representative Western blots and quantification of GFP-Trap immunoprecipitation of CFP-Mff WT in the presence or absence of Parkin. Unsurprisingly, the SUMO-reactive smear of Mff was significantly reduced by knock down of Parkin (B). This smear is more than likely made up of mixed length chains of SUMO and ubiquitin, so it stands to reason that knock down of a ubiquitin ligase reduces its intensity. Interestingly, there was no significant difference in the single lower molecular weight SUMO band, that we believe to be mono-SUMOylated CFP-Mff, upon knock down of Parkin (C). This would argue that ubiquitin and SUMO do not compete at this site and supports the hypothesis of Parkin ubiquitinating Mff at a different residue, but in a SUMO-K151-dependent manner.

To definitively determine whether Parkin is recruited to Mff by SUMO or targets the SUMOylatable residue of Mff, GFP-Trap was used to immunoprecipitate CFP-Mff WT, K151R or E153A from transfected HEK293T cells, in the presence of absence of Parkin (Figure 5.17). As was previously demonstrated (Figure 5.8), knock down of Parkin significantly reduces ubiquitination of WT Mff, but has no effect on the non-SUMOylatable K151R mutant. However, knock down of Parkin did significantly reduce ubiquitination of CFP-Mff E153A. This means that it is the lysine residue, rather than its ability to be SUMOylated, that is affected by knock down of Parkin, and strongly indicates that, at least in this isoform of Mff, K151 is the only site of ubiquitination by Parkin.

While this was disappointing, the identification of K151 as a Parkin target in Mff is a novel finding. Importantly, the data showing that the non-SUMOylatable E153A mutant is significantly less ubiquitinated than the WT (Figure 5.14, Figure 5.17) strongly suggests that one or more of the other, as-yet unidentified, ubiquitin ligases of Mff is being recruited by Mff SUMOylation. There remains the possibility that mutation of E153 disrupts a ubiquitin consensus, but the ability of Parkin to ubiquitinate the E153A mutant suggests that this is not the case. These findings also pose the question of why Parkin is able to bind to SUMO, if not to target it to SUMOylated substrates.

5.4.7 Parkin can be SUMOylated

The experiments defining the non-covalent binding between Parkin and SUMO also yielded an unexpected result. Not only could YFP-SUMO co-immunoprecipitate Myc-Parkin at its predicted molecular weight from co-transfected HEK293T cells, but also higher molecular weight, Parkin-reactive species that were specific to the WT YFP-SUMO constructs, and not apparent in co-immunoprecipitations with the non-conjugatable ΔGG mutants (Figure 5.18). As far as we are aware, this is the first indication that Parkin could be a SUMO substrate. To support this finding, a bacterial SUMOylation assay was also carried out (Figure 5.19). Bacteria lack the molecular machinery required for SUMOylation, so were co-transformed with plasmids encoding the E1 and E2 SUMOylation enzymes as well as the SUMO isoforms, along with Parkin. In this system as well, T7-tagged Parkin was detected at its predicted molecular weight regardless of addition of SUMO and its machinery, while higher molecular weight, T7-reactive species were detected only upon addition of SUMO machinery and SUMO proteins.

If substantiated, this discovery is very interesting. Parkin is a widely-studied protein known to be regulated by myriad PTMs and being a SUMO substrate would add another layer of regulation to an already complex network of regulatory pathways. However, validation of this finding would require far more work.

So far, we have only shown that Parkin can be SUMOylated by over-expressing both Parkin and SUMO, in effect forcing the attachment. While it is unlikely that the SUMO machinery will indiscriminately SUMOylate any available lysine residue if the proteins are present in large enough concentrations, if this modification cannot be detected at endogenous levels, it is unlikely to have any physiological relevance. Parkin also does not contain a consensus SUMOylation motif. This does not rule it out as a SUMO substrate, as >50% of known SUMO substrates lack any kind of consensus motif (Blomster et al., 2009), but it does make identification of the SUMOylatable residue(s) more difficult. Ongoing work is aimed at identifying the functional domain of Parkin which can be SUMOylated, by use of overlapping truncated Parkin fragments, to narrow down the search for lysine residue(s) of interest.

Chapter 6 General Discussion

6.1 Summary of research

Western blot analysis of cardiac tissue from an *ex vivo* model of I/R injury revealed changes in the cellular abundance and mitochondrial association of several fission/fusion-related proteins over the course of ischaemia and reperfusion. Total amounts of HK2, Dyn2, Parkin and MAPL were unchanged by I/R, whereas Drp1, Mfn2, Mff and Fis1 were significantly decreased during reperfusion, Mff also decreased by ischaemia, and Fbxo7 and Fis1 were significantly decreased by ischaemic pre-conditioning (IPC). Mitochondrial association of HK2, Dyn2 and Fbxo7 was significantly decreased by IPC, while association of Drp1 was significantly increased by IPC, but decreased by reperfusion. Association of Parkin was by far the largest change, with an increase during ischaemia, followed by a decrease upon reperfusion. Interestingly, IPC partially attenuated the ischaemia-dependent recruitment.

Ischaemia and reperfusion significantly increased total cellular and mitochondrial ubiquitin-conjugation but had no effect on global or mitochondrial SUMO-conjugation. However, we go on to show that Mff is a novel SUMO substrate, and demonstrate that ischaemic stress (OGD) increases Mff SUMOylation. Analysis of point mutants of Mff reveal that phosphorylation of Mff regulates its SUMOylation, and SUMOylation, to a lesser degree, regulates its ubiquitination and degradation.

The scale of the change to mitochondria-associated Parkin during I/R marked it out as an interesting target for further study. Mitochondrial recruitment of Parkin coincided with a decrease of Mff during ischaemia, consistent with previous work demonstrating Parkin-dependent ubiquitination of Mff during mitophagy (Gao et al., 2015). In HEK293T cells, knock down of Parkin significantly elevated Mff levels, making Mff an ideal candidate for a 'read-out' of Parkin function. Parkin, Fbxo7 and mitophagy have previously been linked (Burchell et al., 2013), so Fbxo7 was also chosen as a protein for deeper investigation.

Knock down analyses showed that Parkin and Fbxo7 independently and additively contribute to ubiquitination of Mff under basal conditions, demonstrating, for the first time, a functional link between Fbxo7-containing CRLs and Mff. Knock down of Parkin significantly slowed and blocked the degradation of Mff over 24 hours, whereas knock down of Fbxo7 slowed, but did not block, Mff degradation in the same time-period. Interestingly, Fbxo7 ablation did appear to alter the ratio of Mff isoforms, indicating that

Parkin and Fbxo7 may regulate Mff in different ways, or primarily target different Mff isoforms, though this has not yet been followed up with further investigation.

Previously published work demonstrated non-covalent binding between Parkin and SUMO (Um and Chung, 2006). I confirmed this interaction by co-immunoprecipitation, both from HEK293T cells and *in vitro*. Overall, the ischaemia-dependent mitochondrial recruitment of Parkin, ischaemia-dependent SUMOylation and loss of Mff from the MOM, together with specific SUMO-binding of Parkin, suggest a role for SUMO in Parkin recruitment to, and ubiquitination of, Mff. I show that, while Fbxo7 has no preference between SUMOylated and non-SUMOylated Mff, Parkin does not ubiquitinate a non-SUMOylatable mutant of Mff, K151R. We therefore initially hypothesised that Parkin could be a SUMO-targeted ubiquitin ligase (STUbL). Subsequent experiments, however, indicated that Parkin directly ubiquitinates Mff at K151, independently of SUMO. This site of Parkin-mediated ubiquitination has not been previously reported. Additionally, immunoprecipitation experiments between Parkin and SUMO indicate the potential for Parkin itself to be a SUMO substrate which, if validated, would be a novel and exciting discovery.

6.2 The mitochondrial proteome is altered during I/R injury

It is well-established that mitochondria are a major target of the damage incurred by ischaemia and reperfusion (Halestrap, 2010, Sanada et al., 2011, Pasdois et al., 2013). Building on this work, the focus of my *ex vivo* experiments was on proteins associated with mitochondrial function and dynamics. IPC is protective against I/R injury but the molecular mechanisms underlying this remain poorly-understood (Yellon et al., 1992, Otani, 2004, Halestrap, 2010, Kalogeris et al., 2014). Therefore, particular attention was paid to proteins whose expression and/or subcellular compartmentalisation was affected by IPC. Summaries of the changes observed in these experiments are given in the tables below (Table 6.1 compares pre-ischaemia to ischaemia; Table 6.2 compares ischaemia with I/R or IPC).

6.2.1 Proteins involved in mitochondrial dynamics

To our knowledge, this is the first study to screen cardiac I/R injured-tissue for changes to mitochondrial dynamics-associated proteins. Using mass spectrometry, Oshima

et al demonstrated that IPC caused significant up- or down-regulation of several mitochondrial proteins compared to I/R in rat liver, while Kim *et al* identified 25 mitochondrial proteins that were differentially expressed in IPC or I/R rabbit cardiac tissue, which were predominantly proteins of the mitochondrial respiratory chain and proteins involved in energy metabolism (Kim et al., 2006b, Oshima et al., 2008). However, neither group included an ischaemic control group, making it difficult to draw conclusions. Forini *et al* also carried out a proteomics screen on mitochondrial proteins following cardiac I/R injury but focussed on proteins associated with metabolic processes (Forini et al., 2015).

By far the most marked change was in mitochondrial association of Parkin, which increased around 20-fold during ischaemia, an effect which was halved by IPC. A similar, but less pronounced, pattern was observed for Fbxo7. With regard to mitophagy, it was interesting that Parkin and Fbxo7 appear to be regulated in different ways; Fbxo7 was degraded during IPC, whereas total Parkin was stable, but less recruited to mitochondria during ischaemia following IPC. These data support the previous report that Fbxo7 is required for mitochondrial Parkin translocation (Burchell et al., 2013) - degradation of Fbxo7 as a result of IPC contributes to reduced mitochondrial translocation of Parkin. Additionally, Mff was lost from the mitochondrial fraction at the same time as Parkin was recruited, consistent with a previous study on Parkin-dependent ubiquitination of Mff during mitophagy (Gao et al., 2015). Taken together, this series of experiments suggest that Parkin is integral to both Fbxo7-mediated mitophagy and degradation of Mff and suggests a direct functional link between Fbxo7 and Mff stability.

6.2.2 Post-translational modifications

Hypoxia has been previously shown to up-regulate SUMO conjugation, which is thought to be a protective mechanism (Guo et al., 2013, Meller et al., 2014, Lee et al., 2007, Luo et al., 2017). With that in mind, we set out to determine whether SUMOylation was increased by IPC, a known cardio-protective mechanism. While there were no global changes to SUMO-2/3-ylation, a small but significant increase was observed in global SUMO-1-ylation as a result of IPC, which we propose could contribute to the cytoprotective effect of IPC. Unsurprisingly, global ubiquitination was significantly increased during reperfusion, a pattern reflected in the mitochondrial fraction. We attribute this to

substantial upregulation of the UPS as part of the unfolded protein response triggered by cytotoxic conditions (Lindholm et al., 2017).

Protein	Ischaemia	
Stress response		
LC3 II/I	=	
Cleaved Caspase-3	=	
LDH	+	
Mitochondria-associated	**Total**	**Mitochondrial**
HK2	=	=
Dyn2	=	=
Drp1	=	=
Fbxo7	=	=
Parkin	=	+
Mfn2		=
PINK1		=
MAPL		=
Mff		-
Fis1		=
Post-translational modifications	**Total**	**Mitochondrial**
Ubiquitin	=	=
SUMO-1	=	=
SUMO-2/3	=	=
SUMO-1 55kDa species		+

Table 6.1 **Protein changes observed in *ex vivo* experiments (1)**. Green plus symbol indicates increased protein, red minus symbol indicates decreased protein, equal symbol indicates no significant change. Protein levels compared with pre-ischaemia (control).

Protein	Reperfusion		Pre-conditioning	
Stress response				
LC3 II/I	+		=	
Cleaved Caspase-3	+		=	
LDH				
Mitochondria-associated	**Total**	**Mito.**	**Total**	**Mito.**
HK2	=	=	=	=
Dyn2	=	=	=	-
Drp1	-	-	=	=
Fbxo7	=	=	-	-
Parkin	=	-	=	-
Mfn2		=		=
PINK1		=		=
MAPL		=		=
Mff		=		=
Fis1		-		=
Post-translational modifications	**Total**	**Mito.**	**Total**	**Mito.**
Ubiquitin	+	+	=	=
SUMO-1	=	=	+	=
SUMO-2/3	=	=	=	=
SUMO-1 55kDa species		=		-

Table 6.2 **Protein changes observed in *ex vivo* experiments (2)**. Green plus symbol indicates increased protein, red minus symbol indicates decreased protein, equal symbol indicates no significant change. Protein levels for reperfusion or ischaemic-preconditioning (IPC) are compared with ischaemia.

6.2.3 Parkin and Fbxo7 regulate Mff independently and differentially

Parkin, Fbxo7 and Mff were each identified in the I/R injury screen as targets for further investigation, Parkin and Fbxo7 for their similar profiles of mitochondrial recruitment and known involvement in mitophagy, and Mff for its ischaemia-dependent decrease. While interactions between these three proteins have not been previously reported, they all have been implicated in mitophagy and Parkinson's disease, which is characterised by aberrant mitochondrial dynamics (Wiemerslage and Lee, 2016, Onyango

et al., 2017). I therefore explored the relationships between the three proteins, particularly focussing on Parkin as the 'common denominator,' but also with the goal of investigating the potential link between Fbxo7 and Mff.

6.2.4 Validation of PINK1-dependent ubiquitination of Mff by Parkin

In keeping with the previous work which identified Mff as a target of Parkin-mediated ubiquitination, loss of Mff from the MOM during ischaemia coincided with Parkin recruitment (Gao et al., 2015). While this was an interesting observation, *ex vivo* hearts are not an easily tractable model for molecular manipulation. Therefore, I used HEK293T cells for the majority of functional experiments because of their ease of culture and molecular biological manipulation.

To complement the *ex vivo* data, knock down of Parkin was performed in HEK293T cells to characterise the effect on Mff. Consistent with Parkin being a ubiquitin ligase of Mff, total levels of Mff were significantly increased by ablation of Parkin. Previous work has cast doubt on the integrity of Parkin over-expression, noting that, like for many E3 ligases, over-expression can lead to enzyme promiscuity and 'false positive' substrate identification (Danielsen et al., 2011, Kanner et al., 2017). Indeed, the study by Gao *et al* relied on over-expressed Parkin to mediate Mff ubiquitination. In light of this, I used only endogenous Parkin for functional studies.

Endogenous Parkin was sufficient to detectably ubiquitinate CFP-Mff, even in the absence of proteasomal inhibitors. This allowed me to investigate Parkin-mediated Mff ubiquitination at steady state. In support of the study by Gao *et al*, Parkin knock down halved steady state ubiquitination of Mff, complementing the doubling of total endogenous Mff with the same treatment.

Canonically, Parkin is only recruited to damaged or depolarised mitochondria by accumulation of PINK1 to initiate mitophagy. However, recent reports have demonstrated that, while Parkin-mediated mitophagy is delayed in PINK1-null cardiac cells, Parkin is still recruited to depolarised mitochondria via a PINK1-independent mechanism (Kubli et al., 2015). Moreover, PINK1-independent phosphorylation of Parkin at S57, rather than the canonical PINK1 site S65, hyperactivates Parkin (George et al., 2017). As the Parkin knock down experiments were performed under basal conditions, I wanted to determine whether or not Parkin-mediated ubiquitination of Mff was PINK1-dependent. Knock down of PINK1 in HEK293T cells had no effect on cellular levels of Parkin, but significantly

increased total Mff, indicating that PINK1 is required, at least in part, for Parkin activation prior to Mff ubiquitination. This also demonstrates that basal levels of PINK1 expression are sufficient to induce Parkin activity, an important factor given that most of the experiments detailed in this thesis were performed under basal conditions.

While the experiments discussed here go a long way toward demonstrating that Parkin ubiquitinates Mff in a PINK1-dependent manner, these data would be more convincing if extended with further rescue experiments. For example, the phenotype (increased Mff) of Parkin knock down should be rescued by episomal expression of WT, but not catalytically dead (C431S mutant) Parkin (Riley et al., 2013). Similarly, to validate that this mechanism is PINK1-dependent, a PINK1-insensitive Parkin mutant such as S65A would also not be able to rescue the phenotype (Ordureau et al., 2015).

6.2.5 Different effects of Mff ubiquitination by Parkin and Fbxo7

As outlined above, immunoprecipitation experiments of CFP-Mff revealed that both Parkin and Fbxo7 contributed to Mff ubiquitination. Interestingly, knock down of Parkin or Fbxo7 resulted in equal and additive loss of Mff ubiquitination. Moreover, knock down of Fbxo7 lead to a significant decrease in total Parkin, and *vice versa*. Therefore, my initial working hypothesis was that the reduction in Mff ubiquitination caused by Fbxo7 knock down was due to decreased Parkin. However, simultaneous knock down of Parkin and Fbxo7 caused further significant decrease in Mff ubiquitination, providing strong evidence that the two proteins act upon Mff independently.

I next tested if Parkin- and Fbxo7-mediated ubiquitination of Mff served different purposes. Ubiquitination of Mff by Parkin has already been linked to its degradation (Gao et al., 2015). To validate this finding, degradation of Mff over a 24-hour time-course was measured, in the presence or absence of Parkin. Cycloheximide (CHX) was used to inhibit protein synthesis, so that the rate of protein decay could be measured. In the absence of Parkin, degradation of Mff was significantly slower than in the presence of Parkin, and total Mff levels decreased by around half as much as in the presence of Parkin over 24 hours. This supports the finding by Gao *et al*. Together with the decrease in Mff ubiquitination observed with Parkin knock down, these data support a hypothesis in which Parkin mediates Mff degradation via ubiquitination. From these experiments, however, the mechanism of Mff degradation remains unclear. The study by Gao *et al* suggests that Parkin targets Mff for autophagic degradation, by showing that a non-ubiquitinatable Mff

mutant interacts less strongly with the autophagic adaptor protein p62 (Gao et al., 2015). However, they do not include any analysis of interactions with other proteins, such as those of the UPS, so other degradative mechanisms cannot be ruled out. Indeed, a study by Tanaka *et al* provided evidence that known substrates of Parkin-mediated ubiquitination, including Mfn2, were selectively decreased during CCCP-induced mitochondrial depolarisation, while several other Parkin substrates, including VDAC, Fis1 and the MIM transporter protein Tim23, were unchanged. The lack of global reduction to mitochondrial Parkin substrates might indicate that certain proteins are cleared vie selective proteasomal degradation, rather than mitophagy (Rojansky et al., 2016, Geisler et al., 2010, Aguileta et al., 2015, Tanaka et al., 2010). In their study, the loss of Parkin substrates like Mfn2 was rescued by blocking the UPS using MG132, a well-characterised proteasome inhibitor (Tanaka et al., 2010). This study therefore suggests that at least some Parkin substrates are degraded via the UPS, indicating that this could equally be true for Mff. Repeating the Parkin knock down experiments with and without MG132 could go some way toward determining the degradative pathway; if Mff is degraded via the UPS, MG132 treatment should increase detectable Parkin-induced ubiquitination, as well as increasing total Mff.

Interestingly, although knock down of Fbxo7 had as much of an effect on Mff ubiquitination as Parkin knock down, Fbxo7 ablation did not increase total Mff or decrease Mff turnover in 24 hours CHX treatment compared to the control. However, during the earlier stages (6- and 12-hour timepoints) of the time-course, Fbxo7 knock down did significantly inhibit Mff degradation. These data suggest that Fbxo7-mediated ubiquitination may have a limited effect on Mff turnover, and that degradation may not be the primary function of Fbxo7-mediated modification. A notable effect of Fbxo7 knock down, however, was a significant decrease in abundance of the predominating ~35kDa band and a significant increase in presence of ~25kDa lower bands. One explanation for these results is that Fbxo7 knock down could affect the ratio between different isoforms of Mff. Very little is known about the roles of different isoforms of Mff, so it is difficult to predict what the consequences of this shift in equilibrium could be. It is also interesting that, although Fbxo7 ablation significantly decreased total Parkin, the functional effect of Parkin knock down i.e. increased Mff, was not observed. We propose that the most likely reason for this is that complete or near-complete knock down of Parkin is required to protect Mff from degradation, which is not achieved by knock down of Fbxo7. Consistent with this, when Parkin and Fbxo7 were simultaneously knocked down, Mff was significantly increased.

Another plausible explanation could be that, rather than smaller isoforms, the lower molecular weight Mff-reactive bands observed upon knock down of Fbxo7 are degradation products. In this were the case, one could argue that Fbxo7 actually opposes the activity of Parkin by protecting Mff against degradation, in an epistatic pathway. In this scenario, the observation of the Parkin knock down phenotype (Mff increase) upon knock down of both Parkin and Fbxo7 could indicate that Fbxo7 functions upstream of Parkin. However, as discussed in Chapter 4, it is not possible from these data to dissect out the pathway, given that knock down of Parkin also reduces Fbxo7, and *vice versa*.

6.2.6 Mitochondrial networks are altered by OGD, and Parkin and Fbxo7 regulate this

In H9c2 cells, OGD causes a small but significant decrease in mitochondrial branch length, presumably due to an increase in mitochondrial fission. Mff degradation during ischaemia/OGD, which is at least partially mediated by Parkin, is likely to be a protective mechanism, designed to stop excessive fission from destroying the mitochondrial network. In the absence of Parkin, OGD causes a larger decrease in mitochondrial branch length. We hypothesise that this is due to accumulation of Mff on the MOM as Parkin is not available to ubiquitinate it and target it for degradation. Thus, elevated levels of Mff recruit more Drp1, leading to excessive fission and shortening of mitochondrial branches. However, we cannot conclude from these experiments alone that the effects of Parkin in mitochondrial networks are via Mff; in future it would be prudent to examine the accumulation of Mff by imaging.

In the presence of Fbxo7, OGD has no effect on the average number of branches within a mitochondrial network (network complexity). However, in the absence of Fbxo7, OGD causes a significant increase in the network complexity. It is unclear whether an increase in network complexity is a result of decreased fission or decreased fusion, as logic dictates that either could alter the network structure. A recent publication used mathematical modelling to determine that the mitochondrial network complexity of control cells is 'poised at criticality' (Zamponi et al., 2018). Zamponi *et al* concluded that promoting either fission or fusion results in a decrease in network complexity, which they equate with a decrease in network adaptability. The increase in complexity observed during OGD in the absence of Fbxo7, therefore, could arise from inhibition of fission or fusion. Speculatively, this could be a result of the perturbed equilibrium in Mff isoforms.

However, not enough is currently known about the different Mff isoforms or the involvement of Fbxo7 in their regulation to draw firm conclusions at this time.

6.3 Mff is regulated by stress-dependent post-translational modifications

SUMOylation has been previously shown to protect cells against ischaemic damage (Lee et al., 2007, Guo et al., 2013, Luo et al., 2017). Despite our *ex vivo* work not identifying any large-scale changes to SUMOylation during I/R injury, this does not rule out the possibility of protective changes to the SUMOylation status of subsets of proteins. A readily observable example of this is the ~55kDa mitochondrial SUMO-1-ylated species, which was significantly increased during ischaemia.

6.3.1 Mff is a novel SUMO substrate

During the course of this study, several of our lab demonstrated for the first time that Mff can be SUMO-1- and SUMO-2/3-ylated (Dr Kevin Wilkinson, Richard Seager & Laura Lee, unpublished data). Interestingly, SUMO-1-ylation of GST-Mff in HEK293T cells was substantially increased during OGD, indicating that Mff SUMOylation is regulated by ischaemic stress (Figure 5.7). This dataset does not include a free GST control, so it cannot be ruled out that this is actually GST SUMOylation, however the molecular weights of the co-purified SUMO bands are what would be expected for SUMOylated GST-Mff. Additionally, data presented in Figure 3.15 do include a free GST control, which has no observable covalent modifications, suggestive that GST cannot be readily SUMOylated.

The data shown in Figures 3.14 and 3.15 go a long way to establishing Mff as a *bona fide* SUMO substrate. Figure 3.14 demonstrates that SUMO-reactive species are co-immunoprecipitated with CFP-Mff, but not GFP alone, thereby ruling out the possibility of GFP SUMOylation. Mutation of a single site in Mff, K151, totally abolishes SUMOylation. This demonstrates that either K151 is the sole site of Mff SUMOylation, or that mutation of K151 renders Mff incapable of binding to another ~70kDa SUMO substrate, perhaps by unfolding the protein. This cannot be definitely ruled out, as the 0.1% SDS-containing buffer used for the pull downs is not totally denaturing. However, Figures 3.14 (C) and Figure 3.15 shows that purification of CFP-Mff or GST-Mff, but not free CFP or GST, also purifies a higher, CFP/GST-reactive molecular weight species. That this upper band is also CFP/GST-reactive rules out the possibility of it being another co-purified protein modification, regardless of the buffer composition. This species is also abolished by

expression of a SUMO-specific protease, as further evidence for Mff SUMOylation (Figure 3.15). Nonetheless, further validation of Mff as a SUMO substrate could be achieved by lysing the cells in a completely denaturing buffer, such as one containing 5% SDS or 8M urea, which would then have to be diluted out prior to immunoprecipitation.

Mff is SUMOylated at a single site, K151. We demonstrate this by mutating K151 (K151R) and observing total ablation of SUMO-1- and SUMO-2/3-ylation. Closer examination of the region around K151 revealed that K151 of Mff sits within a consensus phosphorylation-dependent SUMOylation motif (PDSM). We confirm that SUMOylation of Mff is regulated by phosphorylation at S155; mutation of S155 to a non-phosphorylatable site (S155A) significantly reduces SUMO-2/3-ylation of Mff, while mutation to a phospho-mimetic (S155D) significantly increases SUMO-1-ylation. S155 (and S172) of Mff are phosphorylated by AMP-activated kinase (AMPK). AMPK is stress-regulated – as intracellular ATP concentration falls, the increased AMP binds directly to the regulatory subunit of AMPK, facilitating its activation (Toyama et al., 2016). In this mechanism, ischaemic insult depletes cellular ATP, driving cellular AMP levels to reach a critical concentration at which AMPK Is activated. AMPK-mediated phosphorylation of Mff then enhances its SUMO-1-ylation, as shown in Figure 6.1.

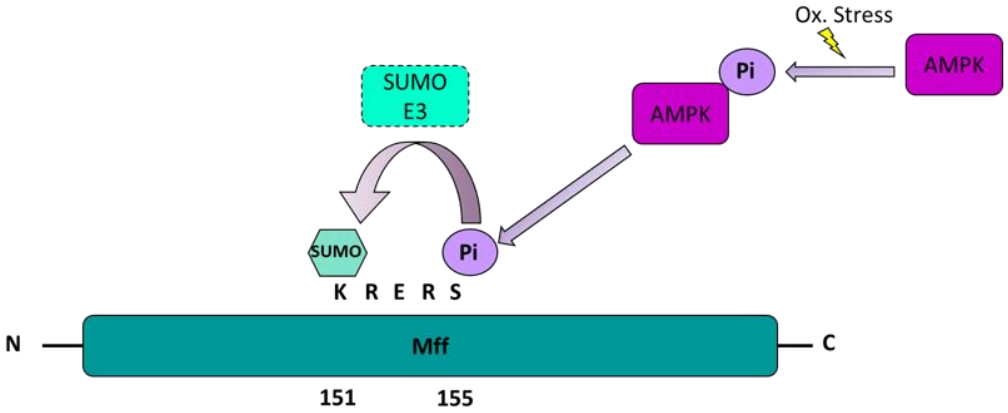

Figure 6.1 **Mff SUMOylation is a stress response**. In response to oxidative stress and low intracellular ATP, AMPK is activated by binding of AMP. AMPK phosphorylates Mff at S155. Phosphorylation of S155 enhances SUMOylation of Mff at K151. The SUMO E3 ligase remains unknown.

6.3.2 Parkin binds SUMO

The finding that Mff is both a substrate for Parkin and is also SUMOylated was particularly intriguing, as a previous publication demonstrated that Parkin could bind non-covalently to SUMO-1, but not SUMO-2 (Um and Chung, 2006). To confirm this report, I

expressed YFP-SUMO and Myc-Parkin in HEK293T cells and used GFP-Trap beads to immunoprecipitate YFP-SUMO. In support of the work carried out by Um and Chung, YFP-SUMO-1 was able to co-immunoprecipitate Myc-Parkin. Surprisingly, the same was observed for YFP-SUMO-2. In their study, Um and Chung used only WT HA-SUMO. To gain more information about the nature of the Parkin-SUMO interaction, I included a -ΔGG mutant of YFP-SUMO, in which the absent C-terminal di-glycine renders SUMO non-conjugatable. In the case of SUMO-1 and SUMO-2, Parkin preferentially bound to the WT form, consistent with the model that Parkin preferentially interacts with SUMO-modified proteins rather than free SUMO. Over the course of my PhD, several findings had hinted at an interplay between Parkin, Mff and SUMO.

- Mff is both a SUMO and a Parkin substrate.
- During ischaemia, SUMOylation of Mff is increased, recruitment of Parkin to the mitochondrial outer membrane is increased, and degradation of Mff is increased.
- Parkin ubiquitinates WT Mff, but not the non-SUMOylatable mutant of Mff, Mff K151R.
- Additionally, Parkin can bind SUMO, and may preferentially bind SUMOylated substrates.
- The only previously published report of Parkin ubiquitinating Mff reported that ubiquitination was at a single site, K302 (Gao et al., 2015).

Taken together, these data provided strong evidence that SUMOylation can recruit Parkin to the SUMO-tagged substrate protein i.e. that Parkin can act as a SUMO-targeted Ubiquitin ligase (STUbL).

If Parkin were a STUbL, a reasonable assumption would be that it would bind with less affinity to non-SUMOylatable Mff and/or with greater affinity to the highly SUMOylated phospho-mimetic mutant. However, co-immunoprecipitation experiments revealed no difference in Parkin binding to any of the mutants used in this study. Nevertheless, the interaction between an E3 ligase and its substrate is usually extremely transient, so may not be accurately measured by co-immunoprecipitation, especially of over-expressed proteins, and substrate binding does not necessarily dictate catalytic efficiency.

6.3.3 Parkin and Fbxo7 ubiquitinate Mff at different sites

The observation that Parkin does not ubiquitinate the non-SUMOylatable K151R mutant of Mff does not necessarily mean that SUMO is required for Parkin activity. Although Parkin has been reported to ubiquitinate Mff only at K302 (Gao et al., 2015), we could not exclude the possibility that the lack of Parkin activity on Mff K151R was because Parkin ubiquitinates Mff at K151. To investigate this possibility, we generated a non-SUMOylatable mutant of Mff that retained the SUMOylatable lysine. In the Mff E153A mutant, K151 is still available for modification, but the SUMO consensus motif is disrupted, ablating SUMOylation at K151. Using this mutant, I could discriminate between the requirement for SUMO and the requirement for K151 for Parkin activity. Immunoprecipitation of CFP-Mff WT, K151R and E153A revealed that Parkin ubiquitinates WT and E153A Mff to the same extent but ubiquitination of K151R is greatly reduced. This provides strong evidence that, contrary to the previously published work, Parkin ubiquitinates Mff at K151, as shown in Figure 6.2.

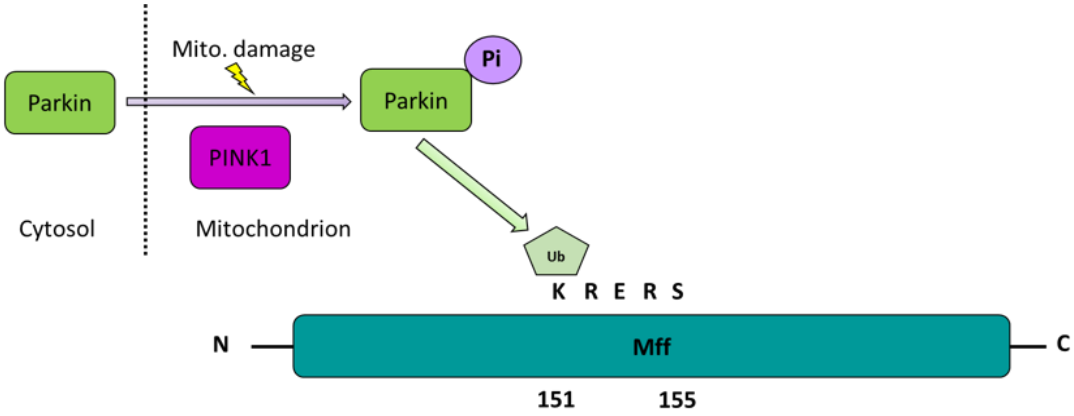

Figure 6.2 **Parkin ubiquitinates Mff at K151.** In response to mitochondrial membrane depolarisation, PINK1 accumulates and recruits Parkin from the cytosol by phosphorylation at S65. Activated Parkin ubiquitinates Mff at K151. Mutation of K151 renders Parkin unable to ubiquitinate Mff, suggesting that this is the only site of Parkin-mediated ubiquitination.

Thus, these data argue against the hypothesis that Parkin is a STUbL for Mff. Nonetheless, it is interesting that the non-SUMOylatable Mff E153A mutant has significantly reduced steady state ubiquitination compared to the WT, similar to the K151R mutant. We interpret these results to indicate that an, as-yet unidentified, ubiquitin ligase of Mff is recruited via SUMOylation at K151 and does not efficiently ubiquitinate Mff E153A despite the availability of K151 because the E153A mutant cannot be SUMOylated.

Mutation of E153 blocks SUMOylation as E153 is an essential part of the Ubc9 recognition and binding motif, and Ubc9 is the only SUMO E2 enzyme. However, there are 100s of ubiquitin E3 ligases, which do not all have the same substrate recognition motif/mechanism, so ubiquitination is not affected by mutation of one residue.

As discussed above, our data suggest that Parkin and Fbxo7 act independently of one another in their mediation of Mff ubiquitination. However, it was not clear whether they both ubiquitinate the same lysine residue. With a site of Parkin-mediated ubiquitination determined, it was easy to interrogate this question. Unlike Parkin, Fbxo7 was able to mediate ubiquitination of Mff K151R, with no preference for WT or K151R. This indicates that Fbxo7 mediates ubiquitination at a site other than K151 (Figure 6.3).

That Fbxo7 is involved in ubiquitinating Mff at a different site to Parkin further supports the hypothesis that Parkin and Fbxo7 act independently in their regulation of Mff, and that Parkin- and Fbxo7-mediated Mff ubiquitination may differ in their effects. There are nine other lysine residues in human Mff; in future systematic mutation of each could identify that Fbxo7 target(s).

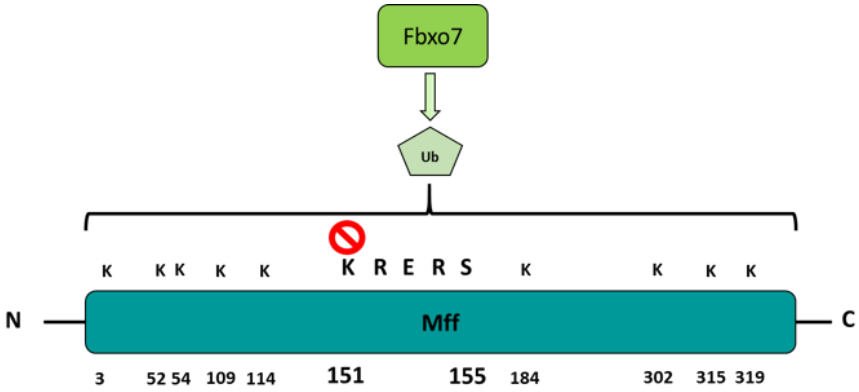

Figure 6.3 **Fbxo7 mediates Mff ubiquitination at a site other than K151.** Mutation of K151 has no bearing on the ability of Fbxo7 to mediate Mff ubiquitination, indicating that Fbxo7 does not ubiquitinate at this site. There are nine other lysine residues in Mff (indicated).

6.4 Parkin is a potential SUMO substrate

An unexpected discovery was that Parkin could be SUMOylated. By expressing YFP-SUMO and Myc-Parkin and performing co-immunoprecipitations, I showed not only that Parkin can non-covalently interact with SUMO, but that it can also be covalently modified by SUMO, as demonstrated by the emergence of Parkin- and SUMO-reactive higher molecular weight species, which were not present in experiments using non-conjugatable ΔGG SUMO mutants. Analysis of the amino acid sequence reveals that Parkin does not

contain a consensus SUMO motif. However, more than half of the known SUMO substrates do not contain a consensus motif, so this does not preclude the possibility that Parkin is a *bona fide* target of SUMOylation (Zhu et al., 2008, Blomster et al., 2009). Additionally, due to difficulties in crystallisation and modelling, a disordered, lysine-containing, portion of the 465 amino acid human Parkin protein, amino acids 75-145, remains largely unstudied (Gladkova et al., 2018). While intriguing, more investigation is required to fully validate this finding, including observation of endogenously SUMOylated Parkin, identification and mutation of the site of SUMOylation, and demonstrating a functional effect at physiological levels.

6.5 Future directions

Investigation of mechanisms of mitochondrial dynamics under oxidative stress

Parkin, Fbxo7 and Mff were chosen for investigation due to the changes observed in ischaemic cardiac tissue (Chapter 3). It was anticipated that the focus of the rest of this thesis would therefore also be ischaemia or an ischaemia-like oxidative stress. However, most of the work presented in Chapters 4 and 5 was carried out under basal conditions. This is not to say that the data are not important; we need to understand the mitochondrial quality control mechanisms that occur basally to be able to critically interpret their behaviour under pathological conditions. Moreover, the basal data obtained here are indicative of substantial roles for Parkin and Fbxo7, both usually studied in the context of disease or dysfunction, in physiological maintenance of the mitochondrial reticulum, through their effects on Mff, a regulator of normal mitochondrial fission.

I demonstrate a stress-inducible mechanism of Mff degradation via AMPK activation, phosphorylation of Mff and enhanced SUMOylation of Mff leading to its ubiquitination. However, I then demonstrate that this is effected by neither Parkin, which ubiquitinates Mff at K151 independently of SUMO, nor Fbxo7, which mediates ubiquitination of Mff at a site other than K151. Additionally, I show that binding of Parkin to Mff is not dependent on its phosphorylation or SUMOylation status, making use of non-SUMOylatable Mff mutants (K151R, E153A) and phospho-mutants (S155A, S155D). Examining the roles of Parkin and Fbxo7 in Mff degradation under conditions of oxidative stress may therefore not be particularly informative. A more interesting question would be the effect of the, as yet unidentified, SUMO-targeted ubiquitin ligase (STUbL) of Mff under conditions of oxidative stress, where we would expect that enhanced Mff SUMOylation would enhance STUbL activity.

Identification of ischaemia-dependent SUMO substrates

Changes in protein SUMOylation under conditions of ischaemic stress have been reported by several independent studies in various systems, including hypoxic neurons, hypoxic embryos, and hibernating ground squirrels (Lee et al., 2007, Guo et al., 2013, Meller et al., 2014). It was therefore surprising that no global changes in SUMOylation were detected in this study. However, as outlined throughout this thesis, global changes in SUMOylation are a relatively crude measure since the dynamics of SUMOylation of individual substrates can increase, decrease or remain unchanged. Measures of total SUMOylation integrate all of these changes, so nuanced but important detail can be lost, as is likely the case in this study. Furthermore, SUMOylation is a very transient modification, and it could be that the 30 minutes ischaemia and 120 minutes reperfusion used in this work, while well-established within the cardiac field (Pasdois et al., 2013), were sub-optimal to detect global changes in SUMOylation. Changes in the temporal parameters of the *ex vivo* work may therefore yield more interesting results with regard to SUMOylation. Similarly, it is important to note that the full set of SUMO and associated enzymes was not investigated in this study. Future work should aim to characterise changes in SUMO conjugating enzymes SAE1/2 and Ubc9, as well as SUMO proteases, to better understand the SUMO response to cardiac I/R injury.

While global changes in protein SUMOylation were not apparent in our model of cardiac I/R injury, a subset of SUMOylated proteins did change in abundance. Identification and analysis of these proteins is an important next step towards understanding any protective role(s) SUMOylation has in the response to cardiac I/R injury, and particularly during IPC. To achieve this, SUMO immunoprecipitation experiments from tissue taken at the different stages of I/R injury could be performed, to yield samples enriched in SUMO substrates. A landmark publication recently detailed an effective protocol for enriching SUMO substrates for quantitative analysis in this way (Barysch et al., 2014). Following immunoprecipitation on an affinity column using SUMO antibodies, SUMOylated substrates were specifically eluted using a buffer containing an epitope-specific SUMO peptide. Identification and relative quantitative analysis of SUMOylated proteins could then be performed using tandem mass tag mass spectrometry (TMT-MS).

Analysis of Mff turnover

My PhD research has shed light on some of the regulatory mechanisms underpinning Mff function and has opened many intriguing questions. We have demonstrated that

stress-inducible phosphorylation of Mff by AMPK regulates SUMOylation and have provided evidence that SUMOylation regulates ubiquitination. If SUMOylation of Mff promotes its ubiquitination, we would predict that non-SUMOylatable mutants of Mff (K151R and E153A) may be more stable than WT Mff. The work presented in this thesis go some way towards demonstrating this, but an incomplete dataset precludes the drawing of firm conclusions. On the other hand, we would predict that the hyper-SUMOylated phospho-mimetic Mff mutant (S155D) would be less stable, as its increased ubiquitination would promote degradation. This will be the subject of future experiments.

Further to this, we would predict that, under stressed conditions, WT Mff would be more rapidly degraded, while non-SUMOylatable Mff might be unaffected, which could be tested in cultured cells through incubation with a mitochondrial uncoupler such as rotenone or FCCP.

It is also important to note that over-expressed WT and K151R Mff mutants were used in this work, and that their rates of degradation may not accurately reflect the true stability of the proteins. A starting point for future studies is to repeat this experiment using endogenous levels of WT and K151R Mff. This could be achieved using a knock down replacement strategy, or using Mff-null MEF cells, currently available in the Henley lab, to express Mff mutants at endogenous levels. Another way to study the effect of Mff SUMOylation on its stability would be using endogenous Mff in conjunction with exogenously expressed SUMO mutants. The Henley lab has a series of SUMO constructs to express WT, non-conjugatable -ΔGG mutant and non-de-conjugatable -PQ mutant SUMO. Using cells expressing WT SUMO as a control, we would predict that Mff stability would be increased by the expression of SUMO-ΔGG, as Mff would remain largely un-SUMOylated, and decreased by expression of SUMO-PQ, as Mff would be permanently SUMOylated.

Identification and characterisation of the STUbL that ubiquitinates Mff

The discovery that Mff is a SUMO substrate and that non-SUMOylatable Mff has reduced ubiquitination hints at a SUMO-mediated ubiquitination mechanism, potentially via the activity of a STUbL. A diagram of proposed STUbL-dependent mechanisms is given in Figure 6.4.

A hypothesis tested as part of this PhD postulated that this could be Parkin, however the data presented here demonstrate that this is not the case. The identification of a STUbL involved in Mff regulation would be very interesting and would contribute to the rapidly

expanding field of inter-modification regulation. Some early and inconclusive experiments performed as part of this PhD revolved around the activity of MAPL, the first identified mitochondria-specific ligase. MAPL was first identified as a ubiquitin ligase, but extensive research performed by the McBride group has demonstrated the ability of MAPL to also conjugate SUMO (Prudent et al., 2015). Data not presented in this thesis revealed that ablation of MAPL resulted in a significant increase in total Mff, hinting that MAPL may be involved in the turnover of Mff. Interestingly, MAPL ablation also lead to a large increase in Mff SUMOylation – an unexpected result for a proposed SUMO ligase. One could speculate that the build-up of SUMOylated Mff is the result of a missing STUbL, with MAPL being a prime candidate.

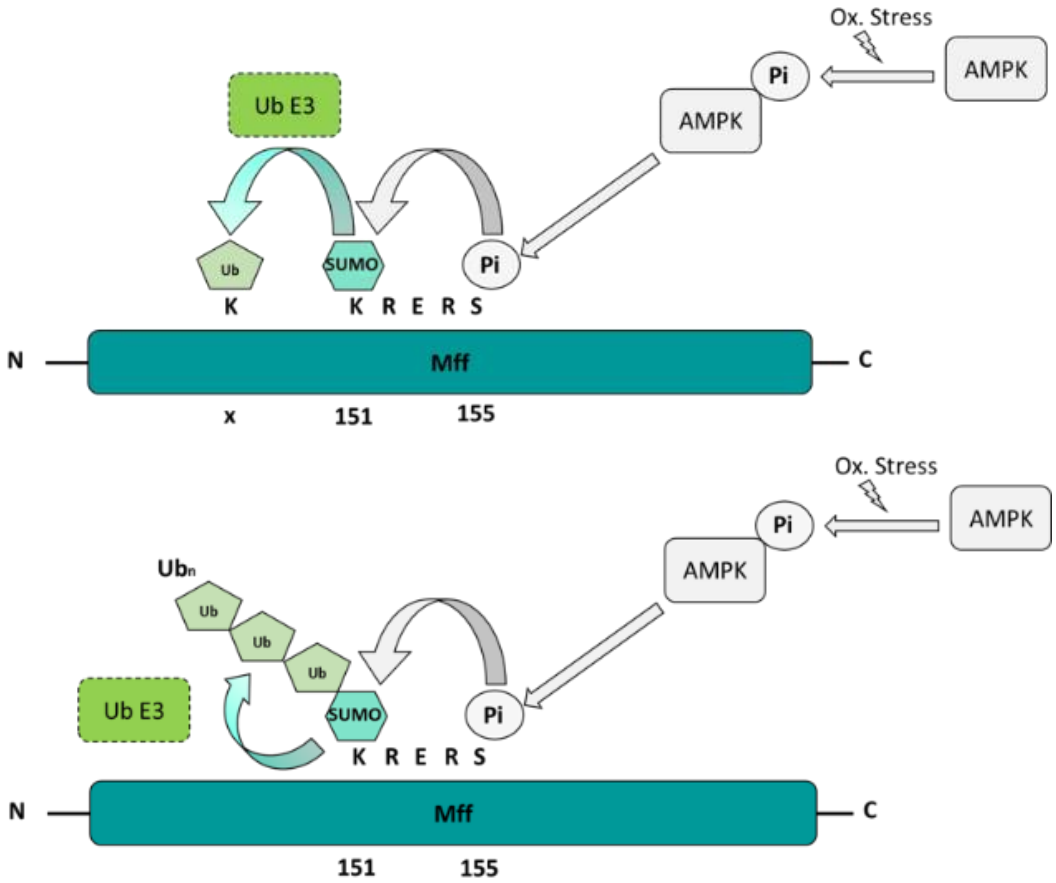

Figure 6.4 **Stress-dependent activation of a STUbL.** As described previously, oxidative stress activates AMPK, leading to phosphorylation of Mff at S155. This promotes SUMOylation at K151, which enhances ubiquitination of Mff by an as-yet unidentified STUbL E3 ligase. It remains unclear whether this STUbL would ubiquitinate Mff at another site (top panel), or directly ubiquitinate the SUMO moiety at K151 (lower panel).

Elucidation of Mff PTM chain composition

Some of the data presented in this thesis, and our hypothetic model, suggest that Mff is the target of mixed SUMO-ubiquitin chains. For example, knock down of the ubiquitin ligase Parkin removes a significant portion of both the ubiquitin- and SUMO-reactive Mff species. I demonstrate that ablation of the Mff SUMOylation consensus significantly reduces its ubiquitination, which supports our model in which SUMO is conjugated to Mff prior to ubiquitin (Figure 6.4). to validate this, samples could be incubated with a constitutively active SENP catalytic domain moiety (Craig et al., 2012). If Mff ubiquitin conjugating is via SUMO, SENP treatment would remove both SUMO and ubiquitin. In the same way, expression of a de-ubiquitinating peptidase (DUB) would remove just ubiquitin, leaving SUMO chains intact. However, these data would be confounded by direct Mff ubiquitination at other sites, such as that mediated by Fbxo7. All other sites of Mff ubiquitination would first need to be mutated/blocked, which requires their prior identification.

Furthermore, identification of the specific ubiquitin chain linkages present on Mff would help to determine the functions of Mff PTMs. While some linkage-specific ubiquitin antibodies have been validated, including those for Lys48- and Lys63-linked chains, it would be difficult to accurately analyse the composition of Mff PTMs by Western blotting alone, by comparing one 'smear' to another (Newton et al., 2008).

A proteomics-based technique could be used, using a 'bottom up' approach in which samples are trypsin-digested prior to liquid chromatography-tandem Mass Spectrometry for peptide identification. Ubiquitination leaves a signature di-glycine moiety of known monoisotopic mass on its substrate following trypsin cleavage, which can be used to identify ubiquitination sites within a substrate. While this allows us to determine ubiquitin chain linkage types, it does not reveal information pertaining to ubiquitin chain architecture (Peng et al., 2003).

A relatively new technique to analyse ubiquitin chain linkages is UbiCRest, in which substrates are subjected to parallel reactions with linkage-specific DUBs, followed by electrophoretic analysis (Hospenthal et al., 2015). This technique also allows users to determine chain architecture, through digestion of heterotypic poly-Ubiquitin chains with different linkage-specific DUBs. In future, this would be interesting to determine the nature (compositional and architectural) of Mff ubiquitination.

Regulation and roles of Fbxo7-mediated ubiquitination of Mff

Data presented here have demonstrated that Parkin-mediated and Fbxo7-mediated ubiquitination of Mff are independent of one another. A site of Parkin ubiquitination has been identified as K151. However, the site of Fbxo7-mediated ubiquitination remains unknown. Systematic replacement of lysine residues of Mff could answer this question; knock down of Fbxo7 would have no effect on ubiquitination of a mutant which it could not target. This experiment could also identify other sites of Mff ubiquitination, allowing us to generate a non-ubiquitinatable mutant.

Identification of the SIM in Parkin

The role of the PINK1-Parkin pathway in mitophagy has been extensively described in the literature, with a large focus on regulation of Parkin activity and its autoinhibition (Burchell et al., 2013, Narendra et al., 2010, Caulfield et al., 2014, Caulfield et al., 2015, Wauer et al., 2015b, Seirafi et al., 2015, Ordureau et al., 2015, Wu et al., 2016, Gladkova et al., 2018). Despite this, only one report has functionally linked Parkin and SUMO (Um and Chung, 2006). Data presented in this thesis have validated the finding of Um and Chung that Parkin and SUMO can interact non-covalently, however the site of this interaction remains unknown. Parkin does not contain a conventional SUMO-interacting motif. Um and Chung demonstrated that binding was not via the Ubl of Parkin but were unable to define the interaction site further. To resolve this, I have already generated a series of overlapping fragments of Parkin, dictated by domain structure (data not shown). In the future, co-immunoprecipitation experiments using these fragments could narrow down the site of the Parkin-SUMO interaction and allow for *in silico* modelling of potential interaction interfaces.

Validation and analysis of Parkin as a SUMO substrate

One of the most interesting discoveries of this project was the finding that Parkin can be modified by SUMO. Parkin, like over half of the known SUMO substrates, does not contain a SUMOylation consensus motif. Nonetheless, using the same Parkin fragments discussed above, immunoprecipitation experiments could help to narrow down the site of potential SUMOylation. Systematic mutation of lysine residues in the candidate fragment could then be used to demonstrate the exact site of SUMOylation. However, for these data to be of importance or physiological relevance, we would need to demonstrate a functional outcome of Parkin SUMOylation. SUMOylation of Parkin could be involved in its

autoinhibition, activation, subcellular localisation, degradation or function, but for Parkin to be named a *bona fide* SUMO substrate this would need to be experimentally demonstrated, ideally using endogenous levels of both Parkin and SUMO. Immunoprecipitation of over-expressed Parkin, like the experiments performed for Mff, would be a good starting point, to demonstrate that endogenous levels of SUMO are sufficient to modify Parkin.

Potential roles of these pathways in regulating neuronal function and dysfunction in disease

While the roles of Parkin, Fbxo7 and Mff in cardiac tissue remain under-investigated, because of the importance of the proteins investigated here in neurodegenerative diseases, the natural next step for this project would be re-capitulation of the experiments presented here in neurons. Both Parkin and Mff are strongly implicated in Parkinson's disease (PD) for their role in mitophagy, and Parkin and Fbxo7 have been shown to function in a similar pathway in PD (Burchell et al., 2013, Gao et al., 2015). Parkin is known to be mutated in many cases of PD, and there are over 120 known PD-associated pathogenic mutations of Parkin (Seirafi et al., 2015). Data from the Henley lab has shown by mass spectrometry that Mff is increased in Fbxo7-depleted neurons (Dr Dan Rocca, unpublished data). As yet, no published work has demonstrated a functional link between all three proteins of these proteins in PD. The Henley lab has acquired *post-mortem* brain tissue from patients who died with PD, as well as controls. It would be interesting to see whether levels of these proteins are altered in these samples. Furthermore, a cellular model of PD has been recently established in the lab using SH-SY5Y cells (Dr Ruth Carmichael, unpublished data). Using this model, it would be interesting to see whether modulation of Parkin, Fbxo7 or Mff levels, or Mff SUMOylation status, could be protective against PD.

6.6 Conclusions and significance

To our knowledge, this is the first study to systematically characterise changes in mitochondrial dynamics proteins and post-translational modifications in cardiac I/R injury. The discovery that Parkin and Fbxo7, both mitophagy-associated proteins, are significantly less recruited to mitochondria during ischaemia following IPC could go some way towards unravelling the illusive molecular mechanisms behind the protective effects of ischaemic pre-conditioning.

I show that Parkin and Fbxo7 contribute to regulation of mitochondrial morphology during ischaemia and demonstrate for the first time that Mff is ubiquitinated by Parkin at K151 and an Fbxo7-containing CRL complex, independently of one another. We show that Mff is a novel SUMO substrate and that SUMOylation of Mff is induced by ischaemia, probably through AMPK-mediated phosphorylation. I also show that SUMOylation of Mff acts to recruit a SUMO-targeted ubiquitin ligase.

The implications of interactions and inter-dependent regulation of Parkin, Fbxo7 and Mff have far-reaching consequences. The experimental data presented in this thesis contribute not only to understanding of the protective effect of cardiac IPC, but also to other pathologies in which aberrant mitochondrial dynamics are a major factor, including neurodegenerative diseases such as PD.

Chapter 7 References

ABUTBUL-IONITA, I., RUJIVIPHAT, J., NIR, I., MCQUIBBAN, G. A. & DANINO, D. 2012. Membrane tethering and nucleotide-dependent conformational changes drive mitochondrial genome maintenance (Mgm1) protein-mediated membrane fusion. *J Biol Chem,* 287**,** 36634-8.

AGUILETA, M. A., KORAC, J., DURCAN, T. M., TREMPE, J. F., HABER, M., GEHRING, K., ELSASSER, S., WAIDMANN, O., FON, E. A. & HUSNJAK, K. 2015. The E3 ubiquitin ligase parkin is recruited to the 26 S proteasome via the proteasomal ubiquitin receptor Rpn13. *J Biol Chem,* 290**,** 7492-505.

ALIROL, E., JAMES, D., HUBER, D., MARCHETTO, A., VERGANI, L., MARTINOU, J.-C., SCORRANO, L. & NEWMEYER, D. 2006. The Mitochondrial Fission Protein hFis1 Requires the Endoplasmic Reticulum Gateway to Induce Apoptosis. *Molecular Biology of the Cell,* 17**,** 4593-4605.

ALKURAYA, F. S., SAADI, I., LUND, J. J., TURBE-DOAN, A., MORTON, C. C. & MAAS, R. L. 2006. SUMO1 haploinsufficiency leads to cleft lip and palate. *Science,* 313**,** 1751.

ALLEN, D. G. & ORCHARD, C. H. 1987. Myocardial contractile function during ischemia and hypoxia. *Circ Res,* 60**,** 153-68.

ALPI, A. F., PACE, P. E., BABU, M. M. & PATEL, K. J. 2008. Mechanistic insight into site-restricted monoubiquitination of FANCD2 by Ube2t, FANCL, and FANCI. *Mol Cell,* 32**,** 767-77.

AMBROSIO, G., ZWEIER, J. L., DUILIO, C., KUPPUSAMY, P., SANTORO, G., ELIA, P. P., TRITTO, I., CIRILLO, P., CONDORELLI, M., CHIARIELLO, M. & ET AL. 1993. Evidence that mitochondrial respiration is a source of potentially toxic oxygen free radicals in intact rabbit hearts subjected to ischemia and reflow. *J Biol Chem,* 268**,** 18532-41.

ANDERSON, S., BANKIER, A. T., BARRELL, B. G., DE BRUIJN, M. H., COULSON, A. R., DROUIN, J., EPERON, I. C., NIERLICH, D. P., ROE, B. A., SANGER, F., SCHREIER, P. H., SMITH, A. J., STADEN, R. & YOUNG, I. G. 1981. Sequence and organization of the human mitochondrial genome. *Nature,* 290**,** 457-65.

ANDERSSON, S. G., ZOMORODIPOUR, A., ANDERSSON, J. O., SICHERITZ-PONTEN, T., ALSMARK, U. C., PODOWSKI, R. M., NASLUND, A. K., ERIKSSON, A. S., WINKLER, H. H. & KURLAND, C. G. 1998. The genome sequence of Rickettsia prowazekii and the origin of mitochondria. *Nature,* 396**,** 133-40.

ANDRE, C., GUILLEMIN, M.-C., ZHU, J., KOKEN, M. H. M., QUIGNON, F., HERVE, L., CHELBI-ALIX, M. K., DHUMEAUX, D., WANG, Z.-Y., DEGOS, L., CHEN, Z. & THE, H. D. 1996. The PML and PML/RARα Domains: From Autoimmunity to Molecular Oncology and from Retinoic Acid to Arsenic. *Experimental Cell Research,* 229**,** 253-260.

ANTONNY, B., BURD, C., DE CAMILLI, P., CHEN, E., DAUMKE, O., FAELBER, K., FORD, M., FROLOV, V. A., FROST, A., HINSHAW, J. E., KIRCHHAUSEN, T., KOZLOV, M. M., LENZ, M., LOW, H. H., MCMAHON, H., MERRIFIELD, C., POLLARD, T. D., ROBINSON, P. J., ROUX, A. & SCHMID, S. 2016. Membrane fission by dynamin: what we know and what we need to know. *The EMBO Journal,* 35**,** 2270.

APARICIO, I. M., ESPINO, J., BEJARANO, I., GALLARDO-SOLER, A., CAMPO, M. L., SALIDO, G. M., PARIENTE, J. A., PEÑA, F. J. & TAPIA, J. A. 2016. Autophagy-related proteins are functionally active in human spermatozoa and may be involved in the regulation of cell survival and motility. *Scientific Reports,* 6**,** 33647.

AUCIELLO, F. R., ROSS, F. A., IKEMATSU, N. & HARDIE, D. G. 2014. Oxidative stress activates AMPK in cultured cells primarily by increasing cellular AMP and/or ADP. *Febs Letters,* 588**,** 3361-3366.

AVKIRAN, M. & MARBER, M. S. 2002. Na(+)/H(+) exchange inhibitors for cardioprotective therapy: progress, problems and prospects. *J Am Coll Cardiol,* 39**,** 747-53.

BABA, D., MAITA, N., JEE, J. G., UCHIMURA, Y., SAITOH, H., SUGASAWA, K., HANAOKA, F., TOCHIO, H., HIROAKI, H. & SHIRAKAWA, M. 2005. Crystal structure of thymine DNA glycosylase conjugated to SUMO-1. *Nature,* 435**,** 979-82.

BABOSHINA, O. V. & HAAS, A. L. 1996. Novel Multiubiquitin Chain Linkages Catalyzed by the Conjugating Enzymes E2EPF and RAD6 Are Recognized by 26 S Proteasome Subunit 5. *Journal of Biological Chemistry,* 271**,** 2823-2831.

BACH, D., PICH, S., SORIANO, F. X., VEGA, N., BAUMGARTNER, B., ORIOLA, J., DAUGAARD, J. R., LLOBERAS, J., CAMPS, M., ZIERATH, J. R., RABASA-LHORET, R., WALLBERG-HENRIKSSON, H., LAVILLE, M., PALACíN, M., VIDAL, H., RIVERA, F., BRAND, M. & ZORZANO, A. 2003. Mitofusin-2 Determines Mitochondrial Network Architecture and Mitochondrial Metabolism: A NOVEL REGULATORY MECHANISM ALTERED IN OBESITY. *Journal of Biological Chemistry,* 278**,** 17190-17197.

BACHMAIR, A., FINLEY, D. & VARSHAVSKY, A. 1986. In vivo half-life of a protein is a function of its amino-terminal residue. *Science,* 234**,** 179-86.

BADER, M., BENJAMIN, S., WAPINSKI, O. L., SMITH, D. M., GOLDBERG, A. L. & STELLER, H. 2011. A conserved F box regulatory complex controls proteasome activity in Drosophila. *Cell,* 145**,** 371-82.

BAILEY, D. & O'HARE, P. 2004. Characterization of the localization and proteolytic activity of the SUMO-specific protease, SENP1. *J Biol Chem,* 279**,** 692-703.

BAINES, C. P. 2010. The cardiac mitochondrion: nexus of stress. *Annu Rev Physiol,* 72**,** 61-80.

BARANDUN, J., DELLEY, C. L. & WEBER-BAN, E. 2012. The pupylation pathway and its role in mycobacteria. *BMC Biol,* 10**,** 95.

BARICAULT, L., SEGUI, B., GUEGAND, L., OLICHON, A., VALETTE, A., LARMINAT, F. & LENAERS, G. 2007. OPA1 cleavage depends on decreased mitochondrial ATP level and bivalent metals. *Exp Cell Res,* 313**,** 3800-8.

BARYSCH, S. V., DITTNER, C., FLOTHO, A., BECKER, J. & MELCHIOR, F. 2014. Identification and analysis of endogenous SUMO1 and SUMO2/3 targets in mammalian cells and tissues using monoclonal antibodies. *Nat Protoc,* 9**,** 896-909.

BAYER, P., ARNDT, A., METZGER, S., MAHAJAN, R., MELCHIOR, F., JAENICKE, R. & BECKER, J. 1998. Structure determination of the small ubiquitin-related modifier SUMO-1. *J Mol Biol,* 280**,** 275-86.

BENSON, M. D., LI, Q. J., KIECKHAFER, K., DUDEK, D., WHORTON, M. R., SUNAHARA, R. K., INIGUEZ-LLUHI, J. A. & MARTENS, J. R. 2007. SUMO modification regulates inactivation of the voltage-gated potassium channel Kv1.5. *Proc Natl Acad Sci U S A,* 104**,** 1805-10.

BERGER, A. K., CORTESE, G. P., AMODEO, K. D., WEIHOFEN, A., LETAI, A. & LAVOIE, M. J. 2009. Parkin selectively alters the intrinsic threshold for mitochondrial cytochrome c release. *Hum Mol Genet,* 18**,** 4317-28.

BERNIER-VILLAMOR, V., SAMPSON, D. A., MATUNIS, M. J. & LIMA, C. D. 2002. Structural Basis for E2-Mediated SUMO Conjugation Revealed by a Complex between Ubiquitin-Conjugating Enzyme Ubc9 and RanGAP1. *Cell,* 108**,** 345-356.

BHANDARI, P., SONG, M., CHEN, Y., BURELLE, Y. & DORN, G. W., 2ND 2014. Mitochondrial contagion induced by Parkin deficiency in Drosophila hearts and its containment by suppressing mitofusin. *Circ Res,* 114**,** 257-65.

BISCHOFF, F. R., KLEBE, C., KRETSCHMER, J., WITTINGHOFER, A. & PONSTINGL, H. 1994. RanGAP1 induces GTPase activity of nuclear Ras-related Ran. *Proc Natl Acad Sci U S A,* 91**,** 2587-91.

BLOMSTER, H. A., HIETAKANGAS, V., WU, J., KOUVONEN, P., HAUTANIEMI, S. & SISTONEN, L. 2009. Novel proteomics strategy brings insight into the prevalence of SUMO-2 target sites. *Mol Cell Proteomics,* 8**,** 1382-90.

BLOMSTER, H. A., IMANISHI, S. Y., SIIMES, J., KASTU, J., MORRICE, N. A., ERIKSSON, J. E. & SISTONEN, L. 2010. In Vivo Identification of Sumoylation Sites by a Signature Tag and Cysteine-targeted Affinity Purification. *The Journal of Biological Chemistry,* 285**,** 19324-19329.

BOHREN, K. M., NADKARNI, V., SONG, J. H., GABBAY, K. H. & OWERBACH, D. 2004. A M55V Polymorphism in a Novel SUMO Gene (SUMO-4) Differentially Activates Heat Shock Transcription Factors and Is Associated with Susceptibility to Type I Diabetes Mellitus. *Journal of Biological Chemistry,* 279**,** 27233-27238.

BOSSIS, G. & MELCHIOR, F. 2006. Regulation of SUMOylation by reversible oxidation of SUMO conjugating enzymes. *Mol Cell,* 21**,** 349-57.

BOSSY, B., PETRILLI, A., KLINGLMAYR, E., CHEN, J., LUTZ-MEINDL, U., KNOTT, A. B., MASLIAH, E., SCHWARZENBACHER, R. & BOSSY-WETZEL, E. 2010. S-Nitrosylation of DRP1 does not affect enzymatic activity and is not specific to Alzheimer's disease. *J Alzheimers Dis,* 20 Suppl 2**,** S513-26.

BRAAK, H., DEL TREDICI, K., RUB, U., DE VOS, R. A., JANSEN STEUR, E. N. & BRAAK, E. 2003. Staging of brain pathology related to sporadic Parkinson's disease. *Neurobiol Aging,* 24**,** 197-211.

BRASCHI, E., ZUNINO, R. & MCBRIDE, H. M. 2009. MAPL is a new mitochondrial SUMO E3 ligase that regulates mitochondrial fission. *EMBO Rep,* 10**,** 748-54.

BRAUNWALD, E. & KLONER, R. A. 1985. Myocardial reperfusion: a double-edged sword? *J Clin Invest,* 76**,** 1713-9.

BRAY, M.-A., SHEEHY SEAN, P. & PARKER KEVIN, K. 2008. Sarcomere alignment is regulated by myocyte shape. *Cell Motility,* 65**,** 641-651.

BRECKENRIDGE, D. G., STOJANOVIC, M., MARCELLUS, R. C. & SHORE, G. C. 2003. Caspase cleavage product of BAP31 induces mitochondrial fission through endoplasmic reticulum calcium signals, enhancing cytochrome c release to the cytosol. *J Cell Biol,* 160**,** 1115-27.

BREMM, A., FREUND, S. M. & KOMANDER, D. 2010. Lys11-linked ubiquitin chains adopt compact conformations and are preferentially hydrolyzed by the deubiquitinase Cezanne. *Nat Struct Mol Biol,* 17**,** 939-47.

BRUICK, R. K. & MCKNIGHT, S. L. 2001. A Conserved Family of Prolyl-4-Hydroxylases That Modify HIF. *Science,* 294**,** 1337.

BURCHELL, V. S., NELSON, D. E., SANCHEZ-MARTINEZ, A., DELGADO-CAMPRUBI, M., IVATT, R. M., POGSON, J. H., RANDLE, S. J., WRAY, S., LEWIS, P. A., HOULDEN, H., ABRAMOV, A. Y., HARDY, J., WOOD, N. W., WHITWORTH, A. J., LAMAN, H. & PLUN-FAVREAU, H. 2013. The Parkinson's disease-linked proteins Fbxo7 and Parkin interact to mediate mitophagy. *Nat Neurosci,* 16**,** 1257-65.

BURNS, K. E. & DARWIN, K. H. 2010. Pupylation versus ubiquitylation: tagging for proteasome-dependent degradation. *Cell Microbiol,* 12**,** 424-31.

BURROUGHS, A. M., IYER, L. M. & ARAVIND, L. 2012. The natural history of ubiquitin and ubiquitin-related domains. *Front Biosci (Landmark Ed),* 17**,** 1433-60.

CADENAS, S. 2018. ROS and redox signaling in myocardial ischemia-reperfusion injury and cardioprotection. *Free Radic Biol Med,* 117**,** 76-89.

CADENAS, S., ARAGONÉS, J. & LANDÁZURI, M. O. 2010. Mitochondrial reprogramming through cardiac oxygen sensors in ischaemic heart disease. *Cardiovascular Research,* 88**,** 219-228.

CANDILIO, L., MALIK, A., ARITI, C., BARNARD, M., DI SALVO, C., LAWRENCE, D., HAYWARD, M., YAP, J., ROBERTS, N., SHEIKH, A., KOLVEKAR, S., HAUSENLOY, D. J. & YELLON,

D. M. 2015. Effect of remote ischaemic preconditioning on clinical outcomes in patients undergoing cardiac bypass surgery: a randomised controlled clinical trial. *Heart,* 101**,** 185-92.

CAULFIELD, T. R., FIESEL, F. C., MOUSSAUD-LAMODIERE, E. L., DOURADO, D. F., FLORES, S. C. & SPRINGER, W. 2014. Phosphorylation by PINK1 releases the UBL domain and initializes the conformational opening of the E3 ubiquitin ligase Parkin. *PLoS Comput Biol,* 10**,** e1003935.

CAULFIELD, T. R., FIESEL, F. C. & SPRINGER, W. 2015. Activation of the E3 Ubiquitin Ligase Parkin. *Biochemical Society transactions,* 43**,** 269-274.

CESARI, R., MARTIN, E. S., CALIN, G. A., PENTIMALLI, F., BICHI, R., MCADAMS, H., TRAPASSO, F., DRUSCO, A., SHIMIZU, M., MASCIULLO, V., D'ANDRILLI, G., SCAMBIA, G., PICCHIO, M. C., ALDER, H., GODWIN, A. K. & CROCE, C. M. 2003. Parkin, a gene implicated in autosomal recessive juvenile parkinsonism, is a candidate tumor suppressor gene on chromosome 6q25-q27. *Proc Natl Acad Sci U S A,* 100**,** 5956-61.

CHAN, N. C., SALAZAR, A. M., PHAM, A. H., SWEREDOSKI, M. J., KOLAWA, N. J., GRAHAM, R. L., HESS, S. & CHAN, D. C. 2011. Broad activation of the ubiquitin-proteasome system by Parkin is critical for mitophagy. *Hum Mol Genet,* 20**,** 1726-37.

CHANG, C.-R. & BLACKSTONE, C. 2007. Cyclic AMP-dependent Protein Kinase Phosphorylation of Drp1 Regulates Its GTPase Activity and Mitochondrial Morphology. *Journal of Biological Chemistry,* 282**,** 21583-21587.

CHANG, C. R. & BLACKSTONE, C. 2010. Dynamic regulation of mitochondrial fission through modification of the dynamin-related protein Drp1. *Ann N Y Acad Sci,* 1201**,** 34-9.

CHASTAGNER, P., ISRAËL, A. & BROU, C. 2006. Itch/AIP4 mediates Deltex degradation through the formation of K29-linked polyubiquitin chains. *EMBO reports,* 7**,** 1147.

CHAUGULE, V. K., BURCHELL, L., BARBER, K. R., SIDHU, A., LESLIE, S. J., SHAW, G. S. & WALDEN, H. 2011. Autoregulation of Parkin activity through its ubiquitin-like domain. *Embo j,* 30**,** 2853-67.

CHECCHETTO, V. & SZABO, I. 2018. Novel Channels of the Outer Membrane of Mitochondria: Recent Discoveries Change Our View. *BioEssays,* 40**,** 1700232.

CHEN, H. & CHAN, D. C. 2010. Physiological functions of mitochondrial fusion. *Ann N Y Acad Sci,* 1201**,** 21-5.

CHEN, H., DETMER, S. A., EWALD, A. J., GRIFFIN, E. E., FRASER, S. E. & CHAN, D. C. 2003. Mitofusins Mfn1 and Mfn2 coordinately regulate mitochondrial fusion and are essential for embryonic development. *The Journal of Cell Biology,* 160**,** 189.

CHEN, L., GONG, Q., STICE, J. P. & KNOWLTON, A. A. 2009. Mitochondrial OPA1, apoptosis, and heart failure. *Cardiovascular Research,* 84**,** 91-99.

CHEN, W., GABEL, S., STEENBERGEN, C. & MURPHY, E. 1995. A Redox-Based Mechanism for Cardioprotection Induced by Ischemic Preconditioning in Perfused Rat Heart. *Circulation Research,* 77**,** 424.

CHEN, Y. & DORN, G. W., 2ND 2013. PINK1-phosphorylated mitofusin 2 is a Parkin receptor for culling damaged mitochondria. *Science,* 340**,** 471-5.

CHIPUK, J. E., BOUCHIER-HAYES, L. & GREEN, D. R. 2006. Mitochondrial outer membrane permeabilization during apoptosis: the innocent bystander scenario. *Cell Death Differ,* 13**,** 1396-402.

CHIU, Y.-H., SUN, Q. & CHEN, Z. J. 2007. E1-L2 Activates Both Ubiquitin and FAT10. *Molecular Cell,* 27**,** 1014-1023.

CHO, D. H., NAKAMURA, T., FANG, J., CIEPLAK, P., GODZIK, A., GU, Z. & LIPTON, S. A. 2009. S-nitrosylation of Drp1 mediates beta-amyloid-related mitochondrial fission and neuronal injury. *Science,* 324**,** 102-5.

CHO, S.-J., YUN, S.-M., JO, C., LEE, D.-H., CHOI, K. J., SONG, J. C., PARK, S. I., KIM, Y.-J. & KOH, Y. H. 2015. SUMO1 promotes Aβ production via the modulation of autophagy. *Autophagy,* 11**,** 100-112.

CHOU, C. H., LIN, C. C., YANG, M. C., WEI, C. C., LIAO, H. D., LIN, R. C., TU, W. Y., KAO, T. C., HSU, C. M., CHENG, J. T., CHOU, A. K., LEE, C. I., LOH, J. K., HOWNG, S. L. & HONG, Y. R. 2012. GSK3beta-mediated Drp1 phosphorylation induced elongated mitochondrial morphology against oxidative stress. *PLoS One,* 7**,** e49112.

CHOUDHARY, C., KUMAR, C., GNAD, F., NIELSEN, M. L., REHMAN, M., WALTHER, T. C., OLSEN, J. V. & MANN, M. 2009. Lysine acetylation targets protein complexes and co-regulates major cellular functions. *Science,* 325**,** 834-40.

CHRISTENSEN, D. E., BRZOVIC, P. S. & KLEVIT, R. E. 2007. E2-BRCA1 RING interactions dictate synthesis of mono- or specific polyubiquitin chain linkages. *Nat Struct Mol Biol,* 14**,** 941-8.

CHU-PING, M., SLAUGHTER, C. A. & DEMARTINO, G. N. 1992. Purification and characterization of a protein inhibitor of the 20S proteasome (macropain). *Biochim Biophys Acta,* 1119**,** 303-11.

CHUNG, K. K. K., THOMAS, B., LI, X., PLETNIKOVA, O., TRONCOSO, J. C., MARSH, L., DAWSON, V. L. & DAWSON, T. M. 2004. S-Nitrosylation of Parkin Regulates Ubiquitination and Compromises Parkin's Protective Function. *Science,* 304**,** 1328.

CHUPRETA, S., HOLMSTROM, S., SUBRAMANIAN, L. & INIGUEZ-LLUHI, J. A. 2005. A small conserved surface in SUMO is the critical structural determinant of its transcriptional inhibitory properties. *Mol Cell Biol,* 25**,** 4272-82.

CIECHANOVER, A., HELLER, H., ELIAS, S., HAAS, A. L. & HERSHKO, A. 1980. ATP-dependent conjugation of reticulocyte proteins with the polypeptide required for protein degradation. *Proc Natl Acad Sci U S A,* 77**,** 1365-8.

CLAGUE, M. J., COULSON, J. M. & URBÉ, S. 2012. Cellular functions of the DUBs. *Journal of Cell Science,* 125**,** 277.

CLAGUE, M. J. & URBE, S. 2006. Endocytosis: the DUB version. *Trends Cell Biol,* 16**,** 551-9.

CLARK, I. E., DODSON, M. W., JIANG, C., CAO, J. H., HUH, J. R., SEOL, J. H., YOO, S. J., HAY, B. A. & GUO, M. 2006. Drosophila pink1 is required for mitochondrial function and interacts genetically with parkin. *Nature,* 441**,** 1162-6.

COHEN, M. V., YANG, X. M. & DOWNEY, J. M. 2007. The pH hypothesis of postconditioning: staccato reperfusion reintroduces oxygen and perpetuates myocardial acidosis. *Circulation,* 115**,** 1895-903.

COLBY, T., MATTHAI, A., BOECKELMANN, A. & STUIBLE, H. P. 2006. SUMO-conjugating and SUMO-deconjugating enzymes from Arabidopsis. *Plant Physiol,* 142**,** 318-32.

COLLAVIN, L., GOSTISSA, M., AVOLIO, F., SECCO, P., RONCHI, A., SANTORO, C. & DEL SAL, G. 2004. Modification of the erythroid transcription factor GATA-1 by SUMO-1. *Proc Natl Acad Sci U S A,* 101**,** 8870-5.

CRAIG, T. J., JAAFARI, N., PETROVIC, M. M., JACOBS, S. C., RUBIN, P. P., MELLOR, J. R. & HENLEY, J. M. 2012. Homeostatic synaptic scaling is regulated by protein SUMOylation. *J Biol Chem,* 287**,** 22781-8.

CRIBBS, J. T. & STRACK, S. 2007. Reversible phosphorylation of Drp1 by cyclic AMP-dependent protein kinase and calcineurin regulates mitochondrial fission and cell death. *EMBO reports,* 8**,** 939.

CROMPTON, M. 1999. The mitochondrial permeability transition pore and its role in cell death. *Biochemical Journal,* 341**,** 233.

DACZKOWSKI, C. M., DZIMIANSKI, J. V., CLASMAN, J. R., GOODWIN, O., MESECAR, A. D. & PEGAN, S. D. 2017. Structural Insights into the Interaction of Coronavirus Papain-Like Proteases and Interferon-Stimulated Gene Product 15 from Different Species. *Journal of Molecular Biology,* 429**,** 1661-1683.

DADKE, S., COTTERET, S., YIP, S.-C., JAFFER, Z. M., HAJ, F., IVANOV, A., RAUSCHER III, F., SHUAI, K., NG, T., NEEL, B. G. & CHERNOFF, J. 2006. Regulation of protein tyrosine phosphatase 1B by sumoylation. *Nature Cell Biology,* 9**,** 80.

DANIELSEN, J. M., SYLVESTERSEN, K. B., BEKKER-JENSEN, S., SZKLARCZYK, D., POULSEN, J. W., HORN, H., JENSEN, L. J., MAILAND, N. & NIELSEN, M. L. 2011. Mass spectrometric analysis of lysine ubiquitylation reveals promiscuity at site level. *Mol Cell Proteomics,* 10**,** M110.003590.

DARWIN, K. H. & HOFMANN, K. 2010. SAMPyling proteins in archaea. *Trends Biochem Sci,* 35**,** 348-51.

DAY, R. N. & DAVIDSON, M. W. 2009. The fluorescent protein palette: tools for cellular imaging. *Chemical Society reviews,* 38**,** 2887-2921.

DE BRITO, O. M. & SCORRANO, L. 2008. Mitofusin 2 tethers endoplasmic reticulum to mitochondria. *Nature,* 456**,** 605.

DEGTEREV, A., BOYCE, M. & YUAN, J. 2003. A decade of caspases. *Oncogene,* 22**,** 8543-67.

DENG, L., WANG, C., SPENCER, E., YANG, L., BRAUN, A., YOU, J., SLAUGHTER, C., PICKART, C. & CHEN, Z. J. 2000. Activation of the IkappaB kinase complex by TRAF6 requires a dimeric ubiquitin-conjugating enzyme complex and a unique polyubiquitin chain. *Cell,* 103**,** 351-61.

DESHAIES, R. J. & JOAZEIRO, C. A. 2009. RING domain E3 ubiquitin ligases. *Annu Rev Biochem,* 78**,** 399-434.

DESTERRO, J. M. P., RODRIGUEZ, M. S. & HAY, R. T. 1998. SUMO-1 Modification of IκBα Inhibits NF-κB Activation. *Molecular Cell,* 2**,** 233-239.

DESTERRO, J. M. P., THOMSON, J. & HAY, R. T. 1997. Ubch9 conjugates SUMO but not ubiquitin. *FEBS Letters,* 417**,** 297-300.

DI BACCO, A., OUYANG, J., LEE, H. Y., CATIC, A., PLOEGH, H. & GILL, G. 2006. The SUMO-specific protease SENP5 is required for cell division. *Mol Cell Biol,* 26**,** 4489-98.

DI FONZO, A., DEKKER, M. C., MONTAGNA, P., BARUZZI, A., YONOVA, E. H., CORREIA GUEDES, L., SZCZERBINSKA, A., ZHAO, T., DUBBEL-HULSMAN, L. O., WOUTERS, C. H., DE GRAAFF, E., OYEN, W. J., SIMONS, E. J., BREEDVELD, G. J., OOSTRA, B. A., HORSTINK, M. W. & BONIFATI, V. 2009. FBXO7 mutations cause autosomal recessive, early-onset parkinsonian-pyramidal syndrome. *Neurology,* 72**,** 240-5.

DIAZ, F. & MORAES, C. T. 2008. Mitochondrial biogenesis and turnover. *Cell Calcium,* 44**,** 24-35.

DING, W. X., NI, H. M., LI, M., LIAO, Y., CHEN, X., STOLZ, D. B., DORN, G. W., 2ND & YIN, X. M. 2010. Nix is critical to two distinct phases of mitophagy, reactive oxygen species-mediated autophagy induction and Parkin-ubiquitin-p62-mediated mitochondrial priming. *J Biol Chem,* 285**,** 27879-90.

DOIL, C., MAILAND, N., BEKKER-JENSEN, S., MENARD, P., LARSEN, D. H., PEPPERKOK, R., ELLENBERG, J., PANIER, S., DUROCHER, D., BARTEK, J., LUKAS, J. & LUKAS, C. 2009. RNF168 binds and amplifies ubiquitin conjugates on damaged chromosomes to allow accumulation of repair proteins. *Cell,* 136**,** 435-46.

DORN, G. W., 2ND 2013. Mitochondrial dynamics in heart disease. *Biochim Biophys Acta,* 1833**,** 233-41.

DORN, G. W., 2ND 2016. Central Parkin: The evolving role of Parkin in the heart. *Biochim Biophys Acta,* 1857**,** 1307-1312.

DUBEY, A. K., GODBOLE, A. & MATHEW, M. K. 2016. Regulation of VDAC trafficking modulates cell death. *Cell Death Discov,* 2**,** 16085.

DUDA, D. M., BORG, L. A., SCOTT, D. C., HUNT, H. W., HAMMEL, M. & SCHULMAN, B. A. 2008. Structural insights into NEDD8 activation of cullin-RING ligases: conformational control of conjugation. *Cell,* 134**,** 995-1006.

EDDINS, M. J., CARLILE, C. M., GOMEZ, K. M., PICKART, C. M. & WOLBERGER, C. 2006. Mms2-Ubc13 covalently bound to ubiquitin reveals the structural basis of linkage-specific polyubiquitin chain formation. *Nat Struct Mol Biol,* 13**,** 915-20.

EHSES, S., RASCHKE, I., MANCUSO, G., BERNACCHIA, A., GEIMER, S., TONDERA, D., MARTINOU, J. C., WESTERMANN, B., RUGARLI, E. I. & LANGER, T. 2009. Regulation of OPA1 processing and mitochondrial fusion by m-AAA protease isoenzymes and OMA1. *J Cell Biol,* 187**,** 1023-36.

ELBASHIR, S. M., MARTINEZ, J., PATKANIOWSKA, A., LENDECKEL, W. & TUSCHL, T. 2001. Functional anatomy of siRNAs for mediating efficient RNAi in Drosophila melanogaster embryo lysate. *Embo j,* 20**,** 6877-88.

EPSTEIN, A. C. R., GLEADLE, J. M., MCNEILL, L. A., HEWITSON, K. S., O'ROURKE, J., MOLE, D. R., MUKHERJI, M., METZEN, E., WILSON, M. I., DHANDA, A., TIAN, Y.-M., MASSON, N., HAMILTON, D. L., JAAKKOLA, P., BARSTEAD, R., HODGKIN, J., MAXWELL, P. H., PUGH, C. W., SCHOFIELD, C. J. & RATCLIFFE, P. J. 2001. C. elegans EGL-9 and Mammalian Homologs Define a Family of Dioxygenases that Regulate HIF by Prolyl Hydroxylation. *Cell,* 107**,** 43-54.

ERNSTER, L. & SCHATZ, G. 1981. Mitochondria: a historical review. *J Cell Biol,* 91**,** 227s-255s.

EVERETT, R. D., BOUTELL, C. & HALE, B. G. 2013. Interplay between viruses and host sumoylation pathways. *Nature Reviews Microbiology,* 11**,** 400.

EVERSE, J. & KAPLAN, N. O. 1973. Lactate dehydrogenases: structure and function. *Adv Enzymol Relat Areas Mol Biol,* 37**,** 61-133.

EXNER, N., TRESKE, B., PAQUET, D., HOLMSTROM, K., SCHIESLING, C., GISPERT, S., CARBALLO-CARBAJAL, I., BERG, D., HOEPKEN, H. H., GASSER, T., KRUGER, R., WINKLHOFER, K. F., VOGEL, F., REICHERT, A. S., AUBURGER, G., KAHLE, P. J., SCHMID, B. & HAASS, C. 2007. Loss-of-function of human PINK1 results in mitochondrial pathology and can be rescued by parkin. *J Neurosci,* 27**,** 12413-8.

FAELBER, K., GAO, S., HELD, M., POSOR, Y., HAUCKE, V., NOE, F. & DAUMKE, O. 2013. Oligomerization of dynamin superfamily proteins in health and disease. *Prog Mol Biol Transl Sci,* 117**,** 411-43.

FAN, W., CAI, W., PARIMOO, S., LENNON, G. G. & WEISSMAN, S. M. 1996. Identification of seven new humanMHC class I region genes around theHLA-F locus. *Immunogenetics,* 44**,** 97-103.

FAULKNER, A., PURCELL, R., HIBBERT, A., LATHAM, S., THOMSON, S., HALL, W. L., WHEELER-JONES, C. & BISHOP-BAILEY, D. 2014. A thin layer angiogenesis assay: a modified basement matrix assay for assessment of endothelial cell differentiation. *BMC Cell Biol,* 15**,** 41.

FIELDS, S. & SONG, O. 1989. A novel genetic system to detect protein-protein interactions. *Nature,* 340**,** 245-6.

FIESEL, F. C., ANDO, M., HUDEC, R., HILL, A. R., CASTANEDES-CASEY, M., CAULFIELD, T. R., MOUSSAUD-LAMODIERE, E. L., STANKOWSKI, J. N., BAUER, P. O., LORENZO-BETANCOR, O., FERRER, I., ARBELO, J. M., SIUDA, J., CHEN, L., DAWSON, V. L., DAWSON, T. M., WSZOLEK, Z. K., ROSS, O. A., DICKSON, D. W. & SPRINGER, W. 2015. (Patho-)physiological relevance of PINK1-dependent ubiquitin phosphorylation. *EMBO Rep,* 16**,** 1114-30.

FIGUEROA-ROMERO, C., INIGUEZ-LLUHI, J. A., STADLER, J., CHANG, C. R., ARNOULT, D., KELLER, P. J., HONG, Y., BLACKSTONE, C. & FELDMAN, E. L. 2009. SUMOylation of the mitochondrial fission protein Drp1 occurs at multiple nonconsensus sites within the B domain and is linked to its activity cycle. *Faseb j,* 23**,** 3917-27.

FINEGAN, B. A., LOPASCHUK, G. D., GANDHI, M. & CLANACHAN, A. S. 1995. Ischemic preconditioning inhibits glycolysis and proton production in isolated working rat hearts. *Am J Physiol,* 269**,** H1767-75.

FINLEY, D. 2009. Recognition and processing of ubiquitin-protein conjugates by the proteasome. *Annu Rev Biochem,* 78**,** 477-513.

FINNEY, N., WALTHER, F., MANTEL, P. Y., STAUFFER, D., ROVELLI, G. & DEV, K. K. 2003. The cellular protein level of parkin is regulated by its ubiquitin-like domain. *J Biol Chem,* 278**,** 16054-8.

FLOTHO, A. & MELCHIOR, F. 2013. Sumoylation: A Regulatory Protein Modification in Health and Disease. *Annual Review of Biochemistry,* 82**,** 357-385.

FORINI, F., UCCIFERRI, N., KUSMIC, C., NICOLINI, G., CECCHETTINI, A., ROCCHICCIOLI, S., CITTI, L. & IERVASI, G. 2015. Low T3 State Is Correlated with Cardiac Mitochondrial Impairments after Ischemia Reperfusion Injury: Evidence from a Proteomic Approach. *Int J Mol Sci,* 16**,** 26687-705.

FRANK, S., GAUME, B., BERGMANN-LEITNER, E. S., LEITNER, W. W., ROBERT, E. G., CATEZ, F., SMITH, C. L. & YOULE, R. J. 2001. The role of dynamin-related protein 1, a mediator of mitochondrial fission, in apoptosis. *Dev Cell,* 1**,** 515-25.

FRIEDMAN, J. R., LACKNER, L. L., WEST, M., DIBENEDETTO, J. R., NUNNARI, J. & VOELTZ, G. K. 2011. ER Tubules Mark Sites of Mitochondrial Division. *Science (New York, N.y.),* 334**,** 358-362.

FRÖHLICH, C., GRABIGER, S., SCHWEFEL, D., FAELBER, K., ROSENBAUM, E., MEARS, J., ROCKS, O. & DAUMKE, O. 2013. Structural insights into oligomerization and mitochondrial remodelling of dynamin 1-like protein. *The EMBO Journal,* 32**,** 1280.

GALISSON, F., MAHROUCHE, L., COURCELLES, M., BONNEIL, E., MELOCHE, S., CHELBI-ALIX, M. K. & THIBAULT, P. 2011. A novel proteomics approach to identify SUMOylated proteins and their modification sites in human cells. *Mol Cell Proteomics,* 10**,** M110.004796.

GANDRE-BABBE, S., VAN DER BLIEK, A. M. & SHAW, J. 2008. The Novel Tail-anchored Membrane Protein Mff Controls Mitochondrial and Peroxisomal Fission in Mammalian Cells. *Molecular Biology of the Cell,* 19**,** 2402-2412.

GAO, J., QIN, S. & JIANG, C. 2015. Parkin-induced ubiquitination of Mff promotes its association with p62/SQSTM1 during mitochondrial depolarization. *Acta Biochim Biophys Sin (Shanghai),* 47**,** 522-9.

GAO, L., ZHAO, Y., HE, J., YAN, Y., XU, L., LIN, N., JI, Q., TONG, R., FU, Y., GAO, Y., SU, Y., YUAN, A., HE, B. & PU, J. 2018. The desumoylating enzyme sentrin-specific protease 3 contributes to myocardial ischemia reperfusion injury. *J Genet Genomics,* 45**,** 125-135.

GAREAU, J. R. & LIMA, C. D. 2010. The SUMO pathway: emerging mechanisms that shape specificity, conjugation and recognition. *Nat Rev Mol Cell Biol,* 11**,** 861-71.

GAUCI, S., HELBIG, A. O., SLIJPER, M., KRIJGSVELD, J., HECK, A. J. & MOHAMMED, S. 2009. Lys-N and trypsin cover complementary parts of the phosphoproteome in a refined SCX-based approach. *Anal Chem,* 81**,** 4493-501.

GEISLER, S., HOLMSTROM, K. M., SKUJAT, D., FIESEL, F. C., ROTHFUSS, O. C., KAHLE, P. J. & SPRINGER, W. 2010. PINK1/Parkin-mediated mitophagy is dependent on VDAC1 and p62/SQSTM1. *Nat Cell Biol,* 12**,** 119-31.

GEISS-FRIEDLANDER, R. & MELCHIOR, F. 2007. Concepts in sumoylation: a decade on. *Nat Rev Mol Cell Biol,* 8**,** 947-56.

GEORGE, S., WANG, S. M., BI, Y., TREIDLINGER, M., BARBER, K. R., SHAW, G. S. & O'DONOGHUE, P. 2017. Ubiquitin phosphorylated at Ser57 hyper-activates parkin. *Biochim Biophys Acta,* 1861**,** 3038-3046.

GLADKOVA, C., MASLEN, S. L., SKEHEL, J. M. & KOMANDER, D. 2018. Mechanism of parkin activation by PINK1. *Nature,* 559**,** 410-414.

GÖKTEPE, S., ABILEZ, O. J., PARKER, K. K. & KUHL, E. 2010. A multiscale model for eccentric and concentric cardiac growth through sarcomerogenesis. *Journal of Theoretical Biology,* 265**,** 433-442.

GOLEBIOWSKI, F., MATIC, I., TATHAM, M. H., COLE, C., YIN, Y., NAKAMURA, A., COX, J., BARTON, G. J., MANN, M. & HAY, R. T. 2009. System-wide changes to SUMO modifications in response to heat shock. *Sci Signal,* 2**,** ra24.

GOMES, L. C. & SCORRANO, L. 2008. High levels of Fis1, a pro-fission mitochondrial protein, trigger autophagy. *Biochimica et Biophysica Acta (BBA) - Bioenergetics,* 1777**,** 860-866.

GONG, G., SONG, M., CSORDAS, G., KELLY, D. P., MATKOVICH, S. J. & DORN, G. W., 2ND 2015. Parkin-mediated mitophagy directs perinatal cardiac metabolic maturation in mice. *Science,* 350**,** aad2459.

GONG, L., LI, B., MILLAS, S. & YEH, E. T. 1999. Molecular cloning and characterization of human AOS1 and UBA2, components of the sentrin-activating enzyme complex. *FEBS Lett,* 448**,** 185-9.

GONG, L. & YEH, E. T. 2006. Characterization of a family of nucleolar SUMO-specific proteases with preference for SUMO-2 or SUMO-3. *J Biol Chem,* 281**,** 15869-77.

GRAY, M. W. 1992. The Endosymbiont Hypothesis Revisited. *In:* WOLSTENHOLME, D. R. & JEON, K. W. (eds.) *International Review of Cytology.* Academic Press.

GREENE, A. W., GRENIER, K., AGUILETA, M. A., MUISE, S., FARAZIFARD, R., HAQUE, M. E., MCBRIDE, H. M., PARK, D. S. & FON, E. A. 2012. Mitochondrial processing peptidase regulates PINK1 processing, import and Parkin recruitment. *EMBO Reports,* 13**,** 378-385.

GREENE, J. C., WHITWORTH, A. J., KUO, I., ANDREWS, L. A., FEANY, M. B. & PALLANCK, L. J. 2003. Mitochondrial pathology and apoptotic muscle degeneration in Drosophila parkin mutants. *Proc Natl Acad Sci U S A,* 100**,** 4078-83.

GREGOIRE, S. & YANG, X. J. 2005. Association with class IIa histone deacetylases upregulates the sumoylation of MEF2 transcription factors. *Mol Cell Biol,* 25**,** 2273-87.

GRIFFITHS, E. J. & HALESTRAP, A. P. 1995. Mitochondrial non-specific pores remain closed during cardiac ischaemia, but open upon reperfusion. *Biochem J,* 307 (Pt 1)**,** 93-8.

GRIPARIC, L., KANAZAWA, T. & VAN DER BLIEK, A. M. 2007. Regulation of the mitochondrial dynamin-like protein Opa1 by proteolytic cleavage. *J Cell Biol,* 178**,** 757-64.

GUO, C. & HENLEY, J. M. 2014. Wrestling with stress: roles of protein SUMOylation and deSUMOylation in cell stress response. *IUBMB Life,* 66**,** 71-7.

GUO, C., HILDICK, K. L., LUO, J., DEARDEN, L., WILKINSON, K. A. & HENLEY, J. M. 2013. SENP3-mediated deSUMOylation of dynamin-related protein 1 promotes cell death following ischaemia. *Embo j,* 32**,** 1514-28.

GUO, C., WILKINSON, K. A., EVANS, A. J., RUBIN, P. P. & HENLEY, J. M. 2017. SENP3-mediated deSUMOylation of Drp1 facilitates interaction with Mff to promote cell death. *Sci Rep,* 7**,** 43811.

GUZZO, C. M., BERNDSEN, C. E., ZHU, J., GUPTA, V., DATTA, A., GREENBERG, R. A., WOLBERGER, C. & MATUNIS, M. J. 2012. RNF4-Dependent Hybrid SUMO-Ubiquitin Chains are Signals for RAP80 and thereby Mediate the Recruitment of BRCA1 to Sites of DNA Damage. *Science signaling,* 5**,** ra88-ra88.

HAAS, A. L. & BRIGHT, P. M. 1988. The resolution and characterization of putative ubiquitin carrier protein isozymes from rabbit reticulocytes. *J Biol Chem,* 263**,** 13258-67.

HAAS, A. L., BRIGHT, P. M. & JACKSON, V. E. 1988. Functional diversity among putative E2 isozymes in the mechanism of ubiquitin-histone ligation. *J Biol Chem,* 263**,** 13268-75.

HAAS, A. L. & ROSE, I. A. 1982. The mechanism of ubiquitin activating enzyme. A kinetic and equilibrium analysis. *J Biol Chem,* 257**,** 10329-37.

HAAS, A. L., WARMS, J. V., HERSHKO, A. & ROSE, I. A. 1982. Ubiquitin-activating enzyme. Mechanism and role in protein-ubiquitin conjugation. *J Biol Chem,* 257**,** 2543-8.

HAGAR, J. M., HALE, S. L. & KLONER, R. A. 1991. Effect of preconditioning ischemia on reperfusion arrhythmias after coronary artery occlusion and reperfusion in the rat. *Circulation Research,* 68**,** 61.

HAGLUND, K., SIGISMUND, S., POLO, S., SZYMKIEWICZ, I., DI FIORE, P. P. & DIKIC, I. 2003. Multiple monoubiquitination of RTKs is sufficient for their endocytosis and degradation. *Nat Cell Biol,* 5**,** 461-6.

HALESTRAP, A. P. 1999. The mitochondrial permeability transition: its molecular mechanism and role in reperfusion injury. *Biochemical Society Symposium,* 66**,** 181.

HALESTRAP, ANDREW P. 2010. A pore way to die: the role of mitochondria in reperfusion injury and cardioprotection. *Biochemical Society Transactions,* 38**,** 841.

HALESTRAP, A. P., PEREIRA, G. C. & PASDOIS, P. 2015. The role of hexokinase in cardioprotection – mechanism and potential for translation. *British Journal of Pharmacology,* 172**,** 2085-2100.

HAN, X. J., LU, Y. F., LI, S. A., KAITSUKA, T., SATO, Y., TOMIZAWA, K., NAIRN, A. C., TAKEI, K., MATSUI, H. & MATSUSHITA, M. 2008. CaM kinase I alpha-induced phosphorylation of Drp1 regulates mitochondrial morphology. *J Cell Biol,* 182**,** 573-85.

HANG, J. & DASSO, M. 2002. Association of the human SUMO-1 protease SENP2 with the nuclear pore. *J Biol Chem,* 277**,** 19961-6.

HANNICH, J. T., LEWIS, A., KROETZ, M. B., LI, S. J., HEIDE, H., EMILI, A. & HOCHSTRASSER, M. 2005. Defining the SUMO-modified proteome by multiple approaches in Saccharomyces cerevisiae. *J Biol Chem,* 280**,** 4102-10.

HARDER, Z., ZUNINO, R. & MCBRIDE, H. 2004. Sumo1 Conjugates Mitochondrial Substrates and Participates in Mitochondrial Fission. *Current Biology,* 14**,** 340-345.

HASSANPOUR, S. H., DEHGHANI, M. A. & KARAMI, S. Z. 2018. Study of respiratory chain dysfunction in heart disease. *J Cardiovasc Thorac Res,* 10**,** 1-13.

HATCH, A. L., GUREL, P. S. & HIGGS, H. N. 2014. Novel roles for actin in mitochondrial fission. *Journal of Cell Science,* 127**,** 4549.

HAUSENLOY, D. J. & YELLON, D. M. 2013. Myocardial ischemia-reperfusion injury: a neglected therapeutic target. *The Journal of Clinical Investigation,* 123**,** 92-100.

HAY, R. T. 2005. SUMO: a history of modification. *Mol Cell,* 18**,** 1-12.

HAYASHI, T., RIZZUTO, R., HAJNOCZKY, G. & SU, T. P. 2009. MAM: more than just a housekeeper. *Trends Cell Biol,* 19**,** 81-8.

HAYASHI, T., SEKI, M., MAEDA, D., WANG, W., KAWABE, Y., SEKI, T., SAITOH, H., FUKAGAWA, T., YAGI, H. & ENOMOTO, T. 2002. Ubc9 is essential for viability of higher eukaryotic cells. *Exp Cell Res,* 280**,** 212-21.

HEAD, B., GRIPARIC, L., AMIRI, M., GANDRE-BABBE, S. & VAN DER BLIEK, A. M. 2009. Inducible proteolytic inactivation of OPA1 mediated by the OMA1 protease in mammalian cells. *J Cell Biol,* 187**,** 959-66.

HEARSE, D. J., HUMPHREY, S. M. & CHAIN, E. B. 1973. Abrupt reoxygenation of the anoxic potassium-arrested perfused rat heart: a study of myocardial enzyme release. *J Mol Cell Cardiol,* 5**,** 395-407.

HECKER, C. M., RABILLER, M., HAGLUND, K., BAYER, P. & DIKIC, I. 2006. Specification of SUMO1- and SUMO2-interacting motifs. *J Biol Chem,* 281**,** 16117-27.

HENDRIKS, I. A., D'SOUZA, R. C., YANG, B., VERLAAN-DE VRIES, M., MANN, M. & VERTEGAAL, A. C. 2014. Uncovering global SUMOylation signaling networks in a site-specific manner. *Nat Struct Mol Biol,* 21**,** 927-36.

HERIDE, C., URBÉ, S. & CLAGUE, M. J. 2014. Ubiquitin code assembly and disassembly. *Current Biology,* 24**,** R215-R220.

HERRMANN, J. M. & NEUPERT, W. 2000. Protein transport into mitochondria. *Curr Opin Microbiol,* 3**,** 210-4.

HERSHKO, A. & CIECHANOVER, A. 1998. The ubiquitin system. *Annu Rev Biochem,* 67**,** 425-79.

HERSHKO, A., CIECHANOVER, A., HELLER, H., HAAS, A. L. & ROSE, I. A. 1980. Proposed role of ATP in protein breakdown: conjugation of protein with multiple chains of the polypeptide of ATP-dependent proteolysis. *Proc Natl Acad Sci U S A,* 77**,** 1783-6.

HERSHKO, A., HELLER, H., ELIAS, S. & CIECHANOVER, A. 1983. Components of ubiquitin-protein ligase system. Resolution, affinity purification, and role in protein breakdown. *J Biol Chem,* 258**,** 8206-14.

HESCHELER, J., MEYER, R., PLANT, S., KRAUTWURST, D., ROSENTHAL, W. & SCHULTZ, G. 1991. Morphological, biochemical, and electrophysiological characterization of a clonal cell (H9c2) line from rat heart. *Circ Res,* 69**,** 1476-86.

HIETAKANGAS, V., AHLSKOG, J. K., JAKOBSSON, A. M., HELLESUO, M., SAHLBERG, N. M., HOLMBERG, C. I., MIKHAILOV, A., PALVIMO, J. J., PIRKKALA, L. & SISTONEN, L. 2003. Phosphorylation of serine 303 is a prerequisite for the stress-inducible SUMO modification of heat shock factor 1. *Mol Cell Biol,* 23**,** 2953-68.

HIETAKANGAS, V., ANCKAR, J., BLOMSTER, H. A., FUJIMOTO, M., PALVIMO, J. J., NAKAI, A. & SISTONEN, L. 2006. PDSM, a motif for phosphorylation-dependent SUMO modification. *Proceedings of the National Academy of Sciences of the United States of America,* 103**,** 45-50.

HIPP, M. S., KALVERAM, B., RAASI, S., GROETTRUP, M. & SCHMIDTKE, G. 2005. FAT10, a ubiquitin-independent signal for proteasomal degradation. *Mol Cell Biol,* 25**,** 3483-91.

HJERPE, R., THOMAS, Y., CHEN, J., ZEMLA, A., CURRAN, S., SHPIRO, N., DICK, L. R. & KURZ, T. 2012. Changes in the ratio of free NEDD8 to ubiquitin triggers NEDDylation by ubiquitin enzymes. *Biochem J,* 441**,** 927-36.

HO, M. S., TSAI, P. I. & CHIEN, C. T. 2006. F-box proteins: the key to protein degradation. *J Biomed Sci,* 13**,** 181-91.

HOCHSTRASSER, M. 2009. Origin and Function of Ubiquitin-like Protein Conjugation. *Nature,* 458**,** 422.

HOEPFNER, D., SCHILDKNEGT, D., BRAAKMAN, I., PHILIPPSEN, P. & TABAK, H. F. 2005. Contribution of the endoplasmic reticulum to peroxisome formation. *Cell,* 122**,** 85-95.

HOFMANN, R. M. & PICKART, C. M. 1999. Noncanonical MMS2-encoded ubiquitin-conjugating enzyme functions in assembly of novel polyubiquitin chains for DNA repair. *Cell,* 96**,** 645-53.

HOLSCHER, M., SILTER, M., KRULL, S., VON AHLEN, M., HESSE, A., SCHWARTZ, P., WIELOCKX, B., BREIER, G., KATSCHINSKI, D. M. & ZIESENISS, A. 2011. Cardiomyocyte-specific prolyl-4-hydroxylase domain 2 knock out protects from acute myocardial ischemic injury. *J Biol Chem,* 286**,** 11185-94.

HOM, J. & SHEU, S.-S. 2009. Morphological dynamics of mitochondria — A special emphasis on cardiac muscle cells. *Journal of Molecular and Cellular Cardiology,* 46**,** 811-820.

HOM JENNIFER, R., GEWANDTER JENNIFER, S., MICHAEL, L., SHEU, S.-S. & YOON, Y. 2007. Thapsigargin induces biphasic fragmentation of mitochondria through calcium-mediated mitochondrial fission and apoptosis. *Journal of Cellular Physiology,* 212**,** 498-508.

HOPPINS, S., LACKNER, L. & NUNNARI, J. 2007. The machines that divide and fuse mitochondria. *Annu Rev Biochem,* 76**,** 751-80.

HOSPENTHAL, M. K., MEVISSEN, T. E. T. & KOMANDER, D. 2015. Deubiquitinase-based analysis of ubiquitin chain architecture using Ubiquitin Chain Restriction (UbiCRest). *Nature Protocols,* 10**,** 349.

HSIAO, H. H., MEULMEESTER, E., FRANK, B. T., MELCHIOR, F. & URLAUB, H. 2009. "ChopNSpice," a mass spectrometric approach that allows identification of endogenous small ubiquitin-like modifier-conjugated peptides. *Mol Cell Proteomics,* 8**,** 2664-75.

HUANG, C., HAN, Y., WANG, Y., SUN, X., YAN, S., YEH, E. T., CHEN, Y., CANG, H., LI, H., SHI, G., CHENG, J., TANG, X. & YI, J. 2009. SENP3 is responsible for HIF-1 transactivation under mild oxidative stress via p300 de-SUMOylation. *Embo j,* 28**,** 2748-62.

HUANG, D. T., HUNT, H. W., ZHUANG, M., OHI, M. D., HOLTON, J. M. & SCHULMAN, B. A. 2007. Basis for a ubiquitin-like protein thioester switch toggling E1-E2 affinity. *Nature,* 445**,** 394-8.

IMAM, S. Z., ZHOU, Q., YAMAMOTO, A., VALENTE, A. J., ALI, S. F., BAINS, M., ROBERTS, J. L., KAHLE, P. J., CLARK, R. A. & LI, S. 2011. Novel Regulation of Parkin Function through c-Abl-Mediated Tyrosine Phosphorylation: Implications for Parkinson's Disease. *The Journal of Neuroscience,* 31**,** 157.

IMOTO, M., TACHIBANA, I. & URRUTIA, R. 1998. Identification and functional characterization of a novel human protein highly related to the yeast dynamin-like GTPase Vps1p. *Journal of Cell Science,* 111**,** 1341-1349.

INGERMAN, E., PERKINS, E. M., MARINO, M., MEARS, J. A., MCCAFFERY, J. M., HINSHAW, J. E. & NUNNARI, J. 2005. Dnm1 forms spirals that are structurally tailored to fit mitochondria. *The Journal of Cell Biology,* 170**,** 1021.

ISHIHARA, N., NOMURA, M., JOFUKU, A., KATO, H., SUZUKI, S. O., MASUDA, K., OTERA, H., NAKANISHI, Y., NONAKA, I., GOTO, Y., TAGUCHI, N., MORINAGA, H., MAEDA, M., TAKAYANAGI, R., YOKOTA, S. & MIHARA, K. 2009. Mitochondrial fission factor Drp1 is essential for embryonic development and synapse formation in mice. *Nat Cell Biol,* 11**,** 958-66.

IYER, L. M., BURROUGHS, A. M. & ARAVIND, L. 2006. The prokaryotic antecedents of the ubiquitin-signaling system and the early evolution of ubiquitin-like beta-grasp domains. *Genome Biol,* 7**,** R60.

IYER, L. M., KOONIN, E. V. & ARAVIND, L. 2004. Novel predicted peptidases with a potential role in the ubiquitin signaling pathway. *Cell Cycle,* 3**,** 1440-50.

JACKSON, S. P. & DUROCHER, D. 2013. Regulation of DNA damage responses by ubiquitin and SUMO. *Mol Cell,* 49**,** 795-807.

JASOVA, M., KANCIROVA, I., WACZULIKOVA, I. & FERKO, M. 2017. Mitochondria as a target of cardioprotection in models of preconditioning. *J Bioenerg Biomembr,* 49**,** 357-368.

JIN, J., LI, X., GYGI, S. P. & HARPER, J. W. 2007. Dual E1 activation systems for ubiquitin differentially regulate E2 enzyme charging. *Nature,* 447**,** 1135-8.

JIN, L., WILLIAMSON, A., BANERJEE, S., PHILIPP, I. & RAPE, M. 2008. Mechanism of ubiquitin-chain formation by the human anaphase-promoting complex. *Cell,* 133**,** 653-65.

JIN, S. M., LAZAROU, M., WANG, C., KANE, L. A., NARENDRA, D. P. & YOULE, R. J. 2010. Mitochondrial membrane potential regulates PINK1 import and proteolytic destabilization by PARL. *The Journal of Cell Biology,* 191**,** 933-942.

JOHNSON, E. S. 2004. Protein modification by SUMO. *Annu Rev Biochem,* 73**,** 355-82.

JOHNSON, E. S., MA, P. C. M., OTA, I. M. & VARSHAVSKY, A. 1995. A Proteolytic Pathway That Recognizes Ubiquitin as a Degradation Signal. *Journal of Biological Chemistry,* 270**,** 17442-17456.

JOHNSON, E. S., SCHWIENHORST, I., DOHMEN, R. J. & BLOBEL, G. 1997. The ubiquitin-like protein Smt3p is activated for conjugation to other proteins by an Aos1p/Uba2p heterodimer. *Embo j,* 16**,** 5509-19.

JOSHI, A. U., SAW, N. L., SHAMLOO, M. & MOCHLY-ROSEN, D. 2018. Drp1/Fis1 interaction mediates mitochondrial dysfunction, bioenergetic failure and cognitive decline in Alzheimer's disease. *Oncotarget,* 9**,** 6128-6143.

KABEYA, Y., MIZUSHIMA, N., UENO, T., YAMAMOTO, A., KIRISAKO, T., NODA, T., KOMINAMI, E., OHSUMI, Y. & YOSHIMORI, T. 2000. LC3, a mammalian homologue of yeast Apg8p, is localized in autophagosome membranes after processing. *Embo j,* 19**,** 5720-8.

KAGEYAMA, Y., ZHANG, Z., RODA, R., FUKAYA, M., WAKABAYASHI, J., WAKABAYASHI, N., KENSLER, T. W., REDDY, P. H., IIJIMA, M. & SESAKI, H. 2012. Mitochondrial division ensures the survival of postmitotic neurons by suppressing oxidative damage. *J Cell Biol,* 197**,** 535-51.

KAISER, S. E., RILEY, B. E., SHALER, T. A., TREVINO, R. S., BECKER, C. H., SCHULMAN, H. & KOPITO, R. R. 2011. Protein standard absolute quantification (PSAQ) method for the measurement of cellular ubiquitin pools. *Nature Methods,* 8**,** 691.

KALOGERIS, T., BAO, Y. & KORTHUIS, R. J. 2014. Mitochondrial reactive oxygen species: a double edged sword in ischemia/reperfusion vs preconditioning. *Redox Biol,* 2**,** 702-14.

KALRA, D. K. & ZOGHBI, W. A. 2002. Myocardial hibernation in coronary artery disease. *Current Atherosclerosis Reports,* 4**,** 149-155.

KAMITANI, T., KITO, K., NGUYEN, H. P., WADA, H., FUKUDA-KAMITANI, T. & YEH, E. T. H. 1998. Identification of Three Major Sentrinization Sites in PML. *Journal of Biological Chemistry,* 273**,** 26675-26682.

KAMITANI, T., KITO, K., NGUYEN, H. P. & YEH, E. T. 1997a. Characterization of NEDD8, a developmentally down-regulated ubiquitin-like protein. *J Biol Chem,* 272**,** 28557-62.

KAMITANI, T., NGUYEN, H. P. & YEH, E. T. 1997b. Preferential modification of nuclear proteins by a novel ubiquitin-like molecule. *J Biol Chem,* 272**,** 14001-4.

KANNER, S. A., MORGENSTERN, T. & COLECRAFT, H. M. 2017. Sculpting ion channel functional expression with engineered ubiquitin ligases. *Elife,* 6.

KAPLAN, L. J., BELLOWS, C. F., BLUM, H., MITCHELL, M. & WHITMAN, G. J. R. 1994. Ischemic Preconditioning Preserves End-Ischemic ATP, Enhancing Functional Recovery and Coronary Flow during Reperfusion. *Journal of Surgical Research,* 57**,** 179-184.

KARBOWSKI, M., NEUTZNER, A. & YOULE, R. J. 2007. The mitochondrial E3 ubiquitin ligase MARCH5 is required for Drp1 dependent mitochondrial division. *J Cell Biol,* 178**,** 71-84.

KEE, Y. & HUIBREGTSE, J. M. 2007. Regulation of catalytic activities of HECT ubiquitin ligases. *Biochem Biophys Res Commun,* 354**,** 329-33.

KEELING, P. J. & ARCHIBALD, J. M. 2008. Organelle evolution: what's in a name? *Curr Biol,* 18**,** R345-7.

KERNER, J., LEE, K., TANDLER, B. & HOPPEL, C. L. 2012. VDAC proteomics: post-translation modifications. *Biochim Biophys Acta,* 1818**,** 1520-5.

KERSCHER, O. 2007. SUMO junction—what's your function? New insights through SUMO-interacting motifs. *EMBO Reports,* 8**,** 550-555.

KESSLER, J. D., KAHLE, K. T., SUN, T., MEERBREY, K. L., SCHLABACH, M. R., SCHMITT, E. M., SKINNER, S. O., XU, Q., LI, M. Z., HARTMAN, Z. C., RAO, M., YU, P., DOMINGUEZ-VIDANA, R., LIANG, A. C., SOLIMINI, N. L., BERNARDI, R. J., YU, B., HSU, T., GOLDING, I., LUO, J., OSBORNE, C. K., CREIGHTON, C. J., HILSENBECK, S. G., SCHIFF, R., SHAW, C. A., ELLEDGE, S. J. & WESTBROOK, T. F. 2012. A SUMOylation-Dependent

Transcriptional Subprogram Is Required for Myc-Driven Tumorigenesis. *Science,* 335**,** 348.

KHO, C., LEE, A., JEONG, D., OH, J. G., CHAANINE, A. H., KIZANA, E., PARK, W. J. & HAJJAR, R. J. 2011. SUMO1-dependent modulation of SERCA2a in heart failure. *Nature,* 477**,** 601.

KIM, J.-W., TCHERNYSHYOV, I., SEMENZA, G. L. & DANG, C. V. 2006a. HIF-1-mediated expression of pyruvate dehydrogenase kinase: A metabolic switch required for cellular adaptation to hypoxia. *Cell Metabolism,* 3**,** 177-185.

KIM, N., LEE, Y., KIM, H., JOO, H., YOUM, J. B., PARK, W. S., WARDA, M., CUONG, D. V. & HAN, J. 2006b. Potential biomarkers for ischemic heart damage identified in mitochondrial proteins by comparative proteomics. *Proteomics,* 6**,** 1237-49.

KIM, P. K., HAILEY, D. W., MULLEN, R. T. & LIPPINCOTT-SCHWARTZ, J. 2008a. Ubiquitin signals autophagic degradation of cytosolic proteins and peroxisomes. *Proceedings of the National Academy of Sciences,* 105**,** 20567.

KIM, Y., PARK, J., KIM, S., SONG, S., KWON, S. K., LEE, S. H., KITADA, T., KIM, J. M. & CHUNG, J. 2008b. PINK1 controls mitochondrial localization of Parkin through direct phosphorylation. *Biochem Biophys Res Commun,* 377**,** 975-80.

KIMES, B. W. & BRANDT, B. L. 1976. Properties of a clonal muscle cell line from rat heart. *Exp Cell Res,* 98**,** 367-81.

KIPREOS, E. T. & PAGANO, M. 2000. The F-box protein family. *Genome Biol,* 1**,** Reviews3002.

KIRK, R., LAMAN, H., KNOWLES, P. P., MURRAY-RUST, J., LOMONOSOV, M., MEZIANE EL, K. & MCDONALD, N. Q. 2008. Structure of a conserved dimerization domain within the F-box protein Fbxo7 and the PI31 proteasome inhibitor. *J Biol Chem,* 283**,** 22325-35.

KLINGE, C. M. 2008. Estrogenic control of mitochondrial function and biogenesis. *J Cell Biochem,* 105**,** 1342-51.

KOCH, A., THIEMANN, M., GRABENBAUER, M., YOON, Y., MCNIVEN, M. A. & SCHRADER, M. 2003. Dynamin-like Protein 1 Is Involved in Peroxisomal Fission. *Journal of Biological Chemistry,* 278**,** 8597-8605.

KOCH, S., DELLA-MORTE, D., DAVE, K. R., SACCO, R. L. & PEREZ-PINZON, M. A. 2014. Biomarkers for ischemic preconditioning: finding the responders. *J Cereb Blood Flow Metab,* 34**,** 933-41.

KOIRALA, S., GUO, Q., KALIA, R., BUI, H. T., ECKERT, D. M., FROST, A. & SHAW, J. M. 2013. Interchangeable adaptors regulate mitochondrial dynamin assembly for membrane scission. *Proceedings of the National Academy of Sciences,* 110**,** E1342.

KOLLI, N., MIKOLAJCZYK, J., DRAG, M., MUKHOPADHYAY, D., MOFFATT, N., DASSO, M., SALVESEN, G. & WILKINSON, KEITH D. 2010. Distribution and paralogue specificity of mammalian deSUMOylating enzymes. *Biochemical Journal,* 430**,** 335.

KOMANDER, D. 2009. The emerging complexity of protein ubiquitination. *Biochemical Society Transactions,* 37**,** 937.

KOMANDER, D., CLAGUE, M. J. & URBE, S. 2009a. Breaking the chains: structure and function of the deubiquitinases. *Nat Rev Mol Cell Biol,* 10**,** 550-63.

KOMANDER, D. & RAPE, M. 2012. The ubiquitin code. *Annu Rev Biochem,* 81**,** 203-29.

KOMANDER, D., REYES-TURCU, F., LICCHESI, J. D., ODENWAELDER, P., WILKINSON, K. D. & BARFORD, D. 2009b. Molecular discrimination of structurally equivalent Lys 63-linked and linear polyubiquitin chains. *EMBO Rep,* 10**,** 466-73.

KONOPACKI, F. A., JAAFARI, N., ROCCA, D. L., WILKINSON, K. A., CHAMBERLAIN, S., RUBIN, P., KANTAMNENI, S., MELLOR, J. R. & HENLEY, J. M. 2011. Agonist-induced PKC phosphorylation regulates GluK2 SUMOylation and kainate receptor endocytosis. *Proc Natl Acad Sci U S A,* 108**,** 19772-7.

KOONIN, E. V. 2010. The origin and early evolution of eukaryotes in the light of phylogenomics. *Genome Biology,* 11**,** 209-209.

KOROBOVA, F., GAUVIN, T. J. & HIGGS, H. N. 2014. A role for myosin II in mammalian mitochondrial fission. *Curr Biol,* 24**,** 409-14.

KRAUS, F. & RYAN, M. T. 2017. The constriction and scission machineries involved in mitochondrial fission. *Journal of Cell Science,* 130**,** 2953.

KRUMOVA, P., MEULMEESTER, E., GARRIDO, M., TIRARD, M., HSIAO, H.-H., BOSSIS, G., URLAUB, H., ZWECKSTETTER, M., KÜGLER, S., MELCHIOR, F., BÄHR, M. & WEISHAUPT, J. H. 2011. Sumoylation inhibits α-synuclein aggregation and toxicity. *The Journal of Cell Biology,* 194**,** 49.

KUBLI, D. A., CORTEZ, M. Q., MOYZIS, A. G., NAJOR, R. H., LEE, Y. & GUSTAFSSON, A. B. 2015. PINK1 Is Dispensable for Mitochondrial Recruitment of Parkin and Activation of Mitophagy in Cardiac Myocytes. *PLoS One,* 10**,** e0130707.

KUBLI, D. A., QUINSAY, M. N. & GUSTAFSSON, A. B. 2013a. Parkin deficiency results in accumulation of abnormal mitochondria in aging myocytes. *Commun Integr Biol,* 6**,** e24511.

KUBLI, D. A., ZHANG, X., LEE, Y., HANNA, R. A., QUINSAY, M. N., NGUYEN, C. K., JIMENEZ, R., PETROSYAN, S., MURPHY, A. N. & GUSTAFSSON, A. B. 2013b. Parkin protein deficiency exacerbates cardiac injury and reduces survival following myocardial infarction. *J Biol Chem,* 288**,** 915-26.

KUIKEN, H. J., EGAN, D. A., LAMAN, H., BERNARDS, R., BEIJERSBERGEN, R. L. & DIRAC, A. M. 2012. Identification of F-box only protein 7 as a negative regulator of NF-kappaB signalling. *J Cell Mol Med,* 16**,** 2140-9.

KUNG, C. C., NAIK, M. T., WANG, S. H., SHIH, H. M., CHANG, C. C., LIN, L. Y., CHEN, C. L., MA, C., CHANG, C. F. & HUANG, T. H. 2014. Structural analysis of poly-SUMO chain recognition by the RNF4-SIMs domain. *Biochem J,* 462**,** 53-65.

KURODA, Y., MITSUI, T., KUNISHIGE, M., SHONO, M., AKAIKE, M., AZUMA, H. & MATSUMOTO, T. 2006. Parkin enhances mitochondrial biogenesis in proliferating cells. *Hum Mol Genet,* 15**,** 883-95.

KUZNETSOV, A. V., JAVADOV, S., SICKINGER, S., FROTSCHNIG, S. & GRIMM, M. 2015. H9c2 and HL-1 cells demonstrate distinct features of energy metabolism, mitochondrial function and sensitivity to hypoxia-reoxygenation. *Biochimica et biophysica acta,* 1853**,** 276-284.

LACKNER, L. L., HORNER, J. S. & NUNNARI, J. 2009. Mechanistic Analysis of a Dynamin Effector. *Science,* 325**,** 874.

LACKNER, L. L. & NUNNARI, J. M. 2009. The molecular mechanism and cellular functions of mitochondrial division. *Biochim Biophys Acta,* 1792**,** 1138-44.

LAGIER-TOURENNE, C., POLYMENIDOU, M., HUTT, K. R., VU, A. Q., BAUGHN, M., HUELGA, S. C., CLUTARIO, K. M., LING, S. C., LIANG, T. Y., MAZUR, C., WANCEWICZ, E., KIM, A. S., WATT, A., FREIER, S., HICKS, G. G., DONOHUE, J. P., SHIUE, L., BENNETT, C. F., RAVITS, J., CLEVELAND, D. W. & YEO, G. W. 2012. Divergent roles of ALS-linked proteins FUS/TLS and TDP-43 intersect in processing long pre-mRNAs. *Nat Neurosci,* 15**,** 1488-97.

LALLEMAND-BREITENBACH, V., JEANNE, M., BENHENDA, S., NASR, R., LEI, M., PERES, L., ZHOU, J., ZHU, J., RAUGHT, B. & DE THÉ, H. 2008. Arsenic degrades PML or PML–RARα through a SUMO-triggered RNF4/ubiquitin-mediated pathway. *Nature Cell Biology,* 10**,** 547.

LAMAN, H. 2006. Fbxo7 gets proactive with cyclin D/cdk6. *Cell Cycle,* 5**,** 279-82.

LAMAN, H., FUNES, J. M., YE, H., HENDERSON, S., GALINANES-GARCIA, L., HARA, E., KNOWLES, P., MCDONALD, N. & BOSHOFF, C. 2005. Transforming activity of Fbxo7 is mediated specifically through regulation of cyclin D/cdk6. *Embo j,* 24**,** 3104-16.

LAMOLIATTE, F., BONNEIL, E., DURETTE, C., CARON-LIZOTTE, O., WILDEMANN, D., ZERWECK, J., WENSHUK, H. & THIBAULT, P. 2013. Targeted identification of SUMOylation sites in human proteins using affinity enrichment and paralog-specific reporter ions. *Mol Cell Proteomics,* 12**,** 2536-50.

LANDO, D., PEET, D. J., GORMAN, J. J., WHELAN, D. A., WHITELAW, M. L. & BRUICK, R. K. 2002. FIH-1 is an asparaginyl hydroxylase enzyme that regulates the transcriptional activity of hypoxia-inducible factor. *Genes Dev,* 16**,** 1466-71.

LARSEN, K. & BENDIXEN, C. 2012. Characterization of the porcine FBX07 gene: the first step towards generation of a pig model for Parkinsonian pyramidal syndrome. *Mol Biol Rep,* 39**,** 1517-26.

LEBKOWSKI, J. S., CLANCY, S. & CALOS, M. P. 1985. Simian virus 40 replication in adenovirus-transformed human cells antagonizes gene expression. *Nature,* 317**,** 169-71.

LEBOUCHER, G. P., TSAI, Y. C., YANG, M., SHAW, K. C., ZHOU, M., VEENSTRA, T. D., GLICKMAN, M. H. & WEISSMAN, A. M. 2012. Stress-induced phosphorylation and proteasomal degradation of mitofusin 2 facilitates mitochondrial fragmentation and apoptosis. *Mol Cell,* 47**,** 547-57.

LEE, I. & SCHINDELIN, H. 2008. Structural insights into E1-catalyzed ubiquitin activation and transfer to conjugating enzymes. *Cell,* 134**,** 268-78.

LEE, J. E., WESTRATE, L. M., WU, H., PAGE, C. & VOELTZ, G. K. 2016. Multiple dynamin family members collaborate to drive mitochondrial division. *Nature,* 540**,** 139.

LEE, J. Y., NAGANO, Y., TAYLOR, J. P., LIM, K. L. & YAO, T. P. 2010. Disease-causing mutations in parkin impair mitochondrial ubiquitination, aggregation, and HDAC6-dependent mitophagy. *J Cell Biol,* 189**,** 671-9.

LEE, S., STERKY, F. H., MOURIER, A., TERZIOGLU, M., CULLHEIM, S., OLSON, L. & LARSSON, N. G. 2012a. Mitofusin 2 is necessary for striatal axonal projections of midbrain dopamine neurons. *Hum Mol Genet,* 21**,** 4827-35.

LEE, S. B., KIM, J. J., NAM, H. J., GAO, B., YIN, P., QIN, B., YI, S. Y., HAM, H., EVANS, D., KIM, S. H., ZHANG, J., DENG, M., LIU, T., ZHANG, H., BILLADEAU, D. D., WANG, L., GIAIME, E., SHEN, J., PANG, Y. P., JEN, J., VAN DEURSEN, J. M. & LOU, Z. 2015. Parkin Regulates Mitosis and Genomic Stability through Cdc20/Cdh1. *Mol Cell,* 60**,** 21-34.

LEE, Y.-J., JEONG, S.-Y., KARBOWSKI, M., SMITH, C. L. & YOULE, R. J. 2004. Roles of the Mammalian Mitochondrial Fission and Fusion Mediators Fis1, Drp1, and Opa1 in Apoptosis. *Molecular Biology of the Cell,* 15**,** 5001-5011.

LEE, Y., DAWSON, V. L. & DAWSON, T. M. 2012b. Animal models of Parkinson's disease: vertebrate genetics. *Cold Spring Harb Perspect Med,* 2.

LEE, Y. J., MIYAKE, S., WAKITA, H., MCMULLEN, D. C., AZUMA, Y., AUH, S. & HALLENBECK, J. M. 2007. Protein SUMOylation is massively increased in hibernation torpor and is critical for the cytoprotection provided by ischemic preconditioning and hypothermia in SHSY5Y cells. *J Cereb Blood Flow Metab,* 27**,** 950-62.

LEGESSE-MILLER, A., MASSOL, R. H. & KIRCHHAUSEN, T. 2003. Constriction and Dnm1p Recruitment Are Distinct Processes in Mitochondrial Fission. *Molecular Biology of the Cell,* 14**,** 1953-1963.

LEMASTERS, J. J., BOND, J. M., CHACON, E., HARPER, I. S., KAPLAN, S. H., OHATA, H., TROLLINGER, D. R., HERMAN, B. & CASCIO, W. E. 1996. The pH paradox in ischemia-reperfusion injury to cardiac myocytes. *Exs,* 76**,** 99-114.

LI, J., LU, D., DOU, H., LIU, H., WEAVER, K., WANG, W., LI, J., YEH, E. T. H., WILLIAMS, B. O., ZHENG, L. & YANG, T. 2018. Desumoylase SENP6 maintains osteochondroprogenitor homeostasis by suppressing the p53 pathway. *Nature Communications,* 9**,** 143.

LI, S., XU, S., ROELOFS, B. A., BOYMAN, L., LEDERER, W. J., SESAKI, H. & KARBOWSKI, M. 2015. Transient assembly of F-actin on the outer mitochondrial membrane contributes to mitochondrial fission. *The Journal of Cell Biology,* 208**,** 109.

LI, S. J. & HOCHSTRASSER, M. 1999. A new protease required for cell-cycle progression in yeast. *Nature,* 398**,** 246-51.

LI, W., HESABI, B., BABBO, A., PACIONE, C., LIU, J., CHEN, D. J., NICKOLOFF, J. A. & SHEN, Z. 2000. Regulation of double-strand break-induced mammalian homologous recombination by UBL1, a RAD51-interacting protein. *Nucleic Acids Res,* 28**,** 1145-53.

LI, X., FANG, P., MAI, J., CHOI, E. T., WANG, H. & YANG, X. F. 2013. Targeting mitochondrial reactive oxygen species as novel therapy for inflammatory diseases and cancers. *J Hematol Oncol,* 6**,** 19.

LI, Y. & LIU, X. 2018. Novel insights into the role of mitochondrial fusion and fission in cardiomyocyte apoptosis induced by ischemia/reperfusion. *Journal of Cellular Physiology,* 233**,** 5589-5597.

LICCHESI, J. D. F., MIESZCZANEK, J., MEVISSEN, T. E. T., RUTHERFORD, T. J., AKUTSU, M., VIRDEE, S., OUALID, F. E., CHIN, J. W., OVAA, H., BIENZ, M. & KOMANDER, D. 2011. An Ankyrin-repeat ubiquitin binding domain determines TRABID's specificity for atypical ubiquitin chains. *Nat Struct Mol Biol,* 19**,** 62-71.

LIN, Y., HWANG, W. C. & BASAVAPPA, R. 2002. Structural and functional analysis of the human mitotic-specific ubiquitin-conjugating enzyme, UbcH10. *J Biol Chem,* 277**,** 21913-21.

LINDHOLM, D., KORHONEN, L., ERIKSSON, O. & KOKS, S. 2017. Recent Insights into the Role of Unfolded Protein Response in ER Stress in Health and Disease. *Front Cell Dev Biol,* 5**,** 48.

LINDSKOG, C., LINNÉ, J., FAGERBERG, L., HALLSTRÖM, B. M., SUNDBERG, C. J., LINDHOLM, M., HUSS, M., KAMPF, C., CHOI, H., LIEM, D. A., PING, P., VÄREMO, L., MARDINOGLU, A., NIELSEN, J., LARSSON, E., PONTÉN, F. & UHLÉN, M. 2015. The human cardiac and skeletal muscle proteomes defined by transcriptomics and antibody-based profiling. *BMC Genomics,* 16**,** 475.

LIU, Y. C., LIN, W. Y., JHANG, Y. R., HUANG, S. H., WU, C. P. & WU, H. T. 2011. Efficiency of DNA Transfection of Rat Heart Myoblast Cells H9c2(2-1) by Either Polyethyleneimine or Electroporation. *Applied Biochemistry and Biotechnology,* 164**,** 1172-1182.

LOSÓN, O. C., SONG, Z., CHEN, H., CHAN, D. C. & NEWMEYER, D. D. 2013. Fis1, Mff, MiD49, and MiD51 mediate Drp1 recruitment in mitochondrial fission. *Molecular Biology of the Cell,* 24**,** 659-667.

LUKASIAK, S., SCHILLER, C., OEHLSCHLAEGER, P., SCHMIDTKE, G., KRAUSE, P., LEGLER, D. F., AUTSCHBACH, F., SCHIRMACHER, P., BREUHAHN, K. & GROETTRUP, M. 2008. Proinflammatory cytokines cause FAT10 upregulation in cancers of liver and colon. *Oncogene,* 27**,** 6068.

LUO, J., GURUNG, S., LEE, L., HENLEY, J. M., WILKINSON, K. A. & GUO, C. 2017. Increased SUMO-2/3-ylation mediated by SENP3 degradation is protective against cadmium-induced caspase 3-dependent cytotoxicity. *J Toxicol Sci,* 42**,** 529-538.

LUTZ, A. K., EXNER, N., FETT, M. E., SCHLEHE, J. S., KLOOS, K., LAMMERMANN, K., BRUNNER, B., KURZ-DREXLER, A., VOGEL, F., REICHERT, A. S., BOUMAN, L., VOGT-WEISENHORN, D., WURST, W., TATZELT, J., HAASS, C. & WINKLHOFER, K. F. 2009. Loss of parkin or PINK1 function increases Drp1-dependent mitochondrial fragmentation. *J Biol Chem,* 284**,** 22938-51.

MACDONALD, P. J., FRANCY, C. A., STEPANYANTS, N., LEHMAN, L., BAGLIO, A., MEARS, J. A., QI, X. & RAMACHANDRAN, R. 2016. Distinct Splice Variants of Dynamin-related

Protein 1 Differentially Utilize Mitochondrial Fission Factor as an Effector of Cooperative GTPase Activity. *Journal of Biological Chemistry,* 291**,** 493-507.

MAHAJAN, R., DELPHIN, C., GUAN, T., GERACE, L. & MELCHIOR, F. 1997. A small ubiquitin-related polypeptide involved in targeting RanGAP1 to nuclear pore complex protein RanBP2. *Cell,* 88**,** 97-107.

MAHAJAN, R., GERACE, L. & MELCHIOR, F. 1998. Molecular Characterization of the SUMO-1 Modification of RanGAP1 and Its Role in Nuclear Envelope Association. *The Journal of Cell Biology,* 140**,** 259.

MAHFOUDH-BOUSSAID, A., ZAOUALI, M. A., HADJ-AYED, K., MILED, A. H., SAIDANE-MOSBAHI, D., ROSELLO-CATAFAU, J. & BEN ABDENNEBI, H. 2012. Ischemic preconditioning reduces endoplasmic reticulum stress and upregulates hypoxia inducible factor-1alpha in ischemic kidney: the role of nitric oxide. *J Biomed Sci,* 19**,** 7.

MAHON, P. C., HIROTA, K. & SEMENZA, G. L. 2001. FIH-1: a novel protein that interacts with HIF-1alpha and VHL to mediate repression of HIF-1 transcriptional activity. *Genes Dev,* 15**,** 2675-86.

MAILAND, N., BEKKER-JENSEN, S., FAUSTRUP, H., MELANDER, F., BARTEK, J., LUKAS, C. & LUKAS, J. 2007. RNF8 ubiquitylates histones at DNA double-strand breaks and promotes assembly of repair proteins. *Cell,* 131**,** 887-900.

MANNELLA, C. A. 2006. Structure and dynamics of the mitochondrial inner membrane cristae. *Biochim Biophys Acta,* 1763**,** 542-8.

MANOR, U., BARTHOLOMEW, S., GOLANI, G., CHRISTENSON, E., KOZLOV, M., HIGGS, H., SPUDICH, J. & LIPPINCOTT-SCHWARTZ, J. 2015. A mitochondria-anchored isoform of the actin-nucleating spire protein regulates mitochondrial division. *Elife,* 4**,** e08828.

MANSOUR, H., DE TOMBE, P. P., SAMAREL, A. M. & RUSSELL, B. 2004. Restoration of Resting Sarcomere Length After Uniaxial Static Strain Is Regulated by Protein Kinase Cε and Focal Adhesion Kinase. *Circulation Research,* 94**,** 642.

MANUELL, A. L., QUISPE, J. & MAYFIELD, S. P. 2007. Structure of the chloroplast ribosome: novel domains for translation regulation. *PLoS Biol,* 5**,** e209.

MARBAN, E., KITAKAZE, M., KUSUOKA, H., PORTERFIELD, J. K., YUE, D. T. & CHACKO, V. P. 1987. Intracellular free calcium concentration measured with 19F NMR spectroscopy in intact ferret hearts. *Proc Natl Acad Sci U S A,* 84**,** 6005-9.

MARGOLIN, W. 2005. FtsZ and the division of prokaryotic cells and organelles. *Nat Rev Mol Cell Biol,* 6**,** 862-71.

MARIN, I. & FERRUS, A. 2002. Comparative genomics of the RBR family, including the Parkinson's disease-related gene parkin and the genes of the ariadne subfamily. *Mol Biol Evol,* 19**,** 2039-50.

MARIN, I., LUCAS, J. I., GRADILLA, A. C. & FERRUS, A. 2004. Parkin and relatives: the RBR family of ubiquitin ligases. *Physiol Genomics,* 17**,** 253-63.

MARTIN-PUIG, S., TELLO, D. & ARAGONÉS, J. 2015. Novel perspectives on the PHD-HIF oxygen sensing pathway in cardioprotection mediated by IPC and RIPC. *Frontiers in Physiology,* 6**,** 137.

MARTIN, S., WILKINSON, K. A., NISHIMUNE, A. & HENLEY, J. M. 2007. Emerging extranuclear roles of protein SUMOylation in neuronal function and dysfunction. *Nature reviews. Neuroscience,* 8**,** 948-959.

MASCLE, X. H., LUSSIER-PRICE, M., CAPPADOCIA, L., ESTEPHAN, P., RAIOLA, L., OMICHINSKI, J. G. & AUBRY, M. 2013. Identification of a Non-covalent Ternary Complex Formed by PIAS1, SUMO1, and UBC9 Proteins Involved in Transcriptional Regulation. *The Journal of Biological Chemistry,* 288**,** 36312-36327.

MASPERO, E., MARI, S., VALENTINI, E., MUSACCHIO, A., FISH, A., PASQUALATO, S. & POLO, S. 2011. Structure of the HECT:ubiquitin complex and its role in ubiquitin chain elongation. *EMBO Rep,* 12**,** 342-9.

MATIC, I., SCHIMMEL, J., HENDRIKS, I. A., VAN SANTEN, M. A., VAN DE RIJKE, F., VAN DAM, H., GNAD, F., MANN, M. & VERTEGAAL, A. C. 2010. Site-specific identification of SUMO-2 targets in cells reveals an inverted SUMOylation motif and a hydrophobic cluster SUMOylation motif. *Mol Cell,* 39**,** 641-52.

MATIC, I., VAN HAGEN, M., SCHIMMEL, J., MACEK, B., OGG, S. C., TATHAM, M. H., HAY, R. T., LAMOND, A. I., MANN, M. & VERTEGAAL, A. C. O. 2008. In vivo identification of human small ubiquitin-like modifier polymerization sites by high accuracy mass spectrometry and an in vitro to in vivo strategy. *Mol Cell Proteomics,* 7**,** 132-44.

MATSUDA, N., SATO, S., SHIBA, K., OKATSU, K., SAISHO, K., GAUTIER, C. A., SOU, Y. S., SAIKI, S., KAWAJIRI, S., SATO, F., KIMURA, M., KOMATSU, M., HATTORI, N. & TANAKA, K. 2010. PINK1 stabilized by mitochondrial depolarization recruits Parkin to damaged mitochondria and activates latent Parkin for mitophagy. *J Cell Biol,* 189**,** 211-21.

MATSUOKA, S., SARAI, N., JO, H. & NOMA, A. 2004. Simulation of ATP metabolism in cardiac excitation–contraction coupling. *Progress in Biophysics and Molecular Biology,* 85**,** 279-299.

MATUNIS, M. J., COUTAVAS, E. & BLOBEL, G. 1996. A novel ubiquitin-like modification modulates the partitioning of the Ran-GTPase-activating protein RanGAP1 between the cytosol and the nuclear pore complex. *J Cell Biol,* 135**,** 1457-70.

MATUNIS, M. J., WU, J. & BLOBEL, G. 1998. SUMO-1 Modification and Its Role in Targeting the Ran GTPase-activating Protein, RanGAP1, to the Nuclear Pore Complex. *The Journal of Cell Biology,* 140**,** 499.

MAUPIN-FURLOW, J. A. 2014. Prokaryotic Ubiquitin-Like Protein Modification. *Annual review of microbiology,* 68**,** 155-175.

MCBRIDE, H. M., NEUSPIEL, M. & WASIAK, S. 2006. Mitochondria: more than just a powerhouse. *Curr Biol,* 16**,** R551-60.

MCCORMACK, J. G. & DENTON, R. M. 1989. The role of Ca2+ ions in the regulation of intramitochondrial metabolism and energy production in rat heart. *Molecular and Cellular Biochemistry,* 89**,** 121-125.

MCLELLAND, G. L., SOUBANNIER, V., CHEN, C. X., MCBRIDE, H. M. & FON, E. A. 2014. Parkin and PINK1 function in a vesicular trafficking pathway regulating mitochondrial quality control. *Embo j,* 33**,** 282-95.

MCNULTY, P. H., DARLING, A. & WHITING, J. M. 1996. Glycogen depletion contributes to ischemic preconditioning in the rat heart in vivo. *Am J Physiol,* 271**,** H2283-9.

MEARS, J. A., LACKNER, L. L., FANG, S., INGERMAN, E., NUNNARI, J. & HINSHAW, J. E. 2011. Conformational changes in Dnm1 support a contractile mechanism for mitochondrial fission. *Nat Struct Mol Biol,* 18**,** 20-6.

MEEUSEN, S., DEVAY, R., BLOCK, J., CASSIDY-STONE, A., WAYSON, S., MCCAFFERY, J. M. & NUNNARI, J. 2006. Mitochondrial inner-membrane fusion and crista maintenance requires the dynamin-related GTPase Mgm1. *Cell,* 127**,** 383-95.

MEEUSEN, S., MCCAFFERY, J. M. & NUNNARI, J. 2004. Mitochondrial fusion intermediates revealed in vitro. *Science,* 305**,** 1747-52.

MELLER, C. L., MELLER, R., SIMONS, R. P. & PODRABSKY, J. E. 2014. Patterns of ubiquitylation and SUMOylation associated with exposure to anoxia in embryos of the annual killifish Austrofundulus limnaeus. *J Comp Physiol B,* 184**,** 235-47.

MELUH, P. B. & KOSHLAND, D. 1995. Evidence that the MIF2 gene of Saccharomyces cerevisiae encodes a centromere protein with homology to the mammalian centromere protein CENP-C. *Mol Biol Cell,* 6**,** 793-807.

METZGER, M. B., PRUNEDA, J. N., KLEVIT, R. E. & WEISSMAN, A. M. 2014. RING-type E3 ligases: master manipulators of E2 ubiquitin-conjugating enzymes and ubiquitination. *Biochim Biophys Acta,* 1843**,** 47-60.

MIKKONEN, L., HIRVONEN, J. & JANNE, O. A. 2013. SUMO-1 regulates body weight and adipogenesis via PPARgamma in male and female mice. *Endocrinology,* 154**,** 698-708.

MINTY, A., DUMONT, X., KAGHAD, M. & CAPUT, D. 2000. Covalent modification of p73alpha by SUMO-1. Two-hybrid screening with p73 identifies novel SUMO-1-interacting proteins and a SUMO-1 interaction motif. *J Biol Chem,* 275**,** 36316-23.

MITTAL, R., JHAVERI, V. M., KAY, S. S., GREER, A., SUTHERLAND, K. J., MCMURRY, H. S., LIN, N., MITTAL, J., MALHOTRA, A. K. & PATEL, A. P. 2018. Recent advances in understanding the pathogenesis of cardiovascular diseases and development of treatment modalities. *Cardiovasc Hematol Disord Drug Targets*.

MIURA, K., JIN, J. B. & HASEGAWA, P. M. 2007. Sumoylation, a post-translational regulatory process in plants. *Curr Opin Plant Biol,* 10**,** 495-502.

MOLDOVAN, G. L., PFANDER, B. & JENTSCH, S. 2007. PCNA, the maestro of the replication fork. *Cell,* 129**,** 665-79.

MORETT, E. & BORK, P. 1999. A novel transactivation domain in parkin. *Trends Biochem Sci,* 24**,** 229-31.

MOZAFFARIAN, D., BENJAMIN, E. J., GO, A. S., ARNETT, D. K., BLAHA, M. J., CUSHMAN, M., DE FERRANTI, S., DESPRES, J. P., FULLERTON, H. J., HOWARD, V. J., HUFFMAN, M. D., JUDD, S. E., KISSELA, B. M., LACKLAND, D. T., LICHTMAN, J. H., LISABETH, L. D., LIU, S., MACKEY, R. H., MATCHAR, D. B., MCGUIRE, D. K., MOHLER, E. R., 3RD, MOY, C. S., MUNTNER, P., MUSSOLINO, M. E., NASIR, K., NEUMAR, R. W., NICHOL, G., PALANIAPPAN, L., PANDEY, D. K., REEVES, M. J., RODRIGUEZ, C. J., SORLIE, P. D., STEIN, J., TOWFIGHI, A., TURAN, T. N., VIRANI, S. S., WILLEY, J. Z., WOO, D., YEH, R. W. & TURNER, M. B. 2015. Heart disease and stroke statistics--2015 update: a report from the American Heart Association. *Circulation,* 131**,** e29-322.

MUKHOPADHYAY, D., AYAYDIN, F., KOLLI, N., TAN, S. H., ANAN, T., KAMETAKA, A., AZUMA, Y., WILKINSON, K. D. & DASSO, M. 2006. SUSP1 antagonizes formation of highly SUMO2/3-conjugated species. *J Cell Biol,* 174**,** 939-49.

MUKHOPADHYAY, D. & DASSO, M. 2007. Modification in reverse: the SUMO proteases. *Trends Biochem Sci,* 32**,** 286-95.

MUNOZ-PINEDO, C., GUIO-CARRION, A., GOLDSTEIN, J. C., FITZGERALD, P., NEWMEYER, D. D. & GREEN, D. R. 2006. Different mitochondrial intermembrane space proteins are released during apoptosis in a manner that is coordinately initiated but can vary in duration. *Proc Natl Acad Sci U S A,* 103**,** 11573-8.

MURRY, C. E., JENNINGS, R. B. & REIMER, K. A. 1986. Preconditioning with ischemia: a delay of lethal cell injury in ischemic myocardium. *Circulation,* 74**,** 1124.

MURRY, C. E., RICHARD, V. J., REIMER, K. A. & JENNINGS, R. B. 1990. Ischemic preconditioning slows energy metabolism and delays ultrastructural damage during a sustained ischemic episode. *Circ Res,* 66**,** 913-31.

NACERDDINE, K., LEHEMBRE, F., BHAUMIK, M., ARTUS, J., COHEN-TANNOUDJI, M., BABINET, C., PANDOLFI, P. P. & DEJEAN, A. 2005. The SUMO pathway is essential for nuclear integrity and chromosome segregation in mice. *Dev Cell,* 9**,** 769-79.

NAKAMURA, N., KIMURA, Y., TOKUDA, M., HONDA, S. & HIROSE, S. 2006. MARCH-V is a novel mitofusin 2- and Drp1-binding protein able to change mitochondrial morphology. *EMBO Rep,* 7**,** 1019-22.

NARENDRA, D., TANAKA, A., SUEN, D. F. & YOULE, R. J. 2008. Parkin is recruited selectively to impaired mitochondria and promotes their autophagy. *J Cell Biol,* 183**,** 795-803.

NARENDRA, D. P., JIN, S. M., TANAKA, A., SUEN, D. F., GAUTIER, C. A., SHEN, J., COOKSON, M. R. & YOULE, R. J. 2010. PINK1 is selectively stabilized on impaired mitochondria to activate Parkin. *PLoS Biol,* 8**,** e1000298.

NASSAR, N., HORN, G., HERRMANN, C. A., SCHERER, A., MCCORMICK, F. & WITTINGHOFER, A. 1995. The 2.2 Å crystal structure of the Ras-binding domain of the serine/threonine kinase c-Raf1 in complex with RaplA and a GTP analogue. *Nature,* 375**,** 554-560.

NELSON, D. E., RANDLE, S. J. & LAMAN, H. 2013. Beyond ubiquitination: the atypical functions of Fbxo7 and other F-box proteins. *Open Biol,* 3**,** 130131.

NEMES, Z., DEVREESE, B., STEINERT, P. M., VAN BEEUMEN, J. & FESUS, L. 2004. Cross-linking of ubiquitin, HSP27, parkin, and alpha-synuclein by gamma-glutamyl-epsilon-lysine bonds in Alzheimer's neurofibrillary tangles. *Faseb j,* 18**,** 1135-7.

NEUSPIEL, M., SCHAUSS, A. C., BRASCHI, E., ZUNINO, R., RIPPSTEIN, P., RACHUBINSKI, R. A., ANDRADE-NAVARRO, M. A. & MCBRIDE, H. M. 2008. Cargo-selected transport from the mitochondria to peroxisomes is mediated by vesicular carriers. *Curr Biol,* 18**,** 102-8.

NEWTON, K., MATSUMOTO, M. L., WERTZ, I. E., KIRKPATRICK, D. S., LILL, J. R., TAN, J., DUGGER, D., GORDON, N., SIDHU, S. S., FELLOUSE, F. A., KOMUVES, L., FRENCH, D. M., FERRANDO, R. E., LAM, C., COMPAAN, D., YU, C., BOSANAC, I., HYMOWITZ, S. G., KELLEY, R. F. & DIXIT, V. M. 2008. Ubiquitin chain editing revealed by polyubiquitin linkage-specific antibodies. *Cell,* 134**,** 668-78.

NI, H. M., WILLIAMS, J. A. & DING, W. X. 2015. Mitochondrial dynamics and mitochondrial quality control. *Redox Biol,* 4**,** 6-13.

NUNNARI, J., MARSHALL, W. F., STRAIGHT, A., MURRAY, A., SEDAT, J. W. & WALTER, P. 1997. Mitochondrial transmission during mating in Saccharomyces cerevisiae is determined by mitochondrial fusion and fission and the intramitochondrial segregation of mitochondrial DNA. *Molecular Biology of the Cell,* 8**,** 1233-1242.

OLICHON, A., ELACHOURI, G., BARICAULT, L., DELETTRE, C., BELENGUER, P. & LENAERS, G. 2007. OPA1 alternate splicing uncouples an evolutionary conserved function in mitochondrial fusion from a vertebrate restricted function in apoptosis. *Cell Death Differ,* 14**,** 682-92.

OLSEN, S. K., CAPILI, A. D., LU, X., TAN, D. S. & LIMA, C. D. 2010. Active site remodelling accompanies thioester bond formation in the SUMO E1. *Nature,* 463**,** 906-12.

ONYANGO, I. G., KHAN, S. M. & BENNETT, J. P., JR. 2017. Mitochondria in the pathophysiology of Alzheimer's and Parkinson's diseases. *Front Biosci (Landmark Ed),* 22**,** 854-872.

ORDUREAU, A., HEO, J. M., DUDA, D. M., PAULO, J. A., OLSZEWSKI, J. L., YANISHEVSKI, D., RINEHART, J., SCHULMAN, B. A. & HARPER, J. W. 2015. Defining roles of PARKIN and ubiquitin phosphorylation by PINK1 in mitochondrial quality control using a ubiquitin replacement strategy. *Proc Natl Acad Sci U S A,* 112**,** 6637-42.

ORDUREAU, A., SARRAF, S. A., DUDA, D. M., HEO, J. M., JEDRYCHOWSKI, M. P., SVIDERSKIY, V. O., OLSZEWSKI, J. L., KOERBER, J. T., XIE, T., BEAUSOLEIL, S. A., WELLS, J. A., GYGI, S. P., SCHULMAN, B. A. & HARPER, J. W. 2014. Quantitative proteomics reveal a feedforward mechanism for mitochondrial PARKIN translocation and ubiquitin chain synthesis. *Mol Cell,* 56**,** 360-75.

ORENGO, C. A., JONES, D. T. & THORNTON, J. M. 1994. Protein superfamilles and domain superfolds. *Nature,* 372**,** 631.

OSELLAME, L. D., SINGH, A. P., STROUD, D. A., PALMER, C. S., STOJANOVSKI, D., RAMACHANDRAN, R. & RYAN, M. T. 2016. Cooperative and independent roles of the Drp1 adaptors Mff, MiD49 and MiD51 in mitochondrial fission. *Journal of Cell Science,* 129**,** 2170.

OSHIMA, R., NAKANO, H., KATAYAMA, M., SAKURAI, J., WU, W., KOIZUMI, S., ASANO, T., WATANABE, T., ASAKURA, T., OHTA, T. & OTSUBO, T. 2008. Modification of the hepatic mitochondrial proteome in response to ischemic preconditioning following ischemia-reperfusion injury of the rat liver. *Eur Surg Res,* 40**,** 247-55.

OTANI, H. 2004. Reactive Oxygen Species as Mediators of Signal Transduction in Ischemic Preconditioning. *Antioxidants & Redox Signaling,* 6**,** 449-469.

OTERA, H., MIYATA, N., KUGE, O. & MIHARA, K. 2016. Drp1-dependent mitochondrial fission via MiD49/51 is essential for apoptotic cristae remodeling. *The Journal of Cell Biology,* 212**,** 531.

OTERA, H., WANG, C., CLELAND, M. M., SETOGUCHI, K., YOKOTA, S., YOULE, R. J. & MIHARA, K. 2010. Mff is an essential factor for mitochondrial recruitment of Drp1 during mitochondrial fission in mammalian cells. *The Journal of Cell Biology,* 191**,** 1141.

OWERBACH, D., MCKAY, E. M., YEH, E. T., GABBAY, K. H. & BOHREN, K. M. 2005. A proline-90 residue unique to SUMO-4 prevents maturation and sumoylation. *Biochem Biophys Res Commun,* 337**,** 517-20.

OZKAN, E., YU, H. & DEISENHOFER, J. 2005. Mechanistic insight into the allosteric activation of a ubiquitin-conjugating enzyme by RING-type ubiquitin ligases. *Proc Natl Acad Sci U S A,* 102**,** 18890-5.

OZKAYNAK, E., FINLEY, D., SOLOMON, M. J. & VARSHAVSKY, A. 1987. The yeast ubiquitin genes: a family of natural gene fusions. *Embo j,* 6**,** 1429-39.

PALMER, C. S., OSELLAME, L. D., LAINE, D., KOUTSOPOULOS, O. S., FRAZIER, A. E. & RYAN, M. T. 2011. MiD49 and MiD51, new components of the mitochondrial fission machinery. *EMBO Reports,* 12**,** 565-573.

PALMER, J. W., TANDLER, B. & HOPPEL, C. L. 1985. Biochemical differences between subsarcolemmal and interfibrillar mitochondria from rat cardiac muscle: Effects of procedural manipulations. *Archives of Biochemistry and Biophysics,* 236**,** 691-702.

PAREYSON, D. 2004. Differential diagnosis of Charcot-Marie-Tooth disease and related neuropathies. *Neurological Sciences,* 25**,** 72-82.

PARK, J., LEE, S. B., LEE, S., KIM, Y., SONG, S., KIM, S., BAE, E., KIM, J., SHONG, M., KIM, J. M. & CHUNG, J. 2006. Mitochondrial dysfunction in Drosophila PINK1 mutants is complemented by parkin. *Nature,* 441**,** 1157-61.

PARRATT, J. & VEGH, A. 1994. Pronounced antiarrhythmic effects of ischemic preconditioning. *Cardioscience,* 5**,** 9-18.

PASDOIS, P., PARKER, J. E. & HALESTRAP, A. P. 2013. Extent of Mitochondrial Hexokinase II Dissociation During Ischemia Correlates With Mitochondrial Cytochrome c Release, Reactive Oxygen Species Production, and Infarct Size on Reperfusion. *Journal of the American Heart Association: Cardiovascular and Cerebrovascular Disease,* 2**,** e005645.

PASTORINO, J. G. & HOEK, J. B. 2003. Hexokinase II: the integration of energy metabolism and control of apoptosis. *Curr Med Chem,* 10**,** 1535-51.

PASTORINO, J. G. & HOEK, J. B. 2008. Regulation of hexokinase binding to VDAC. *J Bioenerg Biomembr,* 40**,** 171-82.

PENG, C., RAO, W., ZHANG, L., GAO, F., HUI, H., WANG, K., DAI, S., YANG, Y., LUO, P., MA, Y., MA, W., YU, X. & FEI, Z. 2018. Mitofusin 2 Exerts a Protective Role in Ischemia Reperfusion Injury Through Increasing Autophagy. *Cell Physiol Biochem,* 46**,** 2311-2324.

PENG, J., SCHWARTZ, D., ELIAS, J. E., THOREEN, C. C., CHENG, D., MARSISCHKY, G., ROELOFS, J., FINLEY, D. & GYGI, S. P. 2003. A proteomics approach to understanding protein ubiquitination. *Nat Biotechnol,* 21**,** 921-6.

PESSAYRE, D., MANSOURI, A. & FROMENTY, B. 2002. Nonalcoholic steatosis and steatohepatitis. V. Mitochondrial dysfunction in steatohepatitis. *Am J Physiol Gastrointest Liver Physiol,* 282**,** G193-9.

PETROSKI, M. D. & DESHAIES, R. J. 2005a. Function and regulation of cullin-RING ubiquitin ligases. *Nat Rev Mol Cell Biol,* 6**,** 9-20.

PETROSKI, M. D. & DESHAIES, R. J. 2005b. Mechanism of lysine 48-linked ubiquitin-chain synthesis by the cullin-RING ubiquitin-ligase complex SCF-Cdc34. *Cell,* 123**,** 1107-20.

PHILLIPS, M. J. & VOELTZ, G. K. 2016. Structure and function of ER membrane contact sites with other organelles. *Nat Rev Mol Cell Biol,* 17**,** 69-82.

PICKART, C. M. 2001. Mechanisms Underlying Ubiquitination. *Annual Review of Biochemistry,* 70**,** 503-533.

PICKART, C. M., KASPEREK, E. M., BEAL, R. & KIM, A. 1994. Substrate properties of site-specific mutant ubiquitin protein (G76A) reveal unexpected mechanistic features of ubiquitin-activating enzyme (E1). *J Biol Chem,* 269**,** 7115-23.

PINHEIRO, D. F., FONTES, B., SHIMAZAKI, J. K., HEIMBECKER, A. M., JACYSYN JDE, F., RASSLAN, S., MONTERO, E. F. & UTIYAMA, E. M. 2016. Ischemic preconditioning modifies mortality and inflammatory response. *Acta Cir Bras,* 31**,** 1-7.

PIPER, H. M., GARCIA-DORADO, D. & OVIZE, M. 1998. A fresh look at reperfusion injury. *Cardiovasc Res,* 38**,** 291-300.

PIQUEREAU, J., CAFFIN, F., NOVOTOVA, M., LEMAIRE, C., VEKSLER, V., GARNIER, A., VENTURA-CLAPIER, R. & JOUBERT, F. 2013. Mitochondrial dynamics in the adult cardiomyocytes: which roles for a highly specialized cell? *Frontiers in Physiology,* 4**,** 102.

PIZZO, P. & POZZAN, T. 2007. Mitochondria-endoplasmic reticulum choreography: structure and signaling dynamics. *Trends Cell Biol,* 17**,** 511-7.

PLECHANOVOVA, A., JAFFRAY, E. G., TATHAM, M. H., NAISMITH, J. H. & HAY, R. T. 2012. Structure of a RING E3 ligase and ubiquitin-loaded E2 primed for catalysis. *Nature,* 489**,** 115-20.

PLOTZ, M., GILLISSEN, B., HOSSINI, A. M., DANIEL, P. T. & EBERLE, J. 2012. Disruption of the VDAC2-Bak interaction by Bcl-x(S) mediates efficient induction of apoptosis in melanoma cells. *Cell Death Differ,* 19**,** 1928-38.

PRAEFCKE, G. J. & MCMAHON, H. T. 2004. The dynamin superfamily: universal membrane tubulation and fission molecules? *Nat Rev Mol Cell Biol,* 5**,** 133-47.

PRUDENT, J., ZUNINO, R., SUGIURA, A., MATTIE, S., SHORE, G. C. & MCBRIDE, H. M. 2015. MAPL SUMOylation of Drp1 Stabilizes an ER/Mitochondrial Platform Required for Cell Death. *Mol Cell,* 59**,** 941-55.

PRUNEDA, J. N., LITTLEFIELD, P. J., SOSS, S. E., NORDQUIST, K. A., CHAZIN, W. J., BRZOVIC, P. S. & KLEVIT, R. E. 2012. Structure of an E3:E2~Ub complex reveals an allosteric mechanism shared among RING/U-box ligases. *Mol Cell,* 47**,** 933-42.

QI, X., DISATNIK, M. H., SHEN, N., SOBEL, R. A. & MOCHLY-ROSEN, D. 2011. Aberrant mitochondrial fission in neurons induced by protein kinase C{delta} under oxidative stress conditions in vivo. *Mol Biol Cell,* 22**,** 256-65.

QIAN, T., NIEMINEN, A. L., HERMAN, B. & LEMASTERS, J. J. 1997. Mitochondrial permeability transition in pH-dependent reperfusion injury to rat hepatocytes. *Am J Physiol,* 273**,** C1783-92.

QUAST, S. A., BERGER, A. & EBERLE, J. 2013. ROS-dependent phosphorylation of Bax by wortmannin sensitizes melanoma cells for TRAIL-induced apoptosis. *Cell Death Dis,* 4**,** e839.

RAASI, S., SCHMIDTKE, G., DE GIULI, R. & GROETTRUP, M. 1999. A ubiquitin-like protein which is synergistically inducible by interferon-γ and tumor necrosis factor-α. *European Journal of Immunology,* 29**,** 4030-4036.

RAO, F., DENG, C. Y., WU, S. L., XIAO, D. Z., YU, X. Y., KUANG, S. J., LIN, Q. X. & SHAN, Z. X. 2009. Involvement of Src in L-type Ca2+ channel depression induced by macrophage migration inhibitory factor in atrial myocytes. *J Mol Cell Cardiol,* 47**,** 586-94.

RAVID, T. & HOCHSTRASSER, M. 2008. Diversity of degradation signals in the ubiquitin-proteasome system. *Nat Rev Mol Cell Biol,* 9**,** 679-90.

REIMER, K. A., LOWE, J. E., RASMUSSEN, M. M. & JENNINGS, R. B. 1977. The wavefront phenomenon of ischemic cell death. 1. Myocardial infarct size vs duration of coronary occlusion in dogs. *Circulation,* 56**,** 786-94.

REN, C., YAN, Z., WEI, D., GAO, X., CHEN, X. & ZHAO, H. 2009. Limb remote ischemic postconditioning protects against focal ischemia in rats. *Brain Res,* 1288**,** 88-94.

REVERTER, D. & LIMA, C. D. 2004. A basis for SUMO protease specificity provided by analysis of human Senp2 and a Senp2-SUMO complex. *Structure,* 12**,** 1519-31.

REVERTER, D. & LIMA, C. D. 2005. Insights into E3 ligase activity revealed by a SUMO-RanGAP1-Ubc9-Nup358 complex. *Nature,* 435**,** 687-92.

RICH, P. R. 2003. The molecular machinery of Keilin's respiratory chain. *Biochem Soc Trans,* 31**,** 1095-105.

RICHTER, V., PALMER, C. S., OSELLAME, L. D., SINGH, A. P., ELGASS, K., STROUD, D. A., SESAKI, H., KVANSAKUL, M. & RYAN, M. T. 2014. Structural and functional analysis of MiD51, a dynamin receptor required for mitochondrial fission. *The Journal of Cell Biology,* 204**,** 477.

RILEY, B. E., LOUGHEED, J. C., CALLAWAY, K., VELASQUEZ, M., BRECHT, E., NGUYEN, L., SHALER, T., WALKER, D., YANG, Y., REGNSTROM, K., DIEP, L., ZHANG, Z., CHIOU, S., BOVA, M., ARTIS, D. R., YAO, N., BAKER, J., YEDNOCK, T. & JOHNSTON, J. A. 2013. Structure and function of Parkin E3 ubiquitin ligase reveals aspects of RING and HECT ligases. *Nat Commun,* 4**,** 1982.

RODRIGO-BRENNI, M. C. & MORGAN, D. O. 2007. Sequential E2s drive polyubiquitin chain assembly on APC targets. *Cell,* 130**,** 127-39.

RODRIGUEZ-SINOVAS, A., RUIZ-MEANA, M., DENUC, A. & GARCIA-DORADO, D. 2018. Mitochondrial Cx43, an important component of cardiac preconditioning. *Biochim Biophys Acta,* 1860**,** 174-181.

RODRIGUEZ, J. A., ORBE, J., SAENZ-PIPAON, G., ABIZANDA, G., GEBARA, N., RADULESCU, F., AZCARATE, P. M., ALONSO-PEREZ, L., MERINO, D., PROSPER, F., PARAMO, J. A. & RONCAL, C. 2018. Selective increase of cardiomyocyte derived extracellular vesicles after experimental myocardial infarction and functional effects on the endothelium. *Thromb Res,* 170**,** 1-9.

ROJANSKY, R., CHA, M. Y. & CHAN, D. C. 2016. Elimination of paternal mitochondria in mouse embryos occurs through autophagic degradation dependent on PARKIN and MUL1. *Elife,* 5.

ROJO, M., LEGROS, F., CHATEAU, D. & LOMBÈS, A. 2002. Membrane topology and mitochondrial targeting of mitofusins, ubiquitous mammalian homologs of the transmembrane GTPase Fzo. *Journal of Cell Science,* 115**,** 1663-1674.

ROSSIER, M. F. 2006. T channels and steroid biosynthesis: in search of a link with mitochondria. *Cell Calcium,* 40**,** 155-64.

ROTHFUSS, O., FISCHER, H., HASEGAWA, T., MAISEL, M., LEITNER, P., MIESEL, F., SHARMA, M., BORNEMANN, A., BERG, D., GASSER, T. & PATENGE, N. 2009. Parkin protects mitochondrial genome integrity and supports mitochondrial DNA repair. *Hum Mol Genet,* 18**,** 3832-50.

RUBIO DE LA TORRE, E., LUZON-TORO, B., FORTE-LAGO, I., MINGUEZ-CASTELLANOS, A., FERRER, I. & HILFIKER, S. 2009. Combined kinase inhibition modulates parkin inactivation. *Hum Mol Genet,* 18**,** 809-23.

RUIZ-MEANA, M., NUNEZ, E., MIRO-CASAS, E., MARTINEZ-ACEDO, P., BARBA, I., RODRIGUEZ-SINOVAS, A., INSERTE, J., FERNANDEZ-SANZ, C., HERNANDO, V., VAZQUEZ, J. & GARCIA-DORADO, D. 2014. Ischemic preconditioning protects cardiomyocyte mitochondria through mechanisms independent of cytosol. *J Mol Cell Cardiol,* 68**,** 79-88.

RUJIVIPHAT, J., MEGLEI, G., RUBINSTEIN, J. L. & MCQUIBBAN, G. A. 2009. Phospholipid Association Is Essential for Dynamin-related Protein Mgm1 to Function in Mitochondrial Membrane Fusion. *J Biol Chem,* 284**,** 28682-6.

SADLER, A. J. & WILLIAMS, B. R. G. 2008. Interferon-inducible antiviral effectors. *Nature reviews. Immunology,* 8**,** 559-568.

SAITOH, H. & HINCHEY, J. 2000. Functional Heterogeneity of Small Ubiquitin-related Protein Modifiers SUMO-1 versus SUMO-2/3. *Journal of Biological Chemistry,* 275**,** 6252-6258.

SAMPSON, D. A., WANG, M. & MATUNIS, M. J. 2001. The small ubiquitin-like modifier-1 (SUMO-1) consensus sequence mediates Ubc9 binding and is essential for SUMO-1 modification. *J Biol Chem,* 276**,** 21664-9.

SANADA, S., KOMURO, I. & KITAKAZE, M. 2011. Pathophysiology of myocardial reperfusion injury: preconditioning, postconditioning, and translational aspects of protective measures. *American Journal of Physiology-Heart and Circulatory Physiology,* 301**,** H1723-H1741.

SANGER, J. W., AYOOB, J. C., CHOWRASHI, P., ZURAWSKI, D. & SANGER, J. M. 2000. Assembly of Myofibrils in Cardiac Muscle Cells. *In:* GRANZIER, H. L. & POLLACK, G. H. (eds.) *Elastic Filaments of the Cell.* Boston, MA: Springer US.

SANTEL, A., FRANK, S., GAUME, B., HERRLER, M., YOULE, R. J. & FULLER, M. T. 2003. Mitofusin-1 protein is a generally expressed mediator of mitochondrial fusion in mammalian cells. *Journal of Cell Science,* 116**,** 2763.

SARRAF, S. A., RAMAN, M., GUARANI-PEREIRA, V., SOWA, M. E., HUTTLIN, E. L., GYGI, S. P. & HARPER, J. W. 2013. Landscape of the PARKIN-dependent ubiquitylome in response to mitochondrial depolarization. *Nature,* 496**,** 372-6.

SATO, Y., YOSHIKAWA, A., YAMAGATA, A., MIMURA, H., YAMASHITA, M., OOKATA, K., NUREKI, O., IWAI, K., KOMADA, M. & FUKAI, S. 2008. Structural basis for specific cleavage of Lys 63-linked polyubiquitin chains. *Nature,* 455**,** 358-62.

SCARFFE, L. A., STEVENS, D. A., DAWSON, V. L. & DAWSON, T. M. 2014. Parkin and PINK1: much more than mitophagy. *Trends Neurosci,* 37**,** 315-24.

SCHALLER, S., PARADIS, S., NGOH, G. A., ASSALY, R., BUISSON, B., DROUOT, C., OSTUNI, M. A., LACAPERE, J. J., BASSISSI, F., BORDET, T., BERDEAUX, A., JONES, S. P., MORIN, D. & PRUSS, R. M. 2010. TRO40303, a new cardioprotective compound, inhibits mitochondrial permeability transition. *J Pharmacol Exp Ther,* 333**,** 696-706.

SCHAPER, J., FROEDE, R., HEIN, S., BUCK, A., HASHIZUME, H., SPEISER, B., FRIEDL, A. & BLEESE, N. 1991. Impairment of the myocardial ultrastructure and changes of the cytoskeleton in dilated cardiomyopathy. *Circulation,* 83**,** 504.

SCHEFFNER, M. & KUMAR, S. 2014. Mammalian HECT ubiquitin-protein ligases: biological and pathophysiological aspects. *Biochim Biophys Acta,* 1843**,** 61-74.

SCHIMKE, R. T. 1976. Protein degradation in vivo and its regulation. *Circ Res,* 38**,** I131-7.

SCHNEIDER-POETSCH, T., JU, J., EYLER, D. E., DANG, Y., BHAT, S., MERRICK, W. C., GREEN, R., SHEN, B. & LIU, J. O. 2010. Inhibition of Eukaryotic Translation Elongation by Cycloheximide and Lactimidomycin. *Nature chemical biology,* 6**,** 209-217.

SCHOLZ, D., DIENER, W. & SCHAPER, J. 1994. Altered nucleus/cytoplasm relationship and degenerative structural changes in human dilated cardiomyopathy. *Cardioscience,* 5**,** 127-138.

SCHOTT, R. J., ROHMANN, S., BRAUN, E. R. & SCHAPER, W. 1990. Ischemic preconditioning reduces infarct size in swine myocardium. *Circulation Research,* 66**,** 1133.

SCHULMAN, B. A. & HARPER, J. W. 2009. Ubiquitin-like protein activation by E1 enzymes: the apex for downstream signalling pathways. *Nature reviews. Molecular cell biology,* 10**,** 319-331.

SCHULZ, S., CHACHAMI, G., KOZACZKIEWICZ, L., WINTER, U., STANKOVIC-VALENTIN, N., HAAS, P., HOFMANN, K., URLAUB, H., OVAA, H., WITTBRODT, J., MEULMEESTER, E. & MELCHIOR, F. 2012. Ubiquitin-specific protease-like 1 (USPL1) is a SUMO isopeptidase with essential, non-catalytic functions. *EMBO Rep,* 13**,** 930-8.

SCHWARTZ, D. C. & HOCHSTRASSER, M. 2003. A superfamily of protein tags: ubiquitin, SUMO and related modifiers. *Trends Biochem Sci,* 28**,** 321-8.

SEIRAFI, M., KOZLOV, G. & GEHRING, K. 2015. Parkin structure and function. *Febs j,* 282**,** 2076-88.

SESAKI, H. & JENSEN, R. E. 1999. Division versus Fusion: Dnm1p and Fzo1p Antagonistically Regulate Mitochondrial Shape. *The Journal of Cell Biology,* 147**,** 699-706.

SHARMA, V. K., RAMESH, V., FRANZINI-ARMSTRONG, C. & SHEU, S. S. 2000. Transport of Ca2+ from Sarcoplasmic Reticulum to Mitochondria in Rat Ventricular Myocytes. *Journal of Bioenergetics and Biomembranes,* 32**,** 97-104.

SHEN, Q., YAMANO, K., HEAD, B. P., KAWAJIRI, S., CHEUNG, J. T. M., WANG, C., CHO, J.-H., HATTORI, N., YOULE, R. J., VAN DER BLIEK, A. M. & NEWMEYER, D. D. 2013. Mutations in Fis1 disrupt orderly disposal of defective mitochondria. *Molecular Biology of the Cell,* 25**,** 145-159.

SHEN, Z., PARDINGTON-PURTYMUN, P. E., COMEAUX, J. C., MOYZIS, R. K. & CHEN, D. J. 1996. Associations of UBE2I with RAD52, UBL1, p53, and RAD51 proteins in a yeast two-hybrid system. *Genomics,* 37**,** 183-6.

SHIMADA, T., HORITA, K., MURAKAMI, M. & OGURA, R. 1984. Morphological studies of different mitochondrial populations in monkey myocardial cells. *Cell and Tissue Research,* 238**,** 577-582.

SHIN, H. W., TAKATSU, H., MUKAI, H., MUNEKATA, E., MURAKAMI, K. & NAKAYAMA, K. 1999. Intermolecular and interdomain interactions of a dynamin-related GTP-binding protein, Dnm1p/Vps1p-like protein. *J Biol Chem,* 274**,** 2780-5.

SHIN, J. H., KO, H. S., KANG, H., LEE, Y., LEE, Y. I., PLETINKOVA, O., TROCONSO, J. C., DAWSON, V. L. & DAWSON, T. M. 2011. PARIS (ZNF746) repression of PGC-1alpha contributes to neurodegeneration in Parkinson's disease. *Cell,* 144**,** 689-702.

SHINTANI-ISHIDA, K., NAKAJIMA, M., UEMURA, K. & YOSHIDA, K. 2006. Ischemic preconditioning protects cardiomyocytes against ischemic injury by inducing GRP78. *Biochem Biophys Res Commun,* 345**,** 1600-5.

SHOJAEE, S., SINA, F., BANIHOSSEINI, S. S., KAZEMI, M. H., KALHOR, R., SHAHIDI, G. A., FAKHRAI-RAD, H., RONAGHI, M. & ELAHI, E. 2008. Genome-wide linkage analysis of a Parkinsonian-pyramidal syndrome pedigree by 500 K SNP arrays. *Am J Hum Genet,* 82**,** 1375-84.

SHOSHAN-BARMATZ, V., DE PINTO, V., ZWECKSTETTER, M., RAVIV, Z., KEINAN, N. & ARBEL, N. 2010. VDAC, a multi-functional mitochondrial protein regulating cell life and death. *Mol Aspects Med,* 31**,** 227-85.

SHPETNER, H. S. & VALLEE, R. B. 1989. Identification of dynamin, a novel mechanochemical enzyme that mediates interactions between microtubules. *Cell,* 59**,** 421-32.

SIGISMUND, S., POLO, S. & DI FIORE, P. P. 2004. Signaling through monoubiquitination. *Curr Top Microbiol Immunol,* 286**,** 149-85.

SIMAMURA, E., SHIMADA, H., HATTA, T. & HIRAI, K. 2008. Mitochondrial voltage-dependent anion channels (VDACs) as novel pharmacological targets for anti-cancer agents. *J Bioenerg Biomembr,* 40**,** 213-7.

SIMPSON, M. V. 1953. The release of labeled amino acids from the proteins of rat liver slices. *J Biol Chem,* 201**,** 143-54.

SINGH, G., SIDDIQUI, M. A., KHANNA, V. K., KASHYAP, M. P., YADAV, S., GUPTA, Y. K., PANT, K. K. & PANT, A. B. 2009. Oxygen glucose deprivation model of cerebral stroke in PC-12 cells: glucose as a limiting factor. *Toxicol Mech Methods,* 19**,** 154-60.

SINGH, R. K., ZERATH, S., KLEIFELD, O., SCHEFFNER, M., GLICKMAN, M. H. & FUSHMAN, D. 2012. Recognition and cleavage of related to ubiquitin 1 (Rub1) and Rub1-ubiquitin chains by components of the ubiquitin-proteasome system. *Mol Cell Proteomics,* 11**,** 1595-611.

SIPIDO, K. R. & MARBAN, E. 1991. L-type calcium channels, potassium channels, and novel nonspecific cation channels in a clonal muscle cell line derived from embryonic rat ventricle. *Circ Res,* 69**,** 1487-99.

SKAAR, J. R., D'ANGIOLELLA, V., PAGAN, J. K. & PAGANO, M. 2009. SnapShot: F Box Proteins II. *Cell,* 137**,** 1358, 1358.e1.

SKAAR, J. R., PAGAN, J. K. & PAGANO, M. 2013. Mechanisms and function of substrate recruitment by F-box proteins. *Nat Rev Mol Cell Biol,* 14**,** 369-81.

SKOWYRA, D., CRAIG, K. L., TYERS, M., ELLEDGE, S. J. & HARPER, J. W. 1997. F-box proteins are receptors that recruit phosphorylated substrates to the SCF ubiquitin-ligase complex. *Cell,* 91**,** 209-19.

SKULACHEV, V. P. 2001. Mitochondrial filaments and clusters as intracellular power-transmitting cables. *Trends in Biochemical Sciences,* 26**,** 23-29.

SMIRNOVA, E., GRIPARIC, L., SHURLAND, D.-L., VAN DER BLIEK, A. M. & POLLARD, T. D. 2001. Dynamin-related Protein Drp1 Is Required for Mitochondrial Division in Mammalian Cells. *Molecular Biology of the Cell,* 12**,** 2245-2256.

SMITH, M., TURKI-JUDEH, W. & COUREY, A. J. 2012. SUMOylation in Drosophila Development. *Biomolecules,* 2**,** 331-49.

SOBHIAN, B., SHAO, G., LILLI, D. R., CULHANE, A. C., MOREAU, L. A., XIA, B., LIVINGSTON, D. M. & GREENBERG, R. A. 2007. RAP80 Targets BRCA1 to Specific Ubiquitin Structures at DNA Damage Sites. *Science,* 316**,** 1198.

SONG, J., DURRIN, L. K., WILKINSON, T. A., KRONTIRIS, T. G. & CHEN, Y. 2004. Identification of a SUMO-binding motif that recognizes SUMO-modified proteins. *Proc Natl Acad Sci U S A,* 101**,** 14373-8.

SONG, J., ZHANG, Z., HU, W. & CHEN, Y. 2005. Small ubiquitin-like modifier (SUMO) recognition of a SUMO binding motif: a reversal of the bound orientation. *J Biol Chem,* 280**,** 40122-9.

SONG, M., GONG, G., BURELLE, Y., GUSTAFSSON, A. B., KITSIS, R. N., MATKOVICH, S. J. & DORN, G. W., 2ND 2015. Interdependence of Parkin-Mediated Mitophagy and Mitochondrial Fission in Adult Mouse Hearts. *Circ Res,* 117**,** 346-51.

SONG, Z., CHEN, H., FIKET, M., ALEXANDER, C. & CHAN, D. C. 2007. OPA1 processing controls mitochondrial fusion and is regulated by mRNA splicing, membrane potential, and Yme1L. *J Cell Biol,* 178**,** 749-55.

SONG, Z., GHOCHANI, M., MCCAFFERY, J. M., FREY, T. G. & CHAN, D. C. 2009. Mitofusins and OPA1 mediate sequential steps in mitochondrial membrane fusion. *Mol Biol Cell,* 20**,** 3525-32.

SOUBANNIER, V., MCLELLAND, G. L., ZUNINO, R., BRASCHI, E., RIPPSTEIN, P., FON, E. A. & MCBRIDE, H. M. 2012. A vesicular transport pathway shuttles cargo from mitochondria to lysosomes. *Curr Biol,* 22**,** 135-41.

SPRATT D , E., WALDEN, H. & SHAW G , S. 2014. RBR E3 ubiquitin ligases: new structures, new insights, new questions. *Biochem J,* 458**,** 421-37.

SRINIVAS, V., ZHANG, L.-P., ZHU, X.-H. & CARO, J. 1999. Characterization of an Oxygen/Redox-Dependent Degradation Domain of Hypoxia-Inducible Factor α (HIF-α) Proteins. *Biochemical and Biophysical Research Communications,* 260**,** 557-561.

SRIRAMACHANDRAN, A. M. & DOHMEN, R. J. 2014. SUMO-targeted ubiquitin ligases. *Biochimica et Biophysica Acta (BBA) - Molecular Cell Research,* 1843**,** 75-85.

STATEVA, S. R., SALAS, V., BENAIM, G., MENENDEZ, M., SOLIS, D. & VILLALOBO, A. 2015. Characterization of phospho-(tyrosine)-mimetic calmodulin mutants. *PLoS One,* 10**,** e0120798.

STERNSDORF, T., JENSEN, K., REICH, B. & WILL, H. 1999. The nuclear dot protein sp100, characterization of domains necessary for dimerization, subcellular localization, and modification by small ubiquitin-like modifiers. *J Biol Chem,* 274**,** 12555-66.

STORMS, R. K., HOLOWACHUCK, E. W. & FRIESEN, J. D. 1981. Genetic complementation of the Saccharomyces cerevisiae leu2 gene by the Escherichia coli leuB gene. *Molecular and Cellular Biology,* 1**,** 836-842.

SUN, H., LEVERSON, J. D. & HUNTER, T. 2007. Conserved function of RNF4 family proteins in eukaryotes: targeting a ubiquitin ligase to SUMOylated proteins. *The EMBO Journal,* 26**,** 4102.

SUZUKI, M., JEONG, S. Y., KARBOWSKI, M., YOULE, R. J. & TJANDRA, N. 2003. The solution structure of human mitochondria fission protein Fis1 reveals a novel TPR-like helix bundle. *J Mol Biol,* 334**,** 445-58.

SWATEK, K. N. & KOMANDER, D. 2016. Ubiquitin modifications. *Cell Res,* 26**,** 399-422.

TAGUCHI, N., ISHIHARA, N., JOFUKU, A., OKA, T. & MIHARA, K. 2007. Mitotic phosphorylation of dynamin-related GTPase Drp1 participates in mitochondrial fission. *J Biol Chem,* 282**,** 11521-9.

TAKAHASHI, Y. & KIKUCHI, Y. 2008. Cytoplasmic sumoylation by PIAS-type Siz1-SUMO ligase. *Cell Cycle,* 7**,** 1738-1744.

TANAKA, A., CLELAND, M. M., XU, S., NARENDRA, D. P., SUEN, D. F., KARBOWSKI, M. & YOULE, R. J. 2010. Proteasome and p97 mediate mitophagy and degradation of mitofusins induced by Parkin. *J Cell Biol,* 191**,** 1367-80.

TANAKA, K., NISHIDE, J., OKAZAKI, K., KATO, H., NIWA, O., NAKAGAWA, T., MATSUDA, H., KAWAMUKAI, M. & MURAKAMI, Y. 1999. Characterization of a fission yeast SUMO-1 homologue, pmt3p, required for multiple nuclear events, including the control of telomere length and chromosome segregation. *Mol Cell Biol,* 19**,** 8660-72.

TANG, J., HU, Z., TAN, J., YANG, S. & ZENG, L. 2016. Parkin Protects against Oxygen-Glucose Deprivation/Reperfusion Insult by Promoting Drp1 Degradation. *Oxid Med Cell Longev,* 2016**,** 8474303.

TANG, Z., EL FAR, O., BETZ, H. & SCHESCHONKA, A. 2005. Pias1 interaction and sumoylation of metabotropic glutamate receptor 8. *J Biol Chem,* 280**,** 38153-9.

TASCA, C. I., DAL-CIM, T. & CIMAROSTI, H. 2015. In vitro oxygen-glucose deprivation to study ischemic cell death. *Methods Mol Biol,* 1254**,** 197-210.

TATHAM, M. H., GEOFFROY, M. C., SHEN, L., PLECHANOVOVA, A., HATTERSLEY, N., JAFFRAY, E. G., PALVIMO, J. J. & HAY, R. T. 2008. RNF4 is a poly-SUMO-specific E3 ubiquitin ligase required for arsenic-induced PML degradation. *Nat Cell Biol,* 10**,** 538-46.

TAY, S. P., YEO, C. W., CHAI, C., CHUA, P. J., TAN, H. M., ANG, A. X., YIP, D. L., SUNG, J. X., TAN, P. H., BAY, B. H., WONG, S. H., TANG, C., TAN, J. M. & LIM, K. L. 2010. Parkin enhances the expression of cyclin-dependent kinase 6 and negatively regulates the proliferation of breast cancer cells. *J Biol Chem,* 285**,** 29231-8.

TERMAN, A., DALEN, H., EATON JOHN, W., NEUZIL, J. & BRUNK ULF, T. 2006. Aging of Cardiac Myocytes in Culture: Oxidative Stress, Lipofuscin Accumulation, and Mitochondrial Turnover. *Annals of the New York Academy of Sciences,* 1019**,** 70-77.

THROWER, J. S., HOFFMAN, L., RECHSTEINER, M. & PICKART, C. M. 2000. Recognition of the polyubiquitin proteolytic signal. *The EMBO Journal,* 19**,** 94.

TOYAMA, E. Q., HERZIG, S., COURCHET, J., LEWIS, T. L., JR., LOSON, O. C., HELLBERG, K., YOUNG, N. P., CHEN, H., POLLEUX, F., CHAN, D. C. & SHAW, R. J. 2016. Metabolism. AMP-activated protein kinase mediates mitochondrial fission in response to energy stress. *Science,* 351**,** 275-281.

TREMPE, J. F., SAUVE, V., GRENIER, K., SEIRAFI, M., TANG, M. Y., MENADE, M., AL-ABDUL-WAHID, S., KRETT, J., WONG, K., KOZLOV, G., NAGAR, B., FON, E. A. & GEHRING, K. 2013. Structure of parkin reveals mechanisms for ubiquitin ligase activation. *Science,* 340**,** 1451-5.

TSANG, A., HAUSENLOY, D. J., MOCANU, M. M. & YELLON, D. M. 2004. Postconditioning: a form of "modified reperfusion" protects the myocardium by activating the phosphatidylinositol 3-kinase-Akt pathway. *Circ Res,* 95**,** 230-2.

TSUKIHARA, T., FUKUYAMA, K., MIZUSHIMA, M., HARIOKA, T., KUSUNOKI, M., KATSUBE, Y., HASE, T. & MATSUBARA, H. 1990. Structure of the [2Fe-2S]ferredoxin I from the blue-green Alga Aphanothece sacrum at 2·2 Å resolution. *Journal of Molecular Biology,* 216**,** 399-410.

TWIG, G., ELORZA, A., MOLINA, A. J., MOHAMED, H., WIKSTROM, J. D., WALZER, G., STILES, L., HAIGH, S. E., KATZ, S., LAS, G., ALROY, J., WU, M., PY, B. F., YUAN, J., DEENEY, J. T., CORKEY, B. E. & SHIRIHAI, O. S. 2008a. Fission and selective fusion govern mitochondrial segregation and elimination by autophagy. *Embo j,* 27**,** 433-46.

TWIG, G., HYDE, B. & SHIRIHAI, O. S. 2008b. Mitochondrial fusion, fission and autophagy as a quality control axis: The bioenergetic view. *Biochimica et Biophysica Acta (BBA) - Bioenergetics,* 1777**,** 1092-1097.

ULRICH, H. D. 2005. Mutual interactions between the SUMO and ubiquitin systems: a plea of no contest. *Trends Cell Biol,* 15**,** 525-32.

UM, J. W. & CHUNG, K. C. 2006. Functional modulation of parkin through physical interaction with SUMO-1. *J Neurosci Res,* 84**,** 1543-54.

UZUNOVA, K., GÖTTSCHE, K., MITEVA, M., WEISSHAAR, S. R., GLANEMANN, C., SCHNELLHARDT, M., NIESSEN, M., SCHEEL, H., HOFMANN, K., JOHNSON, E. S., PRAEFCKE, G. J. K. & DOHMEN, R. J. 2007. Ubiquitin-dependent Proteolytic Control of SUMO Conjugates. *Journal of Biological Chemistry,* 282**,** 34167-34175.

VALENTE, A. J., MADDALENA, L. A., ROBB, E. L., MORADI, F. & STUART, J. A. 2017. A simple ImageJ macro tool for analyzing mitochondrial network morphology in mammalian cell culture. *Acta Histochemica,* 119**,** 315-326.

VAN DER BLIEK, A. M., SHEN, Q. & KAWAJIRI, S. 2013. Mechanisms of Mitochondrial Fission and Fusion. *Cold Spring Harb Perspect Biol,* 5.

VANDIVER, M. S., PAUL, B. D., XU, R., KARUPPAGOUNDER, S., RAO, F., SNOWMAN, A. M., KO, H. S., LEE, Y. I., DAWSON, V. L., DAWSON, T. M., SEN, N. & SNYDER, S. H. 2013. Sulfhydration mediates neuroprotective actions of parkin. *Nat Commun,* 4**,** 1626.

VENKITARAMAN, A. R. 2002. Cancer susceptibility and the functions of BRCA1 and BRCA2. *Cell,* 108**,** 171-82.

VENTECLEF, N., JAKOBSSON, T., EHRLUND, A., DAMDIMOPOULOS, A., MIKKONEN, L., ELLIS, E., NILSSON, L. M., PARINI, P., JANNE, O. A., GUSTAFSSON, J. A., STEFFENSEN, K. R. & TREUTER, E. 2010. GPS2-dependent corepressor/SUMO pathways govern anti-inflammatory actions of LRH-1 and LXRbeta in the hepatic acute phase response. *Genes Dev,* 24**,** 381-95.

VIJAY-KUMAR, S., BUGG, C. E. & COOK, W. J. 1987. Structure of ubiquitin refined at 1.8Åresolution. *Journal of Molecular Biology,* 194**,** 531-544.

VINCOW, E. S., MERRIHEW, G., THOMAS, R. E., SHULMAN, N. J., BEYER, R. P., MACCOSS, M. J. & PALLANCK, L. J. 2013. The PINK1-Parkin pathway promotes both mitophagy and selective respiratory chain turnover in vivo. *Proc Natl Acad Sci U S A,* 110**,** 6400-5.

VIRDEE, S., YE, Y., NGUYEN, D. P., KOMANDER, D. & CHIN, J. W. 2010. Engineered diubiquitin synthesis reveals Lys29-isopeptide specificity of an OTU deubiquitinase. *Nat Chem Biol,* 6**,** 750-7.

VOET, D. & VOET, J. G. 2011. *Biochemistry,* Hoboken, N.J., John Wiley & Sons.

WALLACE, D. C. 1999. Mitochondrial Diseases in Man and Mouse. *Science,* 283**,** 1482.

WANG, C. & YOULE, R. J. 2009. The Role of Mitochondria in Apoptosis(). *Annual review of genetics,* 43**,** 95-118.

WANG, H., SONG, P., DU, L., TIAN, W., YUE, W., LIU, M., LI, D., WANG, B., ZHU, Y., CAO, C., ZHOU, J. & CHEN, Q. 2011a. Parkin ubiquitinates Drp1 for proteasome-dependent degradation: implication of dysregulated mitochondrial dynamics in Parkinson disease. *J Biol Chem,* 286**,** 11649-58.

WANG, J., CHEN, L., WEN, S., ZHU, H., YU, W., MOSKOWITZ IVAN, P., SHAW GARY, M., FINNELL RICHARD, H. & SCHWARTZ ROBERT, J. 2011b. Defective sumoylation pathway directs congenital heart disease. *Birth Defects Research Part A: Clinical and Molecular Teratology,* 91**,** 468-476.

WANG, K., LONG, B., JIAO, J.-Q., WANG, J.-X., LIU, J.-P., LI, Q. & LI, P.-F. 2012a. miR-484 regulates mitochondrial network through targeting Fis1. *Nature Communications,* 3**,** 781.

WANG, S., SONG, P. & ZOU, M.-H. 2012b. AMP-activated protein kinase, stress responses and cardiovascular diseases. *Clinical Science (London, England : 1979),* 122**,** 555-573.

WANG, W., WANG, Y., LONG, J., WANG, J., HAUDEK, S. B., OVERBEEK, P., CHANG, B. H., SCHUMACKER, P. T. & DANESH, F. R. 2012c. Mitochondrial fission triggered by hyperglycemia is mediated by ROCK1 activation in podocytes and endothelial cells. *Cell Metab,* 15**,** 186-200.

WANG, X. & SCHWARZ, T. L. 2009. The Mechanism of Ca2+-Dependent Regulation of Kinesin-Mediated Mitochondrial Motility. *Cell,* 136**,** 163-174.

WANG, Y. & DASSO, M. 2009. SUMOylation and deSUMOylation at a glance. *J Cell Sci,* 122**,** 4249-52.

WASIAK, S., ZUNINO, R. & MCBRIDE, H. M. 2007. Bax/Bak promote sumoylation of DRP1 and its stable association with mitochondria during apoptotic cell death. *J Cell Biol,* 177**,** 439-50.

WATERHAM, H. R., KOSTER, J., VAN ROERMUND, C. W. T., MOOYER, P. A. W., WANDERS, R. J. A. & LEONARD, J. V. 2007. A Lethal Defect of Mitochondrial and Peroxisomal Fission. *New England Journal of Medicine,* 356**,** 1736-1741.

WATKINS, S. J., BORTHWICK, G. M. & ARTHUR, H. M. 2011. The H9C2 cell line and primary neonatal cardiomyocyte cells show similar hypertrophic responses in vitro. *In Vitro Cell Dev Biol Anim,* 47**,** 125-31.

WAUER, T. & KOMANDER, D. 2013. Structure of the human Parkin ligase domain in an autoinhibited state. *Embo j,* 32**,** 2099-112.

WAUER, T., SIMICEK, M., SCHUBERT, A. & KOMANDER, D. 2015a. Mechanism of phospho-ubiquitin-induced PARKIN activation. *Nature,* 524**,** 370-4.

WAUER, T., SIMICEK, M., SCHUBERT, A. & KOMANDER, D. 2015b. Mechanism of phospho-ubiquitin induced PARKIN activation. *Nature,* 524**,** 370-374.

WEI, L. & ZHAO, X. 2016. A new MCM modification cycle regulates DNA replication initiation. *Nat Struct Mol Biol,* 23**,** 209-16.

WEISSHAAR STEFAN, R., KEUSEKOTTEN, K., KRAUSE, A., HORST, C., SPRINGER HELEN, M., GÖTTSCHE, K., DOHMEN, R. J. & PRAEFCKE GERRIT, J. K. 2008. Arsenic trioxide stimulates SUMO-2/3 modification leading to RNF4-dependent proteolytic targeting of PML. *FEBS Letters,* 582**,** 3174-3178.

WENZEL, D. M., LISSOUNOV, A., BRZOVIC, P. S. & KLEVIT, R. E. 2011. UBCH7 reactivity profile reveals parkin and HHARI to be RING/HECT hybrids. *Nature,* 474**,** 105-8.

WHITBY, F. G., XIA, G., PICKART, C. M. & HILL, C. P. 1998. Crystal structure of the human ubiquitin-like protein NEDD8 and interactions with ubiquitin pathway enzymes. *J Biol Chem,* 273**,** 34983-91.

WHITWORTH, A. J., LEE, J. R., HO, V. M., FLICK, R., CHOWDHURY, R. & MCQUIBBAN, G. A. 2008. Rhomboid-7 and HtrA2/Omi act in a common pathway with the Parkinson's disease factors Pink1 and Parkin. *Dis Model Mech,* 1**,** 168-74; discussion 173.

WIEMERSLAGE, L. & LEE, D. 2016. Quantification of mitochondrial morphology in neurites of dopaminergic neurons using multiple parameters. *J Neurosci Methods,* 262**,** 56-65.

WILKINSON, K. A. & HENLEY, J. M. 2010. Mechanisms, regulation and consequences of protein SUMOylation. *Biochem J,* 428**,** 133-45.

WILKINSON, K. A., NISHIMUNE, A. & HENLEY, J. M. 2008. Analysis of SUMO-1 modification of neuronal proteins containing consensus SUMOylation motifs. *Neurosci Lett,* 436**,** 239-44.

WILKINSON, K. D. 2005. The discovery of ubiquitin-dependent proteolysis. *Proceedings of the National Academy of Sciences of the United States of America,* 102**,** 15280-15282.

WILLIAMS, R. L. & URBE, S. 2007. The emerging shape of the ESCRT machinery. *Nat Rev Mol Cell Biol,* 8**,** 355-68.

WILSON, J. E. 2003. Isozymes of mammalian hexokinase: structure, subcellular localization and metabolic function. *J Exp Biol,* 206**,** 2049-57.

WONG, K. H., TODD, R. B., OAKLEY, B. R., OAKLEY, C. E., HYNES, M. J. & DAVIS, M. A. 2008. Sumoylation in Aspergillus nidulans: sumO inactivation, overexpression and live-cell imaging. *Fungal Genet Biol,* 45**,** 728-37.

WU, L., MAIMAITIREXIATI, X., JIANG, Y. & LIU, L. 2016. Parkin Regulates Mitochondrial Autophagy After Myocardial Infarction in Rats. *Med Sci Monit,* 22**,** 1553-9.

WU, P. Y., HANLON, M., EDDINS, M., TSUI, C., ROGERS, R. S., JENSEN, J. P., MATUNIS, M. J., WEISSMAN, A. M., WOLBERGER, C. & PICKART, C. M. 2003. A conserved catalytic residue in the ubiquitin-conjugating enzyme family. *Embo j,* 22**,** 5241-50.

XIAO, B., DENG, X., LIM, G. G. Y., XIE, S., ZHOU, Z. D., LIM, K. L. & TAN, E. K. 2017. Superoxide drives progression of Parkin/PINK1-dependent mitophagy following translocation of Parkin to mitochondria. *Cell Death Dis,* 8**,** e3097.

XIONG, H., WANG, D., CHEN, L., CHOO, Y. S., MA, H., TANG, C., XIA, K., JIANG, W., RONAI, Z., ZHUANG, X. & ZHANG, Z. 2009. Parkin, PINK1, and DJ-1 form a ubiquitin E3 ligase complex promoting unfolded protein degradation. *J Clin Invest,* 119**,** 650-60.

XU, P., DUONG, D. M., SEYFRIED, N. T., CHENG, D., XIE, Y., ROBERT, J., RUSH, J., HOCHSTRASSER, M., FINLEY, D. & PENG, J. 2009. Quantitative Proteomics Reveals the Function of Unconventional Ubiquitin Chains in Proteasomal Degradation. *Cell,* 137**,** 133-145.

XU, Z., LAM, L. S., LAM, L. H., CHAU, S. F., NG, T. B. & AU, S. W. 2008. Molecular basis of the redox regulation of SUMO proteases: a protective mechanism of intermolecular disulfide linkage against irreversible sulfhydryl oxidation. *Faseb j,* 22**,** 127-37.

YAMANO, K., FOGEL, A. I., WANG, C., VAN DER BLIEK, A. M. & YOULE, R. J. 2014. Mitochondrial Rab GAPs govern autophagosome biogenesis during mitophagy. *eLife,* 3**,** e01612.

YAMANO, K. & YOULE, R. J. 2013. PINK1 is degraded through the N-end rule pathway. *Autophagy,* 9**,** 1758-69.

YAMIN, T. T., AYALA, J. M. & MILLER, D. K. 1996. Activation of the native 45-kDa precursor form of interleukin-1-converting enzyme. *J Biol Chem,* 271**,** 13273-82.

YE, Y. & RAPE, M. 2009. Building ubiquitin chains: E2 enzymes at work. *Nature reviews. Molecular cell biology,* 10**,** 755-764.

YEH, E. T., GONG, L. & KAMITANI, T. 2000. Ubiquitin-like proteins: new wines in new bottles. *Gene,* 248**,** 1-14.

YELLON, D. M., ALKHULAIFI, A. M., BROWNE, E. E. & PUGSLEY, W. B. 1992. Ischaemic preconditioning limits infarct size in the rat heart. *Cardiovascular Research,* 26**,** 983-987.

YELLON, D. M. & HAUSENLOY, D. J. 2007. Myocardial reperfusion injury. *N Engl J Med,* 357**,** 1121-35.

YEO, C. W., NG, F. S., CHAI, C., TAN, J. M., KOH, G. R., CHONG, Y. K., KOH, L. W., FOONG, C. S., SANDANARAJ, E., HOLBROOK, J. D., ANG, B. T., TAKAHASHI, R., TANG, C. & LIM, K. L. 2012. Parkin pathway activation mitigates glioma cell proliferation and predicts patient survival. *Cancer Res,* 72**,** 2543-53.

YIN, Q., LIN, S. C., LAMOTHE, B., LU, M., LO, Y. C., HURA, G., ZHENG, L., RICH, R. L., CAMPOS, A. D., MYSZKA, D. G., LENARDO, M. J., DARNAY, B. G. & WU, H. 2009. E2 interaction and dimerization in the crystal structure of TRAF6. *Nat Struct Mol Biol,* 16**,** 658-66.

YONASHIRO, R., ISHIDO, S., KYO, S., FUKUDA, T., GOTO, E., MATSUKI, Y., OHMURA-HOSHINO, M., SADA, K., HOTTA, H., YAMAMURA, H., INATOME, R. & YANAGI, S. 2006. A novel mitochondrial ubiquitin ligase plays a critical role in mitochondrial dynamics. *Embo j,* 25**,** 3618-26.

YOON, Y., KRUEGER, E. W., OSWALD, B. J. & MCNIVEN, M. A. 2003. The mitochondrial protein hFis1 regulates mitochondrial fission in mammalian cells through an interaction with the dynamin-like protein DLP1. *Mol Cell Biol,* 23**,** 5409-20.

YOON, Y., PITTS, K. R., MCNIVEN, M. A. & BONIFACINO, J. 2001. Mammalian Dynamin-like Protein DLP1 Tubulates Membranes. *Molecular Biology of the Cell,* 12**,** 2894-2905.

YOSHIDA, Y. 2018. *Insights into the Mechanisms of Chloroplast Division*.

YOU, J. & PICKART, C. M. 2001. A HECT Domain E3 Enzyme Assembles Novel Polyubiquitin Chains. *Journal of Biological Chemistry,* 276**,** 19871-19878.

YOULE, R. J. & NARENDRA, D. P. 2011. Mechanisms of mitophagy. *Nat Rev Mol Cell Biol,* 12**,** 9-14.

YU, J. Y., DERUITER, S. L. & TURNER, D. L. 2002. RNA interference by expression of short-interfering RNAs and hairpin RNAs in mammalian cells. *Proc Natl Acad Sci U S A,* 99**,** 6047-52.

YUNUS, A. A. & LIMA, C. D. 2006. Lysine activation and functional analysis of E2-mediated conjugation in the SUMO pathway. *Nature Structural &Amp; Molecular Biology,* 13**,** 491.

ZAISS, D. M., STANDERA, S., KLOETZEL, P. M. & SIJTS, A. J. 2002. PI31 is a modulator of proteasome formation and antigen processing. *Proc Natl Acad Sci U S A,* 99**,** 14344-9.

ZAMPONI, N., ZAMPONI, E., CANNAS, S. A., BILLONI, O. V., HELGUERA, P. R. & CHIALVO, D. R. 2018. Mitochondrial network complexity emerges from fission/fusion dynamics. *Scientific Reports,* 8**,** 363.

ZHANG, C. W., HANG, L., YAO, T. P. & LIM, K. L. 2015. Parkin Regulation and Neurodegenerative Disorders. *Front Aging Neurosci,* 7**,** 248.

ZHANG, F. P., MIKKONEN, L., TOPPARI, J., PALVIMO, J. J., THESLEFF, I. & JANNE, O. A. 2008. Sumo-1 function is dispensable in normal mouse development. *Mol Cell Biol,* 28**,** 5381-90.

ZHANG, P. & HINSHAW, J. E. 2001. Three-dimensional reconstruction of dynamin in the constricted state. *Nat Cell Biol,* 3**,** 922-6.

ZHANG, Y.-Q. & SARGE, K. D. 2008. Sumoylation regulates lamin A function and is lost in lamin A mutants associated with familial cardiomyopathies. *The Journal of Cell Biology,* 182**,** 35.

ZHENG, N., WANG, P., JEFFREY, P. D. & PAVLETICH, N. P. 2000. Structure of a c-Cbl-UbcH7 complex: RING domain function in ubiquitin-protein ligases. *Cell,* 102**,** 533-9.

ZHOU, C., HUANG, Y., SHAO, Y., MAY, J., PROU, D., PERIER, C., DAUER, W., SCHON, E. A. & PRZEDBORSKI, S. 2008. The kinase domain of mitochondrial PINK1 faces the cytoplasm. *Proc Natl Acad Sci U S A,* 105**,** 12022-7.

ZHOU, W., RYAN, J. J. & ZHOU, H. 2004. Global analyses of sumoylated proteins in Saccharomyces cerevisiae. Induction of protein sumoylation by cellular stresses. *J Biol Chem,* 279**,** 32262-8.

ZHOU, Z. D., SATHIYAMOORTHY, S., ANGELES, D. C. & TAN, E. K. 2016. Linking F-box protein 7 and parkin to neuronal degeneration in Parkinson's disease (PD). *Mol Brain,* 9**,** 41.

ZHOU, Z. D., XIE, S. P., SATHIYAMOORTHY, S., SAW, W. T., SING, T. Y., NG, S. H., CHUA, H. P., TANG, A. M., SHAFFRA, F., LI, Z., WANG, H., HO, P. G., LAI, M. K., ANGELES, D. C., LIM, T. M. & TAN, E. K. 2015. F-box protein 7 mutations promote protein aggregation in mitochondria and inhibit mitophagy. *Hum Mol Genet,* 24**,** 6314-30.

ZHU, J., ZHU, S., GUZZO, C. M., ELLIS, N. A., SUNG, K. S., CHOI, C. Y. & MATUNIS, M. J. 2008. Small ubiquitin-related modifier (SUMO) binding determines substrate recognition and paralog-selective SUMO modification. *J Biol Chem,* 283**,** 29405-15.

ZHU, P. P., PATTERSON, A., STADLER, J., SEEBURG, D. P., SHENG, M. & BLACKSTONE, C. 2004. Intra- and intermolecular domain interactions of the C-terminal GTPase effector domain of the multimeric dynamin-like GTPase Drp1. *J Biol Chem,* 279**,** 35967-74.

ZIMORSKI, V., KU, C., MARTIN, W. F. & GOULD, S. B. 2014. Endosymbiotic theory for organelle origins. *Current Opinion in Microbiology,* 22**,** 38-48.

ZOU, J., YUE, F., LI, W., SONG, K., JIANG, X., YI, J. & LIU, L. 2014. Autophagy inhibitor LRPPRC suppresses mitophagy through interaction with mitophagy initiator Parkin. *PLoS One,* 9**,** e94903.

ZÜCHNER, S., MERSIYANOVA, I. V., MUGLIA, M., BISSAR-TADMOURI, N., ROCHELLE, J., DADALI, E. L., ZAPPIA, M., NELIS, E., PATITUCCI, A., SENDEREK, J., PARMAN, Y., EVGRAFOV, O., JONGHE, P. D., TAKAHASHI, Y., TSUJI, S., PERICAK-VANCE, M. A., QUATTRONE, A., BATTOLOGLU, E., POLYAKOV, A. V., TIMMERMAN, V., SCHRÖDER, J. M. & VANCE, J. M. 2004. Mutations in the mitochondrial GTPase mitofusin 2 cause Charcot-Marie-Tooth neuropathy type 2A. *Nature Genetics,* 36**,** 449.

ZUNINO, R., SCHAUSS, A., RIPPSTEIN, P., ANDRADE-NAVARRO, M. & MCBRIDE, H. M. 2007. The SUMO protease SENP5 is required to maintain mitochondrial morphology and function. *J Cell Sci,* 120**,** 1178-88.

ZWEIER, J. L., FLAHERTY, J. T. & WEISFELDT, M. L. 1987. Direct measurement of free radical generation following reperfusion of ischemic myocardium. *Proc Natl Acad Sci U S A,* 84**,** 1404-7.

Chapter 8 Appendix

8.1 Supplementary Figure 1

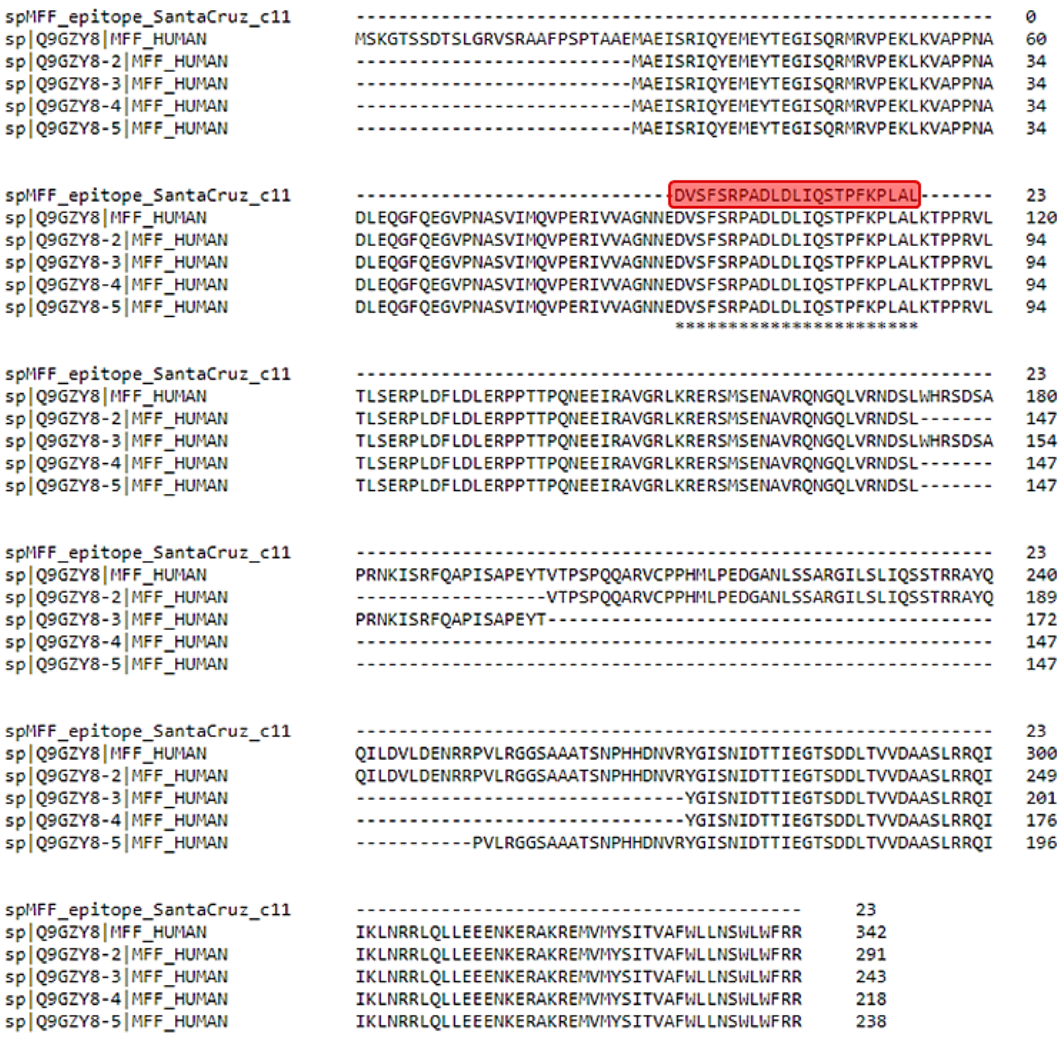

Figure 8.1 **Mff epitope is present in all 5 human isoforms**. Sequence alignment of region containing Santa Cruz Mff monoclonal antibody (C-11) epitope with Full length human Mff (isoform 1) and isoforms 2-5. Region containing epitope sequence is highlighted (red) and present in all Mff isoforms. Alignment produced using ClustalOmega. Uniprot identifiers are as shown (Q9GZY8: full length Mff (as used in Mff constructs), Q9GZY8-2-5 are shorter isoforms 2-5).